INFORMATION TO USERS

This manuscript has been reproduced from the microfilm master. UMI films the text directly from the original or copy submitted. Thus, some thesis and dissertation copies are in typewriter face, while others may be from any type of computer printer.

The quality of this reproduction is dependent upon the quality of the copy submitted. Broken or indistinct print, colored or poor quality illustrations and photographs, print bleedthrough, substandard margins, and improper alignment can adversely affect reproduction.

In the unlikely event that the author did not send UMI a complete manuscript and there are missing pages, these will be noted. Also, if unauthorized copyright material had to be removed, a note will indicate the deletion.

Oversize materials (e.g., maps, drawings, charts) are reproduced by sectioning the original, beginning at the upper left-hand corner and continuing from left to right in equal sections with small overlaps.

ProQuest Information and Learning
300 North Zeeb Road, Ann Arbor, MI 48106-1346 USA
800-521-0600

University of Alberta

SHEAR LAG EFFECT ON WELDED HOT-ROLLED STEEL CHANNEL IN TENSION

By

HUI GUO

A thesis submitted to the Faculty of Graduate Studies and Research in partial fulfillment of the requirements for the degree of Master of Science

in

Structural Engineering

Department of Civil and Environmental Engineering

Edmonton, Alberta

Fall 2005

ABSTRACT

Current design standards dealing with shear lag problem for tension members mostly are based on research conducted on bolted tension members. Relatively few researches are available to study the behavior of welded hot-rolled steel sections in tension. In particular, questions need to be answered about the strength of welded tension members with small L/W (weld length to distance between welds) ratios, which will lead to more severe shear lag effect. Thus, extensive investigation was conducted here in order to better understand the behavior of welded members in tension. A total of ten full-scale tests were conducted on hot-rolled steel channel sections, with different combinations of parameters that may affect the efficiency of the section. Following the tests, non-linear numerical models were developed to study the behavior of welded channel members in tension, and to compare with the test results. Furthermore, a parametric study was performed using these models to expand experimental database to cover all available hot-rolled channel sections. It was found that all the tested channel specimens failed either in net section fracture away from the connection or in weld fracture. Non-uniform stress distribution at connection was observed due to the shear lag effect. However, it has no effect on the final carrying capacity of the specimens. Based on the findings from this research and others, a reduction factor of 0.95 is recommended in designing the resistance of welded channel members in tension.

ACKNOWLEDGEMENTS

This project is funded by Steel Structures Education Foundation and the Natural Science and Engineering Research Council of Canada to Dr. J.J. R. Cheng.

The technical assistance of Larry Burden and Richard Helfrich is acknowledged, both are the technicians in I.F. Morrison Structural Laboratory, Department of Civil and Environmental Engineering, University of Alberta.

Many thanks are given to Dr. Mohammad Behbahanifard and Angus Lam, PhD student in the Department of Civil and Environmental Engineering, University of Alberta for their assistance in using the finite element program.

Special thanks to my family for supporting me and lightening my life in darkness.

TABLE OF CONTENTS

LIST OF TABLES

LIST OF FIGURES

LIST OF SYMBOLS

A	-	gross cross sectional area
A_0	-	initial cross-section area
A_{ne}	-	effective net area
A_n	-	net sectional area
E	-	modulus of elasticity
F_y	-	yield strength of material
F_u	-	ultimate strength of material
L	-	longitudinal welding length
P_{ten}	-	specimen tension strength assuming uniform stress distribution over channel cross section
P_{mea}	-	specimen tension strength based on measured welding size
P_{ult}	-	ultimate strength of specimen
t	-	thickness of the member
T_r	-	factored tensile resistance of the member
U	-	net area efficiency, shear lag coefficient
U_{AISC}	-	net area efficiency based on AISC specification
U_{para}	-	net area efficiency of parametric study result
$U_{S16\text{-}01}$	-	net area efficiency based on CSA-S16-01-2001 standard
w	-	channel width
$\bar{x}$	-	connection eccentricity, distance from the face of the connection to the center of gravity of the member

ϕ - resistance factor

σ_{true} - true stress

σ_{nom} - engineering stress

ε_{nom} - engineering strain

ε_{true} - total true strain

ε^{p}_{true} - plastic true strain

1. INTRODUCTION

1.1 General

Hot-rolled steel sections, such as channels and angles, are widely used in steel structures as axially loaded tension or compression members. For example, they are frequently used as bracing members in a steel tower or as chord and web members in a truss. For axially loaded compression channel members, their failure modes are often governed by local or overall buckling, in which case the material properties cannot be fully utilized; while for axially loaded tension channel members, their capacity is mainly based on the material properties and the way in which members are connected at the ends. Physical tests of tension members have shown that the actual fracture load is usually less than the theoretical strength of the cross-section (product of the net area of the section and the material tensile strength). There are several possible reasons for this fact:

(a) the method of making holes (punched or drilled);

(b) the ratio of the gauge of the holes to the fastener diameter;

(c) the ductility of the material;

(d) the amount of elements being connected.

Of all the above potential factors, it is the fourth one that is the most significant and thus is the focus of the investigation reported herein. In practice, a member may be connected by all its elements or just some of its elements. For practical and economical reason, most open sections, such as I sections, channel sections, and angle sections, are not connected by all the elements of the section. Therefore, the elements that are not connected may not be fully effective in the region of the connection and at the vicinity of

the connection a non-uniform stress distribution occurs. This non-uniform stress distribution could lead to a reduced ultimate strength of the member. For plate or slotted tubular tension member, although the full section is available to carry the load, the stress near the connection (bolt or weld) is much higher than those away from the connection, thus a non-uniform stress distribution still exists. In addition, the length of the connected element also plays a significant role on the carrying capacity of the section. If the length of the connection is long enough, it allows tensile stresses transfer to connected member gradually. This will reduce the degree of non-uniform stress distribution at the critical section; hence lessen the effect on the carrying capacity. Since the internal transfer of stresses from one part to the other part is by shear, this phenomenon is commonly referred to as shear lag effect and is shown schematically in Fig. 1.1 for a welded plate in tension.

1.2 Statement of the Problem

The current design standard CAN/CSA S16-01 (2001) for shear-lag problems (for both bolted and welded connections) is mostly based on Chesson and Munse's research results of bolted and riveted tension members (1963a, 1963b). Although there is some similarity between the failure mechanism of a welded connection and that of a bolted connection, there is a significant difference between these two cases. Recently shear-lag effect on welded tension members has started to receive attention. It is found that in some cases the shear-lag effect is not as severe as that for bolted members, which have the presence of holes at the connection producing more severe non-uniform stress at the connection. Some studies have demonstrated that the shear-lag reduction factor "U" for

welded connections would be much higher than that stipulated in our present design code (Cheng et al. 1998).

Previous research on welded tension members, such as Esterling and Giroux's study for hot-roll channel section (1993), was focused on L/W ratio (ratio of the weld length to the distance between welds) between 1.5 and 2.0; in this case shear lag effect is not as severe as for the case which L/W is close to or less than 1.0. Hence our research will focus on the cases in which L/W is close to 1.0, which is not well defined in the current design standard. As we can expect, a more severe non-uniform stress distribution will occur over the cross-section of the member when L/W is smaller, which will lead to more severe shear-lag effect. Furthermore, with a decrease in weld length, imperfections in the weld in the form of gouge or notch may trigger premature weld failure, which will be discussed hereafter.

A limited number of tests have been completed on hot-roll channel sections in this investigation, with different weld details on either single or double channel sections. For the single channel specimens, a single channel is welded at both ends to gusset plates, in which case there will be significant bending at the vicinity of connection, since at initial loading stage the axial force is eccentric with respect to the centroid of the cross-section. A pair of channels welded symmetrically back to back onto gusset plates at the ends in the double channel specimens, and there will be no eccentricity for the specimens. The welding layout includes longitudinal welds and combination of transverse and longitudinal welds. The length of weld, the size of weld, and the L/W ratio are the important variables in design of the specimens.

1.3 Objectives and Scope

The objective of this research work is to investigate the behavior of welded tension members. Hot-rolled channel sections with different combinations of welding details are studied in this project. Existing design standards are to be evaluated to assess the level of safety currently being provided. The research includes laboratory tests, non-linear finite element analyses, along with a comparison to other research programs. Finally, recommendations are made to improve the existing design provisions and to address the future research needs for the problem.

The specific objectives of this investigation are summarized as follows:

(a) Conduct a limited number of full-scale tension tests of welded single and double channel specimens to examine the shear-lag effect for a series of welding parameters;

(b) Develop finite element models using ABAQUS/Standard program (2002), and carry out a parametric study to further study the behavior of welded channel sections in tension and to enlarge experimental database;

(c) Compare the capacity and behavior difference between single channel and double channel specimens, and check the effect of eccentricity;

(d) Compare the test results with previous studies and current design equations, and propose more rational design criteria, if possible;

(e) Recommend future study on this topic.

1.4 Organization of the Thesis

The thesis consists of seven chapters. Chapter One gives a general statement about the shear-lag problem, objectives, and scope of this investigation. Chapter Two

reviews the previous work done on the net section efficiency for both welded and bolted tension members along with current design standards in North America. Details of laboratory research program, including the geometry of specimens, test setup, and test procedure, are discussed in Chapter Three. Chapter Four provides the test results and discussion of the results. Chapter Five presents the finite element models used to simulate the test results. The parametric study of welded channel sections in tension using the numerical models is included in Chapter Six. Comparison between the findings from this study with other research results is also covered in Chapter Six. Chapter Seven contains summaries and recommendations of the research, future research needs on this topic are also included.

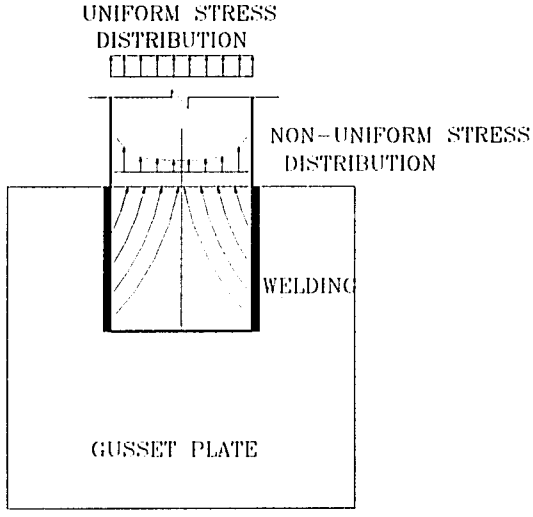

Fig. 1.1 Shear Lag Phenomenon

2. LITERATURE REVIEW

2.1 Bolted Connections

The first recorded research on the shear lag problem was conducted by Mckibben (1906), in which the shear lag effect in hot-rolled steel angle tension member was studied. The end connections were made using either bolts or rivets. Detailed literature reviews of shear lag effect on bolted hot-rolled and cold-formed steel member connections can be found in the papers done by Wu and Kulak (1993), Laboube and Yu (1995), and Yip and Cheng (2000), and will not be repeated here. However, research work done by Chesson and Munse (1963a, 1963b), which formed the basis of current design standard such as CSA Standard S16-01 (2001) and AISC-LRFD Specification (1999), will be described here briefly.

Chesson and Munse conducted experimental tests on bolted and riveted connections to investigate the behavior of various cross sections of truss-type members (1963a). They evaluated the test results by calculating the ratio of ultimate experimental load to the product of the material tensile stress and the gross area of specimens. Several factors were found to have influence on the net section efficiency, namely, the net section area, a geometrical character of cross section, ductility of material, bearing strength, and shear lag effect. After a study of about 200 valid test results, Chesson and Munse seldom found the ratio exceeding 0.9, therefore they suggested an upper limit efficiency of 0.85. Chesson and Munse (1963b) reported on two other studies that recommended the maximum efficiency factors of 0.75 and 0.85. Combining these studies with their own results, Chesson and Munse developed an empirical equation to incorporate various

factors that influence the net section efficiency (1963b). The two most important factors were the calculation of net section area (A_n) and shear lag effect (U). The shear lag reduction factor was given by:

[2.1] $$U = 1 - \frac{\bar{x}}{L}$$

where

$\bar{x}$ = distance from the face of the connection to center of gravity of the member;

L = connection length.

2.2 Welded Connections

In 1931, the American Bureau of Welding released the results of a broad study in which safe working stresses for welds were established. Both single and double plate tension specimens were tested, welded either longitudinally or both longitudinally and transversely, with the ratio of weld length L to the distance between two parallel welds W (L/W) ranging from 0.27 to 1.6. Most of the tests failed at the weld, while a few specimens fractured at the plate section. Although the test results were scattered, they were considered by AISC Specification in the development of the earlier version of design provisions dealing with shear lag problem in the welded members. The provisions with minor modifications are still being used in current design standards (CSA S16-01 and AISC-LRFD-1999).

Easterling and Giroux (1993) at Virginia Tech. conducted a series of experimental and analytical tests to study the shear lag effect on welded tension members. There were 27 specimens tested in the research program, including hot-rolled angles, plates, and channel sections welded back to back onto gusset plates. The gusset plates were then

gripped in a material testing machine and pulled until failure. Fillet weld was used for all specimens, weld configurations for angle and channel specimens were longitudinal, transverse and a combination of longitudinal and transverse weld; for plate specimens, longitudinal and a combination of longitudinal and transverse weld were used. Strain gauges were used in one of the tests for each member type to study the stress distribution at the vicinity of weld connection. Five strain gauges mounted at critical section and three strain gauges were mounted longitudinally along the weld length direction to measure strain distribution. L / W ratio for plate specimens ranged from 1.0 to 1.67, for angle specimens it was between 0.88 and 2.25 and for channel specimens it was 1.67. From the test results, Easterling et al. concluded that shear lag controlled the strength of angle and plate specimens only. For the plate specimens connected only by longitudinal welds, they found the weld length did not affect shear lag effect. The transverse weld in the tension members would not affect the member strength. Since all the channel specimens either ruptured at mid length or fractured at welds and none of them failed at critical section near the weld, they concluded that shear lag effect did not govern the carrying capacity of channel specimens. To account for eccentricities and fabrication imperfection in welded specimens, Easterling and Giroux put an upper limit of 0.9 for the shear lag reduction factor.

Cheng et al. (1998) conducted nine tubular HSS (Hollow Structural Section) tension tests to study the shear lag effect on the slotted tubular tension members. For the HSS102x6.4 specimens, L/W ratio was 1.06, and for the HSS102x4.8 specimens, L/W ratio was 0.94. For the two specimens made by HSS219x8.0, one L/W ratio was 1.0 and the other was 0.8. Welds across the gusset plate thickness were provided to all specimens

except the seventh specimen, which finally ruptured at the critical section. Strain gauges and linear variable displacement transducers (LVDTs) were used to measure the strain distribution and the overall deformation. Seven of nine specimens failed at the mid-length of the member, which could be attributed to the stiffening effect provided by the gusset plates and the weld across the thickness of gusset plates. The other two specimens failed at the critical section, due to either the absence of the weld across the thickness of gusset plate or shorter weld length. In all tests, there was extensive deformation before fracture no matter where the fracture took place. It was concluded that the shear lag did not significantly affect the ultimate capacity of slotted round tubular section welded to gusset plates, as long as the weld length was at least 1.3 times the tube diameter and a weld return was provided at the critical section.

Lemenhe and Cheng (2001) investigated the behavior of welded cold-formed steel tension members. The experimental program included five single channel specimens and seven single angle specimens followed by a numerical analysis. The ratio of L/W varied from 1.04 to 1.49. None of the channel specimens failed at the critical section adjacent to the gusset plates. They either failed at the gross area away from connection or ruptured at the welds. There were three angle specimens failed at the net section initiated by tearing in the connected heel at the end of welds. All other angle specimens fractured in the middle of the members. Finally they concluded that the connection length and the cross-section geometry affected the capacity of welded cold-formed angles. Both balanced and unbalanced welds used for angle specimens lead to the same ultimate strength. Shear lag effect at the connection will not control the strength of welded cold-formed channel

specimens under tension. A section efficiency factor of 0.95 was recommended for the welded cold-formed angle section under tension.

2.3 Current Design Standards

2.3.1 CSA Standard S16-01 (2001)

CSA S16-01 (2001) requires that the factored resistance of a tension member be taken as the least of:

(a) Yielding in the gross cross-section area

[2.2] $$T_r = \phi F_y A_g$$

(b) Fracture of the net area

[2.3] $$T_r = 0.85\phi F_u A_n$$

(c) Fracture of the effective net area considering shear lag effect

[2.4] $$T_r = 0.85\phi F_u A_{ne}$$

where

F_y = yield strength of the material;

F_u = ultimate strength of the material;

A_g = gross cross-sectional area;

A_n = net sectional area;

A_{ne} = effective net sectional area;

ϕ = resistance factor, 0.9 is used for all three limit states.

When a tension load is transmitted by welds, the effective net area shall be computed as

[2.5] $A_{ne} = A_{n1} + A_{n2} + A_{n3}$

A_{n1}, A_{n2}, A_{n3} are the net areas of connected plate elements subject to one of the following methods of load transfer:

(a) elements connected by transverse welds,

[2.6] $A_{n1} = wt$

(b) elements connected by longitudinal welds along two parallel edges,

(i) when $2w \leq L$

[2.7] $A_{n2} = 1.00wt$

(ii) when $w \leq L < 2w$

[2.8] $A_{n2} = 0.5wt + 0.25Lt$

(iii) when $L < w$

[2.9] $A_{n2} = 0.75Lt$

where

L = average length of welds on the two edges

W = plate width (distance between welds)

(c) elements connected by a single longitudinal weld,

(i) when $w \leq L$

[2.10] $A_{n3} = (1 - \frac{\bar{x}}{L})wt$

(ii) when $w > L$

[2.11] $A_{n3} = 0.50Lt$

where

$\bar{x}$ = eccentricity of the weld with respect to centroid of the connected element

L = weld length in the direction of loading. The outstanding leg of an angle is considered connected by the single line of weld along the heel.

2.2.2 AISC-LRFD Specification (1999)

In the Load and Resistance Factor Design (LRFD) equations in AISC Specification (1999) the tensile design strength should be the lower value obtained according to limit states of yielding in the gross section and fracture in the net section.

(a) for yielding in the gross section

[2.12] $T_r = \phi F_y A_g$

(b) for fracture in the net section

[2.13] $T_r = \phi F_u A_e$

where

A_e = effective net area,

ϕ = resistance factor, the resistance factor 0.9 is used for yielding limit state and 0.75 for fracture limit state.

The effective area of tension members shall be determined by follows:

(a) When tension load is transmitted directly to each of cross-sectional elements by fasteners or welds, the effective area A_e is equal to the net area A_n or A_g respectively.

(b) When tension load is transmitted by fasteners or welds through some but not all of the cross-sectional elements of the member, the effective area A_e shall be computed as follows:

(i) When the tension load is transmitted only by longitudinal welds to other than a plate member or by longitudinal welds in combination with transverse welds

[2.14] $A_e = UA_g$

where

$U = 1 - (\overline{x}/L) \leq 0.9$

A_g = gross area of the member

(ii) When tension load is transmitted only by transverse welds

[2.15] $A_e = UA$

where

U = 1.0

A = area of directly connected elements

(iii) When tension load is transmitted to a plate only by longitudinal welds along both edges at the end of plate

[2.18] $A_e = UA_g$

where

[2.18a] U=1.0 for $L \geq 2W$

[2.18b] U = 0.87 for $2W > L \geq 1.5W$

[2.18c] U = 0.75 for $1.5W > L \geq W$

L = length of weld along one side

W = distance between welds

3. EXPERIMENTAL PROGRAM

3.1 General Objectives of the Experimental Program

(a) To study the shear lag effect on the behavior of welded hot-rolled channel sections with different weld connection length and weld size;

(b) To study the load-deformation behavior and stress/strain distributions at the critical sections.

Parameters examined in the experimental program included length of welded connection, presence of a transverse weld, weld size, and single vs. double channel connections.

A total of ten specimens were fabricated and tested in the I.F. Morrison Structural Engineering Laboratory at University of Alberta, of which seven specimens were double channel specimens and the remaining three are single channel specimens. Channels were welded to gusset plates using shielding metal arc welding (SMAW). The electrode wires used for the welding were E48018. It is a low hydrogen electrode with a relatively high percentage of iron power in covering and the manganese content is set at the high end of the range. Detailed explanation of this classification system for SMAW electrode is given in Fig. 3.1. The specimens were instrumented with strain gauges to study the strain distribution at the connection area and mid-length. Also, three linear variable displacement transducers (LVDTs) were attached to each specimen to investigate the load-deformation behavior of different parts of each specimen.

3.2 Specimens Description

The specimens were made up of channels and gussets, as shown in Fig. 3.2. A channel section of C75 x 6 was used for all the specimens. The nominal dimensions of the section are listed below:

d = 76 mm, b = 35 mm, w = 4.3 mm, t = 6.9 mm, and area A = 763 mm^2

CSA G40.21-M Grade 300W steel was used for both channels and gusset plates.

It will be seen in the later chapters that the actual cross-sectional area of the channel is very important for calculating the tensile strength of the channels. However, it is very difficult to measure the area directly because of the tapered flange of a channel cross section. Hence a special method was utilized to obtain the actual cross section area. In doing so, a piece of channel was cut and its length (1320 mm) and mass (7908 g) were measured. Since the mass equals steel density times cross section area and the length, and the density of the steel was constant (7850 kg/m^3), therefore the cross-sectional area of a single channel should be 763.2 mm^2.

The sizes of the gusset plates were 300 mm x 480 mm x 12.7 mm (8 pieces) and 300 mm x 370 mm x 12.7mm (16 pieces), as shown in Fig. 3.3 and Fig. 3.4. The holes on the gusset plates and splice plates were drilled in the structural lab and channels were cut into different lengths depending on the weld length of each specimen. All the net edge-to-edge distance between the gusset plates in specimens were 1200 mm except specimen 2, in which case the net distance was 1310 mm. Welding configurations and specimen dimensions are listed in Table 3.1 and Table 3.2, respectively.

The testing program was conducted in two series. In the first series, seven specimens were tested, which included a specimen with transverse weld. After

completion and evaluation of the first seven test results, three additional specimens were fabricated to study the different behavior between single and double channel specimens. A qualified welder performed all the welding, and weld quality was emphasized. E48018 electrodes were used for all specimens. End return of welds was applied for the first seven specimens. Originally specimens 1 and 2 were designed to fail at the welds based on the nominal channel area and design weld size and strength. However, they unexpectedly failed in the middle of the channels. Further investigation showed that actual weld sizes were larger than the nominal ones and the end return of weld contributed to the actual weld strength as well. Hence, the weld length was shortened for the remaining five specimens of the first seven specimens and end return was also removed. Another reason for doing this is that with the reduced weld lengths, specimens would experience more severe shear lag effect, which may cause the specimens fail at critical sections. After the first batch was done, it was decided that different behavior between single and double channel specimens should be further studied. The weld size and length of Specimens 8 and 9 were identical except that one was single channel specimen, and the other was double channel specimen. To make further comparison between single and double channel specimens, single channel specimen 10 was made based on its counterpart specimen 4.

3.3 Material Tension Coupons

A series of tension coupon tests were completed in order to establish basic material properties of the specimens. Five six-meter long channels from the same heat were used to fabricate the specimens. They were numbered one to five. For each six-

meter long channel two tension coupons were cut from the web; and a total ten web tension coupons were made. In addition, two tension coupons were made from the flange of each of the channels numbered 3 and 5, respectively. The location of the coupons cut from the channel is shown in Fig. 3.5. The tension coupons have a gauge length of 50 mm and a width of 12.5 mm. The dimensions of the coupons were prepared in accordance with the requirements of ASTM A370-01 (2001).

In order to examine the weld material properties, one cylindrical shape coupon and two flat coupons were made according to the requirement of AWS5.1-91 (1991). Firstly, two 200 x 50 x 12.7 mm base metal plates were cut from the same heat of steel gusset plates and a 12.7 mm gap was kept between them, and then a welder used plug welding to weld the two plates together with E48018 electrode to form one piece of plate. When this was done, the weld material was cut out from the middle of the plate and milled to the desired cylindrical shape and size, as shown in Fig. 3.6. For flat weld material coupons, a similar procedure was followed except this time the two flat coupons were cut perpendicular to the weld axis, so the coupons were made up of two kinds of material, one was weld and the other was steel plate, and only central part of the coupon was made of welding material, as shown in Fig. 3.7. Also, tension coupons from the steel gusset plates were fabricated and tested. They were very similar to those shown in Fig. 3.7 except they were made by one material.

An extensometer with 50 mm gauge length was used to measure the strains in the coupons during testing. For the first coupon tested, there were two strain gauges mounted on each face of the coupon to calibrate the extensometer readings. MTS1000 testing machine was used to complete the coupon tests and load-deformation data were recorded.

3.4 Test Setup and Instrumentation

A combined bolted-welded connection device was employed to connect the specimens to the clevis grips of the MTS6000, as shown in the Fig. 3.8 to Fig. 3.10. It can be seen that they are very stocky design. There are some reasons to choose these kinds of attachment. Firstly, it can ensure specimens fail prior to connection failure. Secondly, it has little deformation during test since it is a very stiff design. Thirdly, unlike grip connection in which slip may happen during test, there is no slip in clevis connection. Also, to prevent any out-of-plane movement of the gusset plates, shim plates were inserted between the attachment and the gusset plates.

Measurements of loads, deformations, and strains were made as the specimen was loaded. The instrumentation is detailed in Fig. 3.11 and pictorially shown in Fig. 3.12. LVDTs are used to measure the macro deformation of the specimen while strain gauges are utilized to measure the strain distribution at both the vicinity of welding and the mid-length. The layout and number of each strain gauge are listed in Fig. 3.13 to Fig. 3.15. It can be seen that most strain gauges were placed near to the connection between gusset plate and channel. They would help us get a better understanding about the strain and stress distribution in this area. LVDT1 is designed to measure the deformation of each specimen between the gusset plates, LVDT2 can monitor the deformation around the critical section and LVDT3 will record the deformation of the welds. All strain gauges, LVDTs, stroke, and load readings are routed through a data acquisition system with 22 channels.

3.5 Test Procedure

After the specimen was hooked to the MTS6000 testing machine, whitewash was used to highlight the specimen yielding pattern when load reached certain level. Tension load was applied to the specimen through the connection of the gusset plates to the attachments, which was accommodated in the clevis grips of the MTS6000 machine. At the beginning of each test the specimen was subjected to a small load to align itself within the MTS6000. During the test, the specimen was loaded under stroke control mode. Readings of load, deformation, and strain were taken at regular intervals. Loading was paused several times to record static readings. The specimen was loaded to failure by either fracture in the channels or broken in the welds.

Table 3.1 Specimen Configuration

No.	Single/Double Channel	Welding Detail	Weld Size (mm)	Weld length L_w* (mm)	$\frac{L_w}{d}$
1	Double	Longitudinal	5	115**	1.51
2	Double	Longitudinal	10	60**	0.79
3	Double	Longitudinal	8	60	0.79
4	Double	Longitudinal	10	55	0.72
5	Double	Longitudinal + Transverse	5 + 4.3	55	0.72
6	Single	Longitudinal	8	70	0.92
7	Double	Longitudinal	10	50	0.66
8	Single	Longitudinal	5	100	1.32
9	Double	Longitudinal	5	100	1.32
10	Single	Longitudinal	10	55	0.72

* See Fig. 3.2 for the definition of L_w

** Longitudinal welds with end return

Table 3.2 Dimensions of Gusset Plate and Channel

Specimen	Width (mm)	Length (mm)	Net Length of Channel* (mm)
1	300	480	1200
2	300	370	1310
3	300	370	1200
4	300	370	1200
5	300	480	1200
6	300	480	1200
7	300	480	1200
8	300	370	1200
9	300	480	1200
10	300	370	1200

*See Fig 3.2 for the definition of channel net length

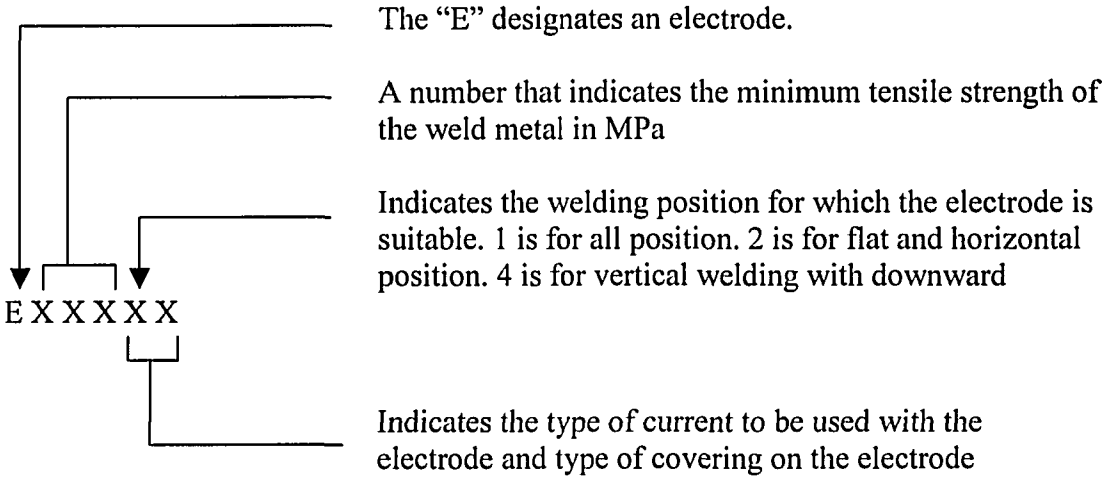

Fig. 3.1 Classification System for Carbon Steel Electrodes for SMAW

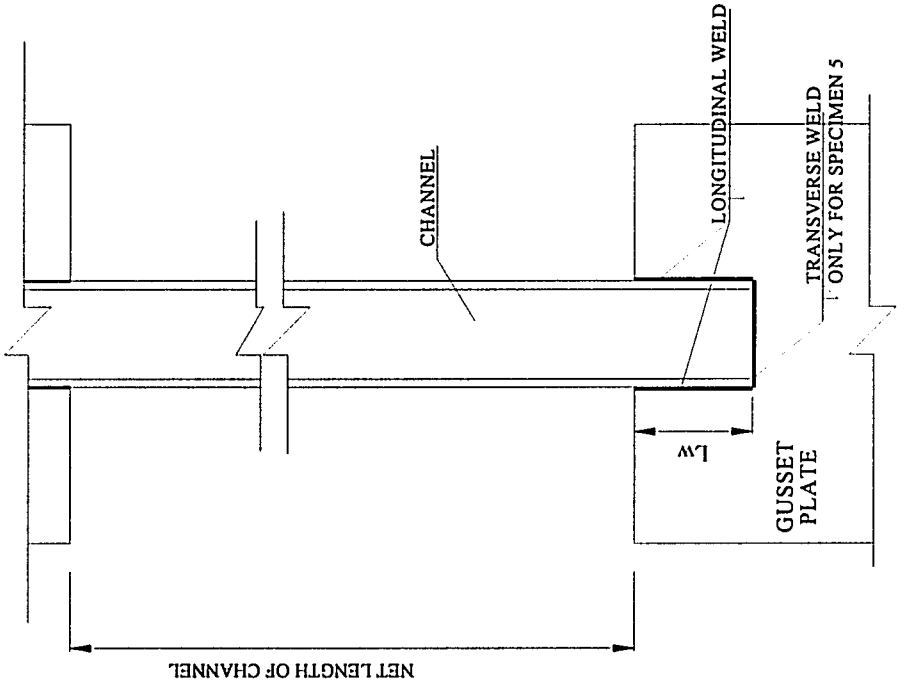

Fig. 3.2 Specimen Configuration

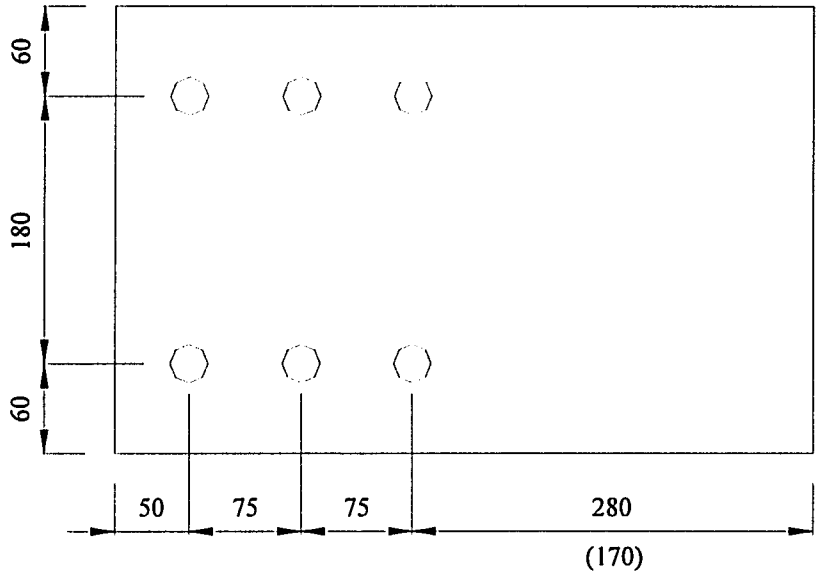

Fig. 3.3 Gusset Plate Dimension

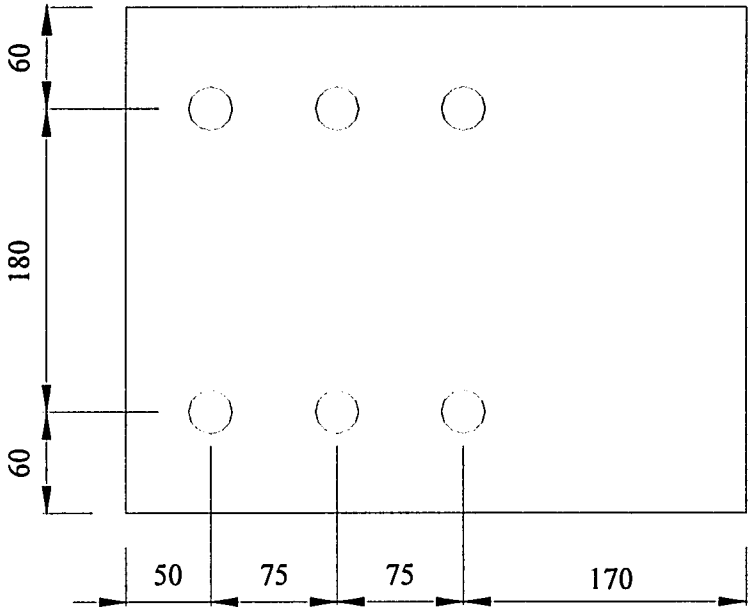

Fig. 3.4 Shim Plate Dimension

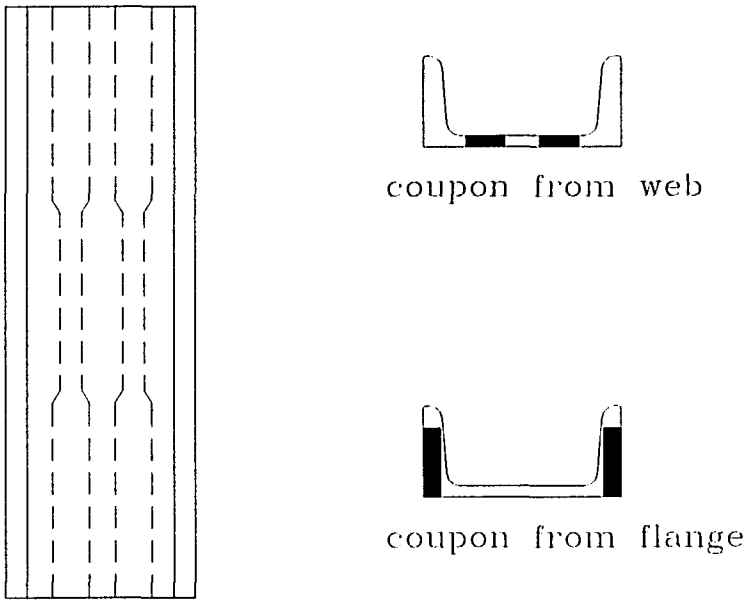

Fig. 3.5 Channel Coupon Locations

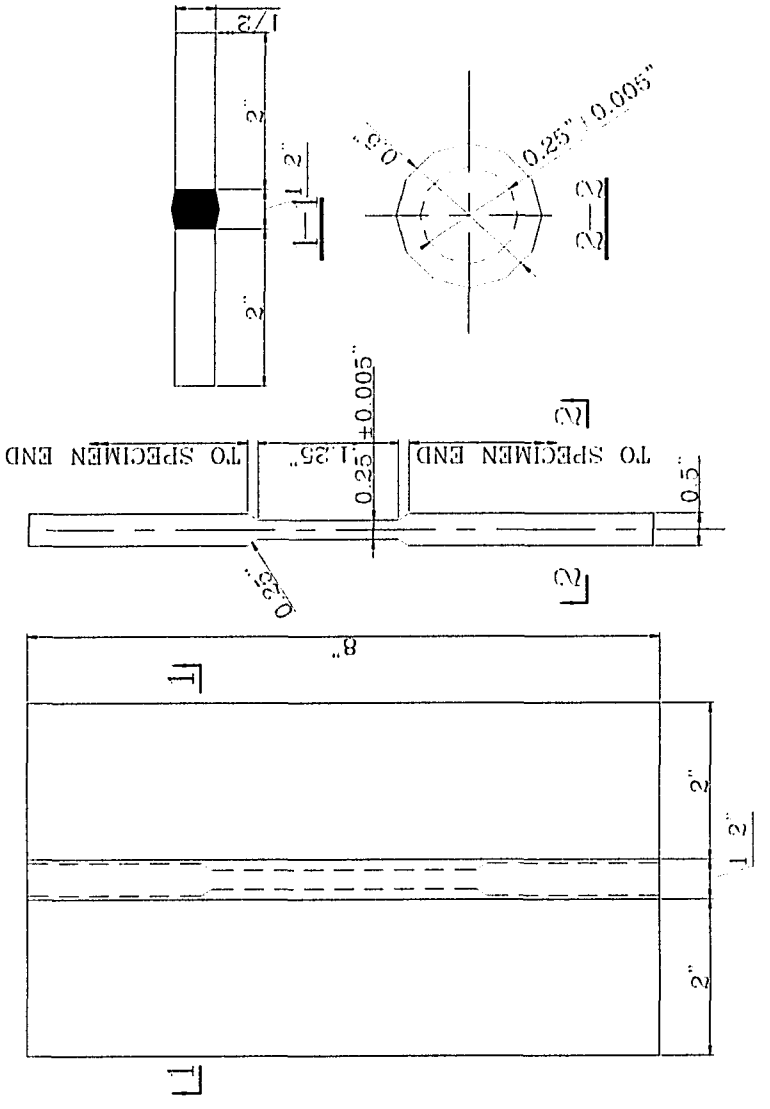

Fig. 3.6 Welding Material Cylindrical Coupon

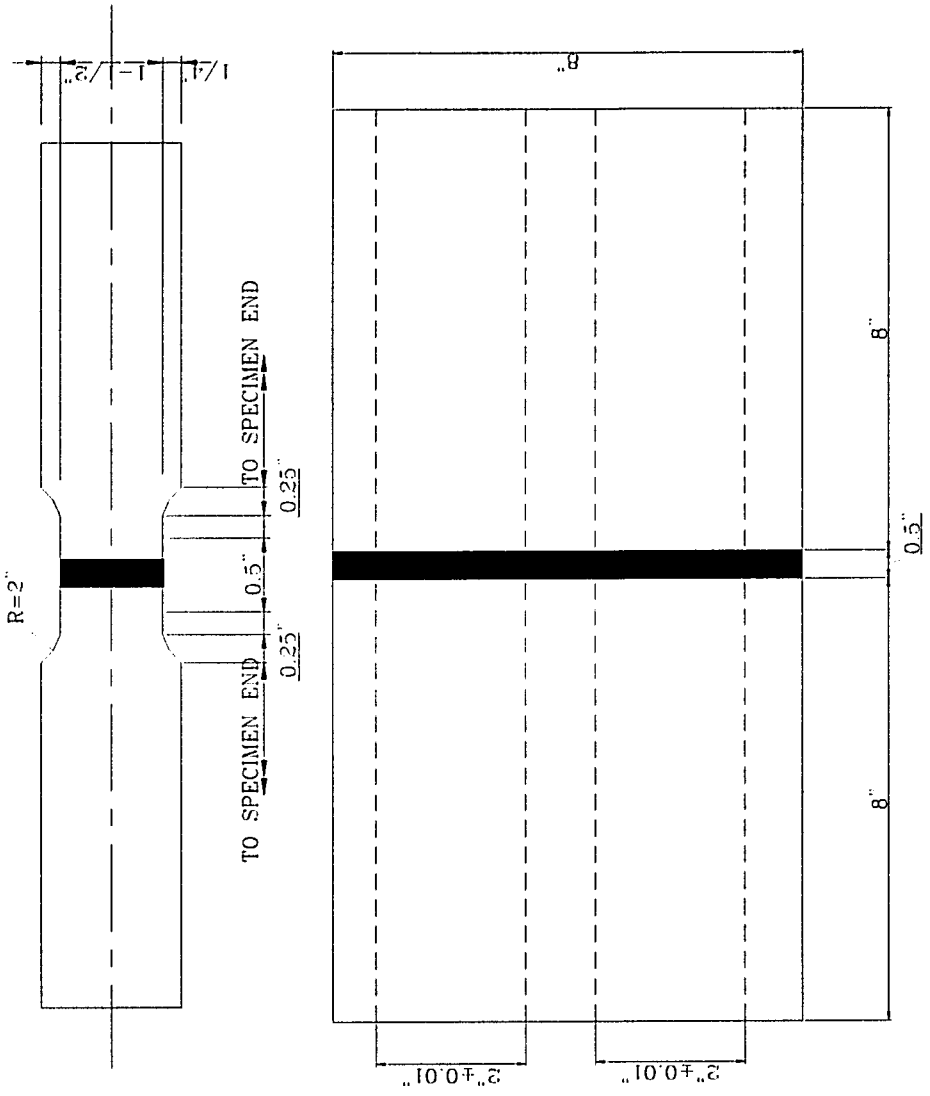

Fig. 3.7 Welding Material Flat Coupon

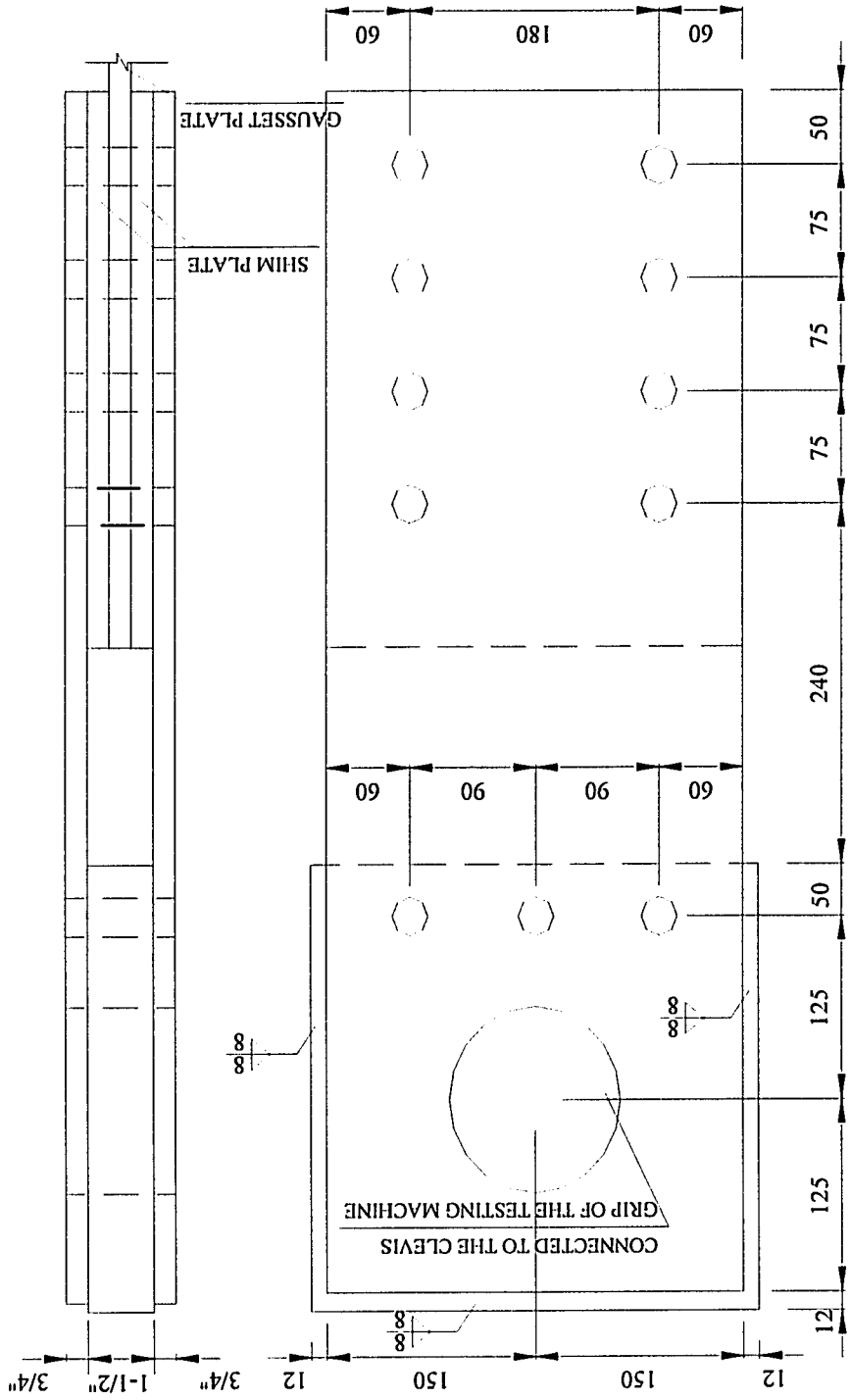

Fig. 3.8 Detail of Top Connection

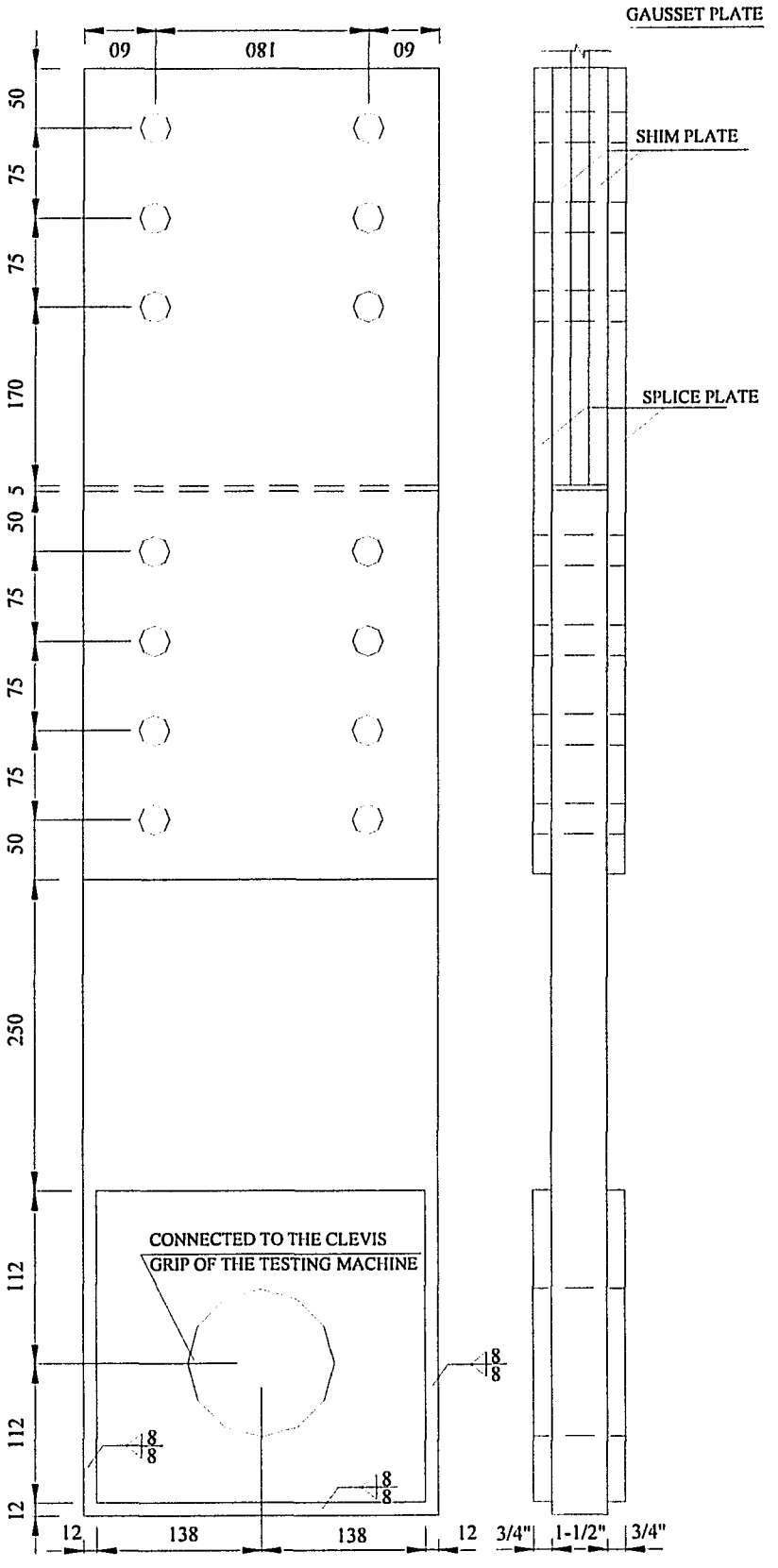

Fig. 3.9 Detail of Bottom Connection

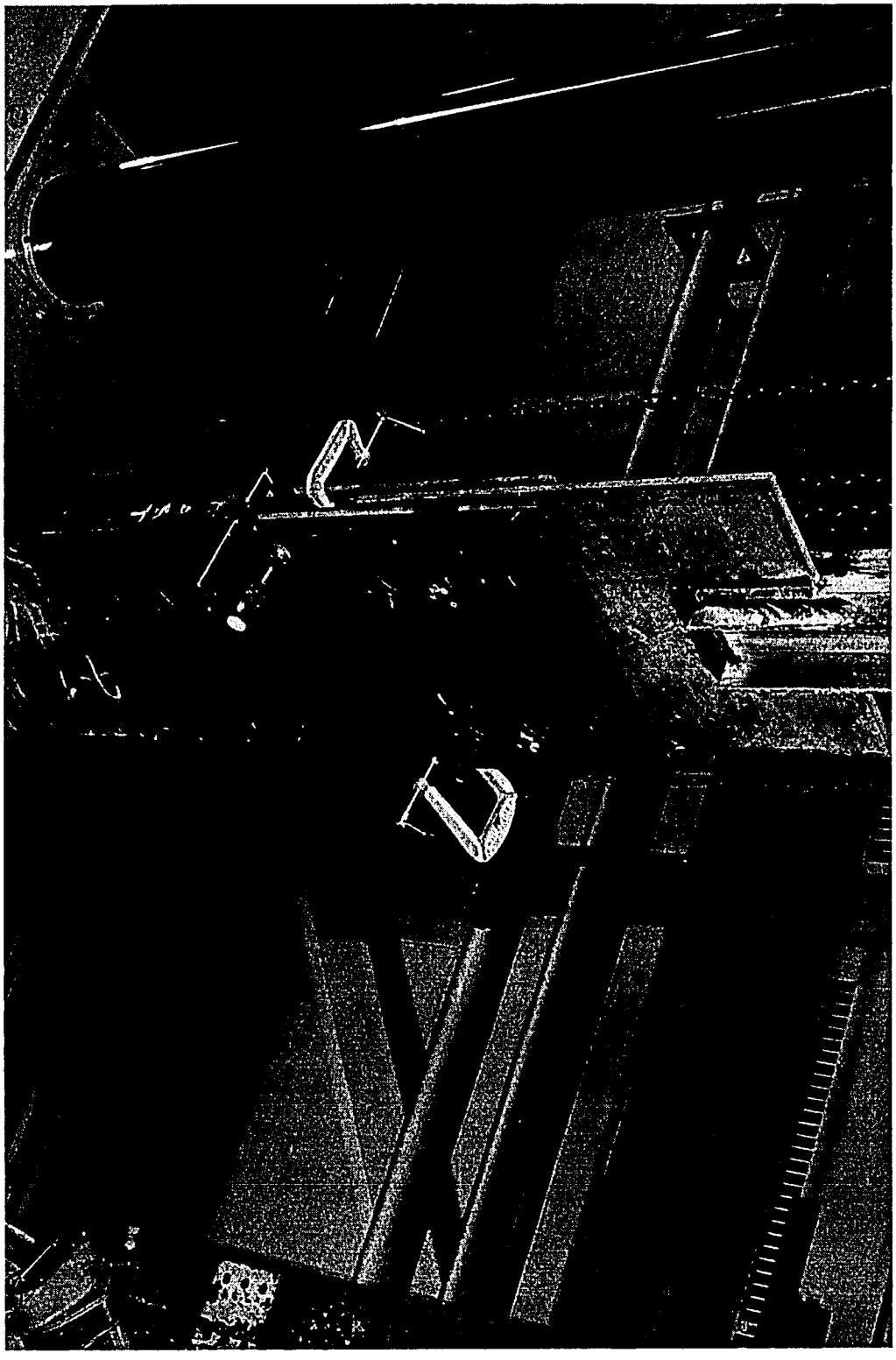

Fig. 3.10 Photograph of Connection and Clevis Device

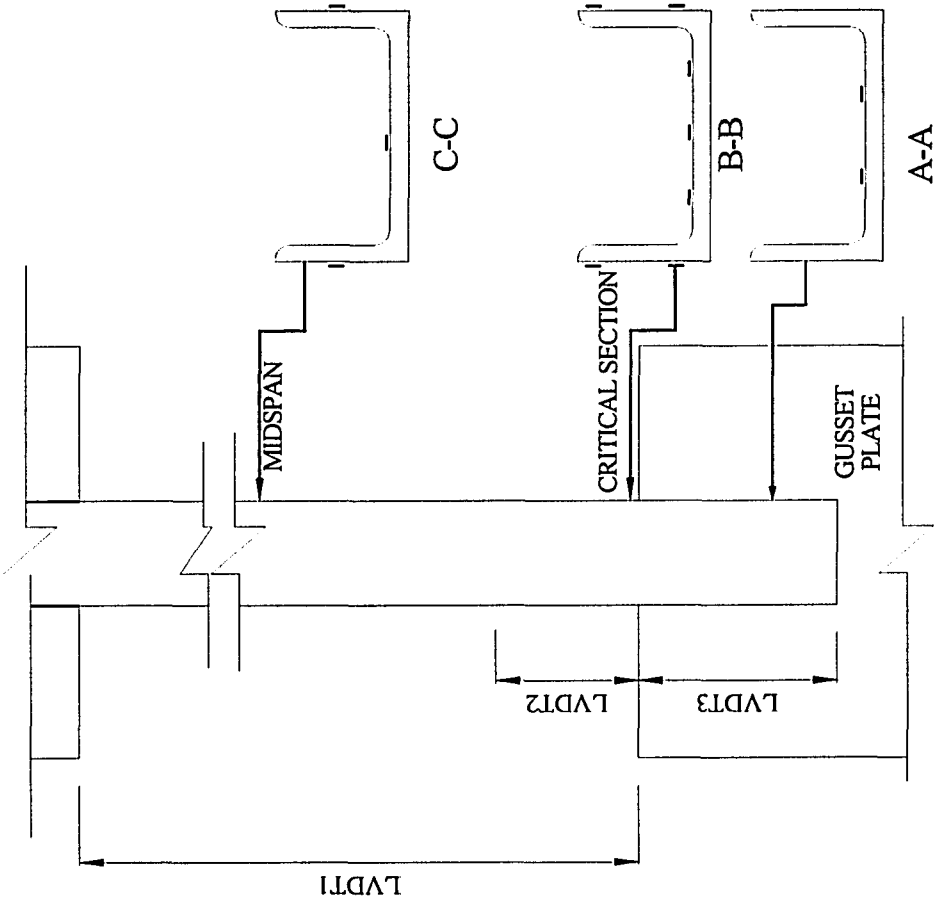

Fig. 3.11 Location of Strain Gauges and LVDTs

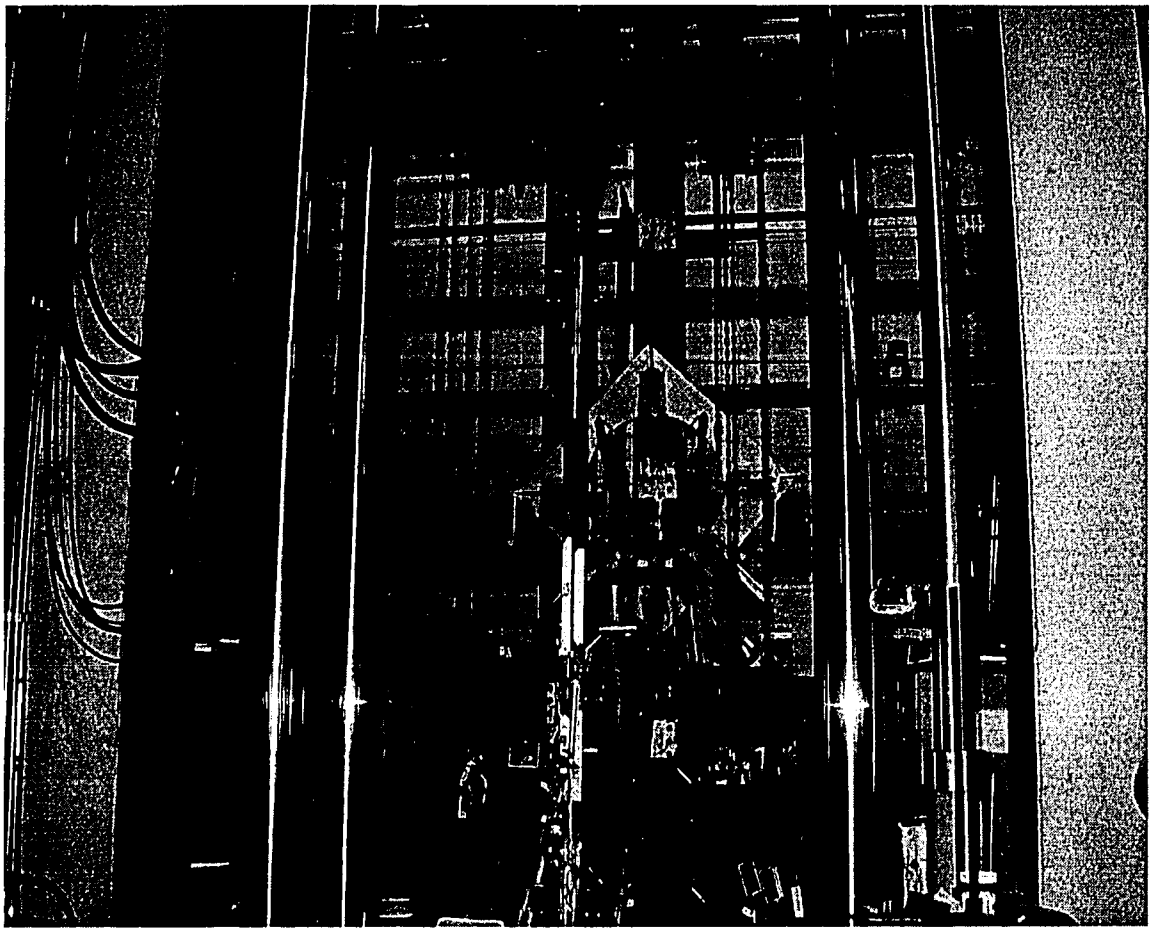

Fig. 3.12 Specimen Test Setup

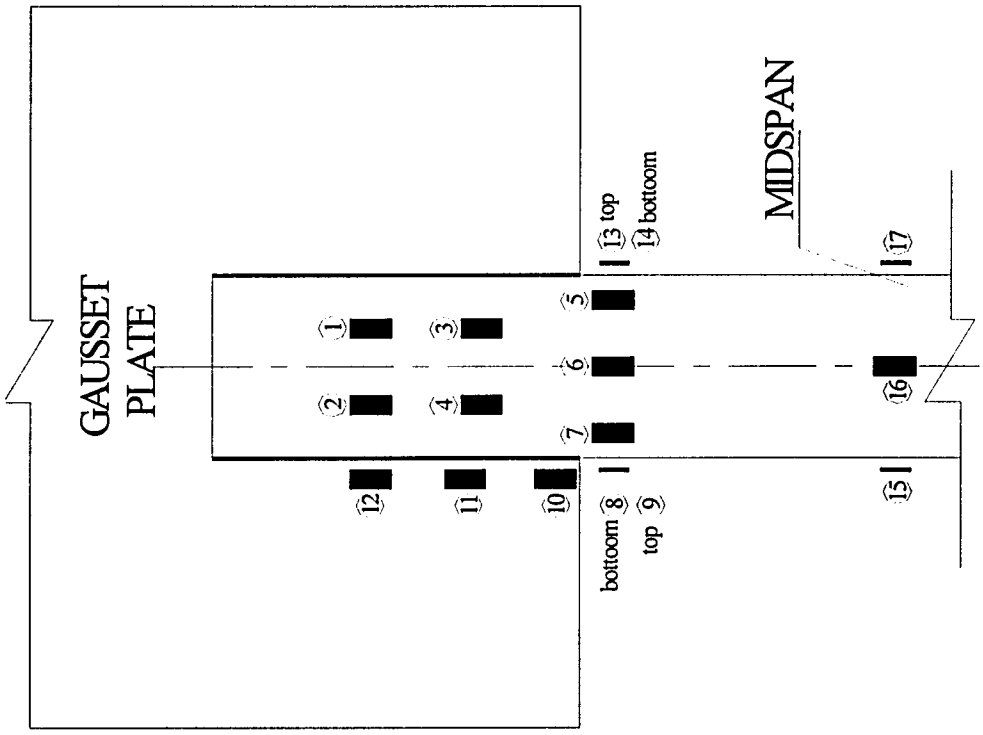

Fig. 3.13 Strain Gauges Layout for Specimen 1

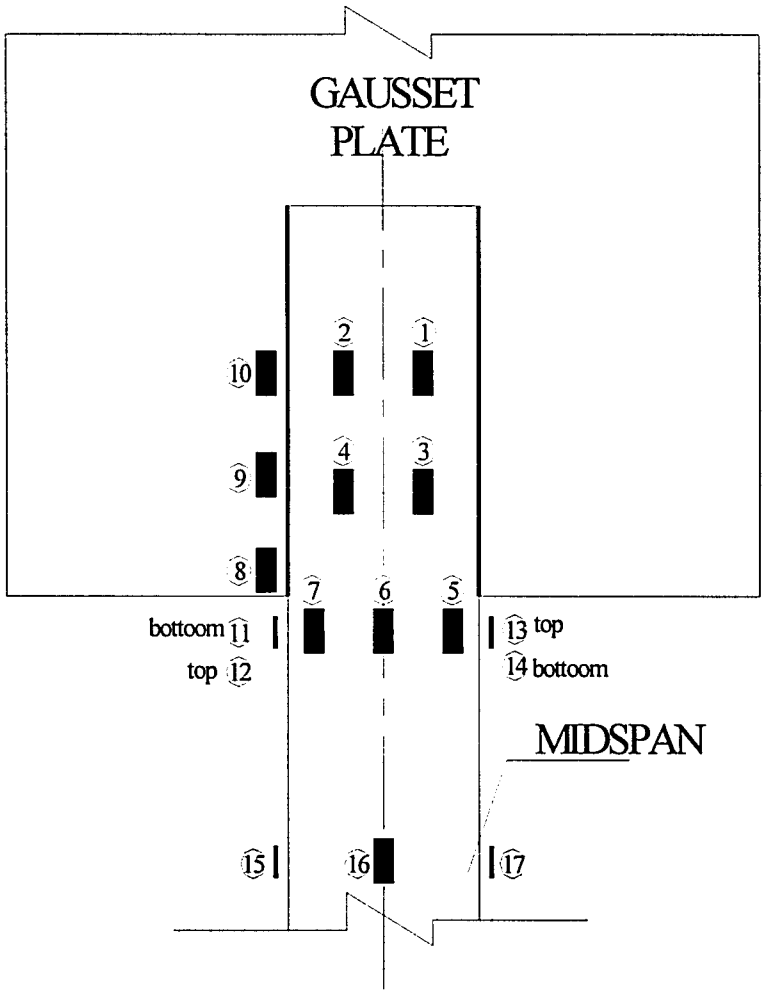

Fig. 3.14 Strain Gauges Layout for Specimens 2, 3, 4, 5, 6, 8, 9, 10

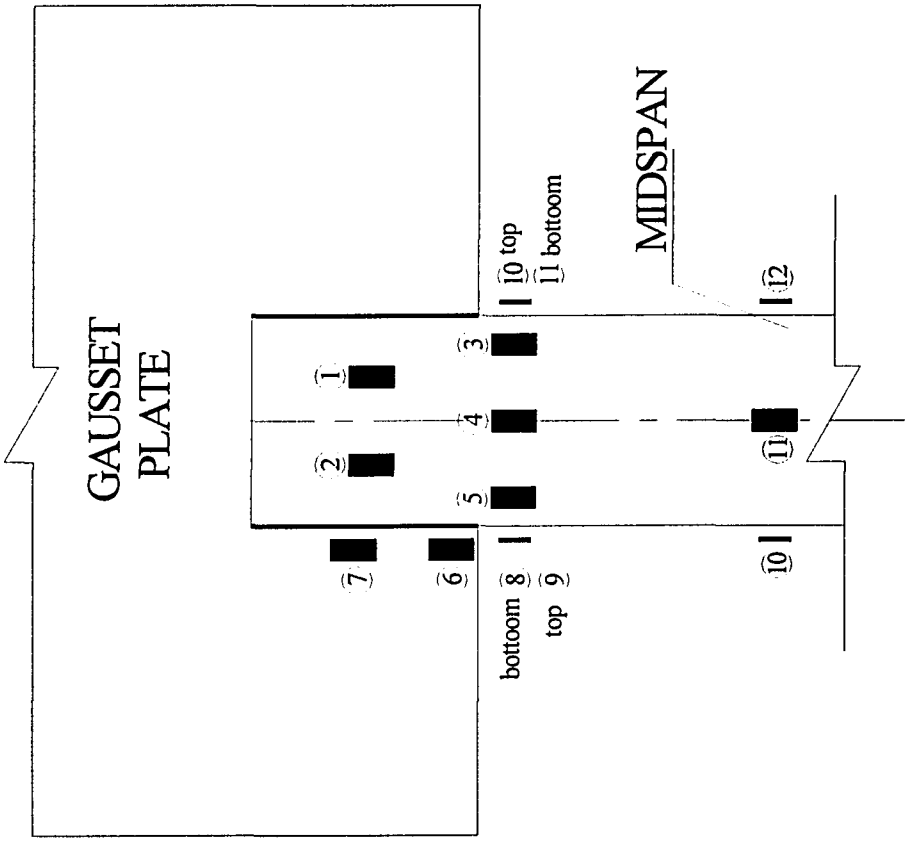

Fig. 3.15 Strain Gauges Layout for Specimen 7

4. TEST RESULTS

4.1 General

This chapter presents the results obtained from the experimental program. The results include the recorded strain distribution at the connection and the mid-length, along with the load-deformation relationships for the full-scale tests. In addition, the material properties are reported from the tension coupon tests. Finally a brief discussion of the test results is presented.

4.2 Tension Coupon Tests

Both channel tension coupon test and welding material tension test results are listed in Tables 4.1 to 4.3. Tension coupon test results of gusset plates are shown in Table 4.4. All results of the mechanical properties of channel material satisfy the required minimum static yield and ultimate tensile strength of CSA G40.21 300W structural steel of 300MPa and 450MPa, respectively. A typical strain-stress curve for these tests is shown in Fig. 4.1. In this figure, both the dynamic and the static curves are drawn together for comparison. It can be seen that after yielding occurs, the static curve is below the dynamic curve. The specified CSA minimum static yield and ultimate tensile strength requirements for weld metal coupon made from E48018 are 400MPa and 480MPa, the test results of the cylinder coupons are 2% and 1% lower than the specified values, respectively. However, the results of the other two flat weld metal coupons are higher than the minimum. Since these two coupons failed in weld metal region, the average results of three coupons are used here, and they are above the minimum requirements by

CSA standard, as listed in Table 4.3. Also the properties of base steel plates that flat weld material coupons made from were tested, results show that they is 300W structural steel and satisfy the CSA G40.21 requirements with much higher yield and tensile strengths. This explains why the flat weld coupons failed in weld material region. The stress versus strain curves of coupon tests are reported in Appendix A.

4.3 Full Scale Tests

The actual weld sizes used in each specimen are measured and listed in Table 4.5. Since two weld legs normally are not equal, they are listed separately as "a" and "b" in the table. The ultimate strength for tests, the predicted channel strength based on tension coupon tests, the predicted weld strength based on measured weld size, failure mode, and various ratios are listed in Table 4.6.

4.3.1 General Observation

There were ten specimens physically tested in this project. Seven of ten specimens were double-channel specimens; others were single-channel specimens. Whitewash was used to highlight the appearance of yielding in channels. Fig. 4.2 shows a typical specimen under test. None of the specimens initially failed at the critical section adjacent to the gusset plate. Specimen 1 fractured in the middle of both channels, as shown in Fig. 4.3. For specimen 2, first it fractured at one channel in the middle with large dynamic energy released, which led the other channel rupture at critical section. According to initial weld connection design, specimens 1 and 2 were expected to fail in the welds, but they failed in the middle of the channels instead. Inspection of the welds showed the actual weld size exceeded the specified ones. Thus the weld length of the

remaining specimens was modified and the end return was removed to allow the weld connection failure could happen in the specimens. Specimens 3 to 7 failed in weld rupture as expected (Fig. 4.4). Specimens 8 and 9 fractured in the heat affected zone, which was right at the vicinity of the attachment of LVDT2, as shown in Fig. 4.5. This kind of failure is also classified as gross section failure. Specimen 10 failed in the welds as well.

For those failed in the middle of channel, as load was applied to certain level, yield lines occurred, featured by flaking of whitewashed in the critical section and extended to mid-length of channel as load increased, as presented in Fig. 4.2. By the time the load reached its ultimate value, the hot-rolled channels started necking and finally fractured at the gross section, as pictorially shown in Fig. 4.3. For specimens 8 and 9 fracture initiated at the vicinity of the attachment of LVDT2, the crack started to appear from the flange welded with small LVDT's attachment and to extend to the other flange through web gradually, as shown in Fig. 4.5. For the specimens failed at welds, the welds fractured suddenly without any obvious necking in channel, as detailed in Fig. 4.4.

Single channel specimens behaved quite differently from double channel specimens during test. The single channel specimen tests were characterized by the bending deformation of the gusset plates and the tendency of the channel try to align its centriod with the applied load. Significant out-of-plane bending was observed, as shown in Fig. 4.6. This is because the gusset plates were relatively flexible in the out-of-plane direction and offered little restraint to the rotation compared to the out-of-plane stiffness of the channel. In double-channel specimen tests, because the centroid of each channel was eccentric to the surface of gusset plate, moments existed in each channel, but the

moments in two channels would balance each other. In other words, the gusset plate passed the centroid of the two channels, there was no bending moment existing in the gusset plates. The space between the backs of two channels kept constant from one end to the other until the specimen failed.

4.3.2 Load-Deformation Relationship

Since specimens were connected to the MTS6000 test machine using clevis grips, there was no slip between specimens and MTS machine. Therefore the stroke recorded by the MTS is the total elongation of the specimen. LVDT1 recorded the elongation of net distance of channel between two gusset plates (1200 mm or 1310 mm). Deformation recorded by LVDT1 is used to plot load-deformation curves. Load-deformation curves for all specimens are plotted in Fig. 4.7 to Fig. 4.16.

Except for specimen 3, the load-deformation curves of all other specimens are characterized by a gradual yielding with typical yield plateau, which was followed by strength hardening. Specimens failed in the gross section of channels have a high level of elongation, while those fractured in the welds have a relatively low level of elongation.

Load-deformation curves of specimens 1, 2 and 9 are a typical gross section fracture ones. Specimen 3 failed prematurely in welds with a very low level of deformation, it failed before it reached yielding. The failure modes of specimens 4 and 7 are very similar, both yielded gross section first and then followed by weld fracture. This kind of curves can be distinguished from those curves failed in gross section by having a relatively smaller deformation (less than 100 mm). With the combination of longitudinal and transverse welding, the deformation of specimen 5 is quite large, though it finally failed in weld fracture.

As can be seen in the load-deformation curve of specimen 6, it is obvious that at the beginning of loading phase, the curve is not linear and the value of deformation is negative, which means the distance between two gusset plates was shortened. This phenomenon can be attributed to the initial accommodation of the out-of-plane bending of gusset plates and channel. However, with the increasing of load this nonlinear behavior diminished. The similar behavior happened to specimens 8 and 10 as well.

4.3.3 Strain Distribution

There were seven strain gauges, except specimen 7 in which five gauges were used, mounted at the critical section of each specimen, see Figs. 3.13 to 3.15. Some typical load vs. strain curves and the comparison of strains at different load levels are shown in Figs. 4.17 to 4.22. The curves for all other specimens are summarized in Appendix B. It can be seen that the strains near the corner of the channel cross section tend to be higher than those at the center of web and the tips of flange, as shown in Figs. 4.19 to 4.22. At the same load level the readings of strain gauges in the web at the critical section are much higher than those in the web between the critical section and the end of channel, as illustrated in Figs. 4.17 and 4.18. This is because the channel at the weld connection region is a transition part where it picks up the applied load. The channel gradually transferred the load to the gusset plate through welds, and at the critical section the channel was subjected to the total load. At the low load level, the strain distribution at critical section was relatively uniform; however, as the load increased, the distribution became highly non-uniform, especially for the strains around the corner. Strains on the gusset plate near welding are quite small compared to those on the channel at the same load level. For single channel specimens the readings from the strain gauges on the gusset

plate are negative at the initial loading stage because of the bending of gusset plates since the strain gauge were on the compression side of the bending, and they became positive as the load increased. As would be expected, the strains were quite uniform at the mid-length of the channels.

4.4 Brief Discussion of Test Results

It is observed that for the specimens failed in weld fracture, fracture planes usually did not pass through the 45^0 theoretical throat area. They are closed either to the gusset plate surface or the channel flange. Specimen 3 failed unexpectedly with only about 4 mm deformation and ultimate load of 494 kN. Measurement of weld size after test showed that average size of one leg was 5.58 mm and the other was 8.90 mm, while the design nominal weld size was 8 mm for Specimen 3. This unsymmetrical welding configuration notably decreased the weld capacity, since one longitudinal weld premature failure triggered the fracture of another parallel longitudinal weld, eventually led to the failure of the whole specimen. The weld length of this specimen might be a concern. But there were three specimens with even shorter weld length, no premature weld failure happened to these specimens. Therefore, the effect of weld length can be excluded from this kind of premature failure.

For specimen fabrication, only shield metal arc welding (SMAW) was used in this project. A commonly used welding process in high production welding is fluxed cored arc welding, which has a different toughness of weld material. However, Ng et al. (2002) and Deng et al. (2003) found that the welding process itself (SMAW or FCAW) had little effect on fillet weld strength. Fillet welds made with weld metals with a specified

toughness did not necessarily have higher strength than weld metals without. Fillet weld capacity was not linearly proportional to weld size. Another important conclusion they made was that low temperature did not have a negative effect on fillet strength, though the ductility of fillet welds at low temperature tends to reduce significantly. Therefore, we can extend validity of our test results to flux cored arc welding and low temperature environment.

If a free body diagram is drawn with respect to the gusset plate and channel, we can find bending moment existing in the channels, even in double-channel specimens, since there is an eccentricity between the centroid of the channel and the surface of gusset plate. The presence of bending moment may affect the capacity of specimen. For the specimens failed in the gross section, say specimens 1, 2, 8 and 9, as shown in Table 4.6, the ratio of ultimate capacity of specimen to calculated tensile strength of channel is at least 0.95, which means the bending moment does not affect specimen capacity much. It is also found that none of specimens with L_w/d (or L/W) greater 1.0 failed in welds even the weld size was as small as 5 mm, which is the minimum weld size in engineering practice.

Comparison of the load capacity of single and double channel specimens with same weld size and weld length can also be made. There are two pairs of specimens having the same weld size and weld length, namely, specimens 4 and 10, specimens 8 and 9. From Fig. 4.19 and Fig. 4.20 it can be seen that at same loading level the strains at the critical section are higher in single channel specimens than those in double channel specimens. Specimen 8 is a single channel specimen with an ultimate capacity 370 kN, while specimen 9 is a double channel specimen with an ultimate capacity 742 kN. Both

of them were made from the same parent material and failed in gross section. The capacity of specimen 8 is almost exactly half of the specimen 9. Although specimens 4 and 10 have different channel material properties, both of them failed in welds instead of gross section, so in this case channel material properties do not affect the capacities of these two specimens. With the same welder and classification of electrode, the capacity of specimen 10 is 341 kN, while for specimen 4 is 607 kN. It can be seen that in this case the capacity of single channel specimen is well above half of the double channel specimen. Hence we can conclude that although there was significant bending deformation during testing for single channel specimens, their capacities were not affected. This conclusion will be further verified by the finite element analysis in Chapter 5.

Specimens 1 and 9 have the same weld size and both of them are double channel specimens, but specimen 1 has longer weld length than specimen 9 does, so as expected the strains in specimen 9 at critical section are higher than those in specimen 1. This is pictorially shown in Fig. 4.21. Double channel specimens 2 and 3 have the same weld length but different welding size, it can be seen in Fig. 4.22 there is not much strain difference at critical section between the two specimens, and so we can conclude that weld size does not notably affect the strain distribution as weld length does.

Specimens 1 and 5 have the same weld size of 5mm in longitudinal welds, however, transverse weld of 4.3 mm was also used in specimen 5. Based on the load versus strain curves close to the end of the specimens, as shown in Figs. 4.23 and 4.24, it can be seen that at ultimate load level (765 kN for specimen 1 and 707 kN for specimen 5), average strain in specimen 1 is about 1200με, while for specimen 5 it is nearly

24000με. Although the ultimate load for specimen 1 is larger than that of specimen 5, its final strain is only about 1/20 of that of specimen 5. This indicates that transverse weld significantly changed the load-transferring pattern of the channel cross-section. The presence of transverse weld mobilized the channel cross-section and caused it pick up the load more effectively. From Fig. 24, it is also found that the ductility of the cross-section was increased remarkably since with the increase of load about 50 kN, the strain was increased about 23000 με. If specimen 5 was fabricated without transverse weld, it would fail in weld failure at very low load since its longitudinal weld length was only 55 mm, less than half of that specimen 1. However, with the contribution of transverse weld, specimen 5 reached a capacity that is very close to that of specimen 1. This proves that transverse weld can improve member capacity. But Easterling et al. (1993) mentioned in their paper that additional transverse welds would not increase member capacity. After checking the configuration of their specimens, it was found that the channel specimens they tested had longer longitudinal weld than that of specimen 5. Since their specimens had long enough longitudinal welds that can fail the specimens at gross section, of course the contribution of transverse weld in their tests could be ignored.

It also can be seen that in Table 4.6, specimens failed in weld have the ratio P_{ult} / P_{weld} ranging from 1.2 to 1.3, this indicates that the weld has 20 to 30% higher strength than the design formula predict. For the specimen failed in gross section, the ratio P_{ult} / P_{weld} ranging from 0.95 to 0.98, which are very close to 1.0. This excludes the idea that channel tensile strength may decrease due to the shear lag effect and load eccentricity.

Table 4.1 Material Properties of Channel Web

Coupon No.	modulus of elasticity (MPa)	dynamic yield strength (MPa)	static yield strength (MPa)	dynamic ultimate strength (MPa)	static ultimate strength (MPa)
C1-a	191000	389	368	534	502
C1-b	198000	378	358	515	483
C2-a	191300	383	368	530	501
C2-b	190600	369	348	502	492
C3-a	192800	382	364	532	502
C3-b	194900	365	344	521	491
C4-a	193100	373	364	525	501
C4-b	191900	378	360	528	501
C5-a	193900	372	352	524	494
C5-b	195700	385	363	533	506
Average	193320	377	359	524	497

Table 4.2 Material Properties of Channel Flange

Coupon No.	modulus of elasticity (MPa)	dynamic yield strength (MPa)	static yield strength (MPa)	dynamic ultimate strength (MPa)	static ultimate strength (MPa)
C3-a	211200	340	321	531	498
C3-b	207100	348	330	536	506
C5-a	201300	347	329	533	500
C5-b	210500	349	330	538	506
Average	207525	346	328	535	503

Table 4.3 Material Properties of Weld Metal

Coupon No.	modulus of elasticity (MPa)	dynamic yield strength (MPa)	static yield strength (MPa)	dynamic ultimate strength (MPa)	static ultimate strength (MPa)
C1	211200	409	392	495	474
C2-a	207100	426	416	554	526
C2-b	201300	438	423	564	542
Average	206500	424	410	538	514

C1 is cylinder coupon, C2-a and C2-b are flat coupon

Table 4.4 Material Properties of Gusset Plate

Coupon No.	modulus of elasticity (MPa)	dynamic yield strength (MPa)	static yield strength (MPa)	dynamic ultimate strength (MPa)	static ultimate strength (MPa)
BC1-a	208700	398	383	556	522
BC1-b	207100	413	397	570	539
Average	207900	406	390	563	531

Table 4.5 Measured Weld Sizes

Specimen	1		2		3		4		5		6		7		8		9		10	
	L	R	L	R	L	R	L	R	L	R	L	R	L	R	L	R	L	R	L	R
a (mm)	5.5	5.9	9.8	10.5	8.9	7.4	9.0	11.5	5.1	5.3	7.0	8.6	8.2	9.1	6.8	7.5	6.8	7.3	11.9	11.8
b (mm)	5.6	5.6	10.6	11.1	5.6	6.9	9.8	8.4	7.1	6.7	6.9	6.3	9.2	9.2	7.1	7.2	6.4	7.1	10.2	12.1

Note: a and b are the sizes of two fillet weld. Transverse weld size for specimen 5 is 4.5 mm.

Table 4.6 Summary of Test Results

Specimen No.	Channel Material	Failure mode	$\frac{L_w}{d}$	P_{ult} (kN)	P_{ten} [1] (kN)	P_{weld} [2] (kN)	$\frac{P_{ult}}{P_{ten}}$	$\frac{P_{ult}}{P_{weld}}$
1	Coupon1	gross section	1.51	750	763	618	0.98	1.21
2	Coupon2	gross section	0.79	730	765	595	0.95	1.23
3	Coupon3	weld	0.79	494	765	390	0.65	1.27
4	Coupon1	weld	0.72	607	763	502	0.80	1.21
5	Coupon4	weld	0.72	707	766	563	0.92	1.26
6	Coupon4	weld	0.92	281	383	235	0.73	1.20
7	Coupon2	weld	0.66	538	765	422	0.70	1.27
8	Coupon5	gross section	1.32	369	383	338	0.96	1.09
9	Coupon5	gross section	1.32	742	767	645	0.97	1.15
10	Coupon5	weld	0.72	341	383	293	0.89	1.31

1. $P_{ten} = F_u^{fl} * A_{fl} + F_u^{web} * A_{web}$, A_{web} is the area of flat part of web, and A_{fl} is the remaining part of channel cross section, F_u^{web} is the average value of each coupon in Table 4.1, and F_u^{fl} is the average value of four flange coupons in Table 4.2.

2. $P_{weld} = 0.67 * A_w * X_u * (1 + 0.5 * \sin^{1.5}\theta)$, A_w is based on measured weld size at throat area and equals to throat area times weld length times 4 for double channel specimens or 2 for single channel specimens, X_u is the average value of weld coupons from Table 4.3, θ is the angle of axis of weld with the line of action of force, for longitudinal weld it is 0^0 and for transverse weld it is 90^0.

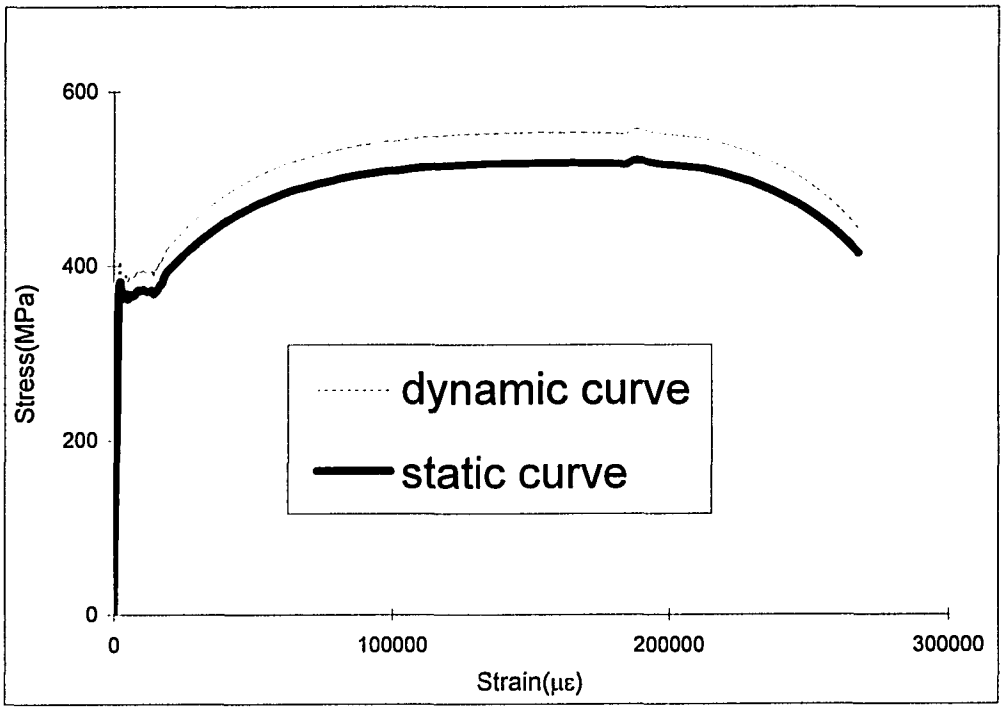

Fig. 4.1 Dynamic vs. Static Strain-Stress Curve of a Typical Coupon Test

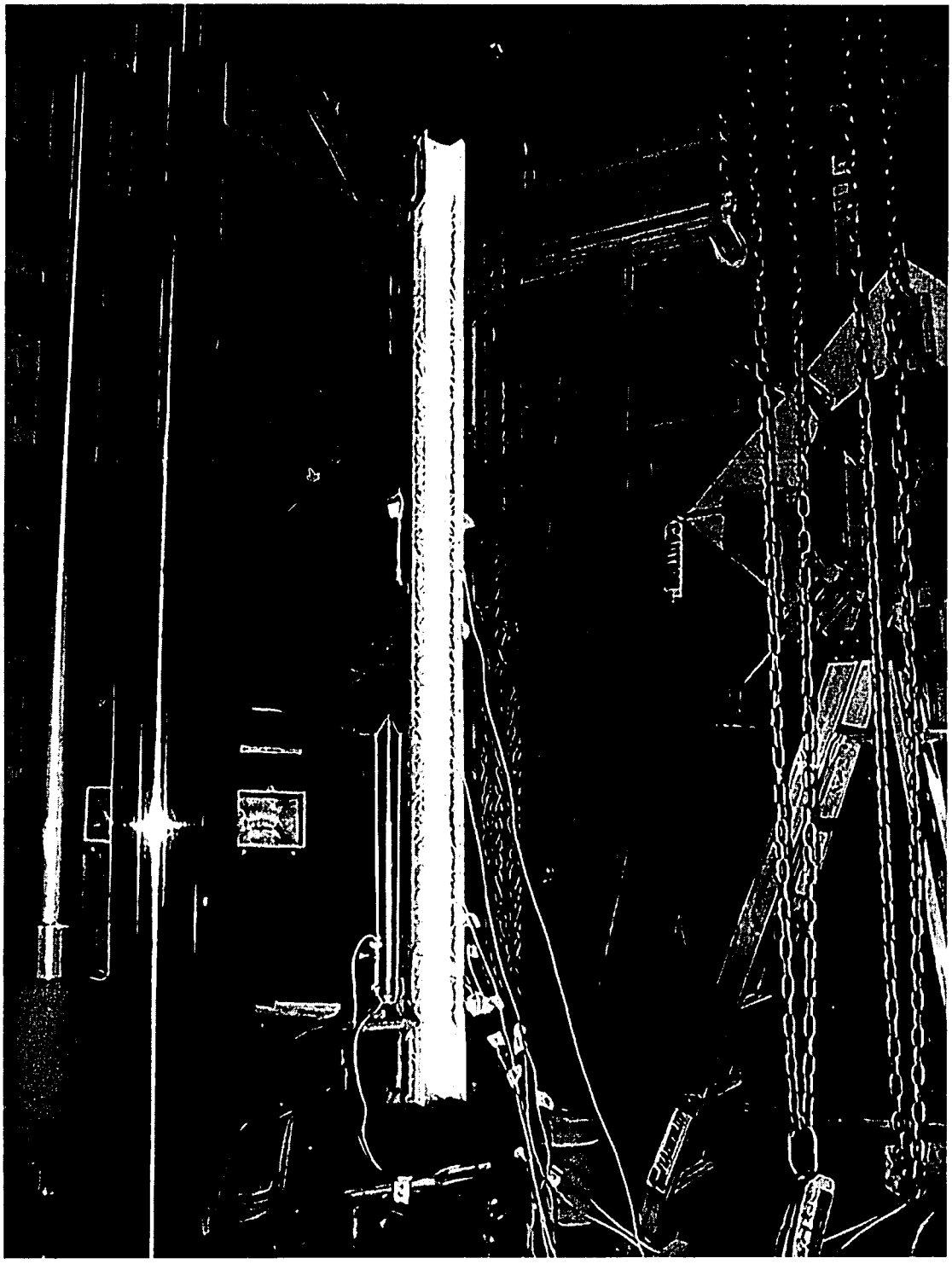

Fig. 4.2 Specimen under Testing

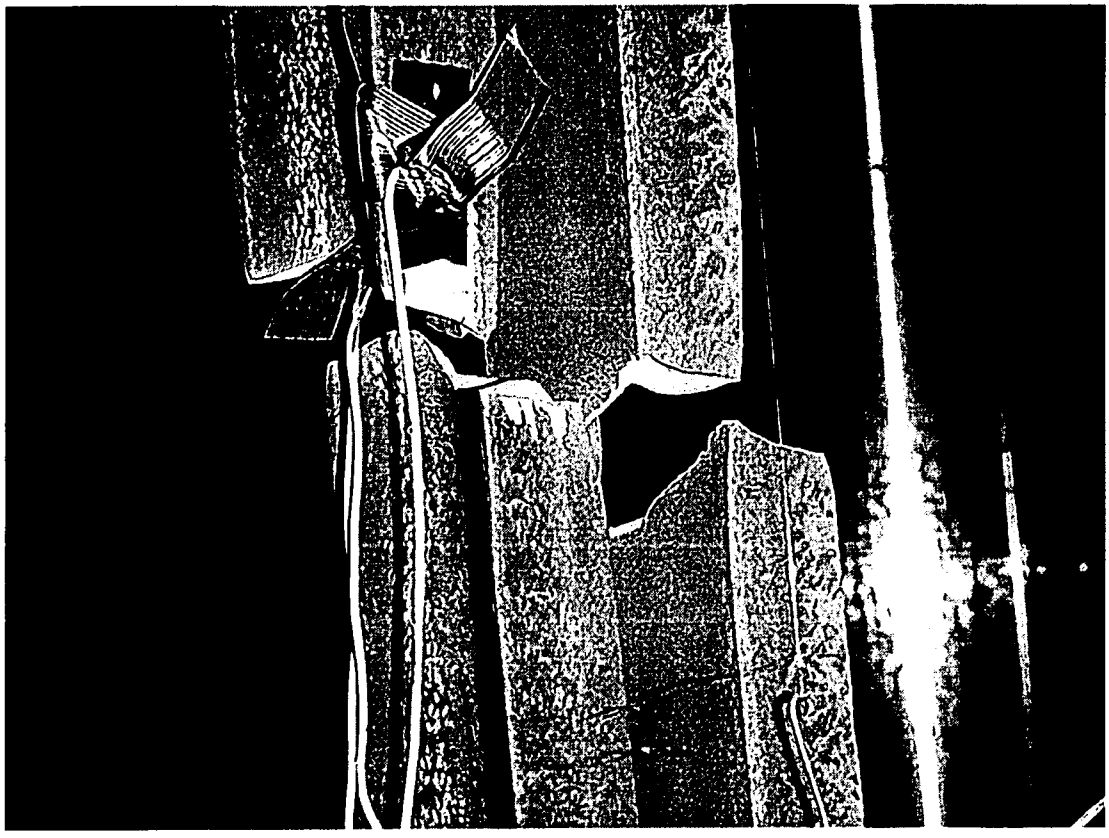

Fig. 4.3 Failure of Specimen 1 at the Mid-Length

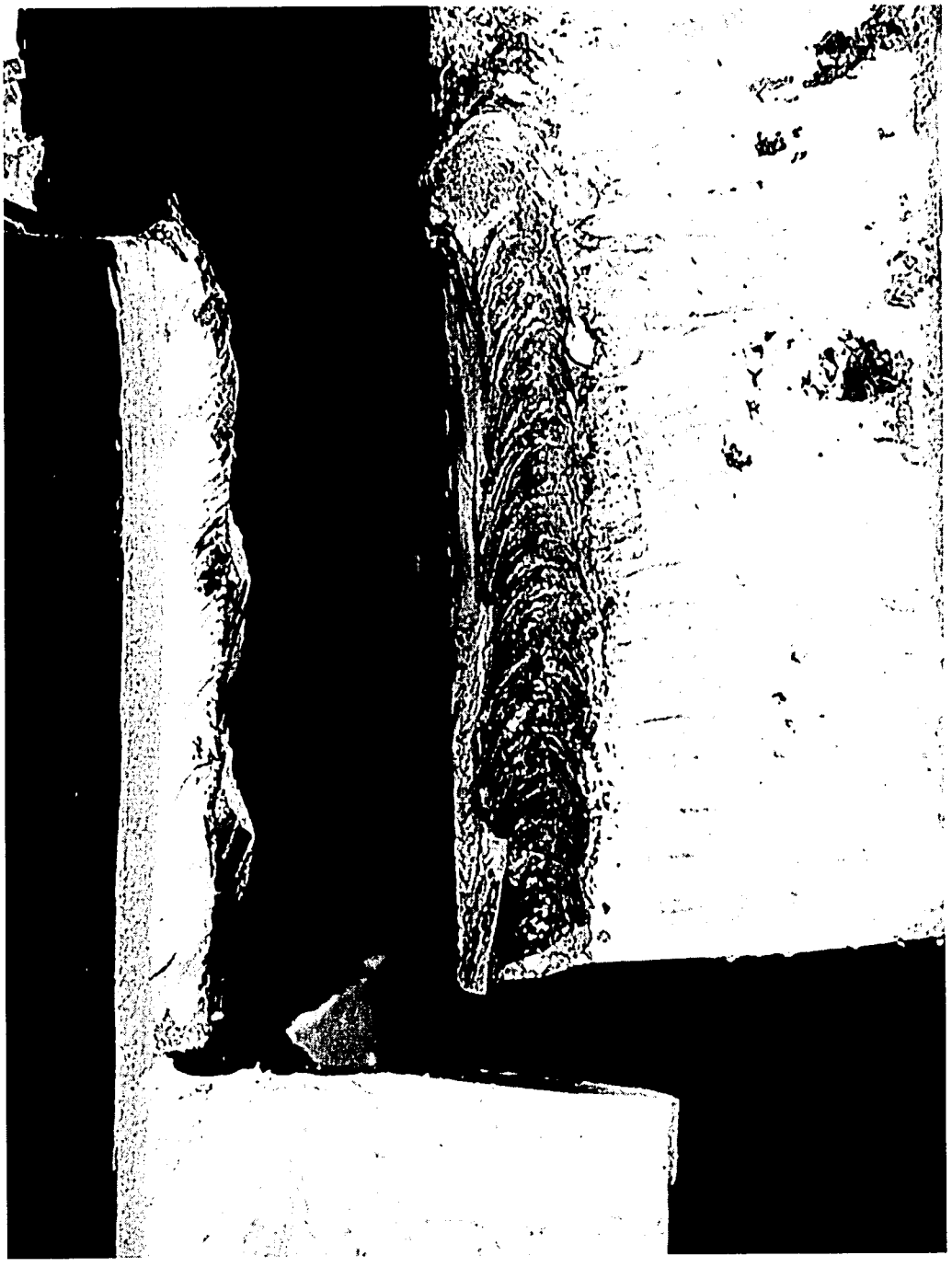

Fig. 4.4 Failure of Specimen 4 in the Welds

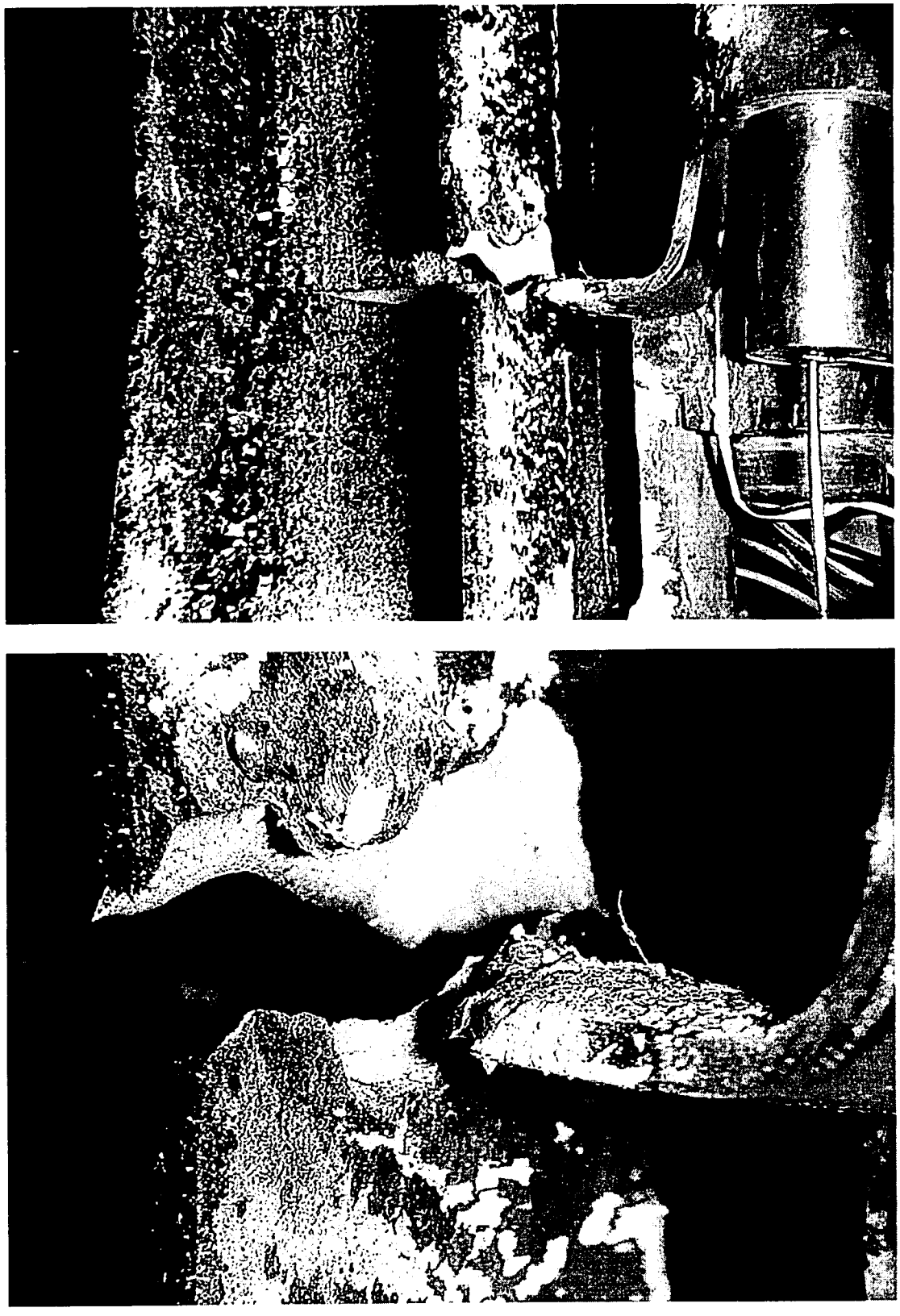

Fig. 4.5 Specimen 8 Fractured at Heat Affected Zone

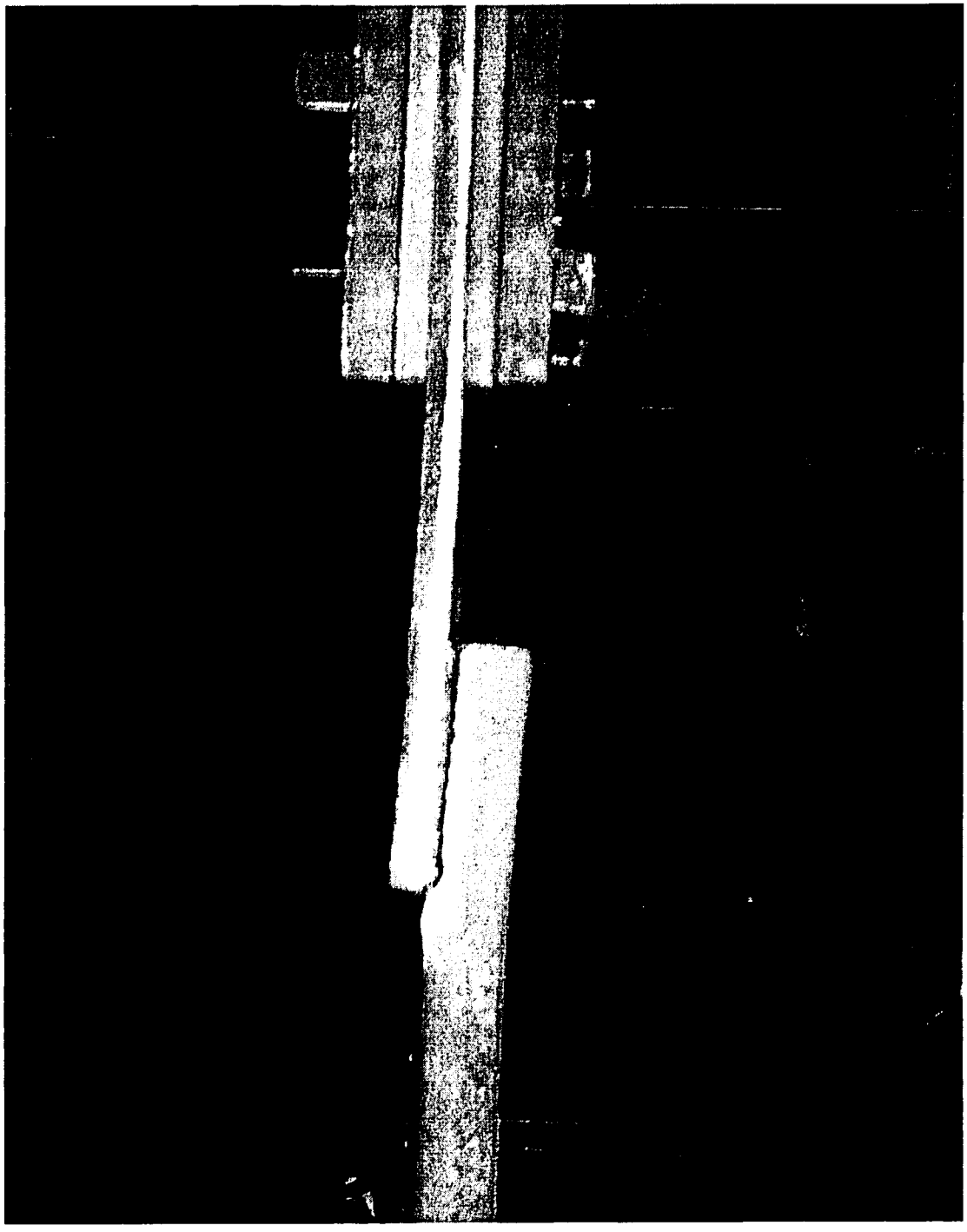

Fig. 4.6 Out-of-Plane Bending of Single Channel Specimen 6

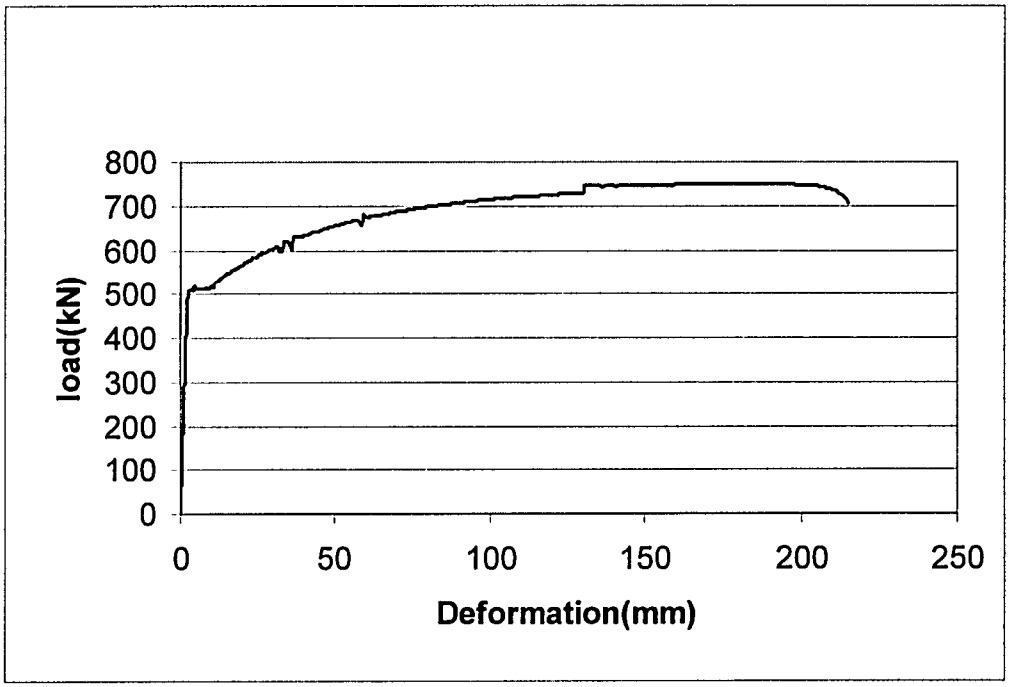

Fig. 4.7 Load-Deformation Curve of Specimen 1

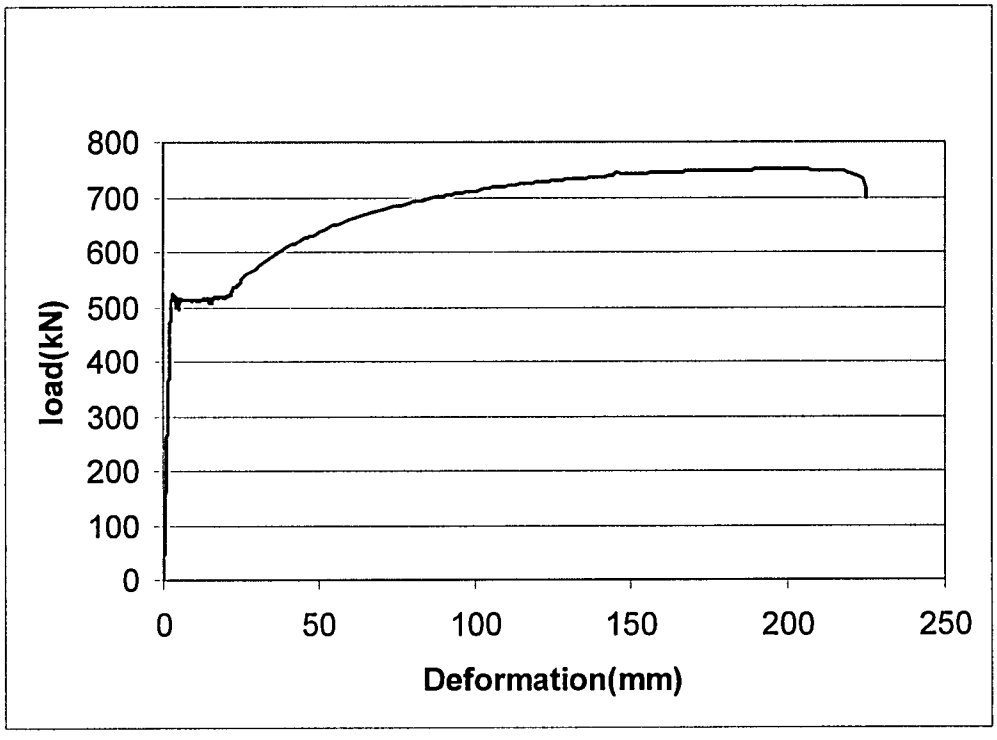

Fig. 4.8 Load-Deformation Curve of Specimen 2

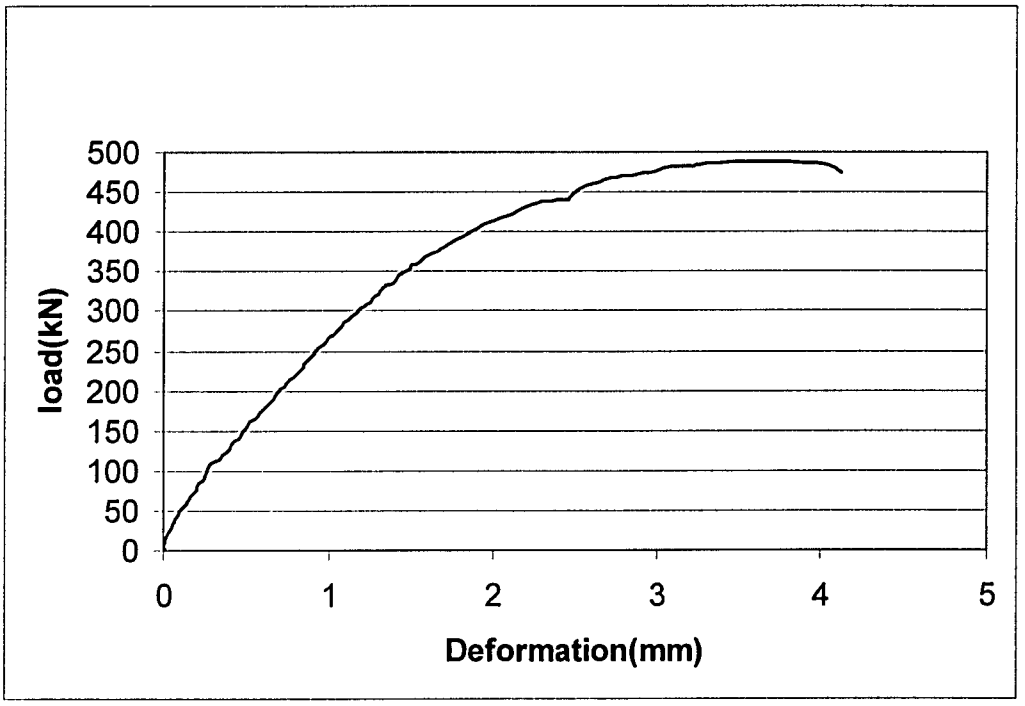

Fig. 4.9 Load-Deformation Curve of Specimen 3

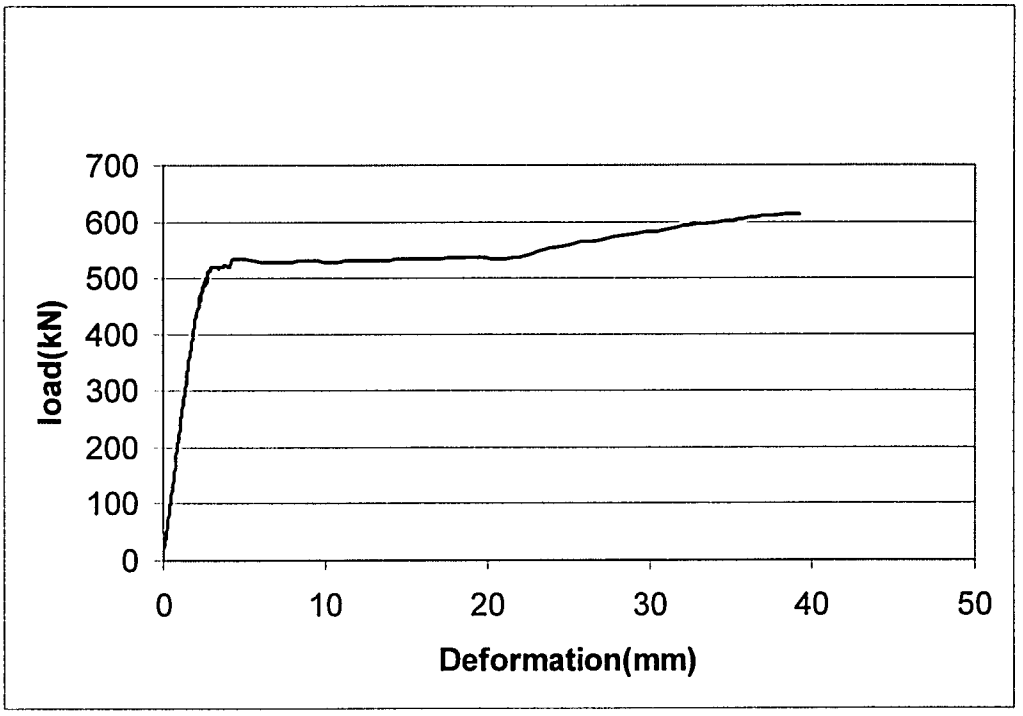

Fig. 4.10 Load-Deformation Curve of Specimen 4

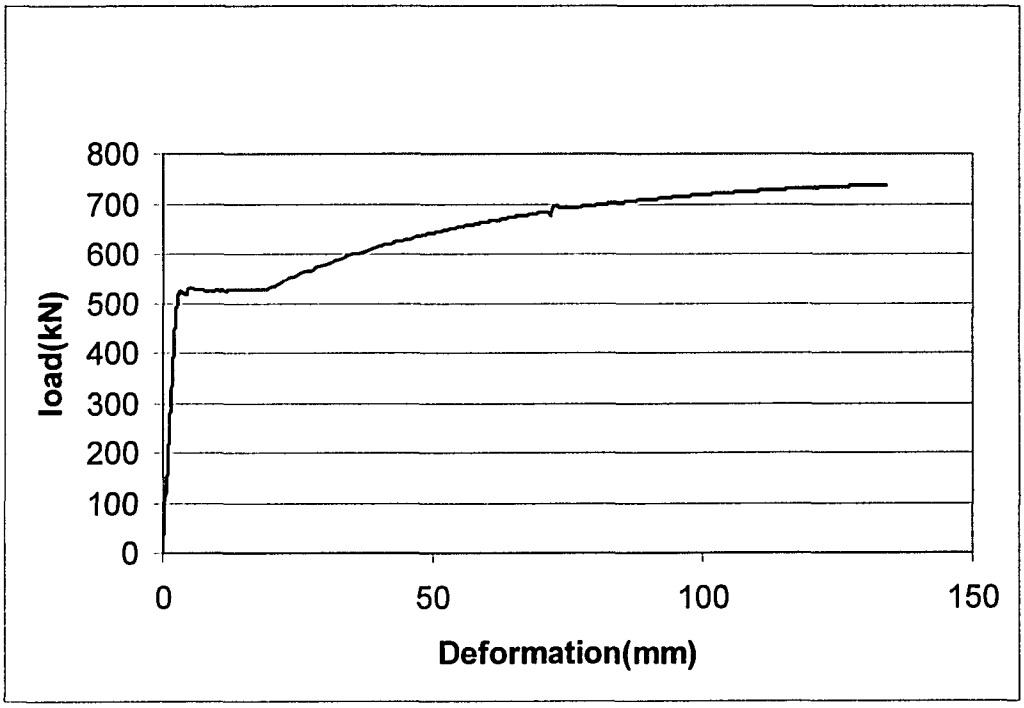

Fig. 4.11 Load-Deformation Curve of Specimen 5

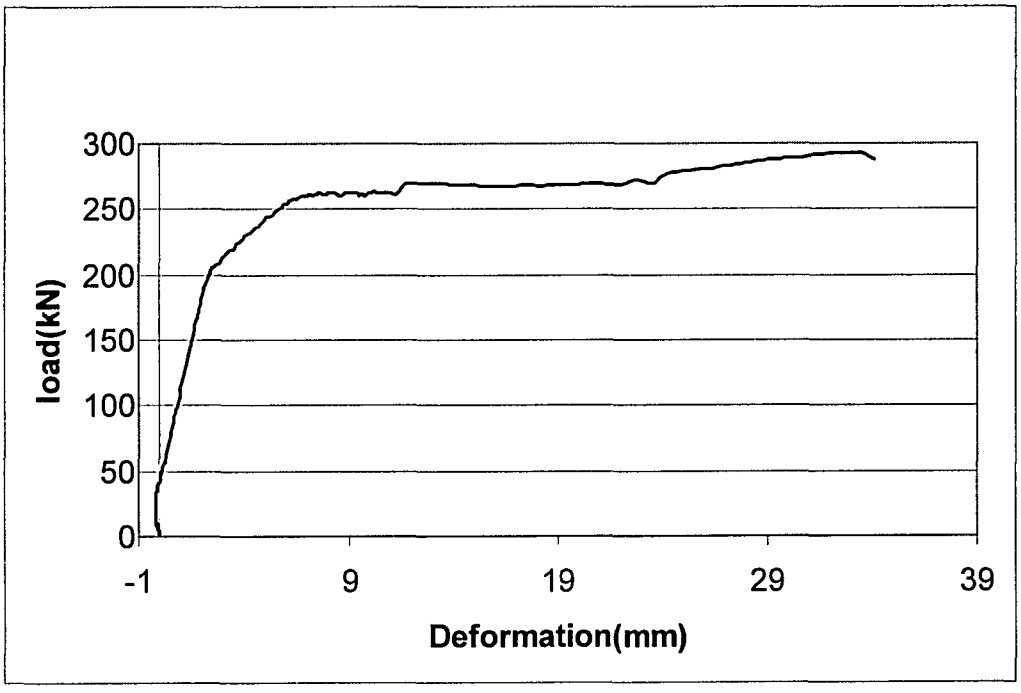

Fig. 4.12 Load-Deformation Curve of Specimen 6

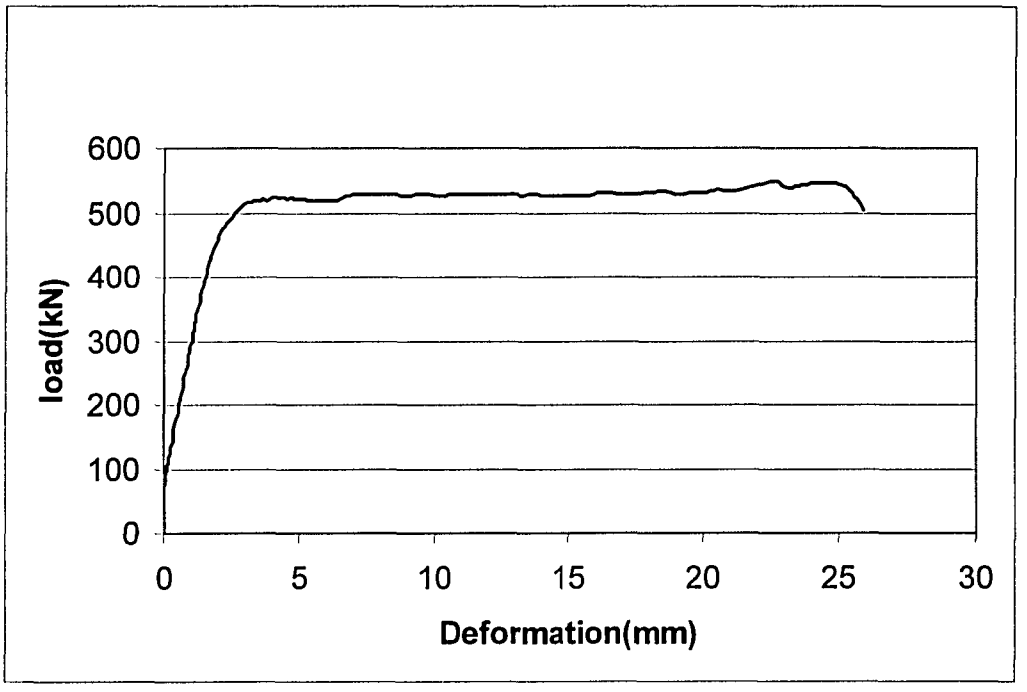

Fig. 4.13 Load-Deformation Curve of Specimen 7

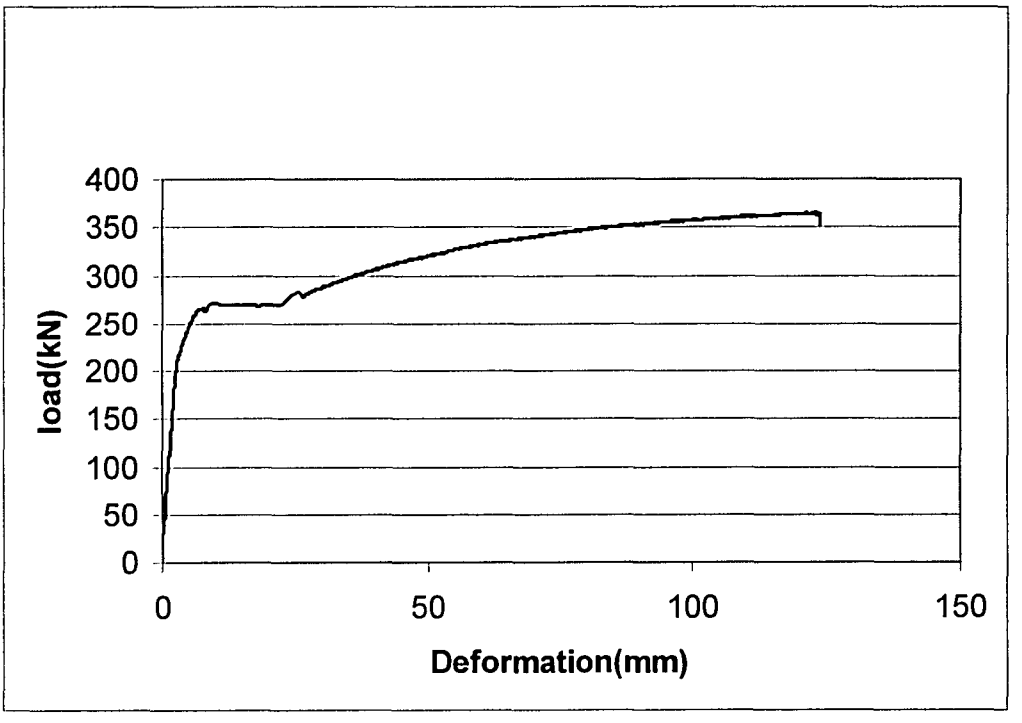

Fig. 4.14 Load-Deformation Curve of Specimen 8

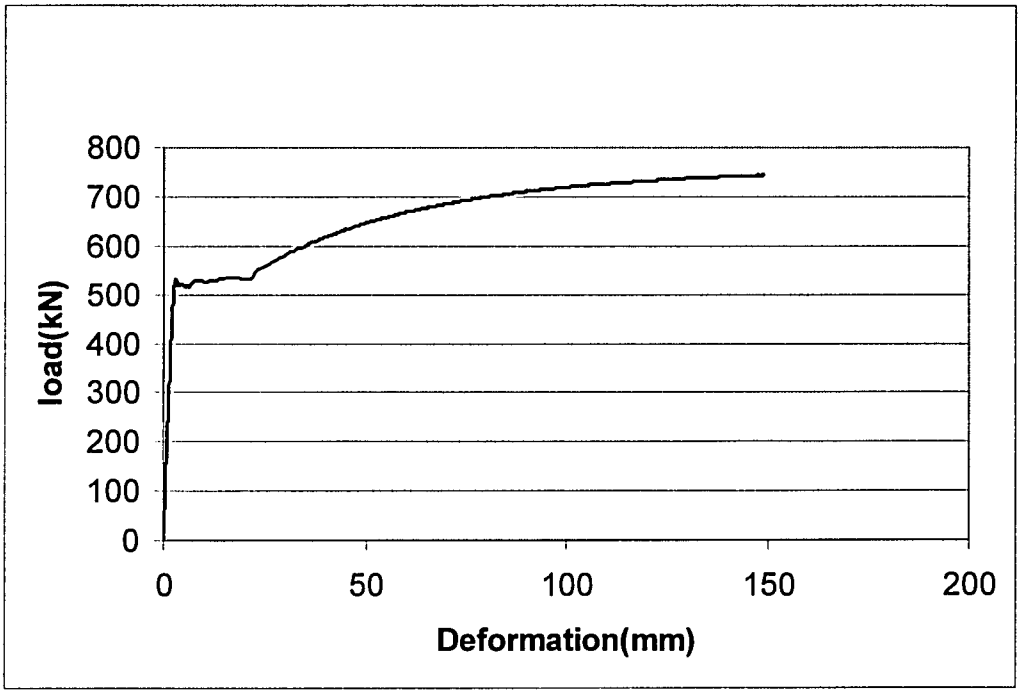

Fig. 4.15 Load-Deformation Curve of Specimen 9

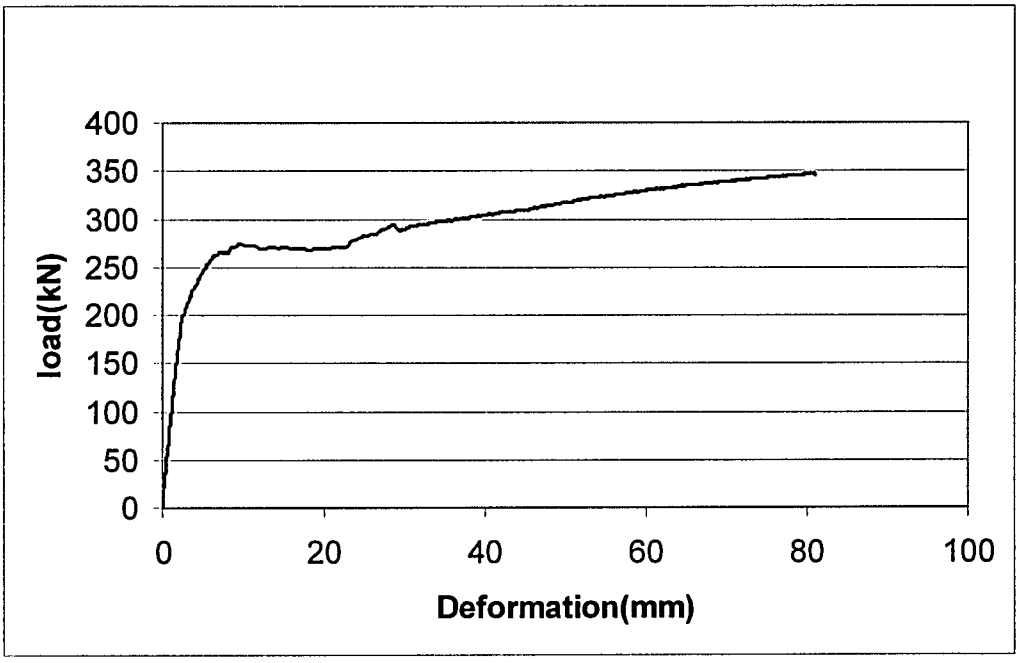

Fig. 4.16 Load-Deformation Curve of Specimen 10

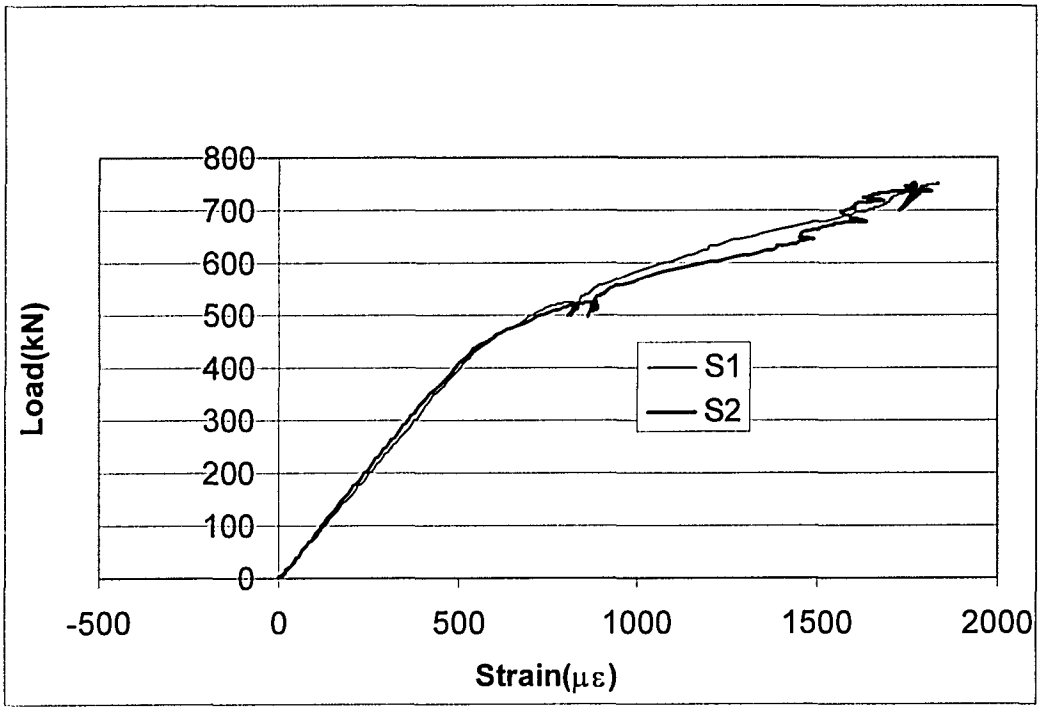

Fig. 4.17 Typical Load-Strain Curves (S1 and S2) of Specimen 2

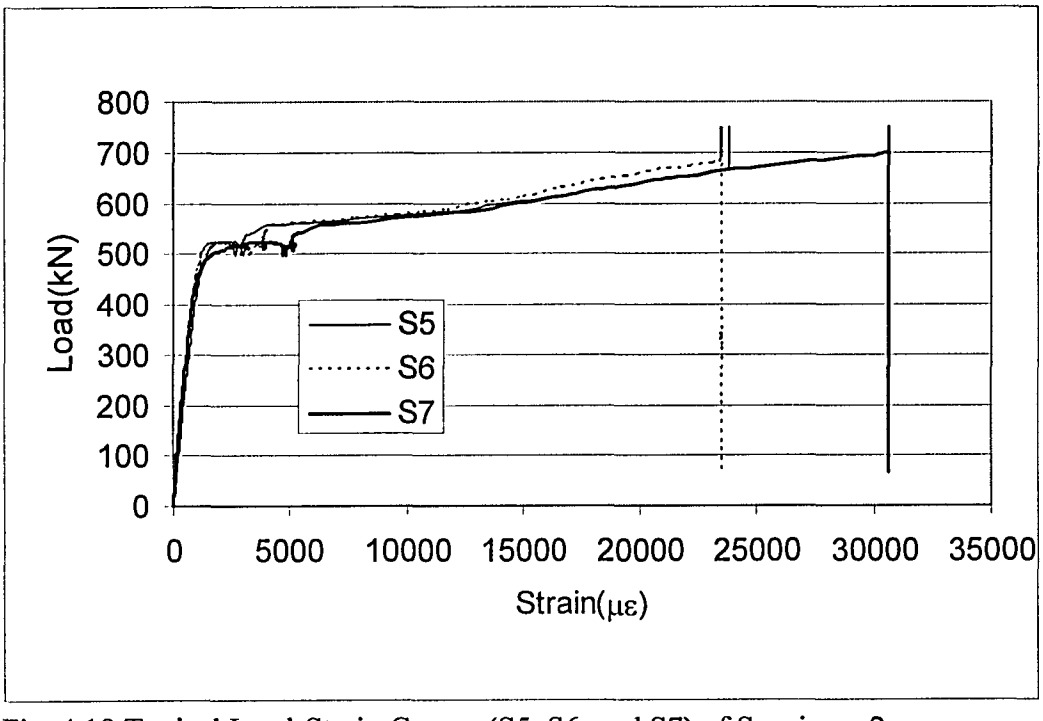

Fig. 4.18 Typical Load-Strain Curves (S5, S6, and S7) of Specimen 2

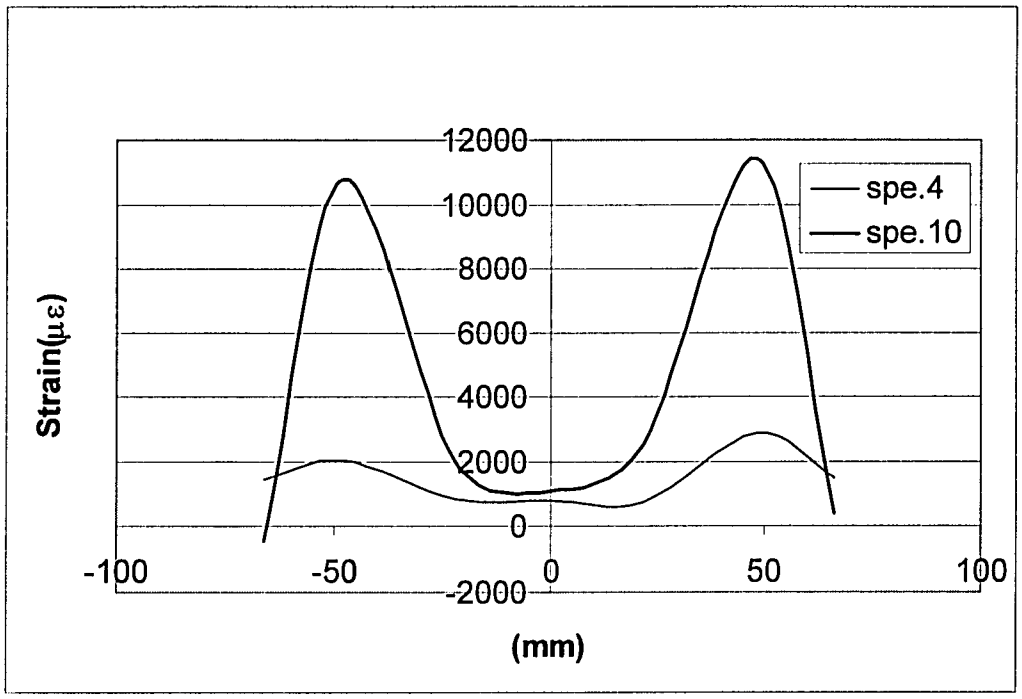

Fig. 4.19 Comparison of Strain of Specimens 4 and 10 at the Critical Section

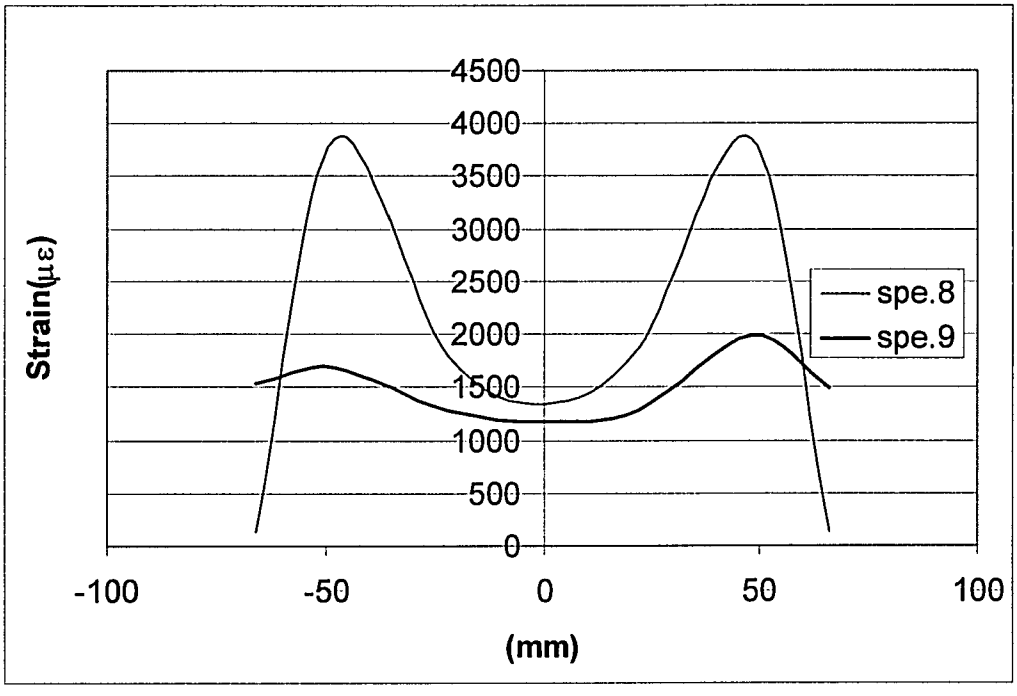

Fig. 4.20 Comparison of Strain of Specimens 8 and 9 at the Critical Section

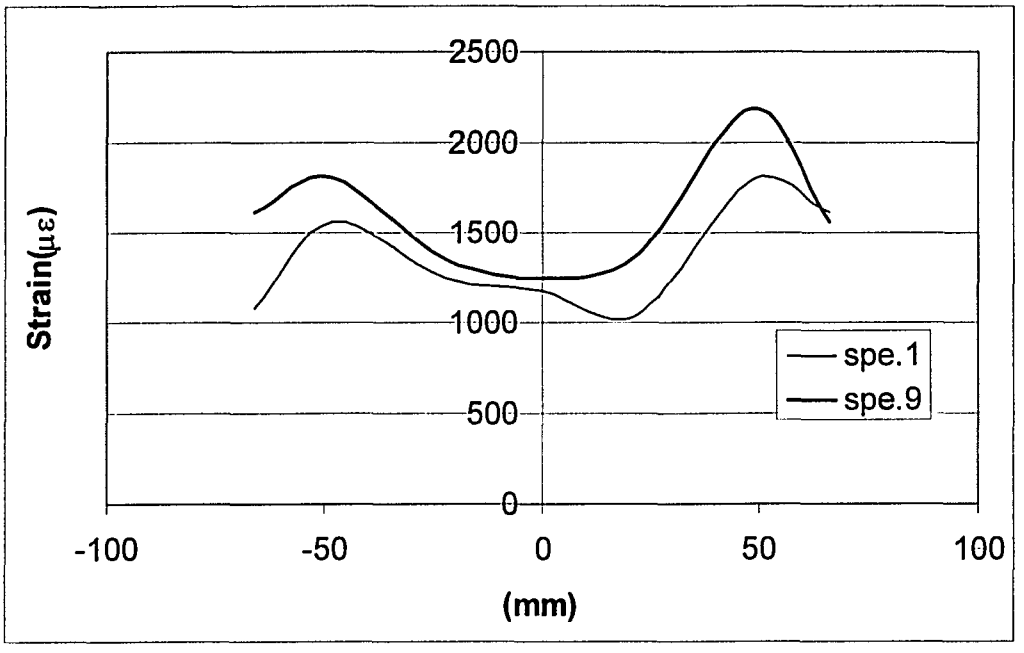

Fig. 4.21 Comparison of Strain of Specimens 1 and 9 at the Critical Section

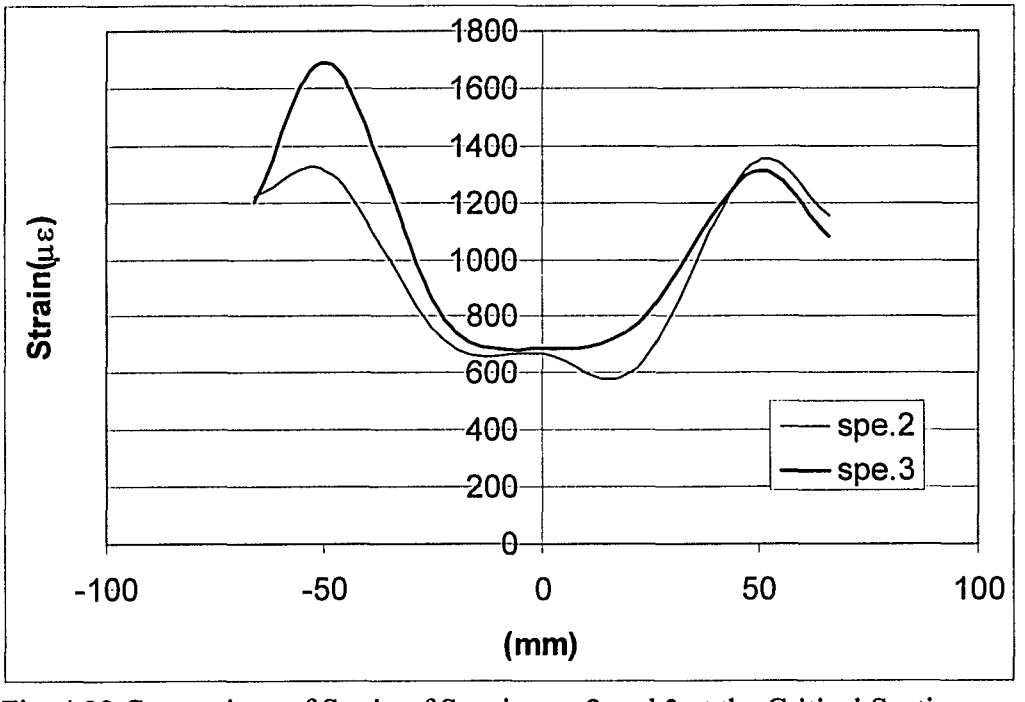

Fig. 4.22 Comparison of Strain of Specimens 2 and 3 at the Critical Section

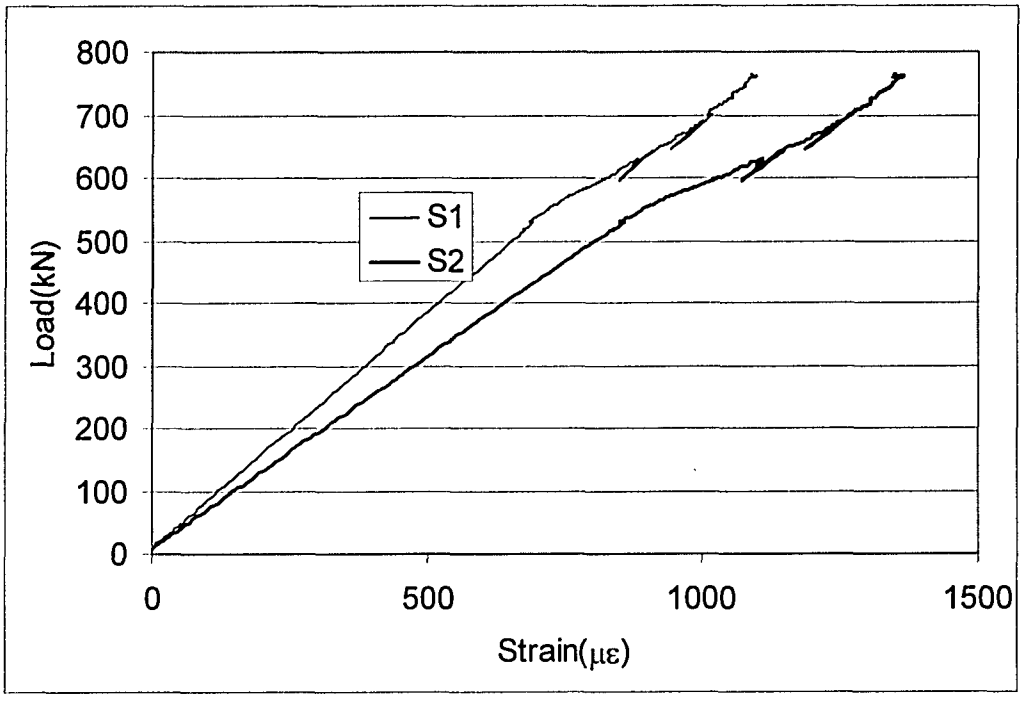

Fig. 4.23 Load-Strain Curves of Strains 1 and 2 of Specimen 1

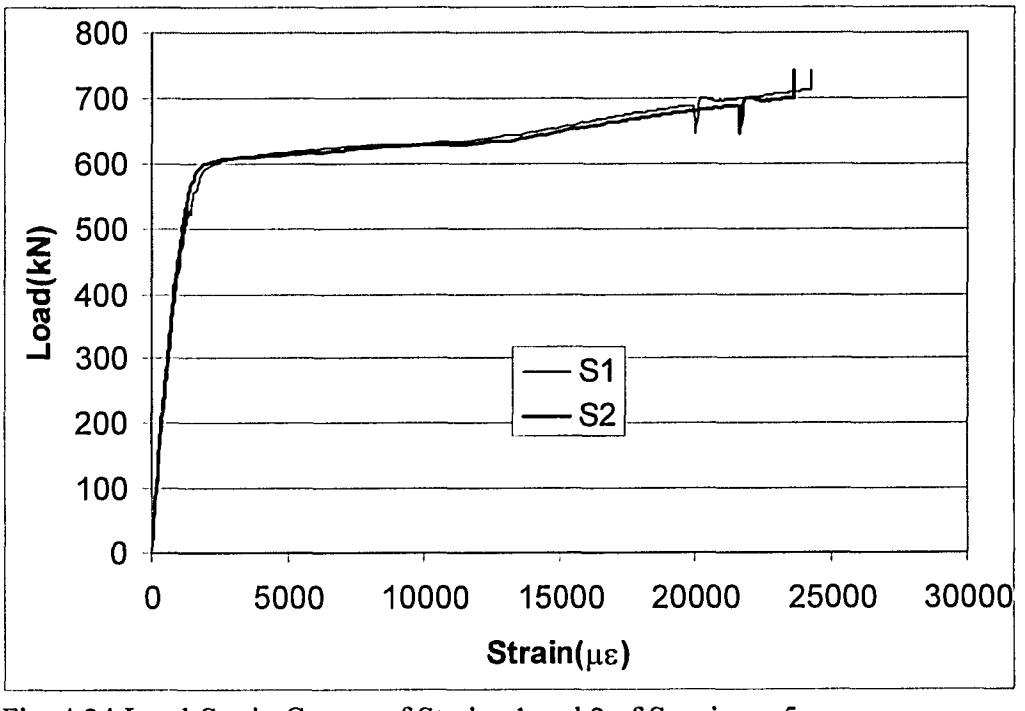

Fig. 4.24 Load-Strain Curves of Strains 1 and 2 of Specimen 5

5. FINITE ELEMENT ANALYSIS

5.1 Introduction

The specific parameter combinations used in the ten physical tests did not cover all the scenarios that might be expected in practical applications. It is desirable to develop a means by which the ultimate strength of welded tension members of other parameter combinations can be predicted, so as to avoid the expense of additional tests. In light of this thought, finite element models were developed after full-scale physical tests. First, these models were validated by comparing the numerical analysis results with the physical test results. It was found that the analysis results of these models agreed well with physical test results in load-deformation behavior, strain distribution at critical section, and deformed shape of specimens. Second, these proven models were used to predict the ultimate failure load of different specimen configurations so that shear lag effect could be assessed for welded tension members. With the expanded database of test results, we can acquire better understanding about shear lag effect of welded hot-rolled channel sections in tension.

5.2 Finite Element Model

A powerful general-purpose non-linear finite element program, ABAQUS/Standard (6.3) was used to conduct the analysis. The quadrilateral shell element S4R with reduced integration was used to form the models. The S4R element is a four-node doubly curved general-purpose shell element that accounts for finite membrane strains. Finite membrane strain allows the thickness of a shell element in the

configuration at time $t + \Delta t$ to be different from its value at time t. There are six degrees of freedom at each node, i.e., three translational (u1, u2, u3) and three rotational (ϕ1, ϕ2, ϕ3) components. In the through thickness direction the shell element is integrated at five points. Considering the symmetry of the specimen, only half-length of the specimen was used in the model. For double channel specimens, based on symmetry again, only one-fourth of the specimen was simulated. The boundary conditions can also be derived from the symmetry. At the mid-length of the double channel specimen, translation in u1 direction was allowed to simulate the stroke control process, while rotations of the ϕ2 and the ϕ 3 were constrained. For the gusset plate of double channel specimens, translation in the u3 direction and rotations in the ϕ 1 and the ϕ2 were forbidden, total degrees of freedom at the top edge were constrained. For single channel specimen, all degrees of freedom were constraint at the top edge of gusset plate except rotation about the ϕ2 direction, constrain to rotations of the ϕ2 and the ϕ3 was applied at mid-length of specimen.

For the specimens failed in gross section, the observed deformation of LVDT3 is very small and welding connection can be treated as rigid connection, so rigid beam MPC element was used to connect channel and gusset plate together. For the specimens failed in welding connection, three dimensional non-linear spring elements were applied to model the non-linear behavior of weld connection. Three spring elements are provided in ABAQUS spring element library and spring2 element was chosen to simulate weld connection. Spring2 element is between two nodes, acting in a fixed direction. Pairs of force-relative displacement values were given on the data lines of input file to define nonlinear spring behavior. These values were derived from the reading of LVDT3 during

experimental test and are listed in Table 5.1. LVDT3 was designed to measure the deformation of weld during the loading process. The typical experimental load-deformation curves of LVDT3 of different weld sizes are shown in Fig. 5.1. There are three directions (x, y, and z) in the spring stiffness, only the spring stiffness in the direction that coincides with the external load is dominant (x direction). Hence to simplified the procedure, the stiffness used in x direction was also used in y and z directions. For double channel specimens, there were four longitudinal welds at each end of a specimen, each individual spring stiffness can be obtained by dividing the load value by four and then by the number of springs defined in each line of weld. This was based on the assumption that the load was shared equally by the four weld lines. For single channel specimens, the load was supposed to be equally shared by two weld lines. Since the resistance of spring is proportional to the number of springs that simulate the weld connection, then spring stiffness derived from experimental tests for the different welds size can be used in the parametric study.

A mesh study was performed in order to find the optimal mesh size for the model. Three kinds of mesh were considered, namely coarse mesh, intermediate mesh and fine mesh. The meshes are shown in Fig. 5.2 and the number of element, element size and predicted ultimate loads are listed in Table 5.2. For three different meshes the predicted loads were almost same. Considering the size of strain gauge mounted on the specimens and computational time, intermediate mesh was chosen as the optimal mesh size. Even in the intermediate mesh, a relatively fine mesh was chosen around the connection region and a relatively coarse mesh was applied to the rest. This strategy was proved to be good enough to satisfy the research purpose while saving computational time. Compatibility

between fine mesh portions and the coarse mesh portion of the model was insured by using constrained equations.

5.3 Material Model

Both geometry and material non-linearities need to be taken into account in the models. An isotropic elastic-plastic-hardening material model was selected for the numerical analysis to reflect the actual behavior of structural steel. Cross section material properties were acquired by testing coupons from both web and flange because it was believed that the strength from flange is different from that of web due to mechanical rolling processing. Engineering stress and engineering strain are converted to true stress and true strain based on coupon test data, which is the syntax required by ABAQUS. The equations for the conversion are as follows:

[5.1] $$\sigma_{true} = \sigma_{nom}(1 + \varepsilon_{nom})$$

[5.2] $$\varepsilon_{true}^{pl} = \ln(1 + \varepsilon_{nom}) - (\frac{\sigma_{true}}{E})$$

[5.3] $$\varepsilon_{true} = \ln(\frac{A_0}{A})$$

where

σ_{true} = true stress

σ_{nom} = engineering stress

E = modulus of elasticity

ε_{true}^{pl} = log plastic strain

ε_{nom} = engineering strain

ε_{true} = total strain

A_0 = initial cross-section area

A = instantaneous cross-section area

From equation [5.3], the localized rupture strain can be calculated by measuring the initial cross-section area and rupture cross-section area of the coupon. Calculation shows that the rupture strain varies from 86% to 102% with an average of 94% in the tested coupons. An investigation of the ductile fracture of steel by Khoo et al. (2000) showed that localized rupture strain was about 80% to120% for structural grade steel, which is approximately the same as the values found here. So the true stress-strain curve is extrapolated to a true plastic strain of 100%, and within this range strain-hardening behavior can be fully simulated by ABAQUS.

5.4 Comparison of Numerical and Physical Test Results

It is found that the finite element analysis results agree well with the test results in three aspects:

(a) load-deformation curve;

(b) strain distribution at the critical section; and

(c) mode of failure and deformed shape.

5.4.1 Load–Deformation Relationship

The deformation for the physical tests can be obtained by the readings of LVDT1, which is the deformation of net span of the specimens. The deformation from the numerical analysis model includes the elongation of gusset plate and channel, but it was found that elongation of gusset plate was very small (much less than 1 mm) in the

numerical model, which can be ignored. Hence the load-deformation curves from LVDT1 results of each test and finite element analysis can be put together for comparison. These comparisons were plotted in Fig. 5.3 to Fig. 5.12. Table 5.3 gives the summary of the ultimate capacities from the numerical analysis and experimental results. The ratios of experimental test ultimate load to analytical ultimate capacity range from 95% to 102% with a mean value of 0.98 and a standard deviation of 0.027.

For the properties used in input file of each model, the most critical data for the model are the material properties and the spring stiffness. Since each material coupon test result was used in the corresponding models, and spring stiffness was obtained from the physical test of each specimen, the fact that numerical results match the physical test results well is not a coincidence.

5.4.2 Strain and Stress Distribution

Although by default ABAQUS calculates five section points through the thickness of a homogeneous shell at the location of a mid surface integration point, it only provides two point values located at the top and bottom surface, so caution should be exercised to figure out the positive and negative direction of the shell element. For the flanges, strain gauges were mounted outside, we should use the strain value at point "5"; while for the web, strain gauges were mounted inside, so strain values at point "1" should be chosen.

A typical comparison of strain distribution at the critical section is shown in Fig 5.13 and all others can be referred to in Appendix C. It can be seen that at different levels of loading, the strain distribution at the web for finite element analysis results is close to those from physical tests and is relatively uniform. This can be explained by the fact that there were two longitudinal welding lines along each side of the web, there is no

outstanding leg, and the load was transferred evenly from both sides. Flanges at the critical section behave like outstanding legs of an angle subjected to tension plus out-of-plane bending. As the load increased, the strain distribution became more non-uniform, this can be seen in Fig. 5.16. The strains of numerical results near a weld line are quite different from those from physical tests. The reason of this discrepancy is that the spring used to simulate the weld in numerical models cannot reflect completely the true behavior of weld during the physical tests. In the physical test, the welds first picks up the load and transfer it to both the flanges and web. The reading of strain gauges near the weld would be affected by the size of the weld and other factors such as variation of weld size along the weld length. As can be expected, a large weld size can improve stress distribution over the channel cross-section; also material properties at the location of a weld may change because they were affected by heating from the welding process. In the numerical models spring stiffness is derived from the stiffness of weld obtained from the experimental tests and does not reflect other physical features of the weld such as weld size and material properties change due to welding process. Therefore, the extent of stress concentration at the vicinity of weld could not be totally reflected by the numerical models. Though there are some differences between the two results, the strain distribution at the critical section from the numerical results follows a pattern similar to those from experimental tests.

Unlike other specimens, due to the presence of transverse welding, strains of numerical results at the web of critical section in specimen 5 are quite different from those of physical test, as can be seen in Fig. 5.14. The transverse weld was not simulated in the model, because the reading in LVDT3 is an overall behavior from both

longitudinal and transverse weld and there was no way to distinguish one contribution from the other. In the experimental test, the transverse weld would affect the reading of strain gauges since it picked up the load right at the location of weld, not like longitudinal welds, which take over the load gradually along the weld length.

For single channel specimens, below a certain load level the tips of flange are under compression during test because of bending. Finite element analysis for single channel specimens showed the same behavior as the single channel specimens did during experimental tests, as shown in Fig. 5.15.

Comparison between experimental and numerical analysis for specimen 3 can also be made. The strain of the experimental test at mid-length of specimen 3 at ultimate load is 1545με, while its corresponding numerical result is 1521με. As can be seen, the latter is close to the result from experimental test. As for other specimens, since the maximum value of strain the strain gauges can measure is around 23000με, and actual strains that other specimens experienced at ultimate load exceeded this value, no comparison can be made between these two strain values at ultimate load. But within the limit that strain gauge can measure, it is found the two strain values from test and analysis are very close to each other, as shown in Fig. 5.17.

Typical stress distribution at loading level of $P = 0.96P_u$ was plotted at the critical section and the mid-length for specimen 4 in Fig. 5.18. We can see that stresses at the critical section are quite non-uniform while at mid-length, the stress is completely uniform.

5.4.3 Failure Mode and Deformed Shape

Fig. 5.19 shows the numerical failure mode for specimens 1 and 2, they both failed at mid-length with obvious necking, which is exactly the same as the physical tests. As for the weld failure mode of numerical model, it was found that the springs that simulate the welds were elongated excessively, which indicated the failure of weld, as shown in Fig. 5.20. Lastly, Fig. 5.21 presents the bending deformed shape of single channel specimen at connection, which was also observed during the experimental test.

5.4.4 Evaluation of Numerical Model

From the results discussed above, it can be seen that all the test to predicted ratios of ultimate strength were well within experimental error for a testing program of this complexity. Within certain range, the strains of numerical results are very close to the measured ones. Furthermore, analytical failure modes and deformed shapes are the same as those observed in the experimental tests. Thus it was felt that the models built herein were successful models and could be utilized in a parametric study.

Table 5.1 LVDT3 Readings from Experimental Tests

Specimen 3		Specimen 4		Specimen 5		Specimen 6		Specimen 7		Specimen 10	
Force (N)	Deform. (mm)	Force (N)	Deform. (mm)	Force (N)	Deform. (mm)	Force (N)	Deform. (mm)	Force (N)	Deform. (mm)	Force (N)	Deform. (mm)
0	0	0	0	0	0	0	0	0	0	0	0
6336	0.082	8486	0.157	9994	0.014	3438	0.21	9733	0.233	5180	0.265
7411	0.145	9967	0.212	15004	0.368	4096	0.418	11977	0.601	6476	0.616
8371	0.305	11042	0.306	15751	0.626	4396	0.43	12895	1.132	6996	1.08
9335	0.568	11631	0.378	16257	0.781	4844	1.116	13363	1.499	7339	1.501
10060	1.05	12588	0.491	16591	0.896	5138	1.758	13690	1.678	7615	2
10188	1.455	13391	0.706	16759	0.974	5235	2.412	14277	2	7883	3.107
		13943	0.935	17206	1						
		14100	1	34413	2						
		16512	2								

* The values listed above are used as the spring stiffness in the numerical models

Table 5.2 Mesh Study

Mesh	No. of Element	Element Size (mm)	Ultimate Load (kN)
Coarse	800	17.5 x 20	748.2
Intermediate	6174	5 x 5	748.0
Fine	9540	3.5 x 5	748.0

Table 5.3 Ratios of Experimental and Numerical Test Results

Specimen No.	Ultimate Load (kN)		Test/Analysis
	Test	Analysis	
1	750	770	0.97
2	718	755	0.95
3	494	518	0.95
4	607	594	1.02
5	707	746	0.95
6	281	277	1.01
7	538	538	1.00
8	369	365	1.01
9	742	748	0.99
10	341	344	0.99

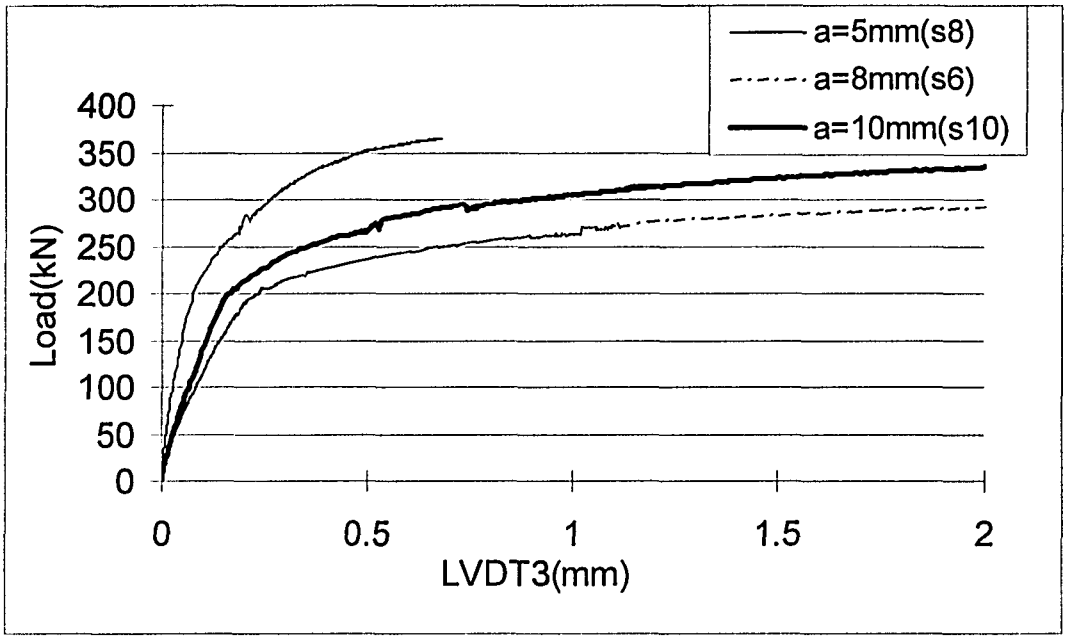

Fig. 5.1 Typical Load-deformation Curves of LVDT3 for Specimens 6, 8, and 10

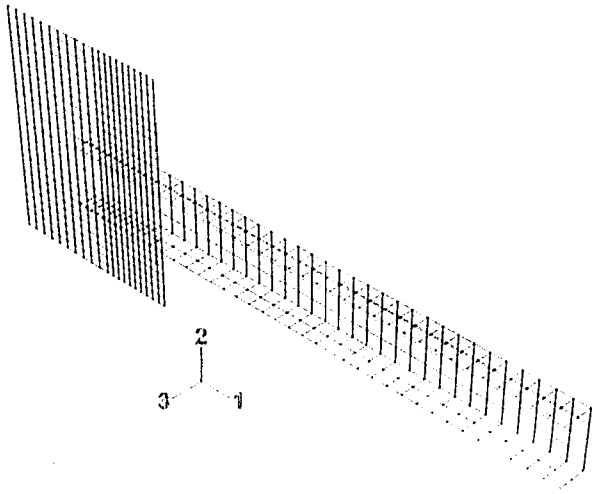

a) Coarse Mesh

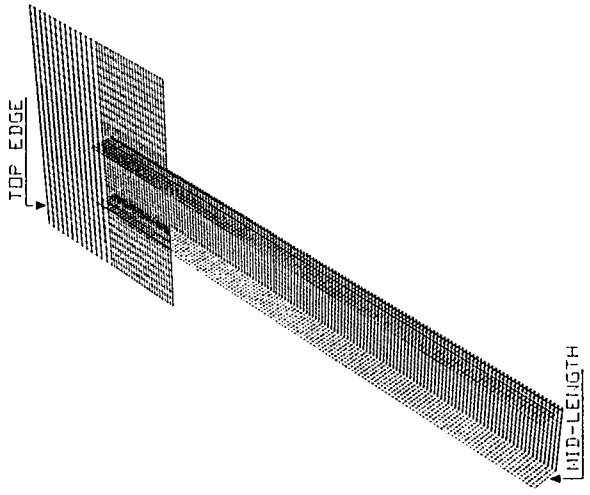

b) Intermediate Mesh

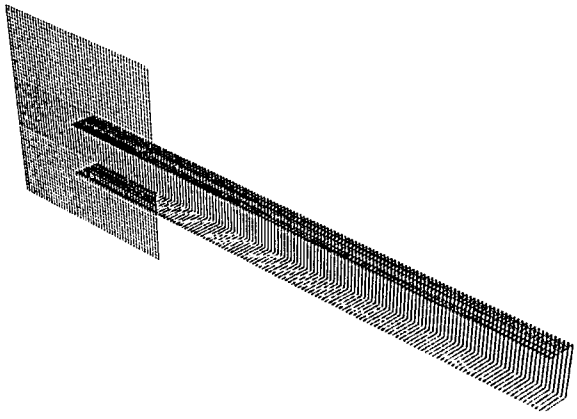

c) Fine Mesh

Fig. 5.2 Different Finite Element Mesh Options

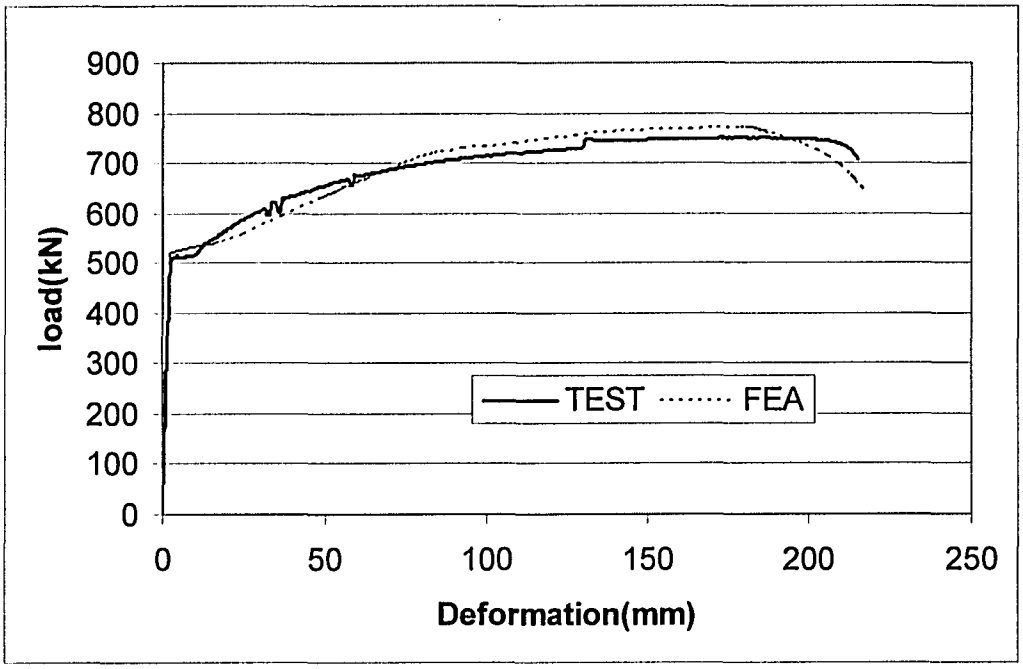

Fig. 5.3 Comparison of Load-deformation Curves of Specimen 1

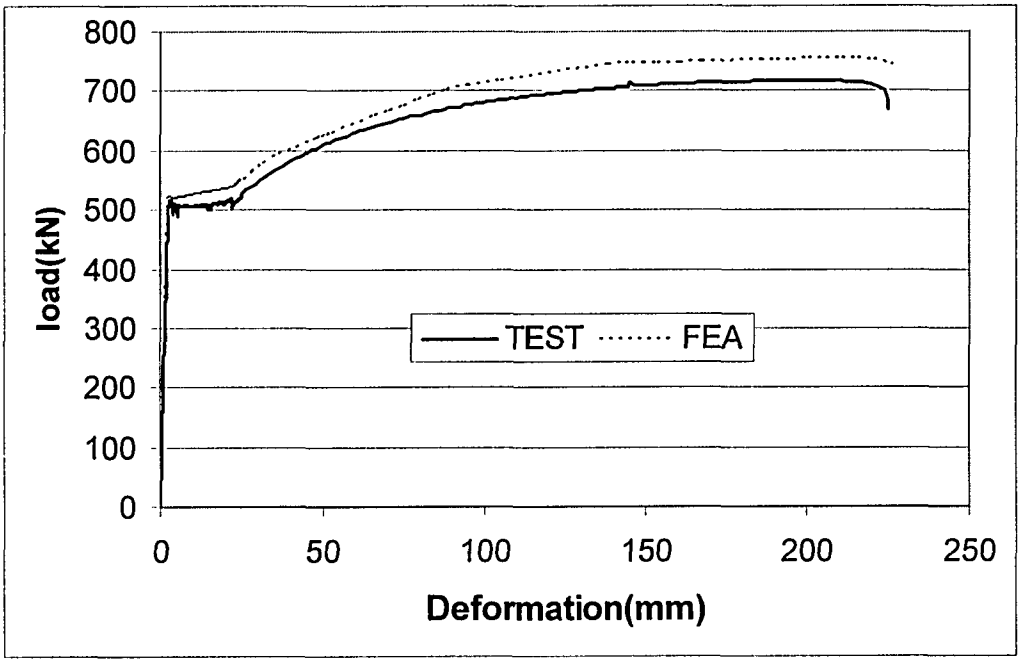

Fig. 5.4 Comparison of Load-deformation Curves of Specimen 2

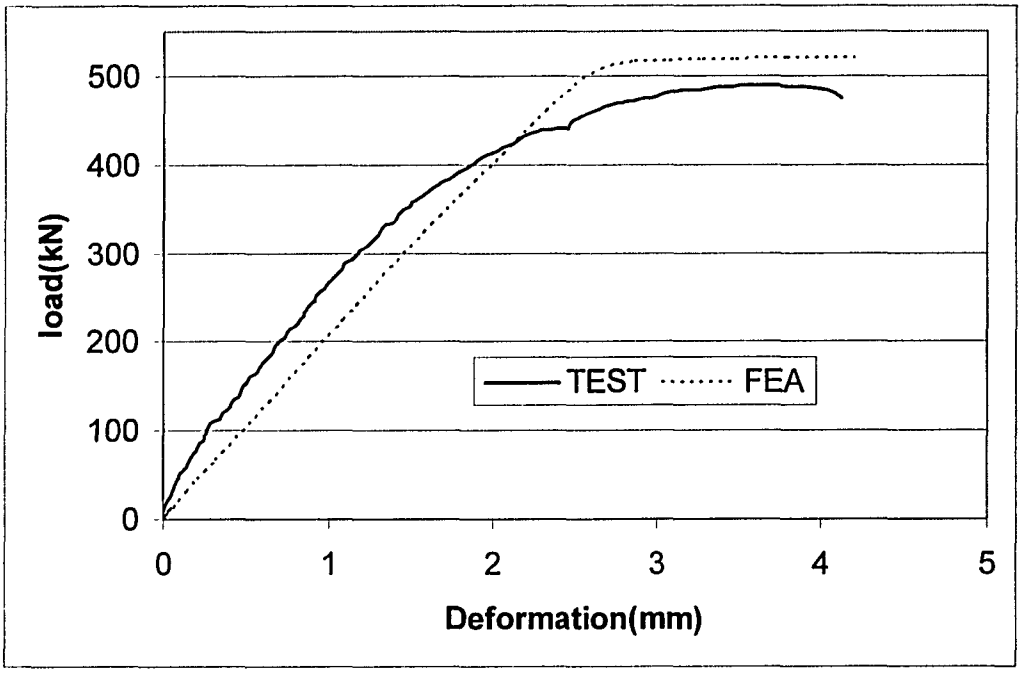

Fig. 5.5 Comparison of Load-deformation Curves of Specimen 3

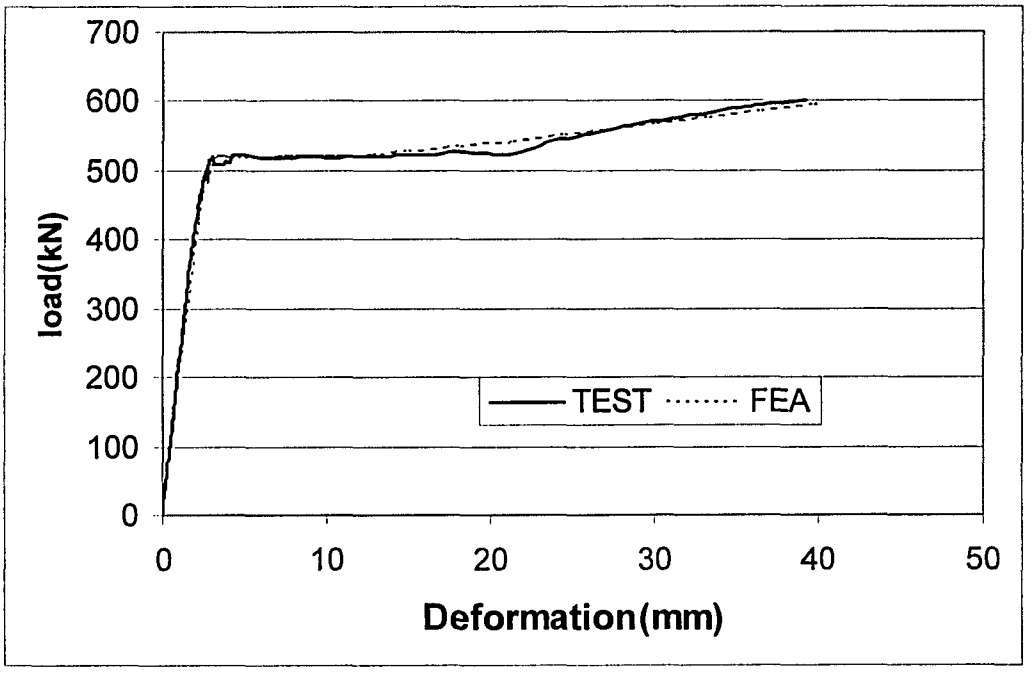

Fig. 5.6 Comparison of Load-deformation Curves of Specimen 4

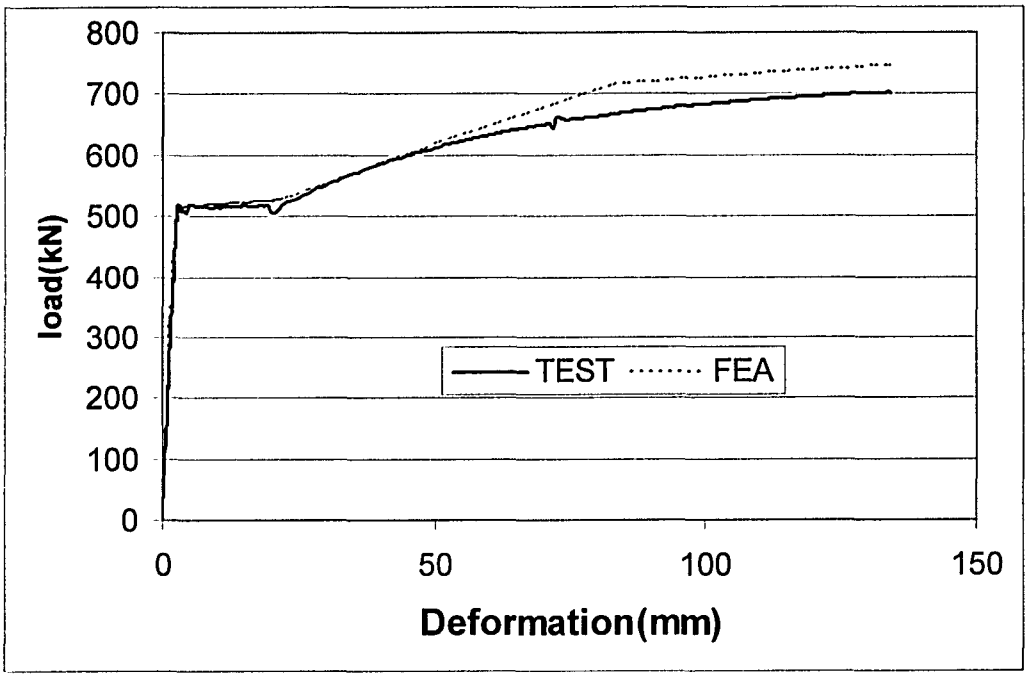

Fig. 5.7 Comparison of Load-deformation Curves of Specimen 5

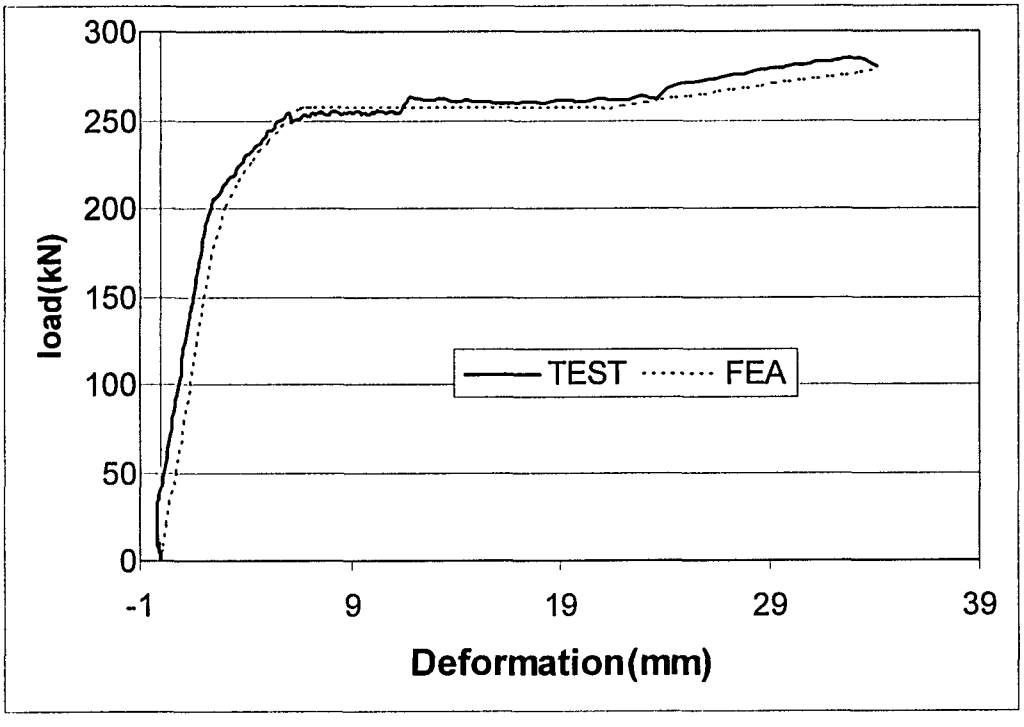

Fig. 5.8 Comparison of Load-deformation Curves of Specimen 6

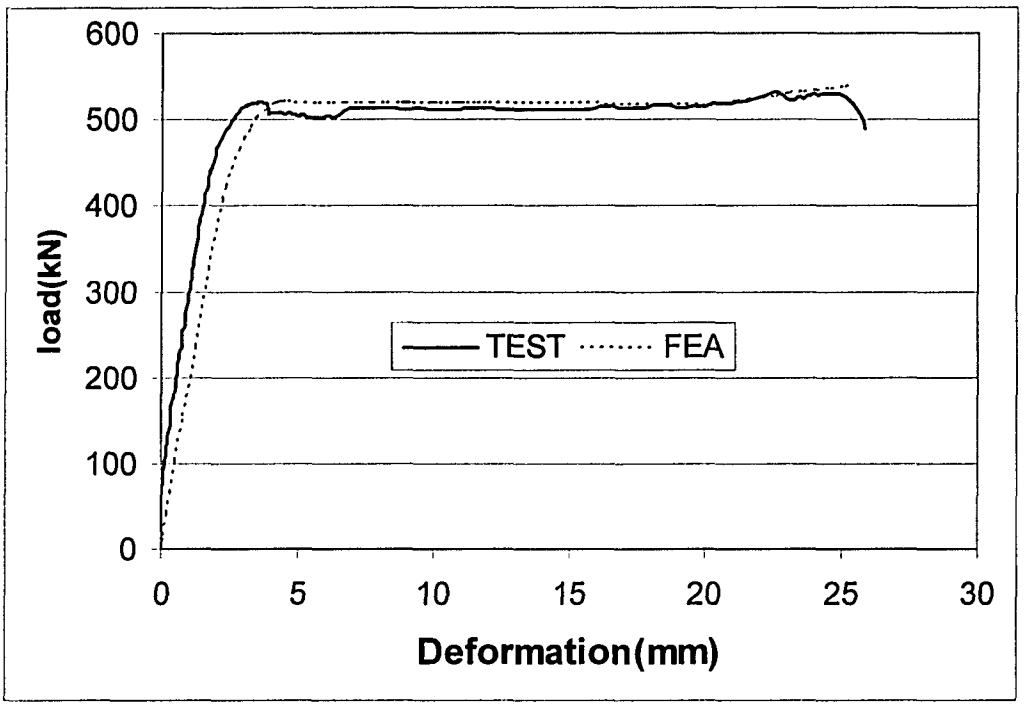

Fig. 5.9 Comparison of Load-deformation Curves of Specimen 7

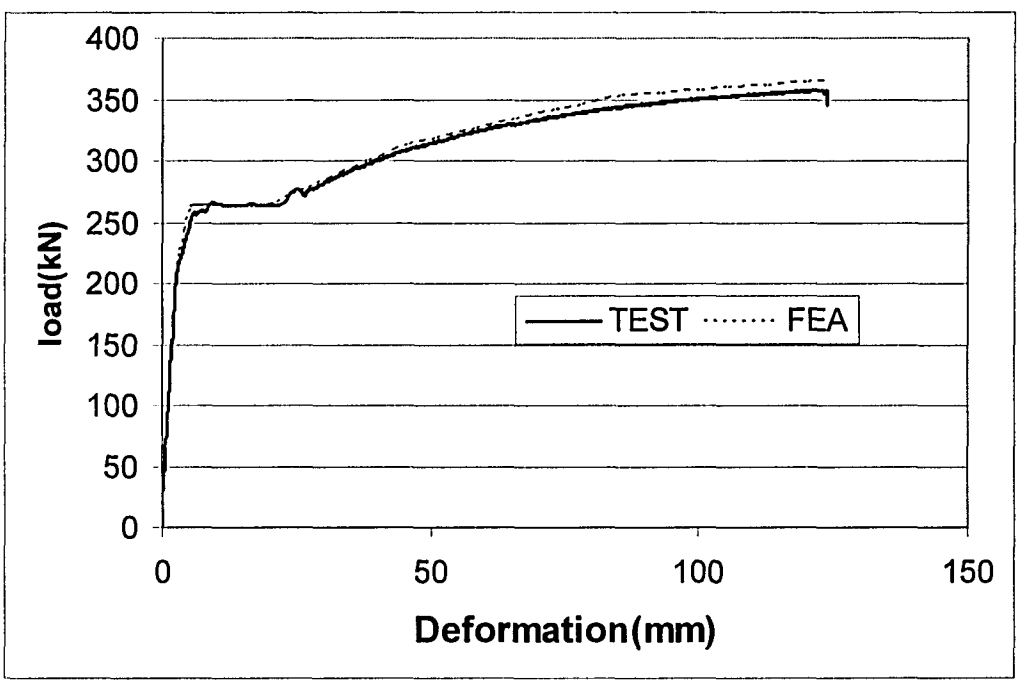

Fig. 5.10 Comparison of Load-deformation Curves of Specimen 8

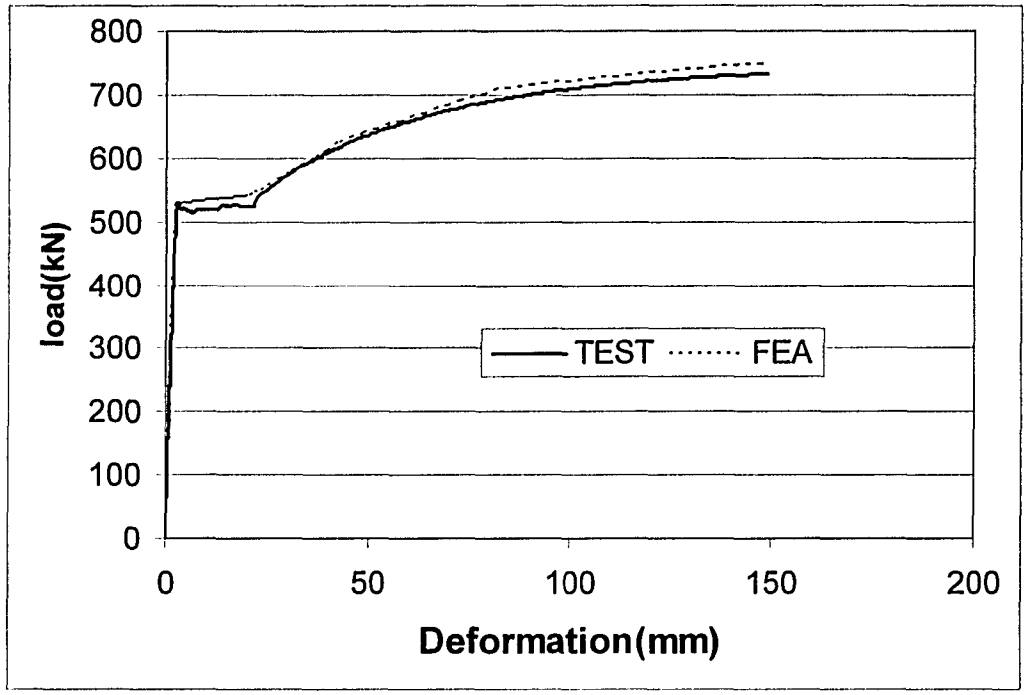

Fig. 5.11 Comparison of Load-deformation Curves of Specimen 9

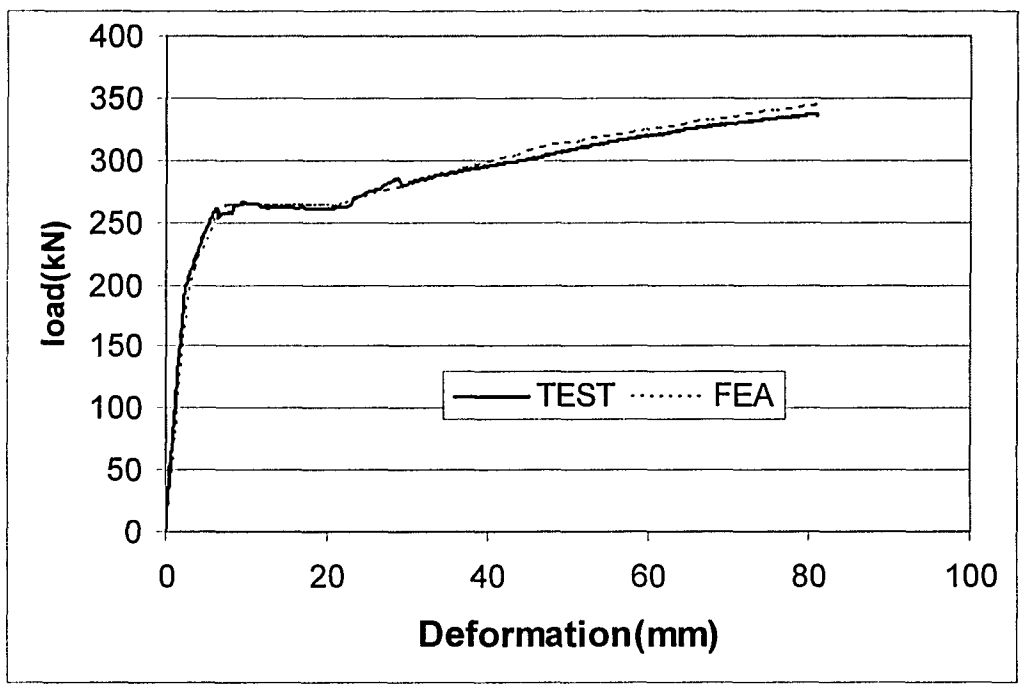

Fig. 5.12 Comparison of Load-deformation Curves of Specimen 10

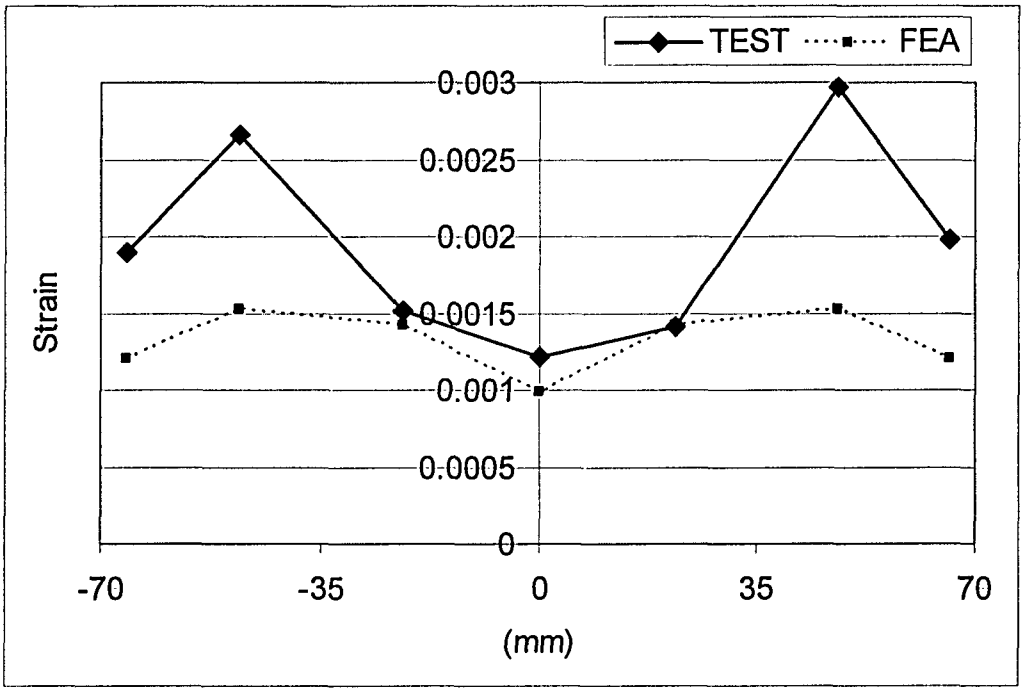

Fig. 5.13 Comparison of Strain Distribution at the Critical Section of Specimen 2

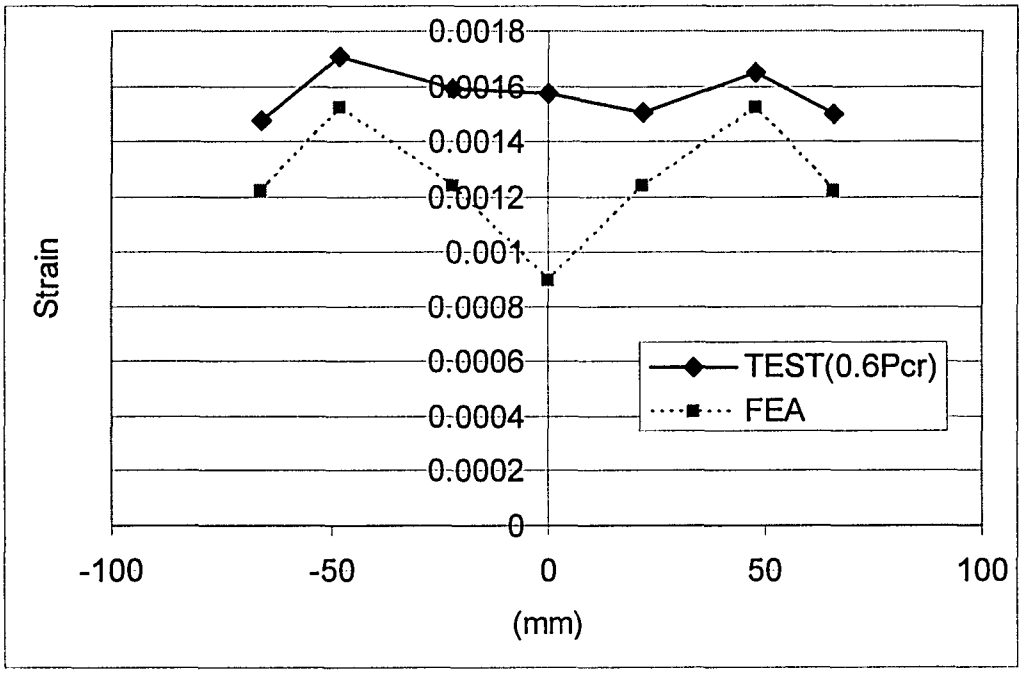

Fig. 5.14 Comparison of Strain Distribution at the Critical Section of Specimen 5

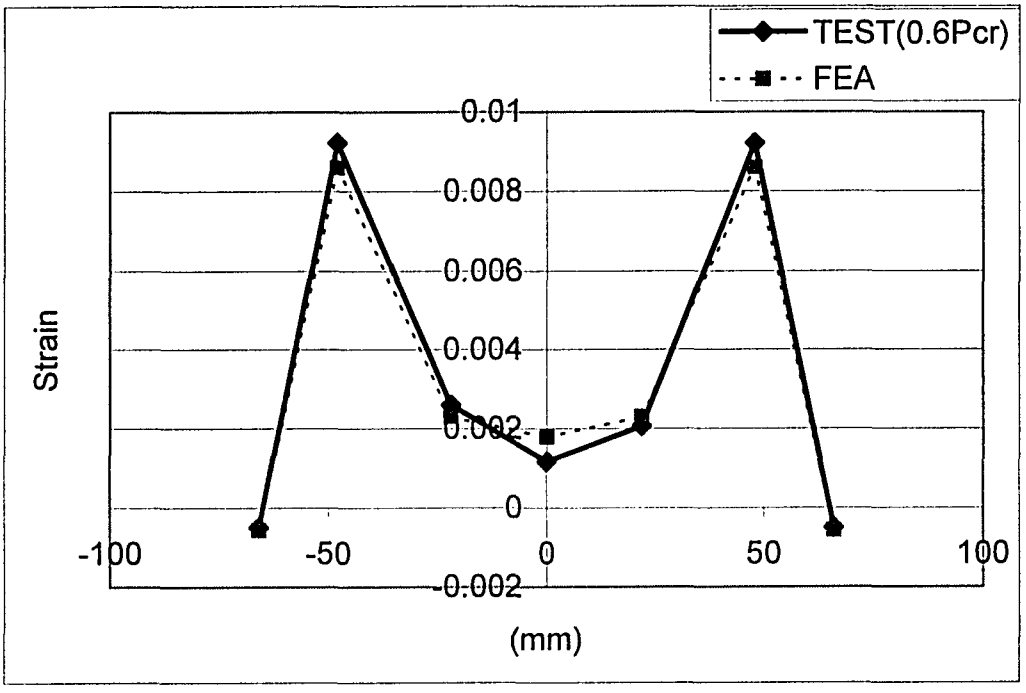

Fig. 5.15 Comparison of Strain at Different Load Levels at the Critical Section of Specimen 10

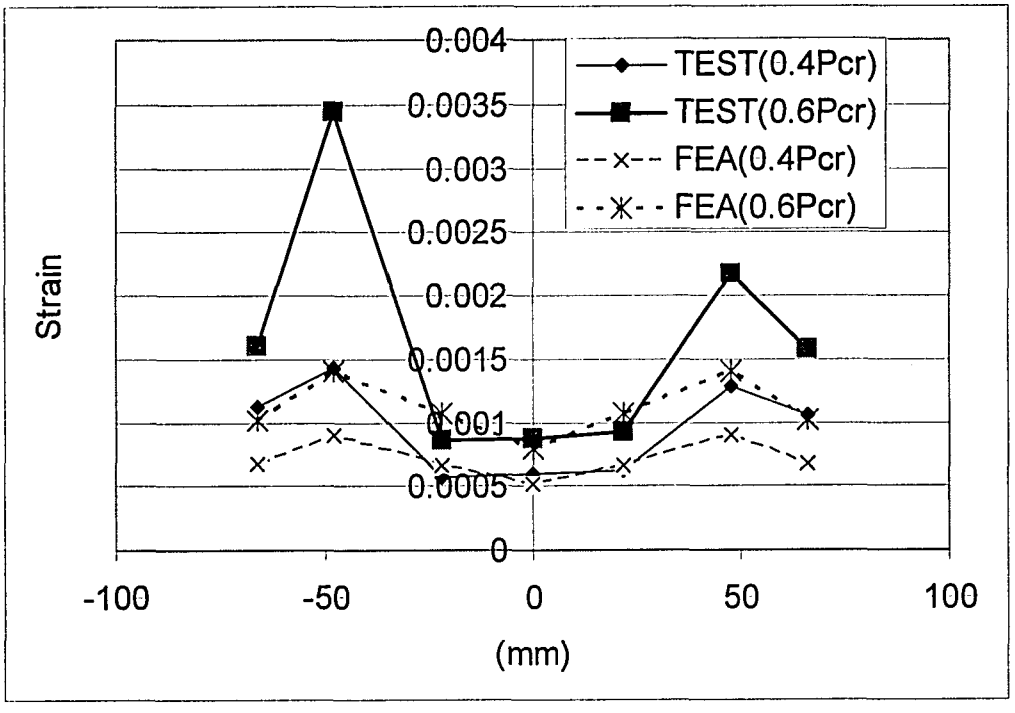

Fig. 5.16 Comparison of Strain at Different Load Levels at the Critical Section of Specimen 4

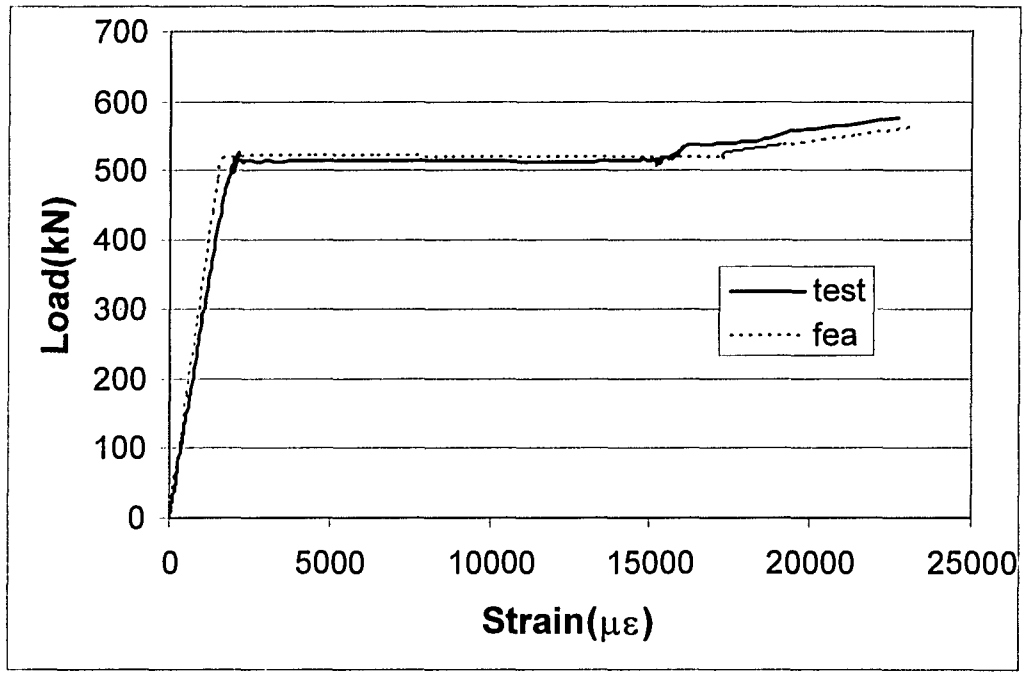

Fig. 5.17 Comparison of Strain of Experimental and Numerical Results of Specimen 2

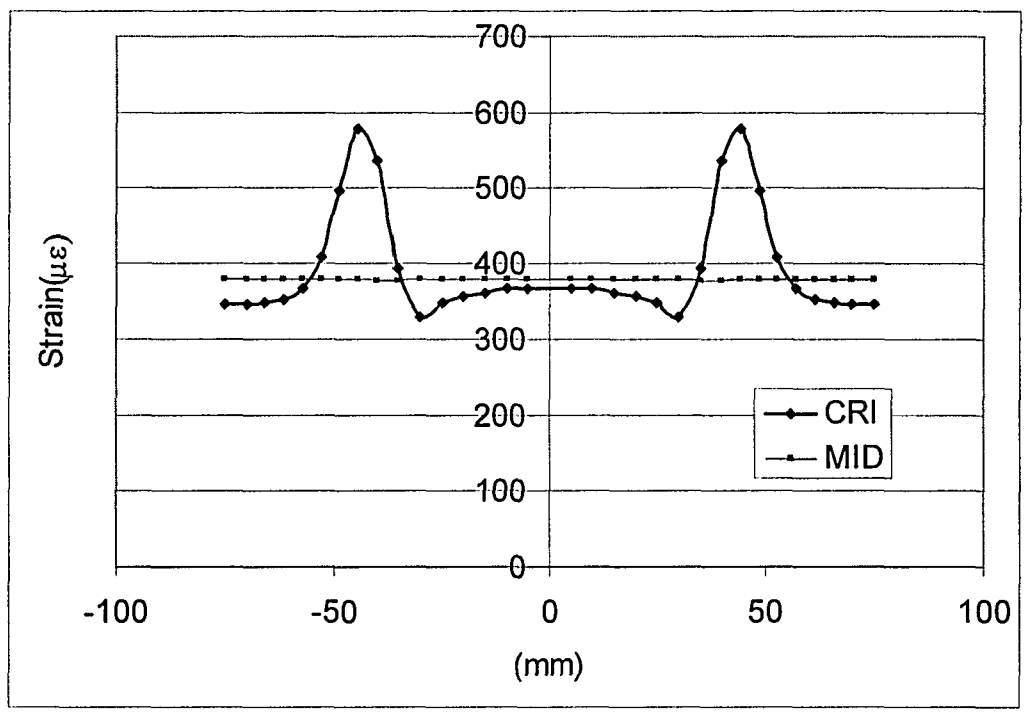

Fig. 5.18 Numerical Stress Distributions at the Critical Section and Mid-length of Specimen 4

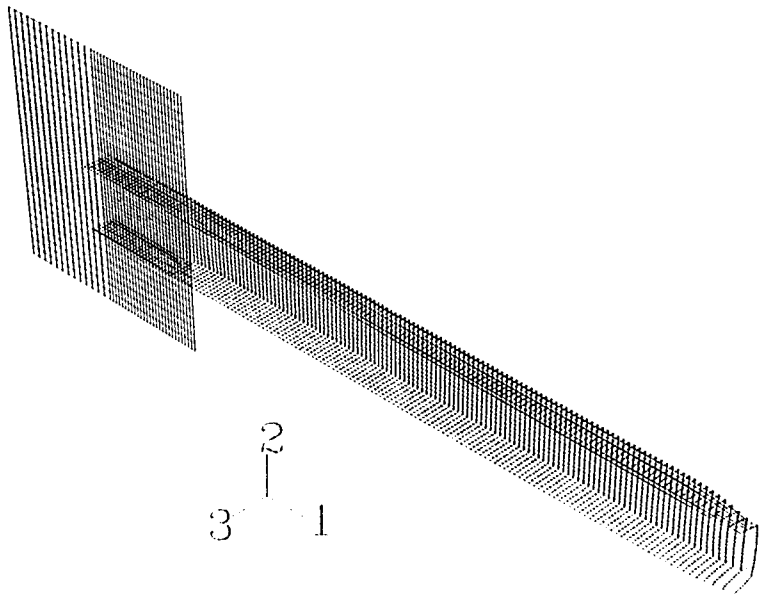

Fig. 5.19 Model Fracture at Mid-Length of Specimens 1 and 2

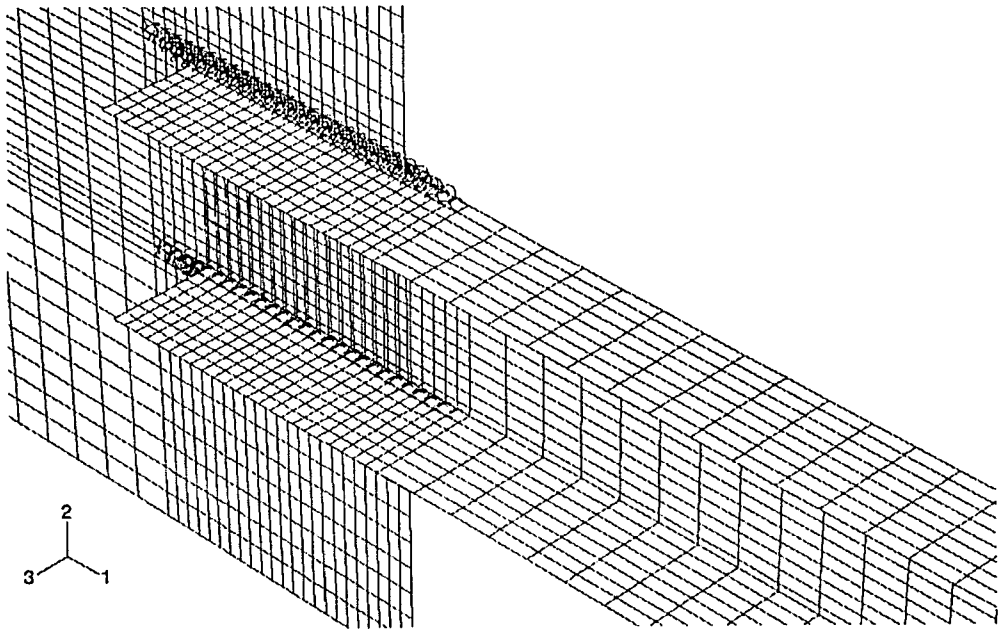

Fig. 5.20 Weld Failure Mode of Numerical Model

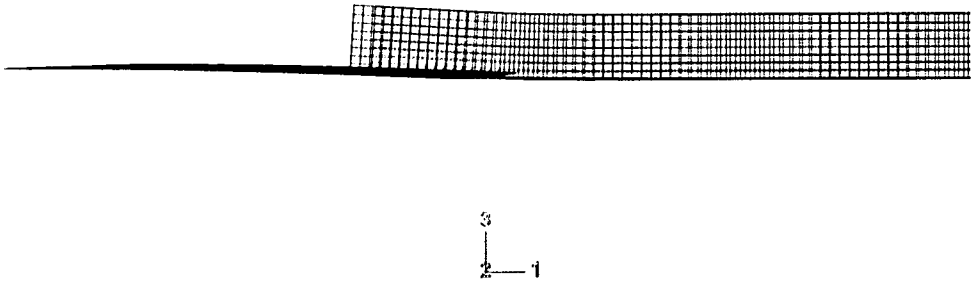

Fig. 5.21 Side View of Deformed Shape of Single Channel Specimen 6

6. PARAMETRIC STUDY

6.1 General

The purpose of this research is to develop simplified equations that account for the shear lag effect for hot-rolled steel channel sections. From the comparison of the experimental and numerical results presented in Chapter 5, it is very clear that the numerical models built in previous chapter can provide excellent predictions of load response, failure mode and strain distribution at the critical section and the mid-length. These proven models can be used to examine a variety of different kinds of combination of parameters that were not tested so that the new suggested equations can be validated in more general case. Since coarse mesh, intermediate mesh, and fine mesh all give the same ultimate carrying capacity as discussed in Chapter 5 and main focus of the parametric study will be on the global behavior of the model, therefore, the coarse mesh will be used here in order to save computational time.

6.2 Determination of Parameters to be Investigated

Through the previous study it is found that a number of variables may or may not have influence on the shear lag behavior of a member. The parameters that need to be considered include the length of specimen, the thickness of gusset plate, single or double channel, the weld size, the ratio of L/W (W is the depth of a channel section), the ratio of flange width H to W, and the ratio of W to web thickness t. Since Ng et al. (2002) concluded that weld capacity was not proportional to the weld size, so only the weld sizes used in the experimental tests will be used for parametric study, namely 5mm, 8mm, and 10mm. As for the combination of longitudinal and transverse weld cases, since LVDT3 measured the integrated effect of both welds, so the LVDT3 data

can only be used in this specific configuration and cannot be applied to other welds size and length. As there are a lot of parameters involved in the parametric study, a good strategy to simplify it is to normalize the parameters to try to cover all cases.

6.2.1 Effect of Specimen Length

Within the practical range of specimen length, it is found that the capacity of specimen will not be affected by changing specimen length. In Fig. 6.1, the capacity of specimen 9 with net channel length 0.6 m, 1.2 m, and 2.4 m were plotted, it can be seen that the capacities of these three specimens are almost identical. Also in Fig. 6.1, the capacities of single channel specimen 8 with different specimen length were checked as well, as can be seen, there is a negligible difference among these three cases. For the extreme cases, in which specimens are too short or too long, are beyond the scope of this research.

6.2.2 Effect of the Thickness of Gusset Plate

For a single channel specimen, the thickness of the gusset plate offers out-of-plane stiffness. As can be expected, the thicker the gusset plate, the more constraint it will offer for out-of-plane bending stiffness. The extent of this constraint may affect the net section efficiency because severe bending may cause stress concentration at the connection. A double channel specimen can be considered as the extreme case of single channel specimen since the out-of-plane stiffness of the gusset plate is irrelevant. Therefore, it is not necessary to examine the thickness effect of gusset plate for double channel specimens. For single channel specimens, both failed in welds and failed in gross section, i.e., specimen 8 and specimen 10 were examined. The thickness of gusset plate used in numerical models is 12.7 mm, 25.4 mm, and 50.8 mm, respectively. It is found that with the same configuration except the thickness of gusset plate, load capacity of a single channel specimen remains constant, as

presented in Fig. 6.2. Therefore, it is confirmed that the thickness of gusset plate has no effect on the net section efficiency.

6.2.3 Effect of Single or Double Channel

During the experimental tests, it was observed that single channel specimens behaved quite differently from double channel specimens. Single channel specimens could align their centroid with the loads so that the eccentricity was reduced. This behavior might result in higher carrying capacity. However, it also caused the bending at the gusset plates, as discussed in previous section. To investigate these effects, ten counterpart numerical models of the experimental tests were built. The ratios of single channel specimens capacity to double channel specimens capacity were plotted in Fig. 6.3, as can be seen, there is negligible different between these two configurations. The average of single to double channel specimen strength ratio is 0.995 with a standard deviation 0.00465. Hence, it can be concluded that the capacity of a single channel specimen is half that of a double channel one.

6.2.4 Effect of Eccentricity $\bar{x}$

The eccentricity $\bar{x}$ is one of the factors that have influence to the net section efficiency. As mentioned in the literature review in Chapter 2, the efficiency of a section would decrease as the eccentricity increases. In CISC Handbook of Steel Construction (2004), for standard channel sections, the eccentricity $\bar{x}$ ranges from 10.8 mm to 20.3 mm. The cross-sections chosen for this parametric study (see Section 6.2.6) will cover this range of eccentricity.

6.2.5 Effect of L/W Ratio

According to the current design standards, of all parameters considered for the shear lag effect of a welded tension member, the ratio of L/W is the most important one. The stresses can spread more evenly over channel cross section with large L/W

ratio. Three L/W ratios for each numerical model studied herein are used here. They are designed based on the weld capacity less, equal, and larger than the capacity of channel section(s), respectively.

6.2.6 Effect of Ratio W/H and Ratio W/t

There are ten groups of standard channel listed in CISC Handbook of Steel Construction (2004). Each group contains two to four types of channel section mainly varying in web thickness. W/H is the ratio of the web width to the flange width. As can be expected, this ratio reflects the relative stiffness of web and flange. W/t is the ratio of the web width to the web thickness, which also indicates the extent of the web stiffness. In the Handbook the range of W/H is 1.9 to 4.4 and the range of W/t is 8.4 to 42.4. Three types of channel section are selected, which are C75x9, C250x23 and C380x50. The range of W/H is 1.9 to 4.43 and the range of W/t is 8.4 to 41.6, in which most cases are covered for standard channel sections in the Handbook. In the meantime, the eccentricity $\bar{x}$ ranges from 11.4 to 20, which includes almost all cases.

6.3 Design of Parametric Study Matrix

Three types of channel cross-section and three ratios of L/W are used for the parametric study, along with three kinds of weld size, a total of 27 numerical models need to be built for the parametric study and they are listed in Table 6.1. For the model name, the first part designates the size of channel section, the second part represents the welding size and the third one signifies the ratio of L/W. The ratios of L/W were chosen to let the models fail either in connection (weld) or in gross section.

6.4 Failure Criterion of Numerical Model

The criterion should be established in order to judge when a numerical model fails. If it fails at gross section, study shows that the average strain in central element in mid-length of channel is 0.199, or simply by studying the deformed shape of numerical model using ABAQUS VIEWER, if there is an onset of unstable behavior in the model, it means the model fails in gross section. If a model fails in weld, it can be seen from ABAQUS VIEWER that the channel slips from its original position and the springs are elongated extensively, as shown in Fig. 5.20, and load-deformation curve for this type of failure mode becomes a horizontal line when it reaches the ultimate load.

6.5 Discussion of the Parametric Study Results

The parametric study results are presented in Table 6.2, along with the section efficiency factor calculated by using equations in CSA-S16-01 (2001) and AISC (1999). Only the specimens and models failed in gross section away from welded connection are included, those failed in welds will not be discussed here. It can be seen that when L/W ratio is equal or greater than 1.7, equations in both CSA16-01 (2001) and AISC (1999) give good prediction of the shear lag coefficient, the difference between them are within 10%. However, when L/W ratio becomes smaller, the difference between numerical test results and those obtained from the equations of S16 and AISC becomes larger. For example, for the model c250-10-0.9, the difference between the numerical result and the section efficiency factor calculated from the equations in AISC is more than 100%. This means that for the small L/W ratio cases, current codes cannot give good prediction of the net section efficiency factor.

6.6 Comparison and Discussion of the Results from Other Research

The results of a similar welded tension member shear lag study done by Easterling and Girous (1993) are listed in Table 6.3. The steel members they studied include plates, angles and channels. The reason why these results are listed here is that by analyzing other steel members, we can better understand about the different behavior of channel sections and other sections under tension. As can be seen, the critical section failure only occurred in plates and angles specimens. Considering out-of-plane stiffness, steel plates are very flexible members and the eccentricity (with regard to the surface of gusset plate) is relatively small, yet most of them still failed at the critical section. Since the critical section is the location where stress concentration happens, plate members have free edges at each side, which allow tearing to happen easily due to stress concentration. The same as plate members, angle members have a free edge at one side, and the experimental test showed that most of angle specimens exhibited a tearing failure initiating at the angle toe.

Unlike plate and angle members, hot-rolled channel section has two symmetric flanges and they are greatly thickened at the intersection of web and flange. When channel members are in tension, there is a possibility that necking may happen at the critical section due to the shear lag effect. However, with the help from the thickened flanges on both sides and the bi-axial stresses in channel web, which increases the channel strength at the critical section, all the channel sections tested by Easterling and Girous (1993) and in this program failed in gross section fracture away from the connection or failed in the welds, none of them failed in the critical section. Experimental tests for tubular section specimens done by Cheng et al. (1998) also indicate that for the cross-section without free edge (tubular sections), the member

strength is not affected by shear lag effect and always failed at mid-length away from the critical section.

Transverse weld in specimen 5 in the experimental test significantly increased load carrying capacity, which in turn could increase the net section efficiency. Easterling and Girous (1993) found the net section efficiency was not increased by additional transverse weld, simply because the specimens they tested had long enough longitudinal welds which could let the specimens fail in gross section. However for specimen 5 in this study, the longitudinal weld is only 55 mm long, as can be seen, the presence of transverse weld contributed a lot to the ultimate load of specimen 5.

It is noticed that the average net section efficiency for the channel sections tested by Easterling and Girous (1993) is 0.90, which is lower than that those values in this study. The reason for this is not clear. Generally speaking, specimen length will not affect the specimen strength, but if the specimens are too short, eventually the strength of the specimens will be affected since the stress concentration zone may overlap. In addition, the material properties in the flange of a channel section are normally lower than the ones from the web. If only material properties from the web were used to calculate the net section efficiency, a lower net section efficiency factor would be expected. Since the information about the specimen length and details of material properties are not available in Easterling and Girous' paper, no conclusion can be made on this issue. It is interesting to note that the net section efficiency of welded cold-formed steel channel sections reported by Lemenhe and Cheng (2001) is also equal or greater than 0.95. None of the cold-formed channel sections tested failed at the critical section.

Table 6.1 Details of Models in the Parametric Study

Model Name	W (mm)	H (mm)	t (mm)	L (mm)	W/H	W/t	Gross Area (mm^2)	$\bar{x}$ (mm)
C75-5-1.5	76	40	9	115	1.9	4.4	1120	11.4
C75-5-2.2	76	40	9	170	1.9	4.4	1120	11.4
C75-5-3.0	76	40	9	230	1.9	4.4	1120	11.4
C75-8-1.5	76	40	9	115	1.9	4.4	1120	11.4
C75-8-2.0	76	40	9	150	1.9	4.4	1120	11.4
C75-8-3.0	76	40	9	230	1.9	4.4	1120	11.4
C75-10-1.0	76	40	9	80	1.9	4.4	1120	11.4
C75-10-1.3	76	40	9	100	1.9	4.4	1120	11.4
C75-10-2.0	76	40	9	150	1.9	4.4	1120	11.4
C250-5-1.4	254	65	6.1	360	3.9	41.6	2880	15.9
C250-5-1.7	254	65	6.1	440	3.9	41.6	2880	15.9
C250-5-2.0	254	65	6.1	500	3.9	41.6	2880	15.9
C250-8-1.3	254	65	6.1	340	3.9	41.6	2880	15.9
C250-8-1.7	254	65	6.1	440	3.9	41.6	2880	15.9
C250-8-2.0	254	65	6.1	500	3.9	41.6	2880	15.9
C250-10-0.9	254	65	6.1	220	3.9	41.6	2880	15.9
C250-10-1.3	254	65	6.1	340	3.9	41.6	2880	15.9
C250-10-1.7	254	65	6.1	440	3.9	41.6	2880	15.9
C380-5-2.2	381	86	10.2	840	4.4	37.4	6430	20
C380-5-2.6	381	86	10.2	1000	4.4	37.4	6430	20
C380-5-3.0	381	86	10.2	1140	4.4	37.4	6430	20
C380-8-2.0	381	86	10.2	800	4.4	37.4	6430	20
C380-8-2.6	381	86	10.2	1000	4.4	37.4	6430	20
C380-8-3.0	381	86	10.2	1140	4.4	37.4	6430	20
C380-10-1.3	381	86	10.2	500	4.4	37.4	6430	20
C380-10-1.7	381	86	10.2	660	4.4	37.4	6430	20
C380-10-2.0	381	86	10.2	800	4.4	37.4	6430	20

Table 6.2 Results of Parametric Study

Model Name	P_{net} (kN)	P_{para} (kN)	Failure Mode	U_{para}	$U_{s16\text{-}01}$	U_{AISC}	U_{para} / $U_{s16\text{-}01}$	U_{para} / U_{AISC}
C75-5-1.5	559	421	WELD	-	-	-	-	-
C75-5-2.2	559	574	G.S*	1.03	0.97	0.96	1.06	1.07
C75-5-3.0	559	574	G.S	1.03	0.98	0.96	1.05	1.07
C75-8-1.5	559	515	WELD	-	-	-	-	-
C75-8-2.0	559	574	G.S	1.03	0.97	0.96	1.06	1.07
C75-8-3.0	559	574	G.S	1.03	0.98	0.96	1.05	1.07
C75-10-1.0	559	544	WELD	-	-	-	-	-
C75-10-1.3	559	573	G.S	1.03	0.85	0.80	1.21	1.29
C75-10-2.0	559	574	G.S	1.03	0.97	0.96	1.06	1.07
C250-5-1.4	1435	1394	G.S	0.97	0.90	0.82	1.07	1.18
C250-5-1.7	1435	1394	G.S	0.97	0.95	0.88	1.02	1.10
C250-5-2.0	1435	1392	G.S	0.97	0.99	0.95	0.98	1.02
C250-8-1.3	1435	1389	G.S	0.97	0.89	0.82	1.09	1.18
C250-8-1.7	1435	1393	G.S	0.97	0.95	0.88	1.02	1.10
C250-8-2.0	1435	1393	G.S	0.97	0.99	0.95	0.98	1.02
C250-10-0.9	1435	1394	G.S	0.97	0.78	0.45	1.24	2.16
C250-10-1.3	1435	1390	G.S	0.97	0.89	0.82	1.09	1.18
C250-10-1.7	1435	1388	G.S	0.97	0.95	0.88	1.02	1.10
C380-5-2.2	3208	3145	G.S	0.98	0.99	0.96	0.99	1.02
C380-5-2.6	3208	3144	G.S	0.98	0.99	0.96	0.99	1.02
C380-5-3.0	3208	3144	G.S	0.98	0.99	0.96	0.99	1.02
C380-8-2.0	3208	3145	G.S	0.98	0.99	0.96	0.99	1.02
C380-8-2.6	3208	1340	G.S	0.98	0.99	0.96	0.99	1.02
C380-8-3.0	3208	3143	G.S	0.98	0.99	0.96	0.99	1.02
C380-10-1.3	3208	3147	G.S	0.98	0.88	0.81	1.11	1.21
C380-10-1.7	3208	3144	G.S	0.98	0.95	0.88	1.03	1.11
C380-10-2.0	3208	3147	G.S	0.98	0.99	0.96	0.99	1.02

*G.S means gross section failure

Table 6.3 Summary of Test Results from Easterling and Girous (1993)

Test Designation	Specimen Configuration	Member Size(mm)	$\frac{L_w}{d}$	Failure Mode	$U_{exp.}$	U_{S16-01}	U_{AISC}	$\frac{U_{exp}}{U_{S16-01}}$	$\frac{U_{exp.}}{U_{AISC}}$
P-L1-1a	Double Plate	102x9.5	1.38	(1)	0.92	0.85	0.75	1.08	1.23
P-L1-1b	Double Plate	76x6.4	1.42	Critical Section	0.94	0.86	0.75	1.09	1.25
P-L1-2	Double Plate	76x6.4	1.42	Critical Section	0.98	0.86	0.75	1.14	1.31
P-L1-3	Double Plate	76x6.4	1.42	Critical Section	1.00	0.86	0.75	1.16	1.33
P-L2-1	Double Plate	76x6.4	1.67	Critical Section	0.98	0.92	0.87	1.07	1.13
P-L2-2	Double Plate	76x6.4	1.67	Critical Section	0.98	0.92	0.87	1.07	1.13
P-L2-3	Double Plate	76x6.4	1.67	Critical Section	0.96	0.92	0.87	1.04	1.1
P-B-1	Double Plate	76x6.4	1.67	Critical Section	0.90	0.92	1.00	0.98	0.9
P-B-2	Double Plate	76x6.4	1.67	Critical Section	0.99	0.92	1.00	1.08	0.99
P-B-3	Double Plate	76x6.4	1.67	Critical Section	0.97	0.92	1.00	1.05	0.97
L-L-1	Double Angle	51x51x4.8	2.24	Critical Section	0.81	0.88	0.87	0.92	0.93
L-L-2	Double Angle	51x51x4.8	2.24	Critical Section	0.82	0.88	0.87	0.93	0.94
L-L-3	Double Angle	51x51x4.8	2.24	Critical Section	0.82	0.88	0.87	0.93	0.94
L-B-1a	Double Angle	102x76x6.4	0.88	Critical Section	0.82	0.86	0.80	0.93	1.03
L-B-1b	Double Angle	51x51x4.8	1.5	Weld Failure	-	0.88	0.81	-	-
L-B-1c	Double Angle	51x51x4.8	1.5	Critical Section	0.80	0.88	0.81	0.91	0.99
L-B-2	Double Angle	51x51x4.8	1.5	Critical Section	0.75	0.88	0.81	0.85	0.93
L-B-3	Double Angle	51x51x4.8	1.5	Critical Section	0.80	0.88	0.81	0.91	0.99
L-T-1	Double Angle	102x76x6.4	-	Weld Failure	-	0.60	0.59	-	-

(1) Testing machine capacity exceeded

Table 6.3 (cont'd)

Test Designation	Specimen Configuration	Member Size(mm)	$\frac{L_w}{d}$	Failure Mode	$U_{exp.}$	U_{S16-01}	U_{AISC}	$\frac{U_{exp}}{U_{S16-01}}$	$\frac{U_{exp.}}{U_{AISC}}$
C-L-1	Double Channel	C75x6	1.67	Gross Section	0.89	0.86	0.91	1.03	0.98
C-L-2	Double Channel	C75x6	1.67	Gross Section	0.90	0.86	0.91	1.05	0.99
C-L-3	Double Channel	C75x6	1.67	Gross Section	0.91	0.86	0.91	1.06	1.00
C-B-1	Double Channel	C75x6	1.67	Gross Section	0.90(2)	0.90	0.91	1.05	0.99
C-B-2	Double Channel	C75x6	1.67	Gross Section	0.92	0.90	0.91	1.02	1.01
C-B-3	Double Channel	C75x6	1.67	Gross Section	0.88	0.90	0.91	0.98	0.97
C-T-1	Double Channel	C100x8	-	Weld Failure	-	0.43	0.44	-	-
C-T-2	Double Channel	C75x6	-	Weld Failure	-	0.43	0.49	-	-

(2) There is a typo in original paper and is corrected here

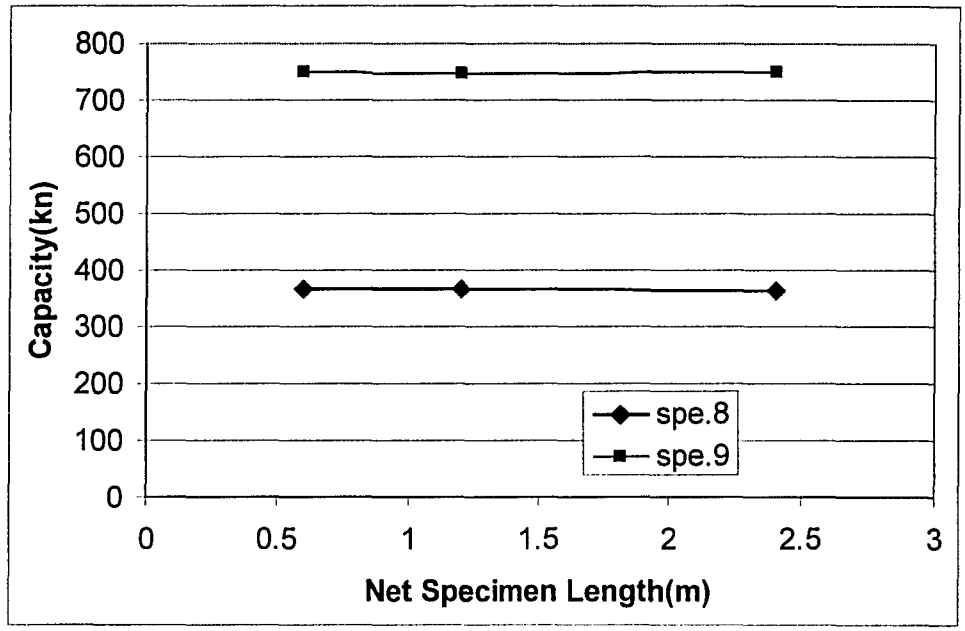

Fig. 6.1 Comparison of Load Capacity of Different Specimen Length

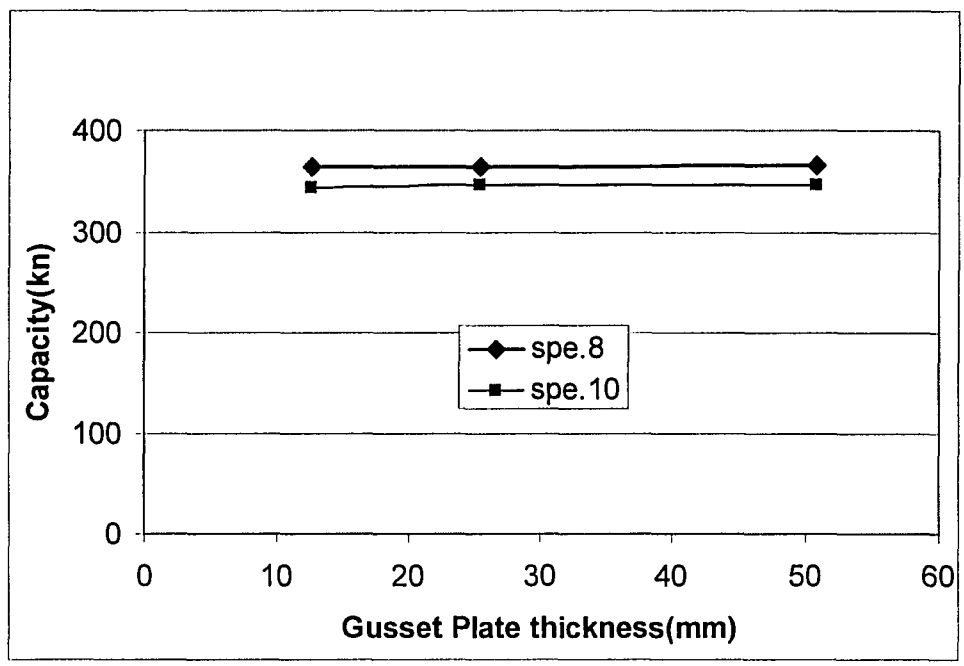

Fig. 6.2 Comparison of Load Capacity of Different Thickness of Gusset Plate

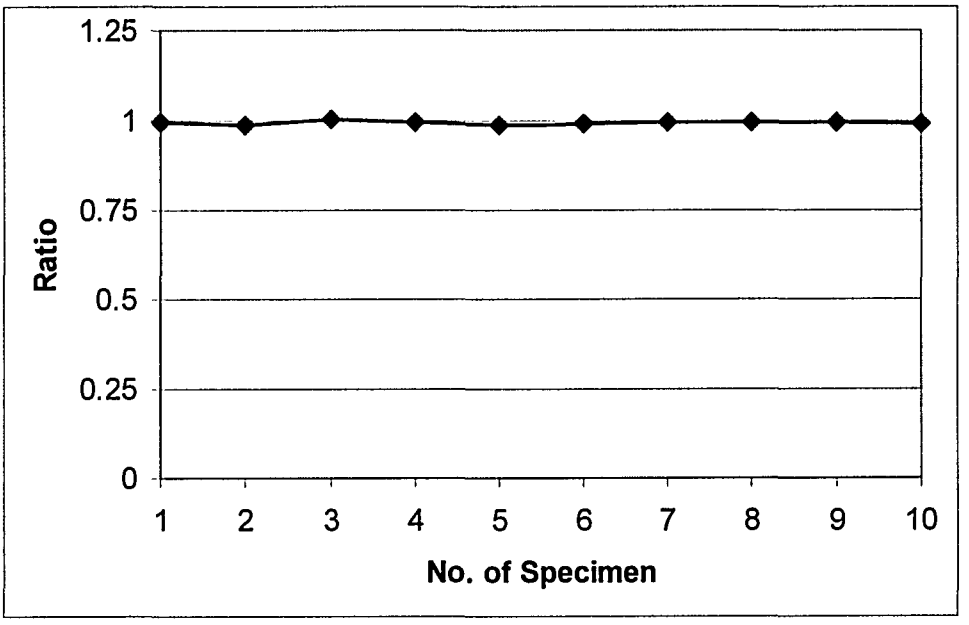

Fig. 6.3 Comparison of Load Capacity of Single to Their Corresponding Double Channel Specimens

7. SUMMARY, CONCLUSIONS, AND RECOMMENDATIONS

7.1 Summary

This project is to evaluate the influence of shear lag effect to the net section efficiency of welded hot-rolled steel channel sections in tension. Firstly, ten specimens with different design variables were fabricated and tested, which included different weld length, weld size, longitudinal and transverse welds, single or double channels. The connections were designed to fail either in the member or in the welds. Secondly, numerical models were established based on the corresponding test specimens and the test results. The third step was to expand the test results by a parametric study using the numerical models. The parametric study was designed to cover the whole spectrum of hot-rolled steel channel sections in the CISC steel handbook. Typical channel sections were chosen in the parametric study to investigate the influence of different parameters, such as the specimen length, the thickness of gusset plates, the eccentricity $\bar{x}$, the L/W ratios, the ratios of W/H and W/t.

All ten test specimens failed either in gross section fracture at the mid-length or in weld fracture. From the readings of strain gauges at the critical section, it is confirmed that shear lag effect does exist in the welded tension channel members. However, the final strength of these members was not affected by the shear lag effect since none of them failed at the critical section. This was also confirmed by Esterling et al (1993). This can be attributed to the shape of the channel cross-section and the bi-axial stresses in the channel web caused by the welds.

The results of the parametric study showed that the net section efficiency of welded hot-rolled steel channels was not affected by the cross section eccentricity $\bar{x}$ and ratios of W/H and W/t. The study also showed that the weld size had no effect on the net section efficiency as long as failure does not occur in weld. This conclusion could also apply to the weld length since it was found that if gross section failure occurred prior to weld failure, specimens with same weld size but different weld length have the same net section efficiency.

The average net section efficiency factor based on both experimental and numerical test results, excluding the specimens failed in the welds, was found to be 0.98 with a standard deviation 0.0247. Theoretically, the net section efficiency of hot-rolled steel channel in tension should be 1.0 since none of the specimens failed in the critical sections. The fact that it is lower than 1.0 can be attributed to the imperfection of the steel members, the load eccentricity, the variable material properties, the fluctuation of workmanship, the limited number of test results, etc. The lower than 1.0 net section efficiency factor was also reported by Easterling and Giroux (1993).

From the specimen failed in combination of longitudinal and transverse welds, i.e., specimen 5, it was found that the transverse weld participated fully in resisting the applied load. The transverse weld also improved the connection ductility when compared to the connection with longitudinal welds only. The transverse weld changed the load transfer mechanism in the connection and allowed more uniform stress distribution in the channel section.

It was also observed that the actually weld strength was about 20% to 30% higher than those predicted by the design equations in CSA S16-01 (2001). This means that the equations used in S16-01 are conservative.

7.2 Conclusions

Based on the study reported herein and previous research results obtained by others, it can be concluded that:

1. All the test specimens failed either in gross section fracture away from the connection or in weld fracture.
2. Non-uniform stress distribution at connection was observed due to shear lag effect. However, it has no effect on the final carrying capacity of the specimens.
3. The load eccentricity has limited influence on the capacity of both single channel and double channel specimens.
4. For the weld failure, the test to predicted ratios were between 1.2 to 1.3, which indicates the equations in current codes are conservative.
5. Weld length affects stress distributions notably than weld size does.
6. Numerical models yielded good agreement with the test results. Based on the parametric study, member length, thickness of gusset plate, eccentricity, and channel size have little effect on the net section efficiency.
7. The results from this study indicate the deficiency of the current design standards, more specifically for welded channel sections.

8. It is recommended a reduction factor of 0.95 to be used for welded channel section in tension to account for the effects of possible eccentricity and out-of-plane deformation.
9. From this study and other researches, it is concluded that for sections with no free edge weld, such as channel sections and HSS sections, the shear lag phenomenon has little effect on the carrying capacity of the section. However, it is believed that the shear lag behavior will have significant effect on the sections with free edge welds, such as angle sections and plate sections, especially when the L/W ratio is low.

7.3 Recommendations for Future Research

1. Additional experimental tests are required for the specimens with combined longitudinal and transverse welds, and transverse weld only. This will allow better understanding of the behavior of transverse weld and provide experimental data for developing numerical models with transverse weld.
2. More experimental data are needed for welded channel sections in order to further refine the net section efficiency factor.
3. Research is needed for the welded angle sections and plate sections in order to develop design criteria of the section efficiency factors for these sections.
4. Minimum weld length and minimum weld size should be investigated for welded connection to avoid premature weld failure.

REFERENCES

American Institute of Steel Construction (1999). Load and Resistance Factor Design Specification for Structural Steel Buildings. American Institute of Steel Construction, Chicago, Illinois.

American Society for Testing Materials (2001). A370 Standard Test Methods and Definitions for Mechanical Testing of Steel Product. ASTM, Philadelphia, PA

AWS, 1991 "Specification for Carbon Steel Electrodes for Shield Metal Arc Welding." ANSI/AWS A5.1-91, American Welding Society, Miami, FL.

Canadian Standard Association (2001). CAN/CSA-S16-01 Limited State Design of Steel Structures. Canadian Standard Association, Rexdale, Ontario.

Canadian Standard Association (1997). CAN/CSA-G40.21-97 Structural Quality Steels. Canadian Standard Association, Rexdale, Ontario.

Cheng, J.J.R, Kulak, G.L., and Khoo, H.A. (1998). "Strength of Slotted Tubular Tension Members". Canadian Journal of Civil Engineering. Vol. 25, No. 6, pp.982-991.

Chesson, E. and Munse, W. H. (1963a). "Riveted and Bolted Joints: Truss-Type Tensile Connection ". Journal of Structural Division, ASCE, Vol. 89, No. ST1, pp.67-106.

Chesson, E. and Munse, W. H. (1963b). "Riveted and Bolted Joints: Net Section Design". Journal of Structural Division, ASCE, Vol. 89, No. ST1, pp.107-126.

Davis, R. P. and Boomsliter, G. P. (1934). "Tensile Tests of Welded and Riveted Structural Member". Journal of the American Welding Society, April, pp.21-27.

Deng, K., Grondin, Driver, R .G. (2003) "Effect of Loading Angle on the Behavior of Fillet Welds." Structural Engineering Report 251, Department of Civil and Environmental Engineering, University of Alberta, Edmonton, Alberta.

Easterling, W. S. and Giroux, G. L. (1993). "Shear Lag Effects in Steel Tension Members". Engineering Journal, American Institute of Steel Construction, Vol. 30, pp.77-89.

Gibson, G. J. Wake, B. T. (1942). "An Investigation of Welded Connection for Angle Tension Members". The Journal of the American Welding Society, Welding Research Supplement, Vol. 21, Part II, pp.44s-49s.

Hibbit, Karlsson, & Sorenson, Inc. (HKS). (2002) ABAQUS/Standard Getting Start with ABAQUS Version 6.3. Hibbit, Karlsson, & Sorenson, Inc., Pawtucket, Rhode Island.

Hibbit, Karlsson, & Sorenson, Inc. (HKS). (2002) ABAQUS/Standard User's Manual Version 6.3. Hibbit, Karlsson, & Sorenson, Inc., Pawtucket, Rhode Island.

Lemenhe, A. and Cheng, J. J. R. (2001). "Behaviour of Welded Cold-formed Steel Tension Members". Structural Engineering Report No.223, Department of Civil Engineering, University of Alberta, Edmonton, Alberta.

Mckibben, F. P. (1906a). "Tension Test of Steel Angle". Proceedings of the ASTM, Vol. 6, pp.267-274.

Mckibben, F. P. (1906b). "Tension Test of Steel Angle with Various Types of End Connections". Proceedings of the ASTM, Vol. 7, pp.287-295.

Ng, A.K.F., Driver, R. G., and Grondin, G. Y. (2002) "Behavior of Transverse Fillet Welds." Structural Engineering Report 245, Department of Civil and Environmental Engineering, University of Alberta, Edmonton, Alberta.

Wu, Y. and Kulak, G. L. (1993). "Shear Lag in Bolted Single and Double Angle Tension Members". Structural Engineering Report No.187, Department of Civil Engineering, University of Alberta, Edmonton, Alberta.

APPENDIX A

Stress vs. Strain Curves of Coupon Tests

This Appendix includes stress-stain curves of coupon tests.

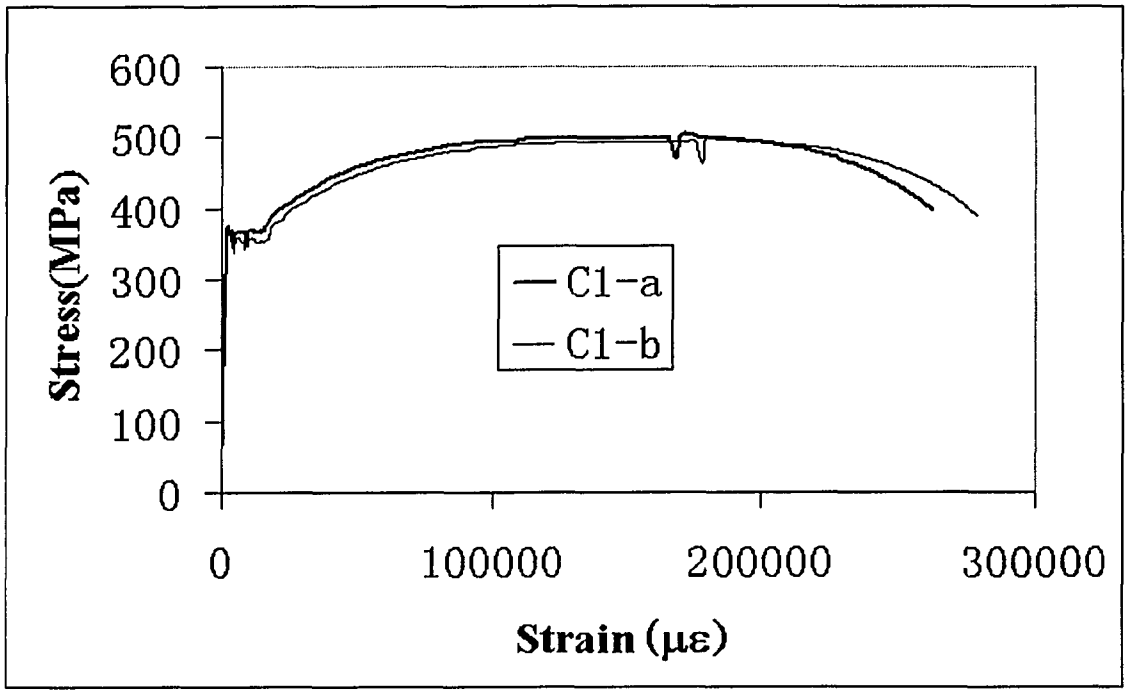

Fig. A1 Stress vs. Strain Curves of Channel Web Coupons - C1

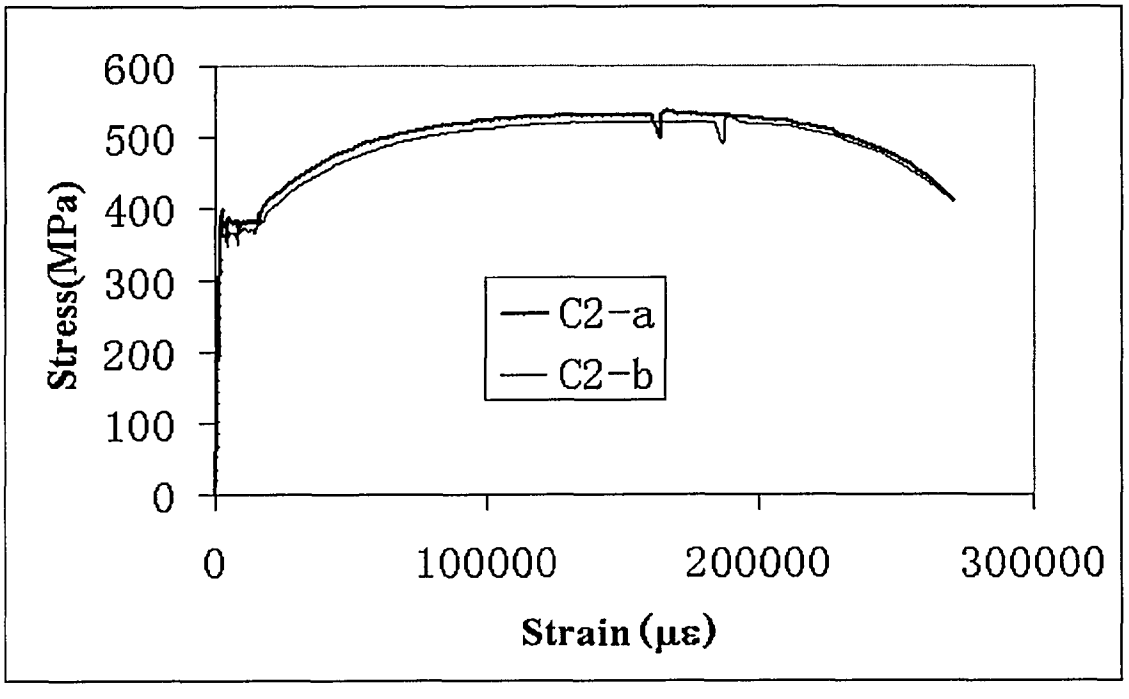

Fig. A2 Stress vs. Strain Curves of Channel Web Coupons - C2

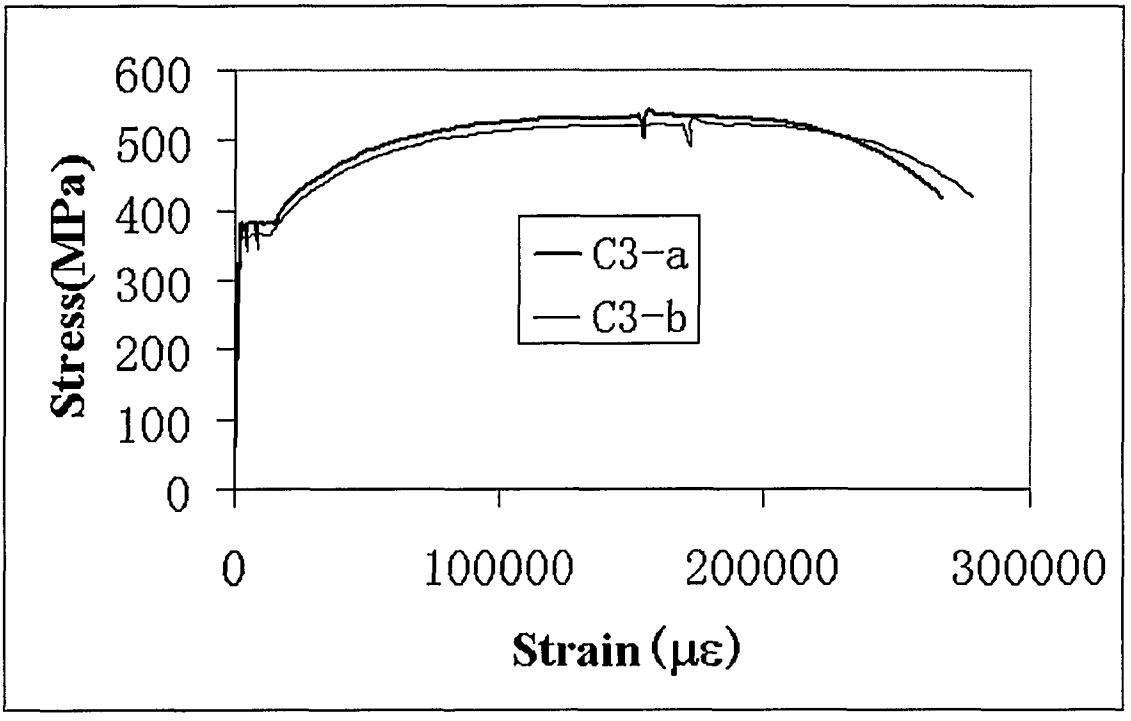

Fig. A3 Stress vs. Strain Curves of Channel Web Coupons - C3

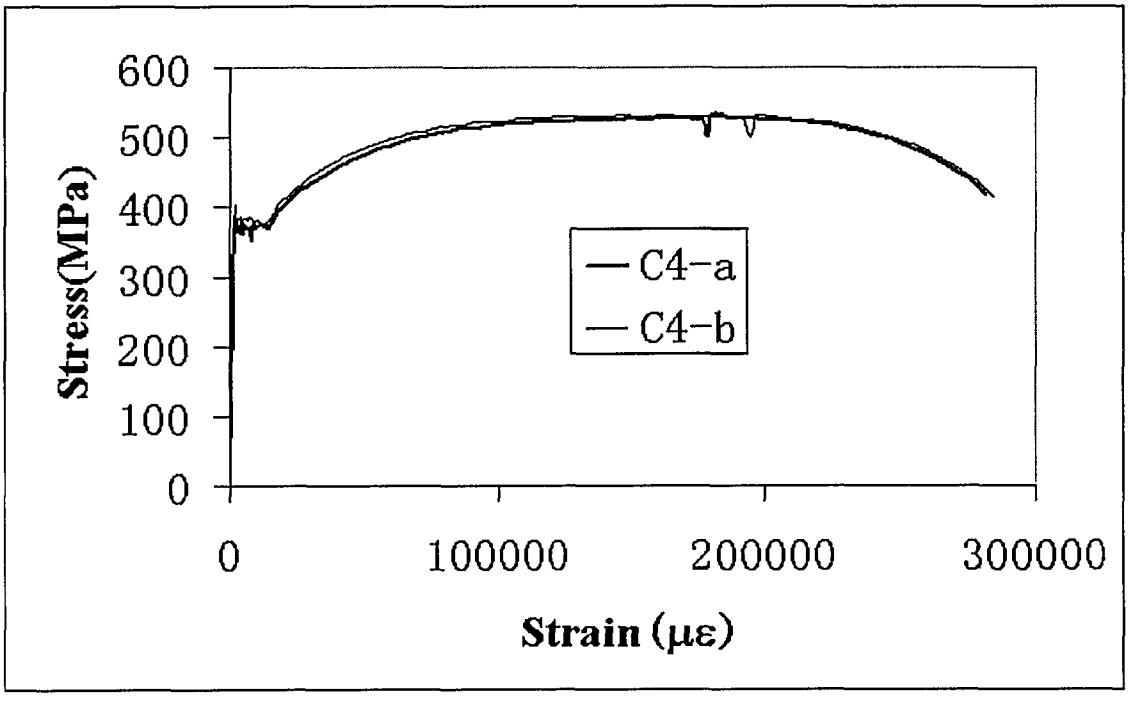

Fig. A4 Stress vs. Strain Curves of Channel Web Coupons - C4

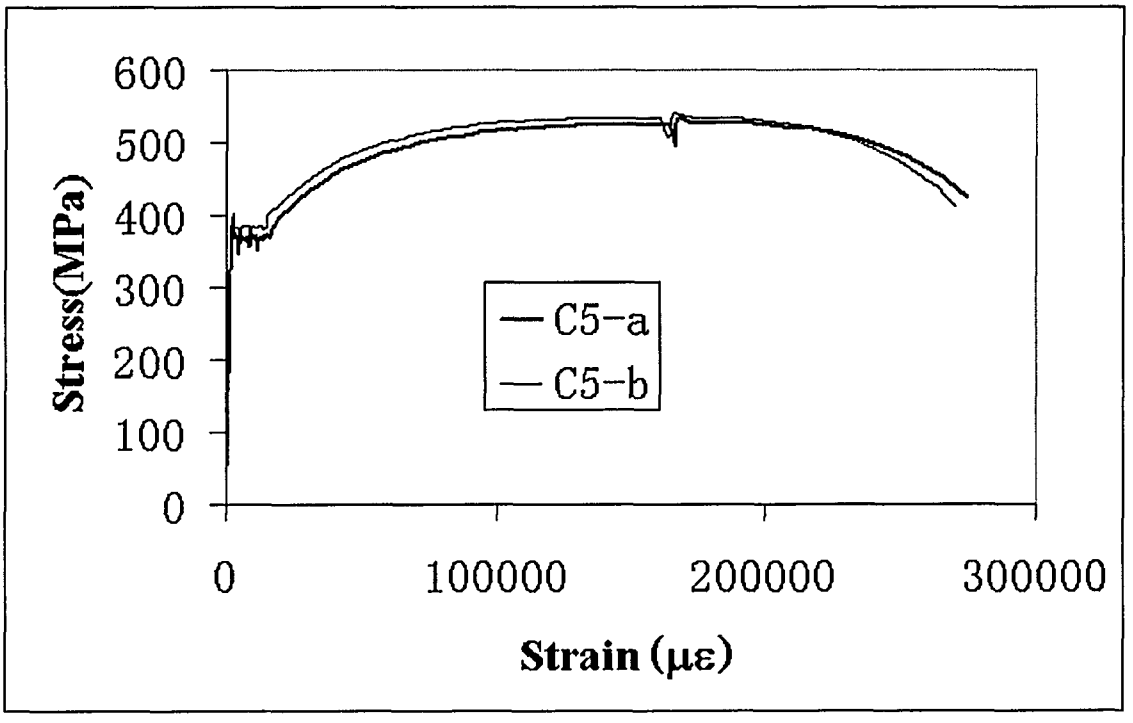

Fig. A5 Stress vs. Strain Curves of Channel Web Coupons - C5

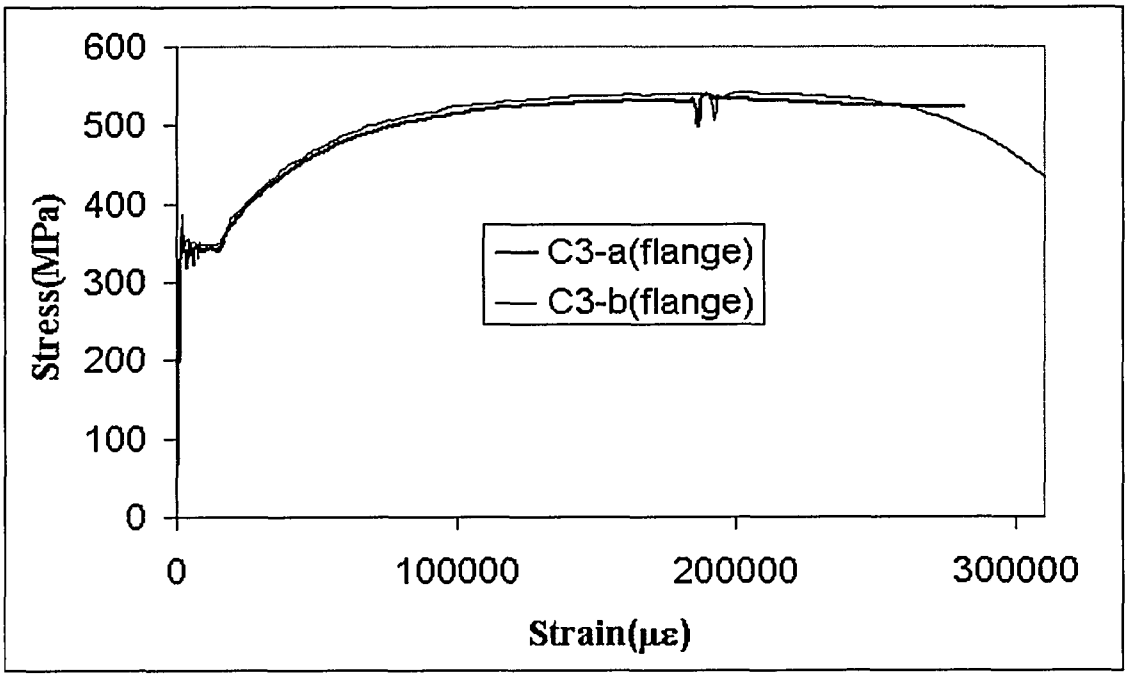

Fig. A6 Stress vs. Strain Curves of Channel Flange Coupons - C3

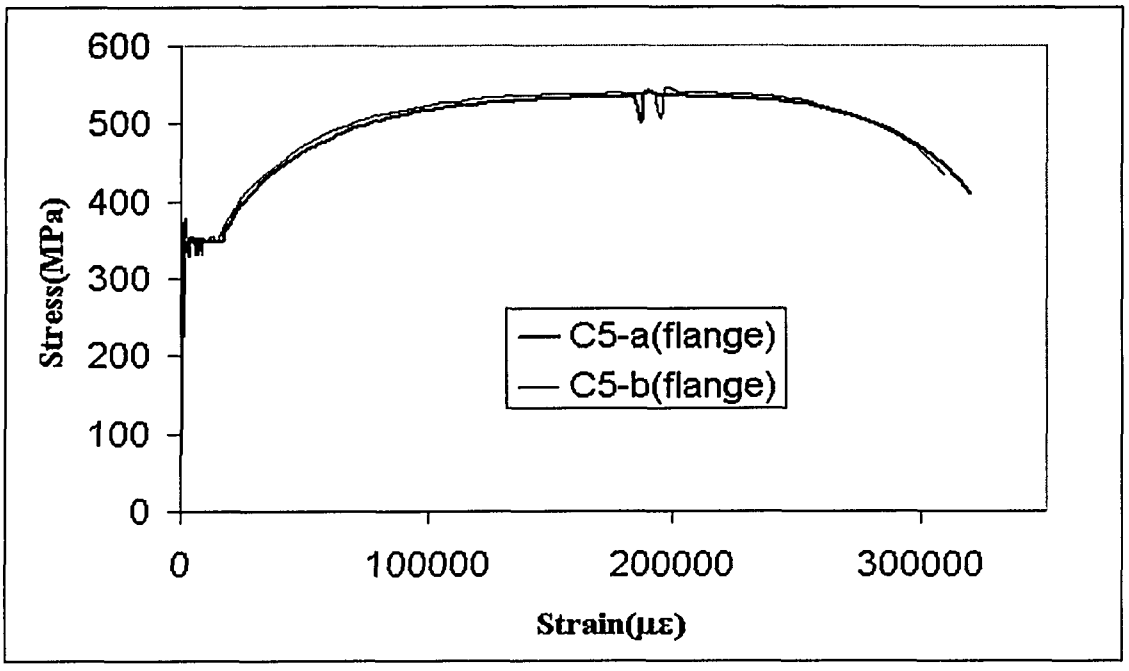

Fig. A7 Stress vs. Strain Curves of Channel Flange Coupons - C5

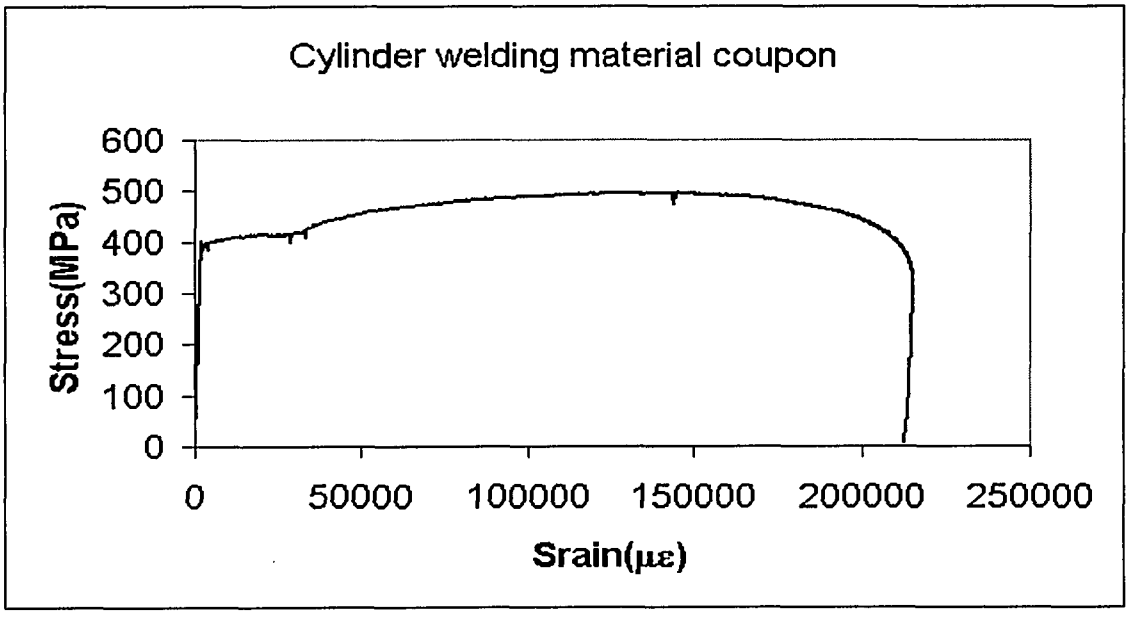

Fig. A8 Stress vs. Strain Curve of Cylindrical Weld Metal Coupon

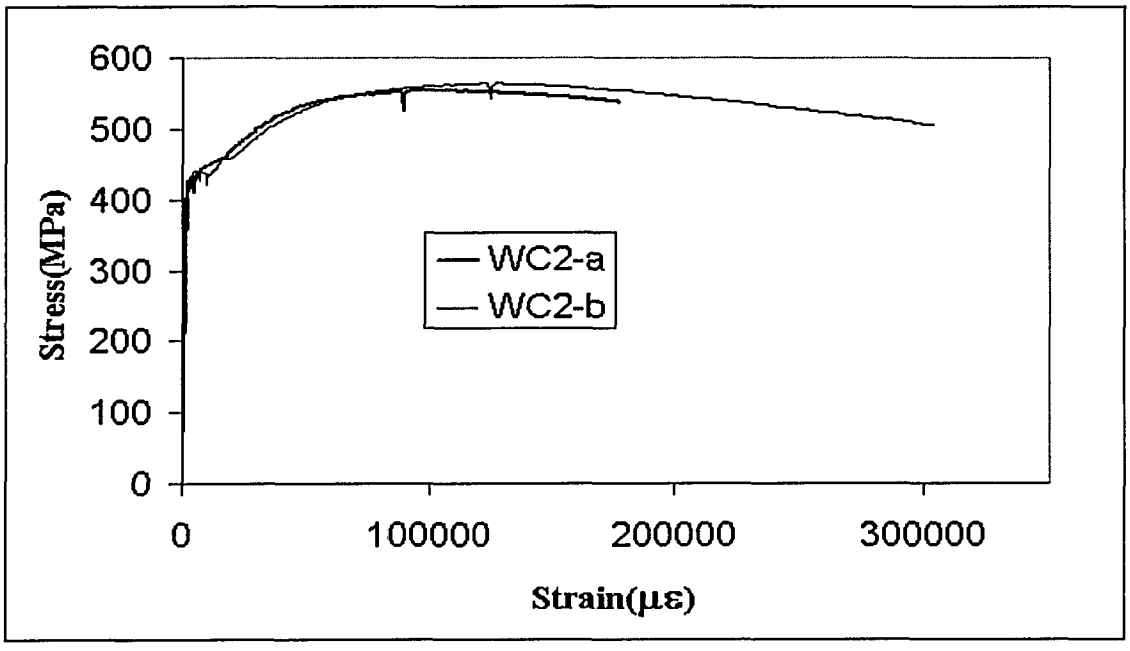

Fig. A9 Stress vs. Strain Curves of Flat Filler Weld Metal Coupons

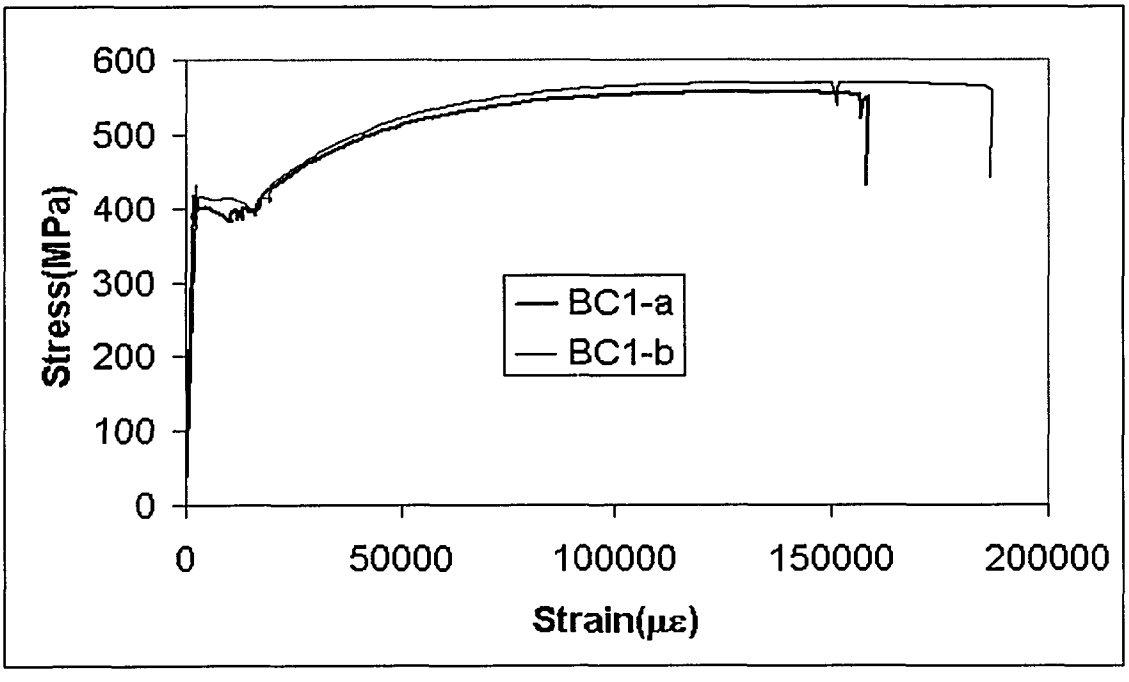

Fig. A10 Stress vs. Strain Curves of Gusset Plate Coupons

APPENDIX B

Load vs. Strain Curves and Comparison of Strains at Different Load Levels

This appendix includes load vs. strain curves for all specimens and comparison of strains at different load levels. In each figure title, Fig. Bxx-yy, the first number "xx" refers to the specimen number, and the second number "yy" refers to the numbering for each specimen. Strain gauge numbering is listed in Fig. B1 and Fig. B2.

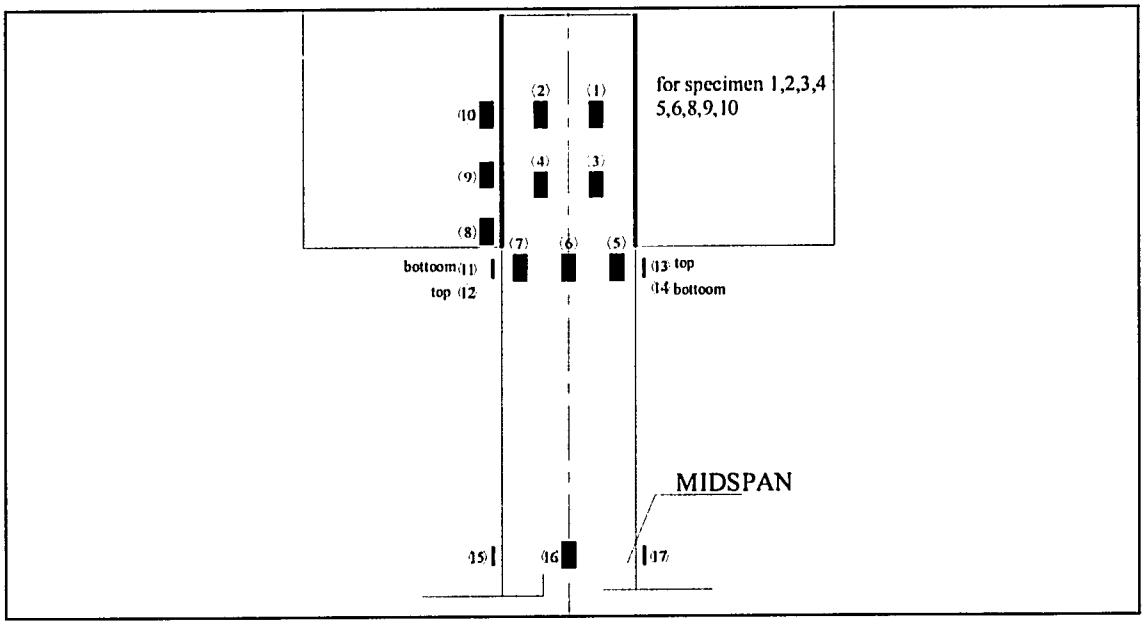

Fig. B1 Strain Gauge Numbering for Specimens 1 to 6 and 8 to 10

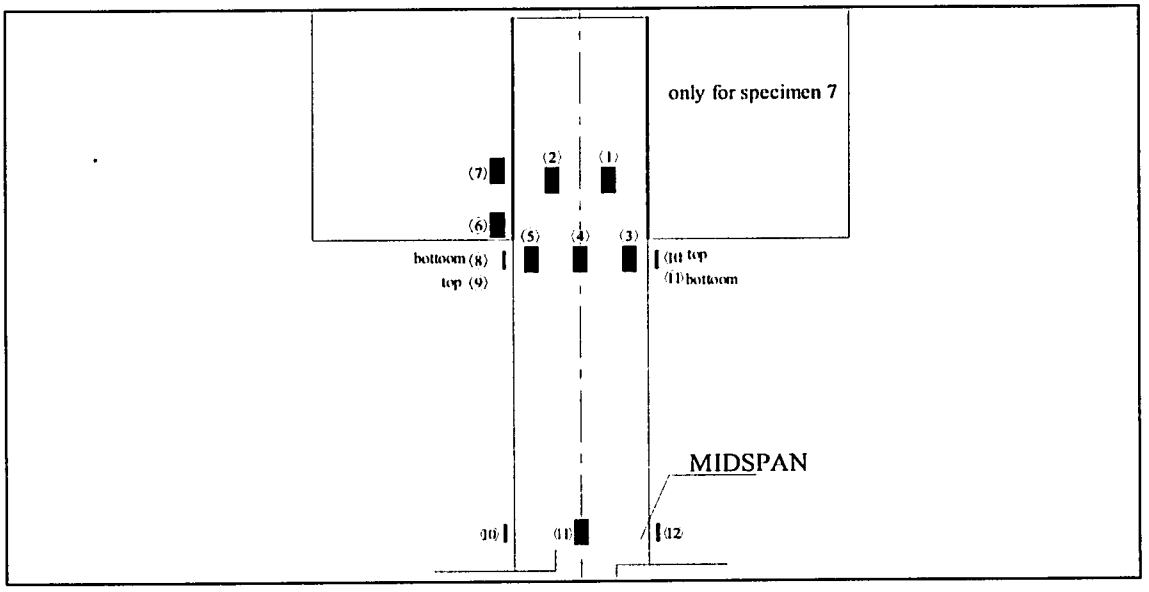

Fig. B2 Strain Gauge Numbering for Specimen 7

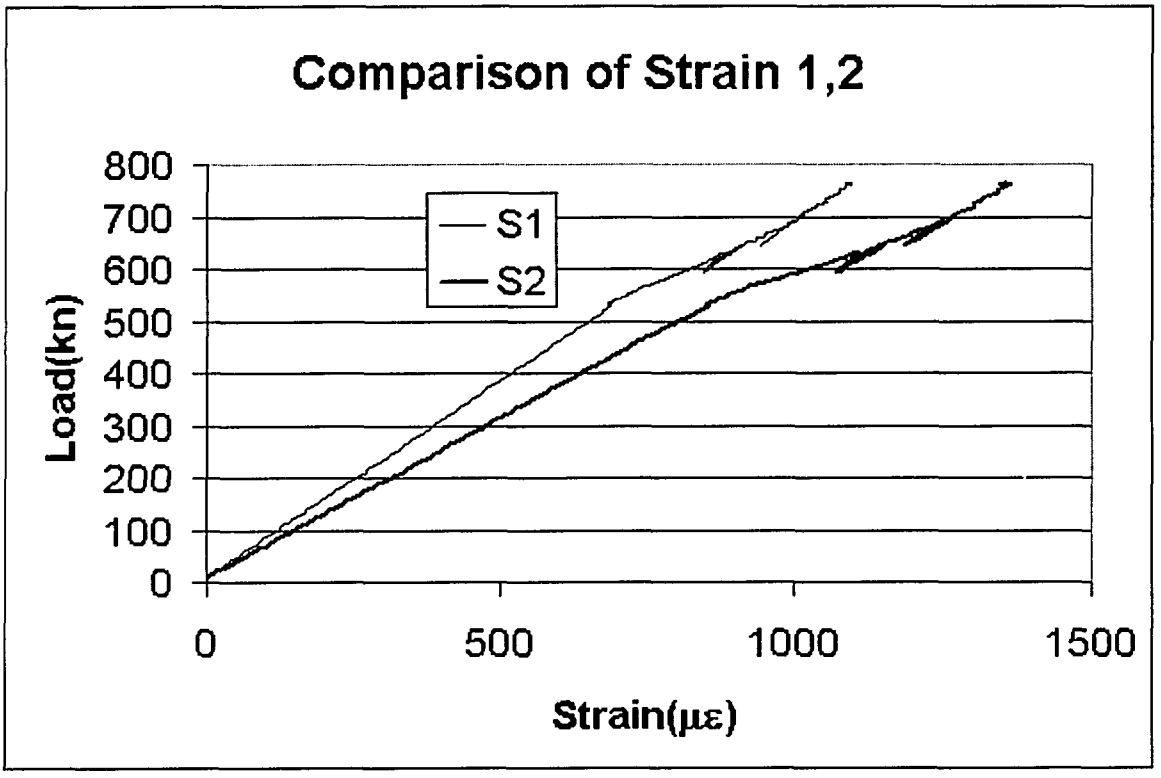

Fig. B1-1 Load vs. Strain 1, 2 of Specimen 1

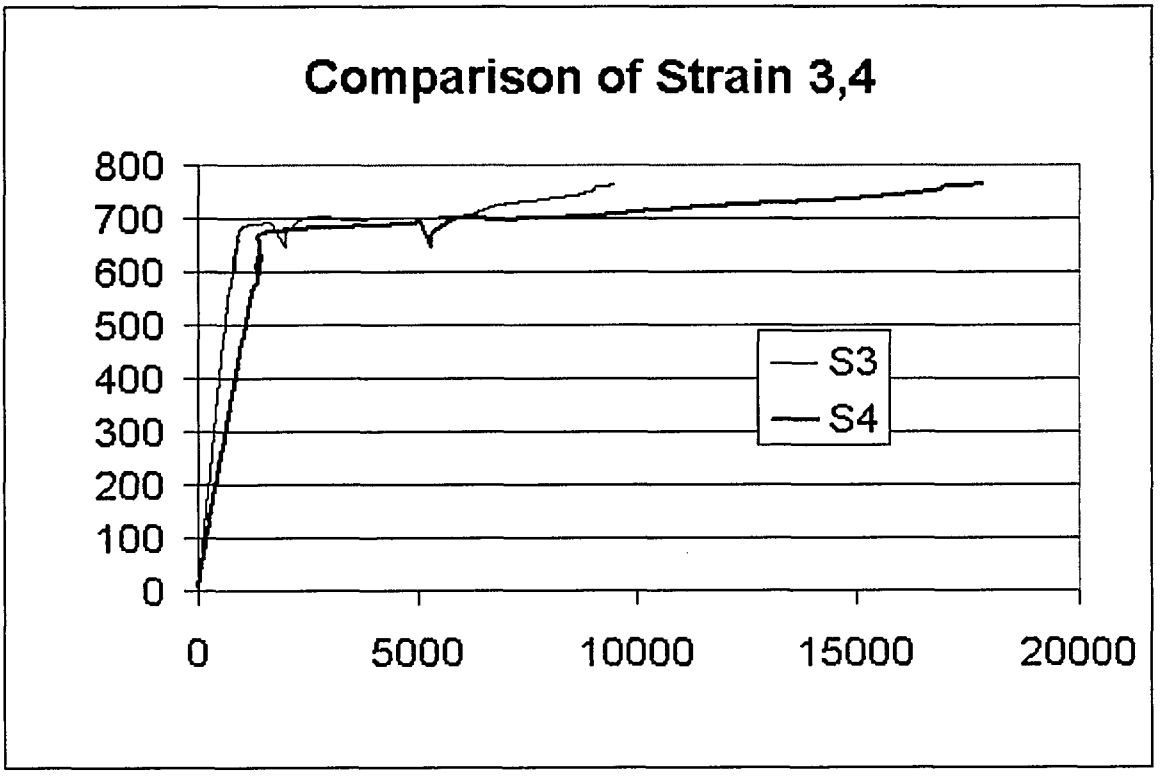

Fig. B1-2 Load vs. Strain 3, 4 of Specimen 1

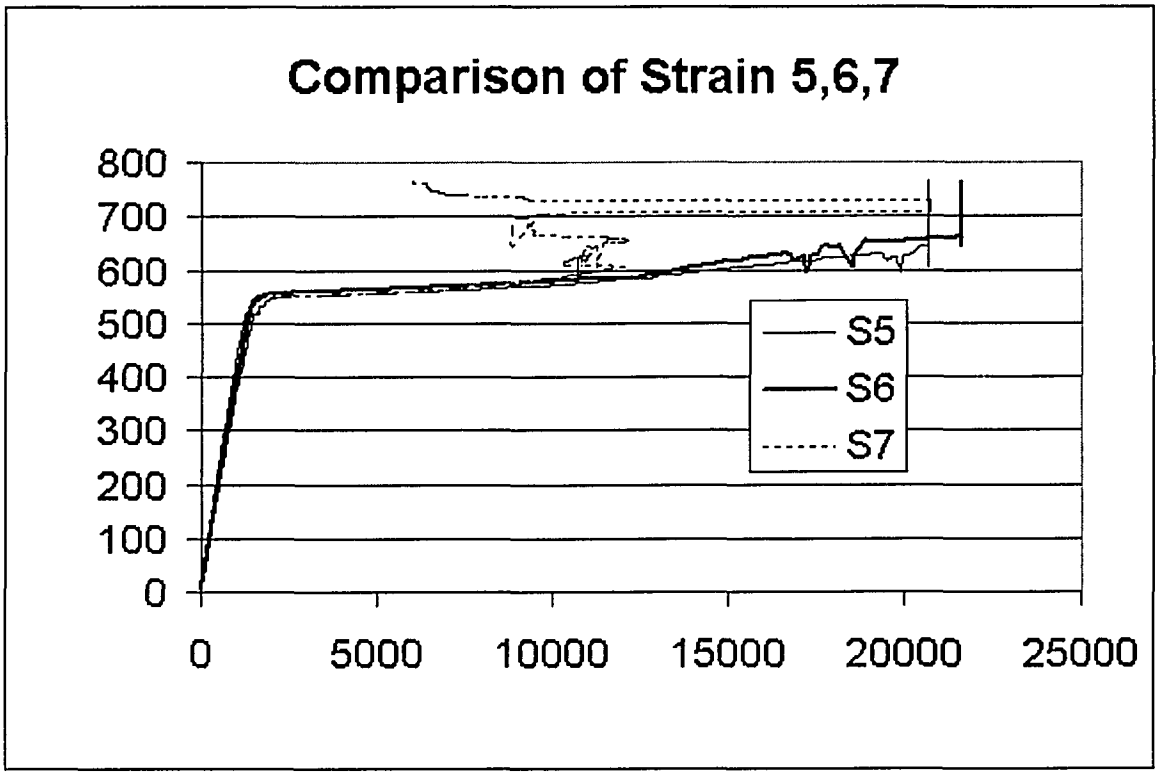

Fig. B1-3 Load vs. Strain 5, 6, 7 of Specimen 1

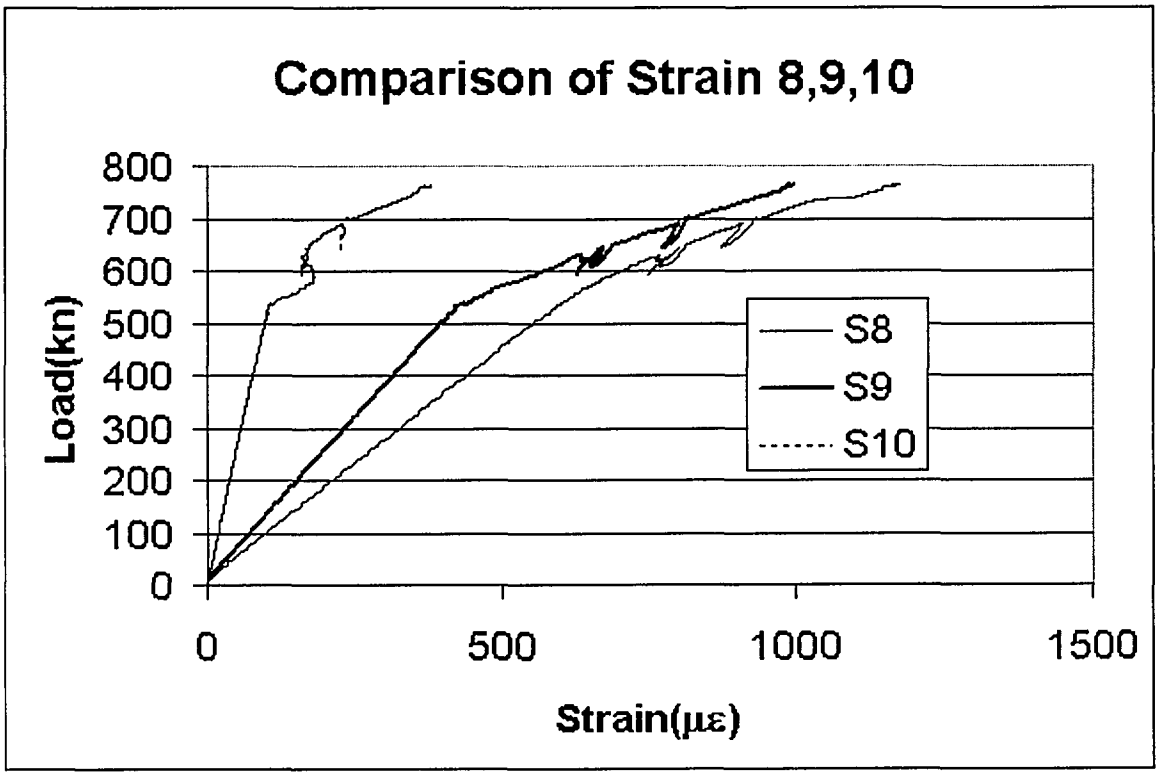

Fig. B1-4 Load vs. Strain 8, 9, 10 of Specimen 1

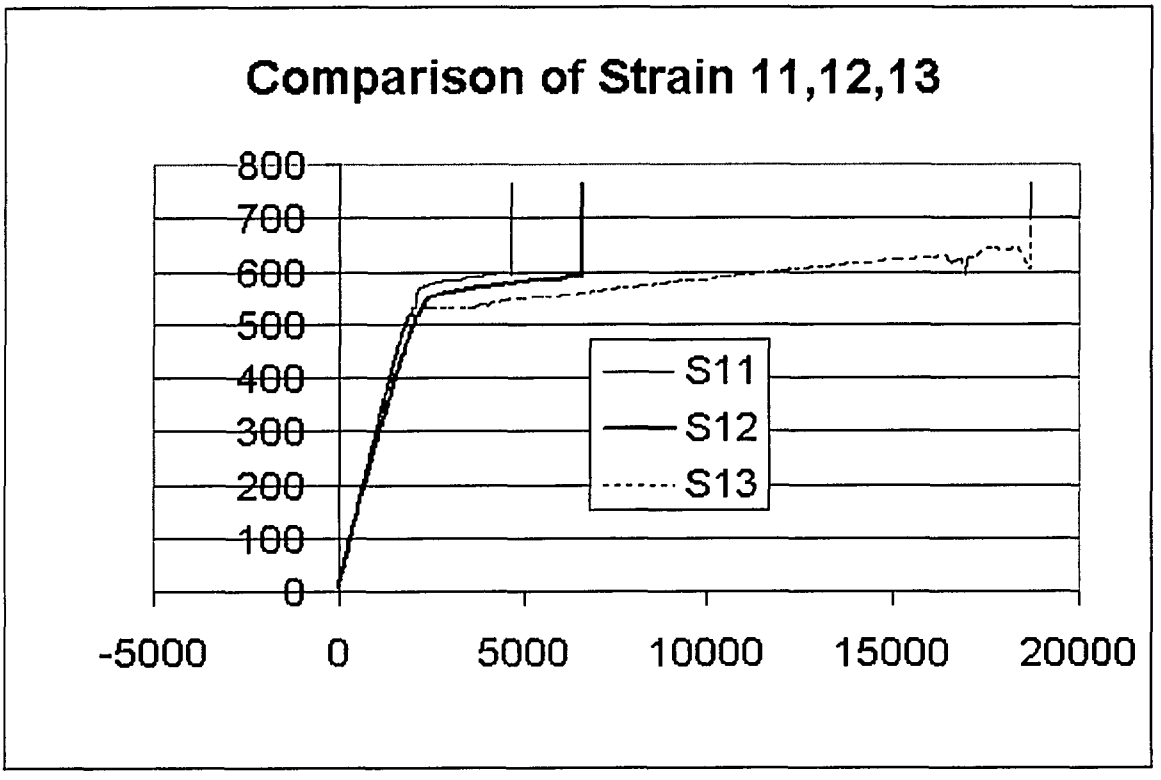

Fig. B1-5 Load vs. Strain 11, 12, 13 of Specimen 1

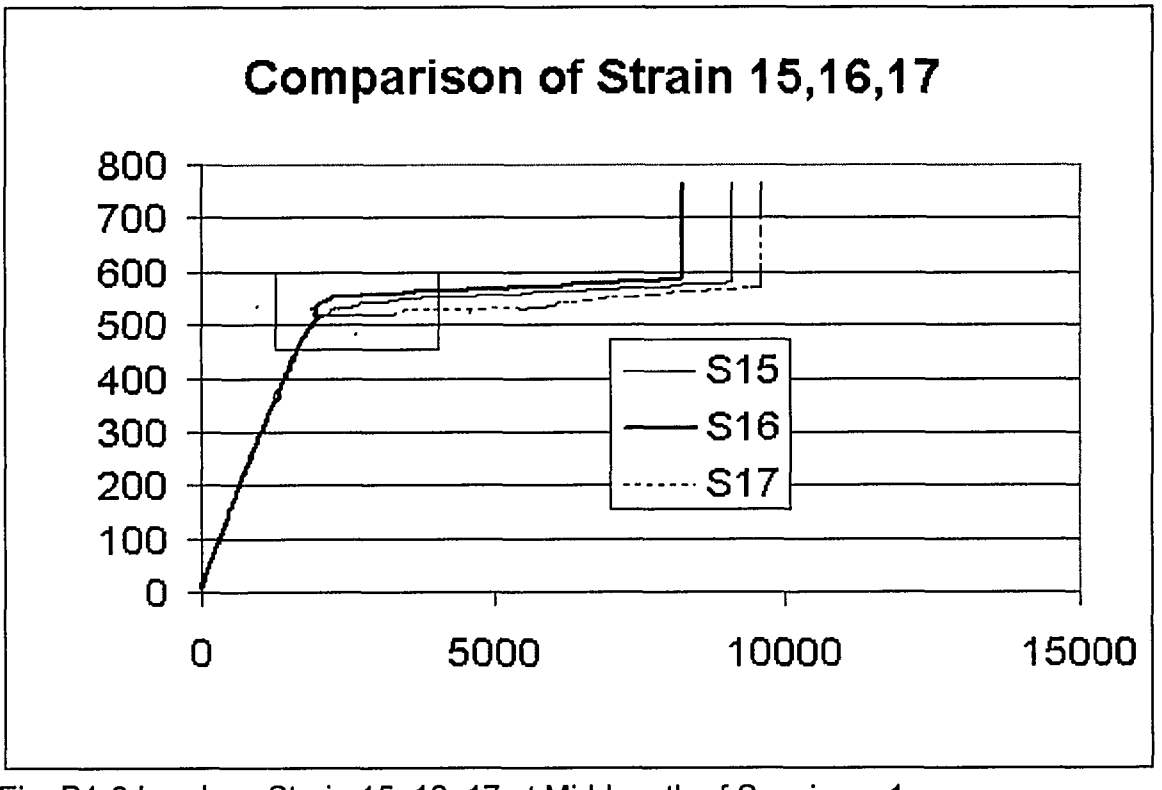

Fig. B1-6 Load vs. Strain 15, 16, 17 at Mid-length of Specimen 1

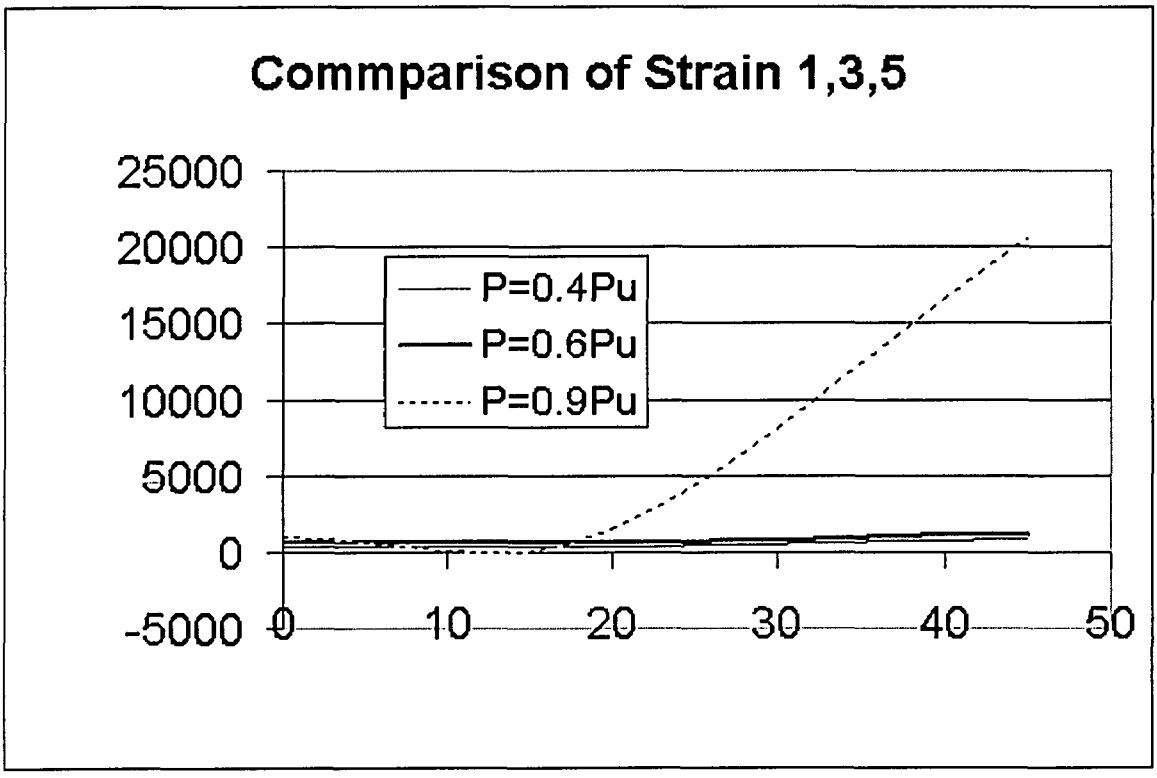

Fig. B1-7 Comparison of Strain 1, 3, 5 at Different Load Levels of Specimen 1

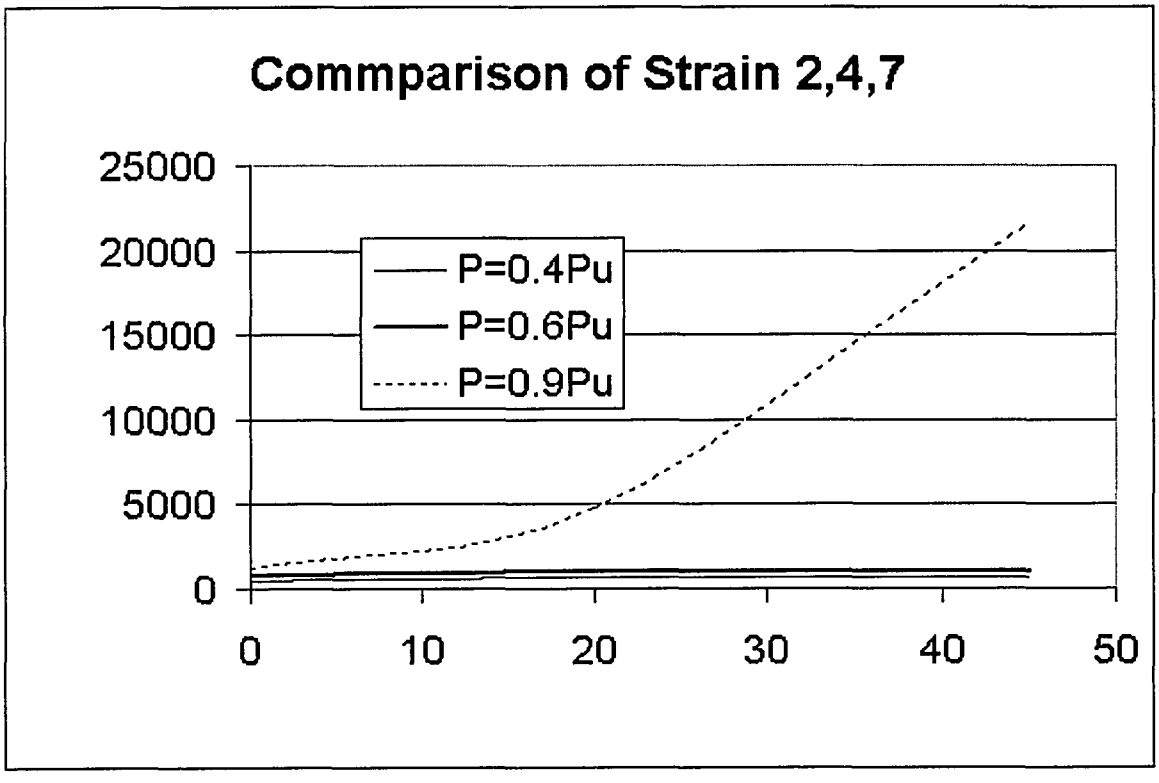

Fig. B1-8 Comparison of Strain 2, 4, 7 at Different Load Levels of Specimen 1

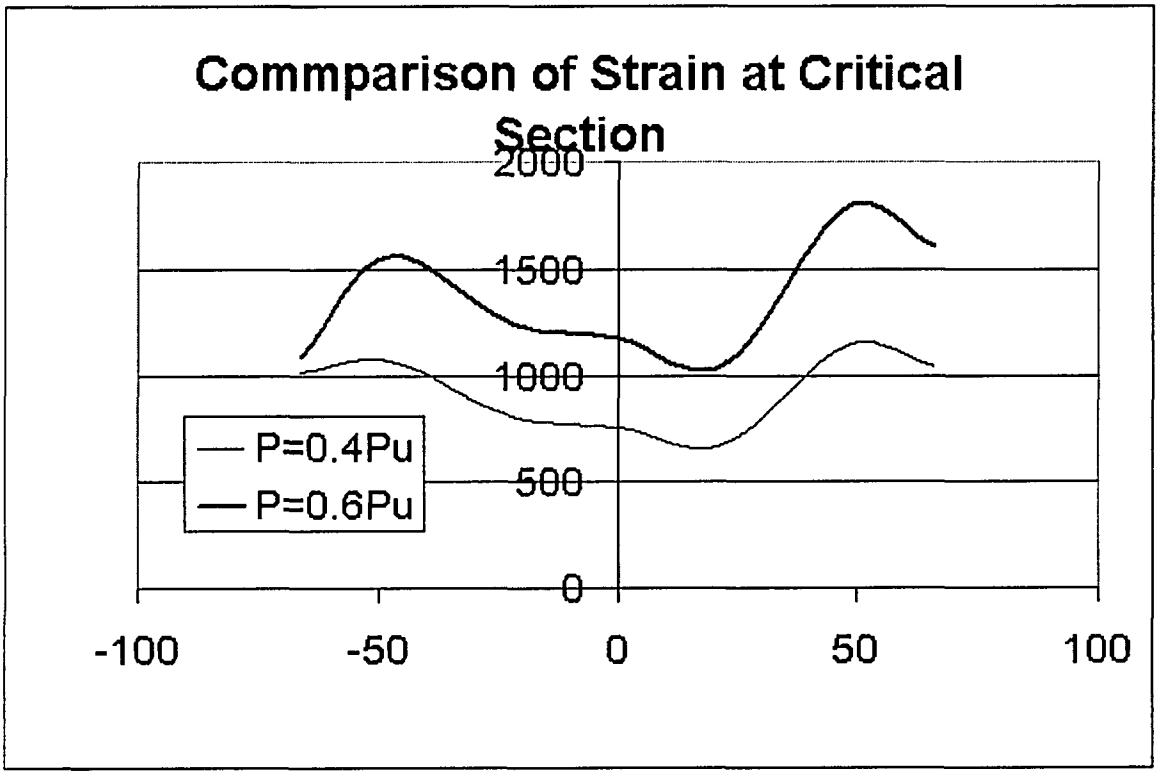

Fig. B1-9 Comparison of Strain at Critical Section at Different Load Levels of Specimen 1

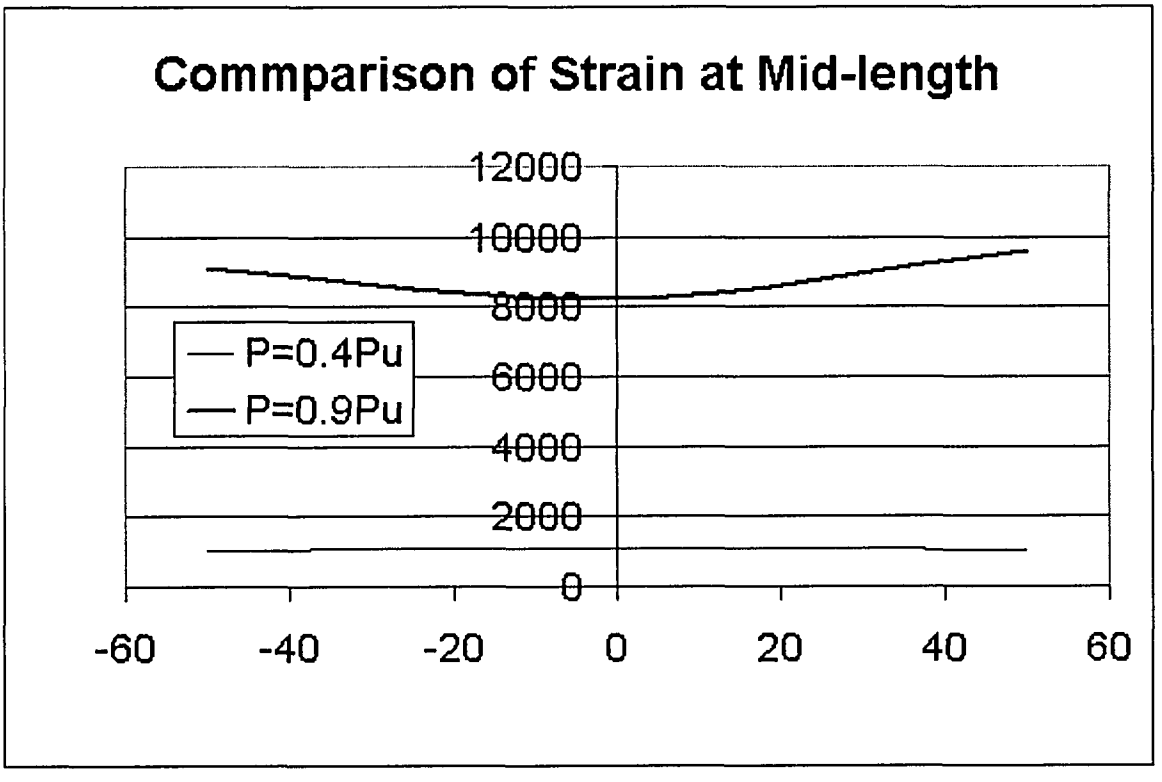

Fig. B1-10 Comparison of Strain at Mid-length at Different Load Levels of Specimen 1

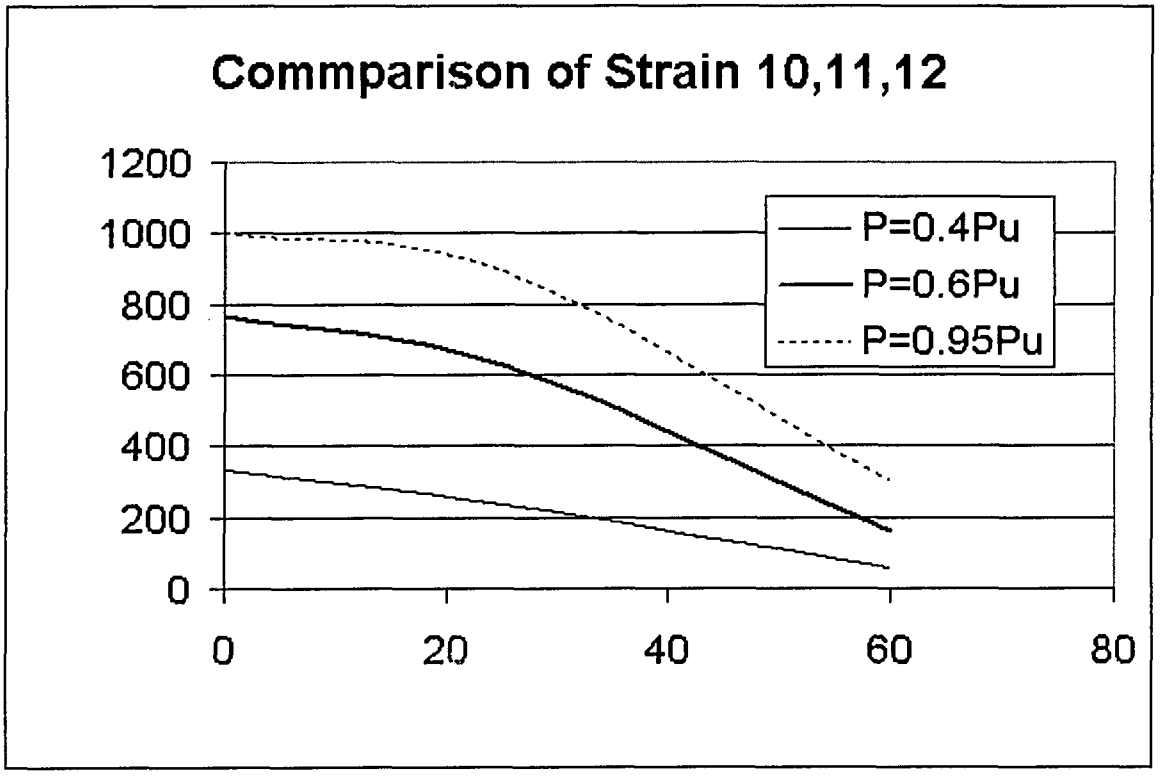

Fig. B1-11 Comparison of Strain 8, 9, 10 at Different Load Levels of Specimen 1

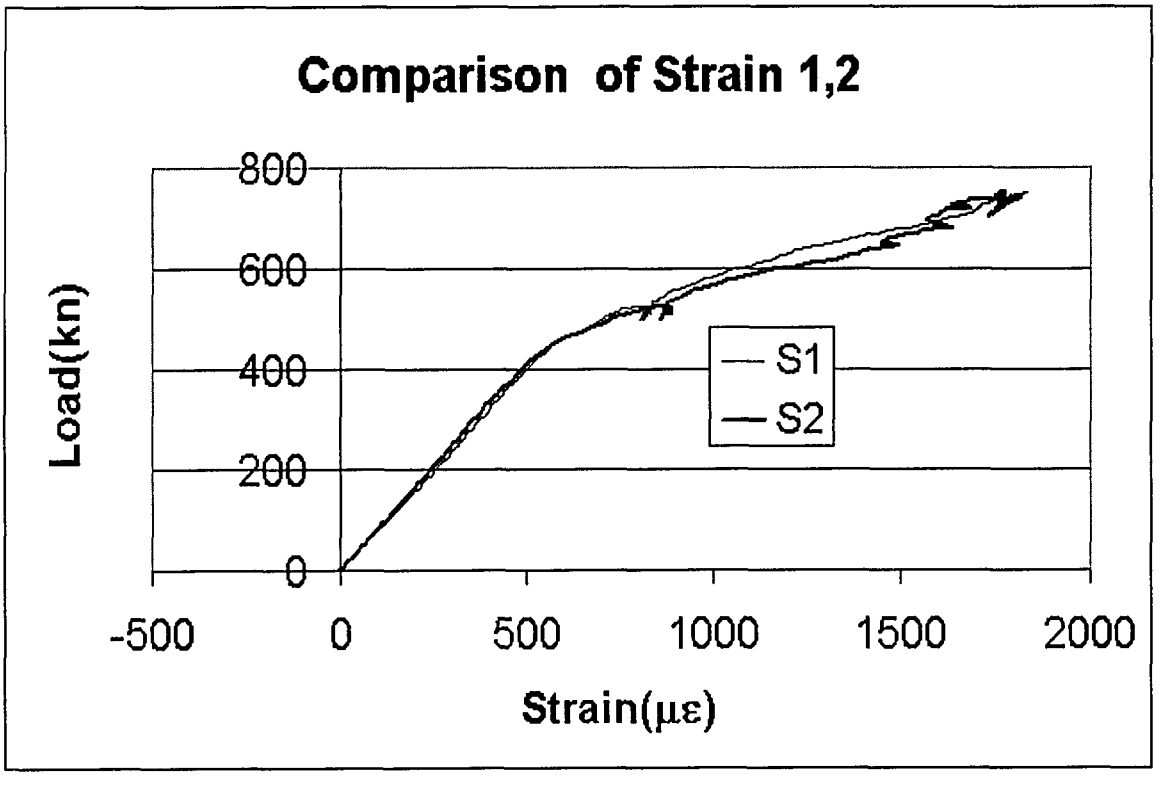

Fig. B2-1 Load vs. Strain 1, 2 of Specimen 2

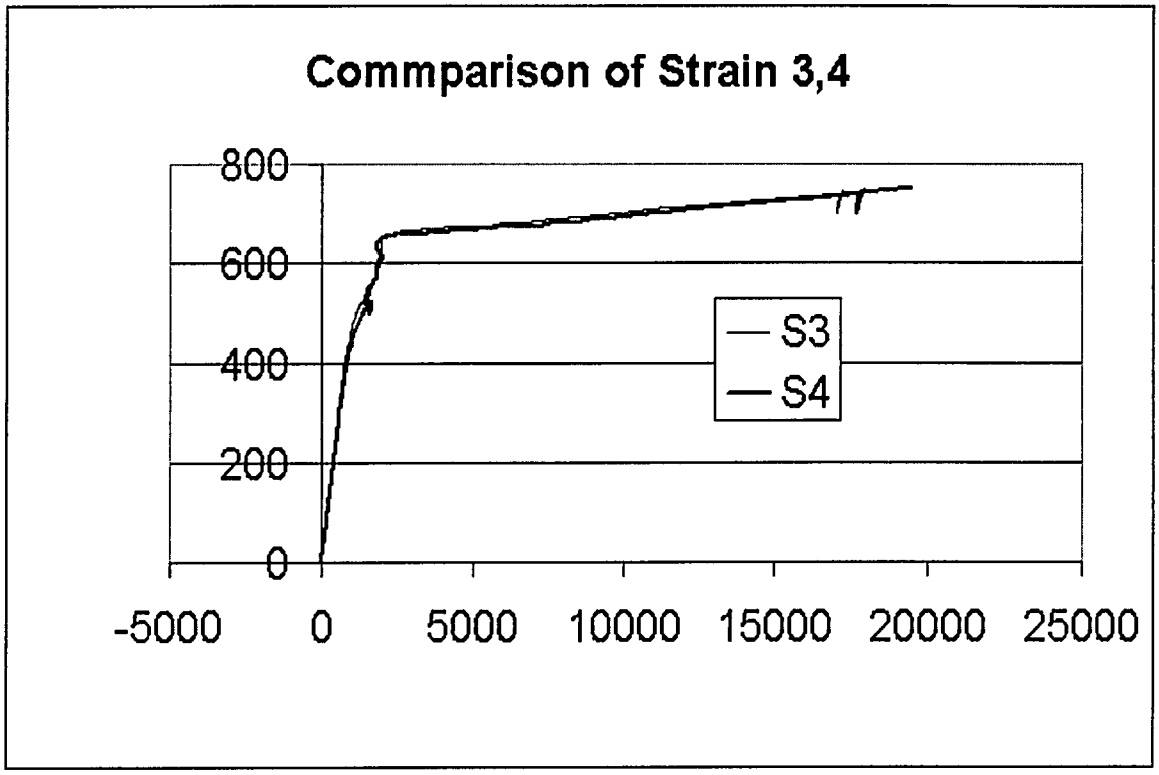

Fig. B2-2 Load vs. Strain 3,4 of Specimen 2

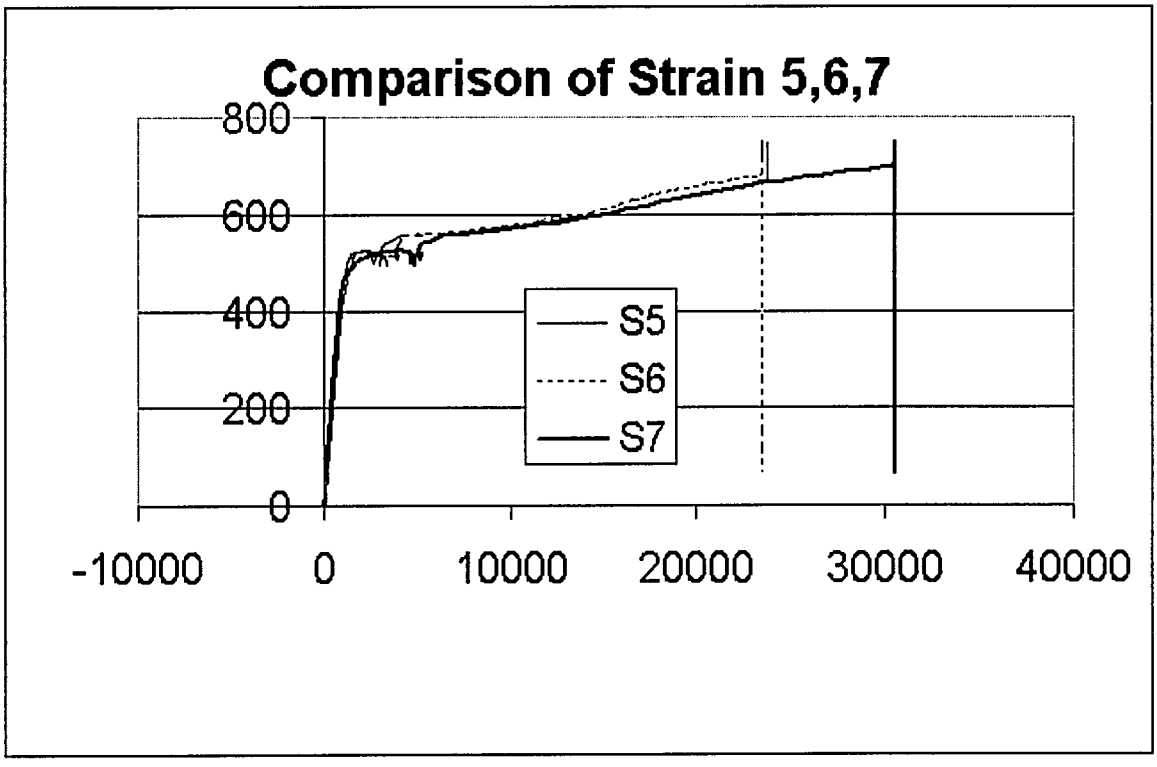

Fig. B2-3 Load vs. Strain 5,6,7 of Specimen 2

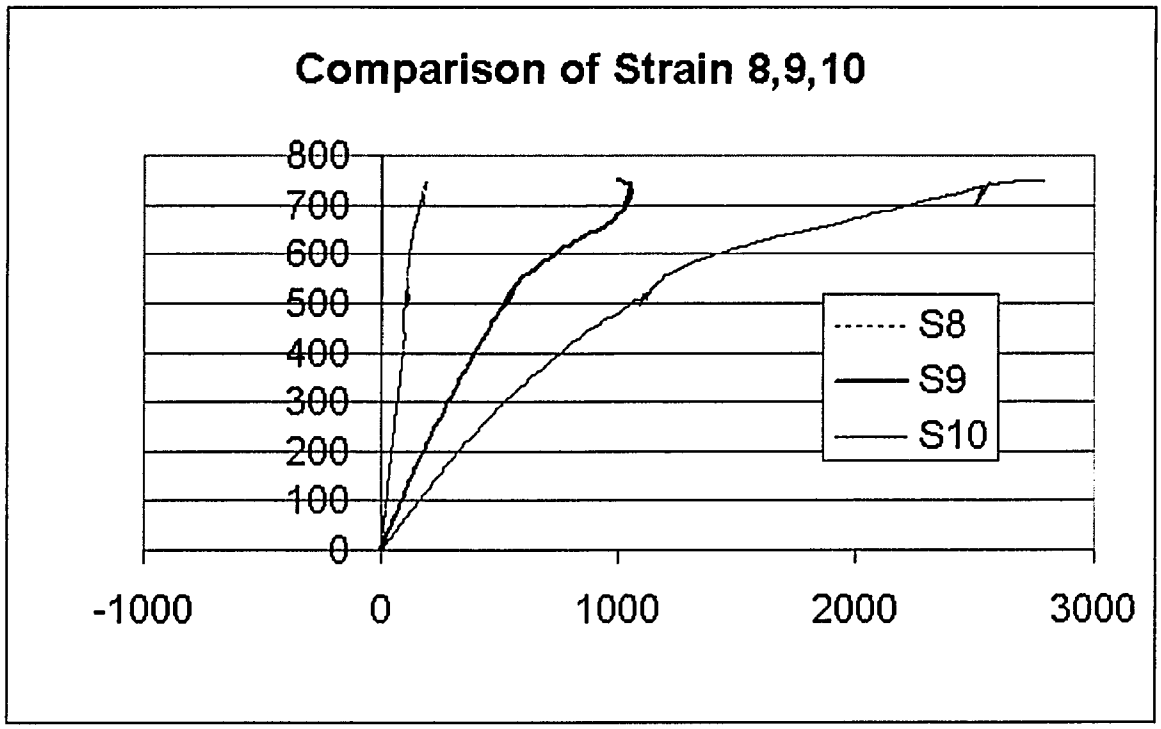

Fig. B2-4 Load vs. Strain 8,9,10 of Specimen 2

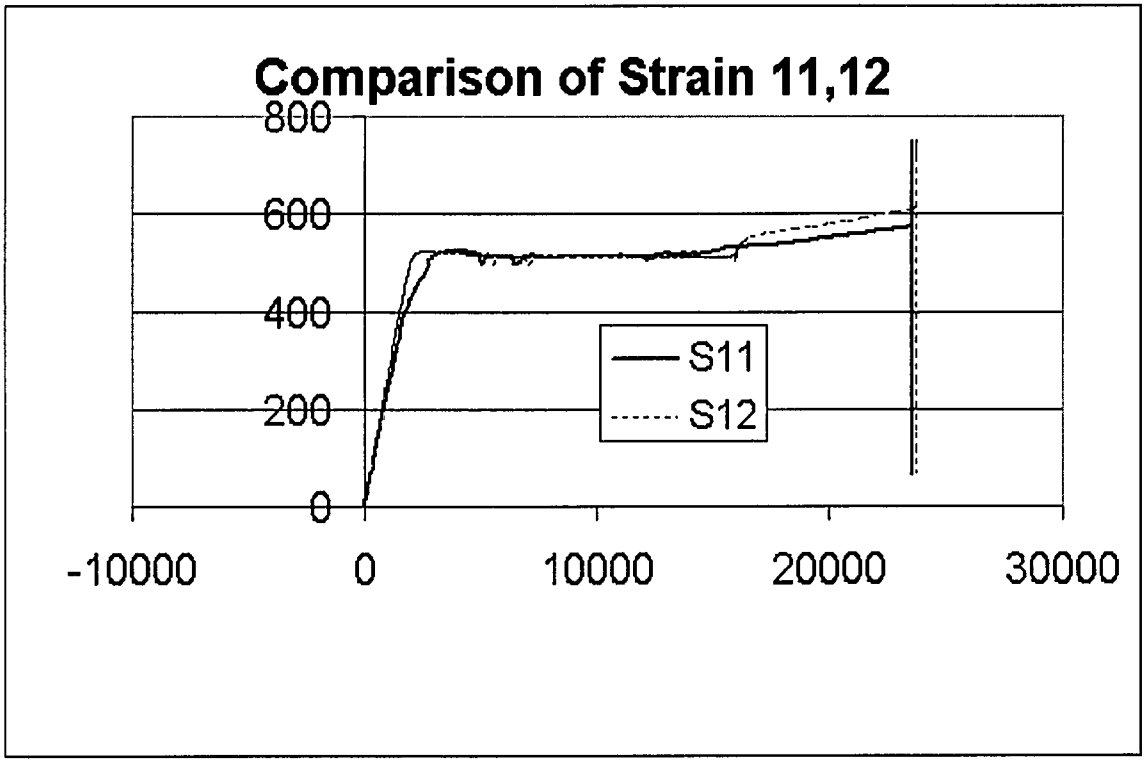

Fig. B2-5 Load vs. Strain 11,12 of Specimen 2

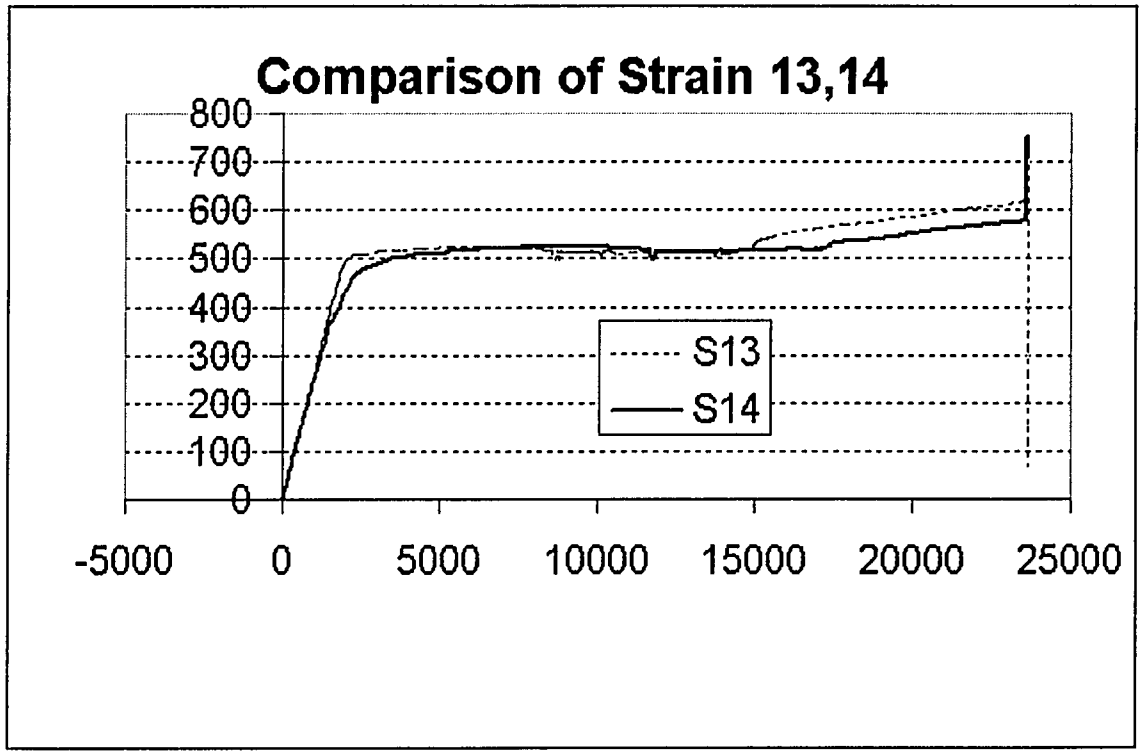

Fig. B2-6 Load vs. Strain 13,14 of Specimen 2

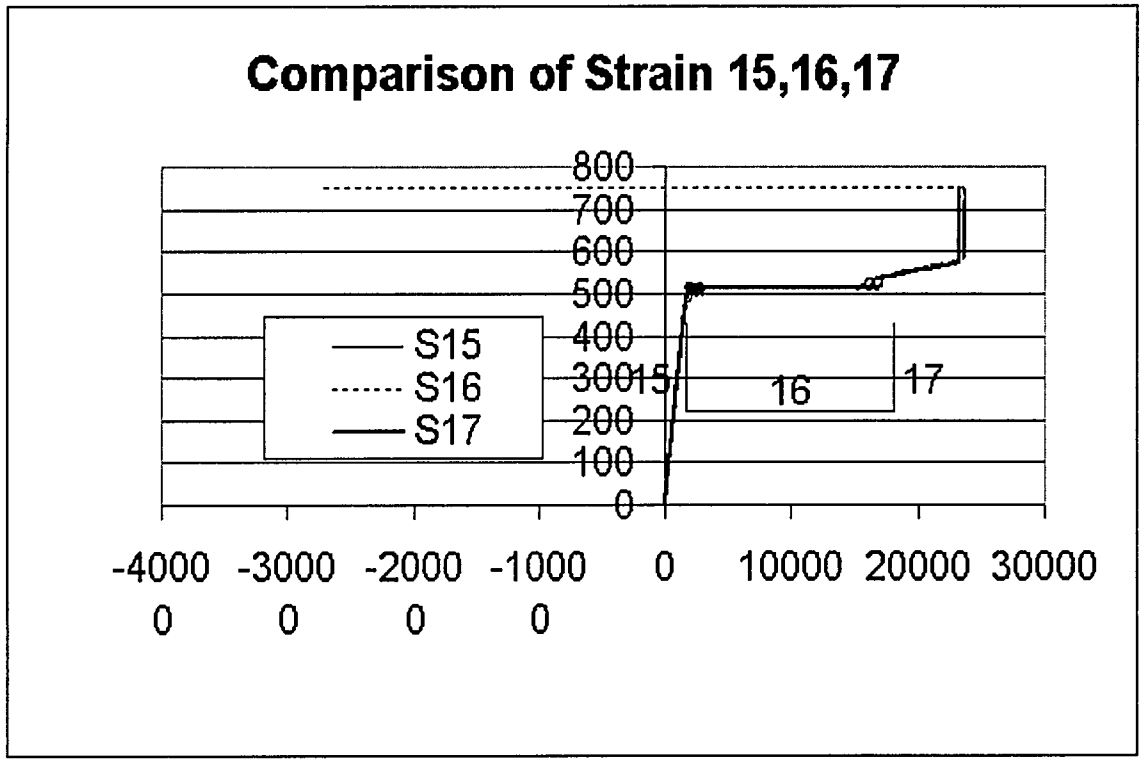

Fig. B2-7 Load vs. Strain 15,16,17 at mid-length of Specimen 2

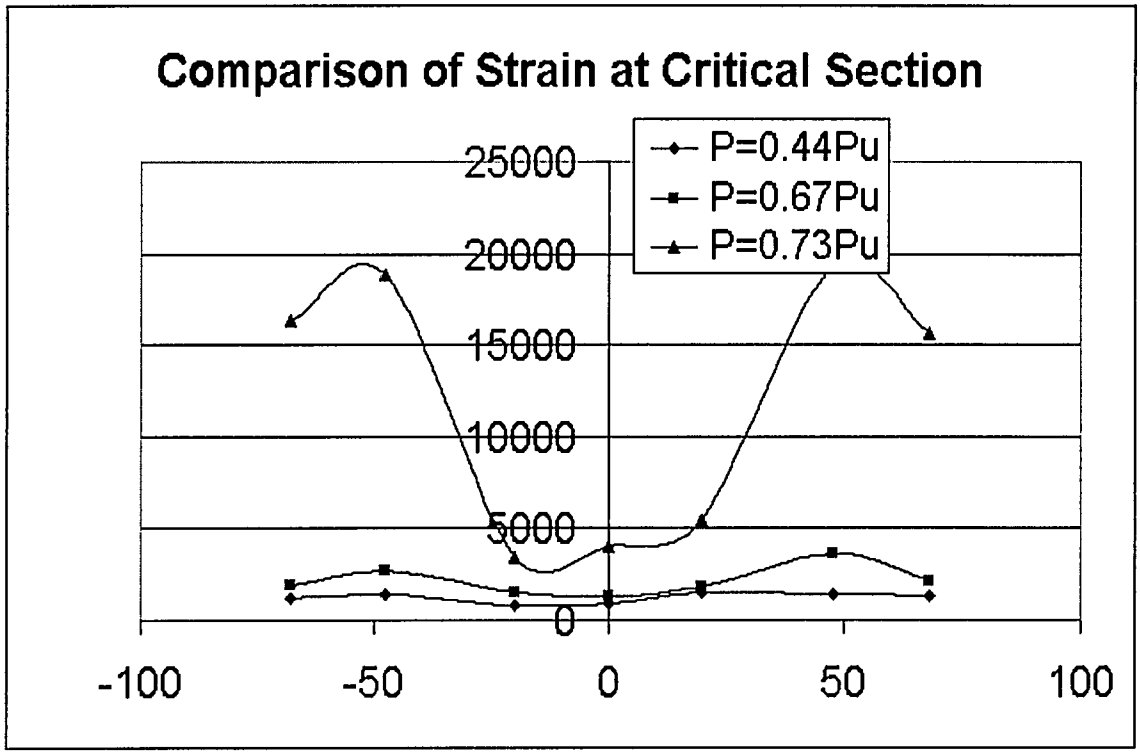

Fig. B2-8 Comparison of Strain at Critical Section at Different Load Level of Specimen 2

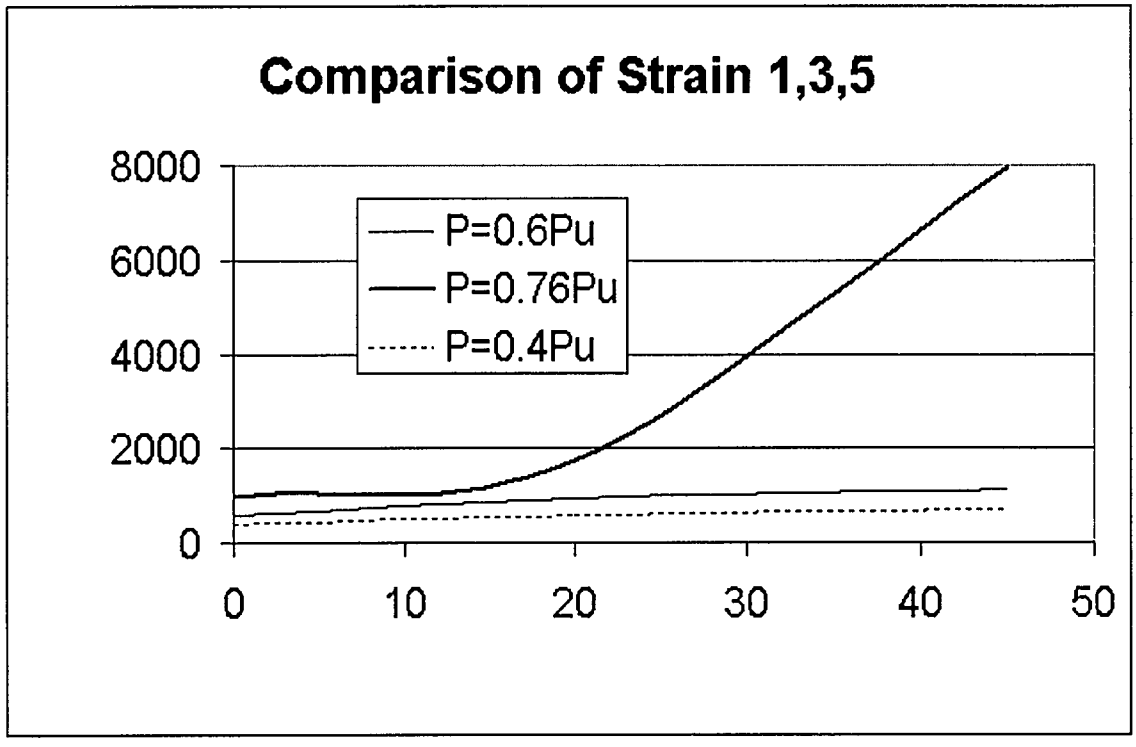

Fig. B2-9 Comparison of Strain 1,3,5 at Different Load Level of Specimen 2

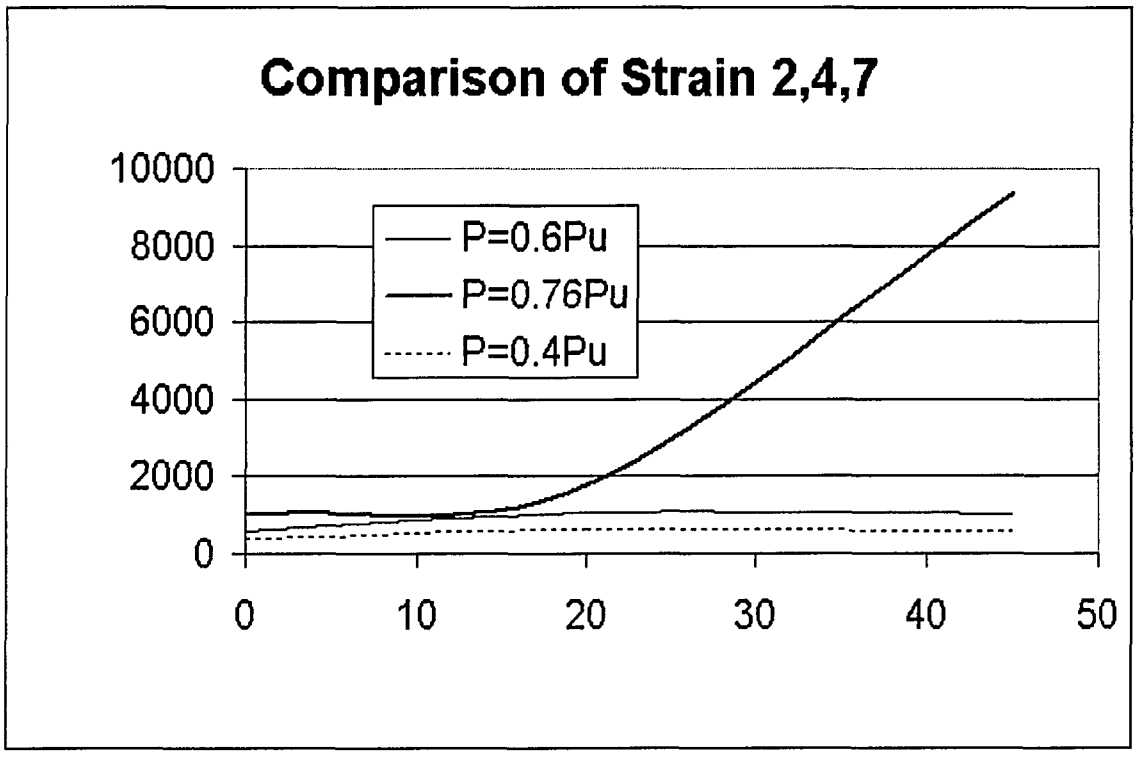

Fig. B2-10 Comparison of Strain 2,4,7 at Different Load Level of Specimen 2

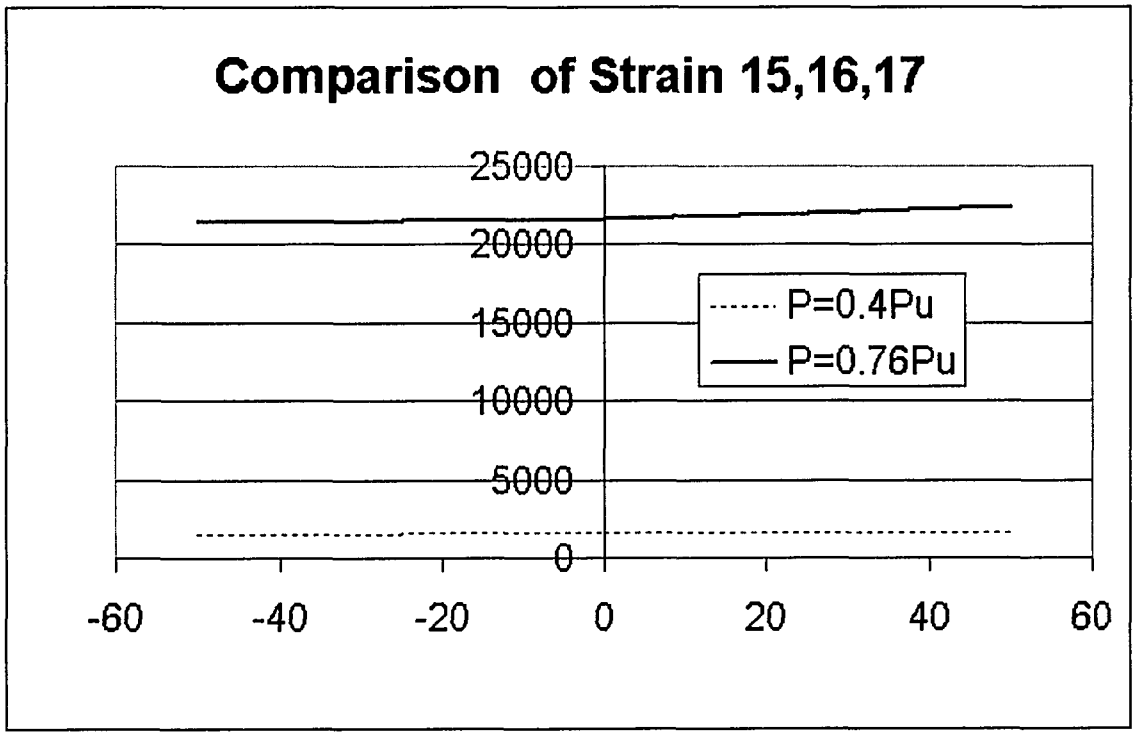

Fig. B2-11 Comparison of Strain 15,16,17 at Different Load Level of Specimen 2

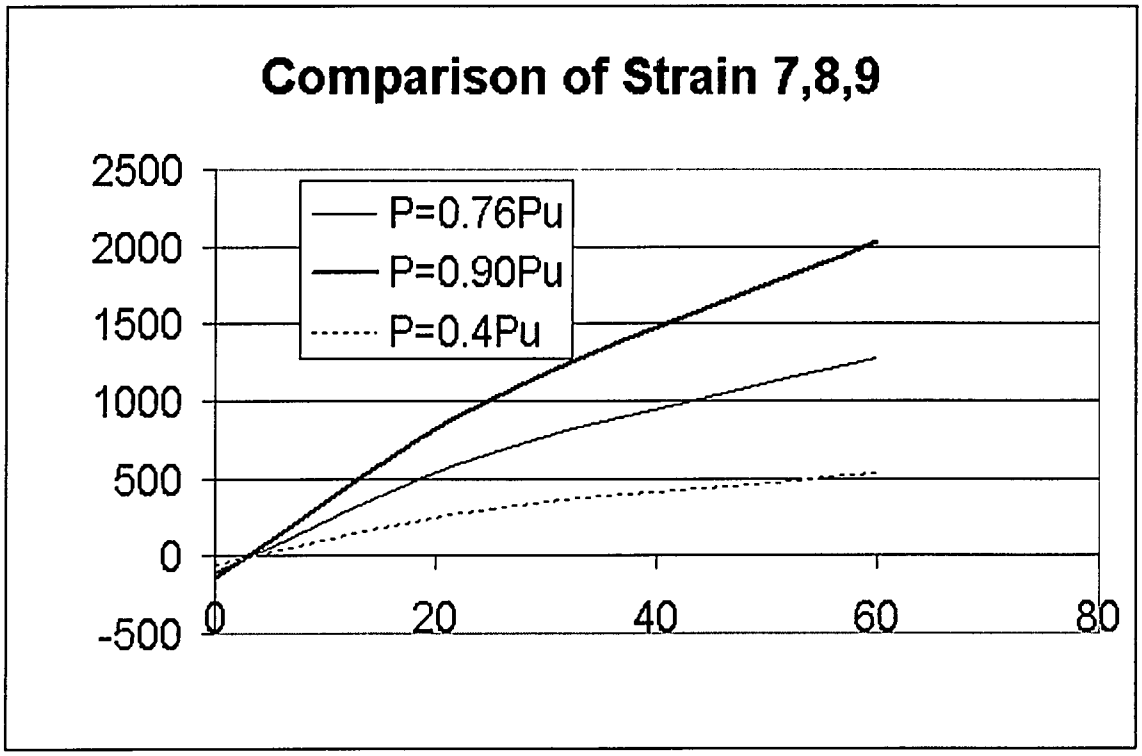

Fig. B2-12 Comparison of Strain 8,9,10 at Different Load Level of Specimen 2

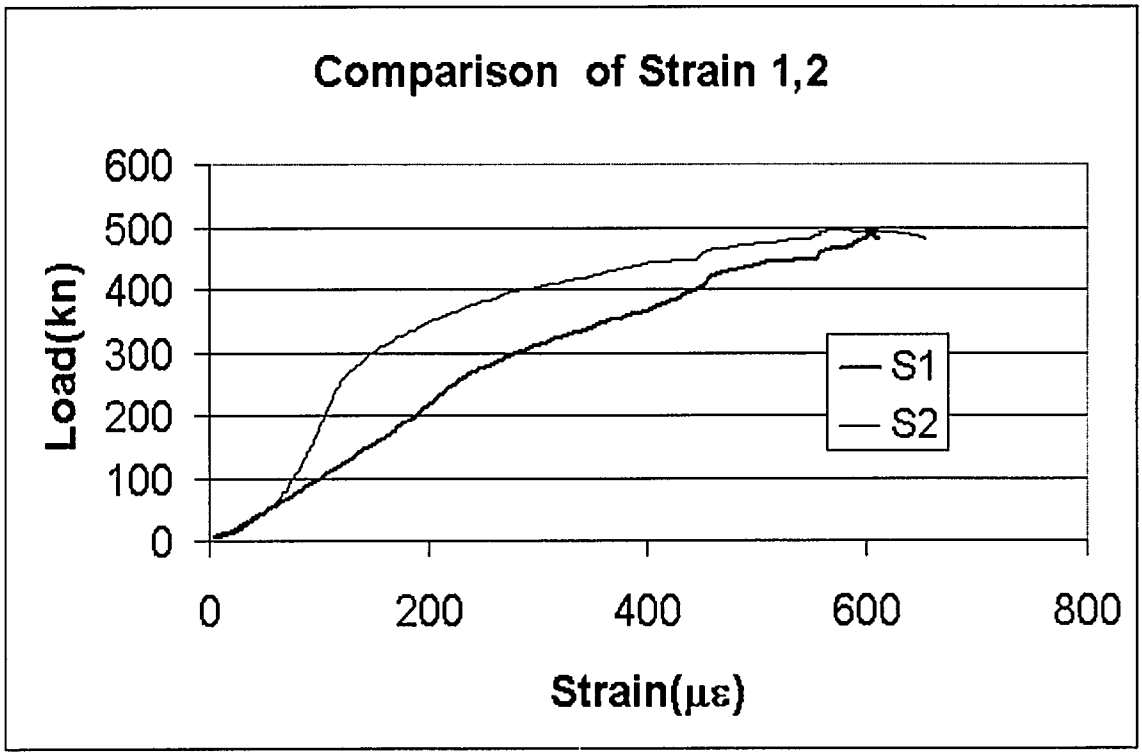

Fig. B3-1 Load vs. Strain 1,2 of Specimen 3

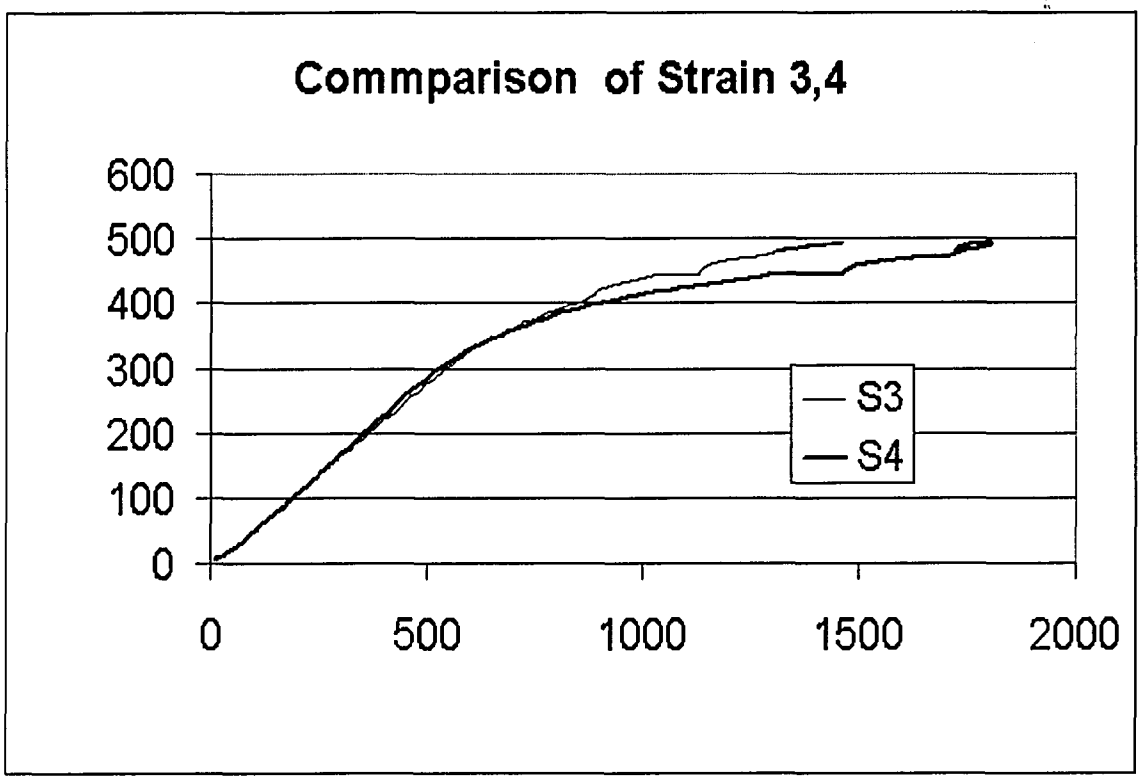

Fig. B3-2 Load vs. Strain 3,4 of Specimen 3

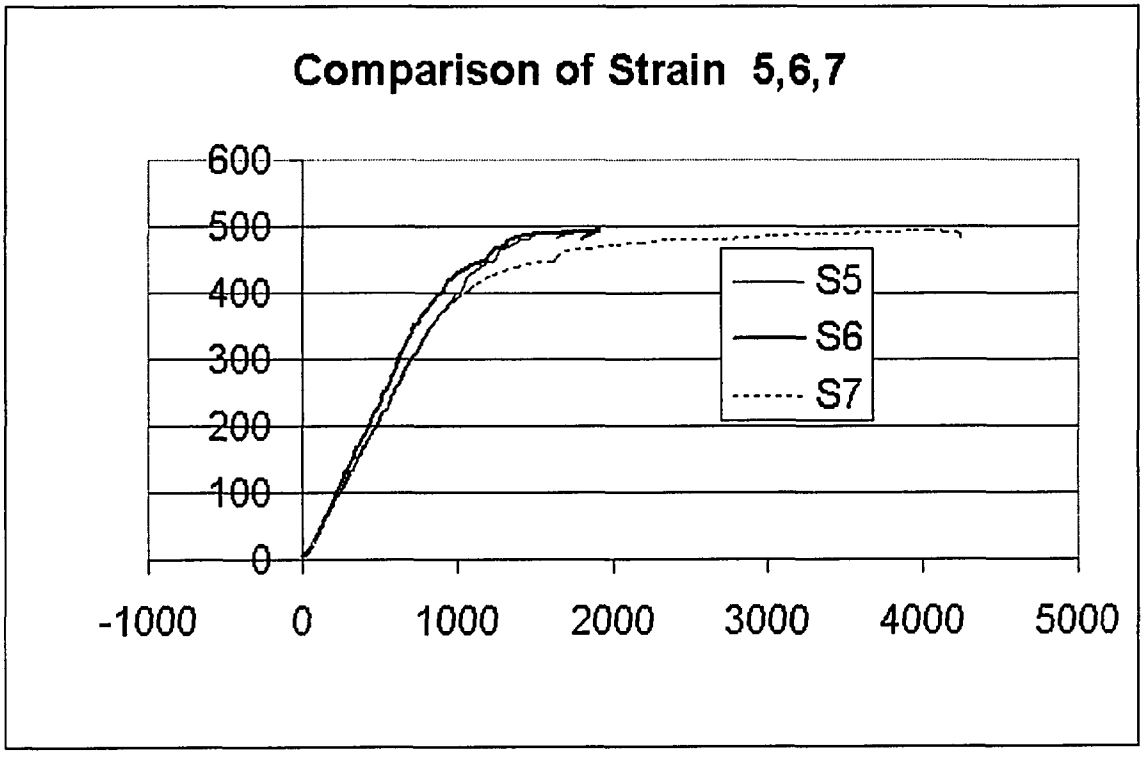

Fig. B3-3 Load vs. Strain 5,6,7 of Specimen 3

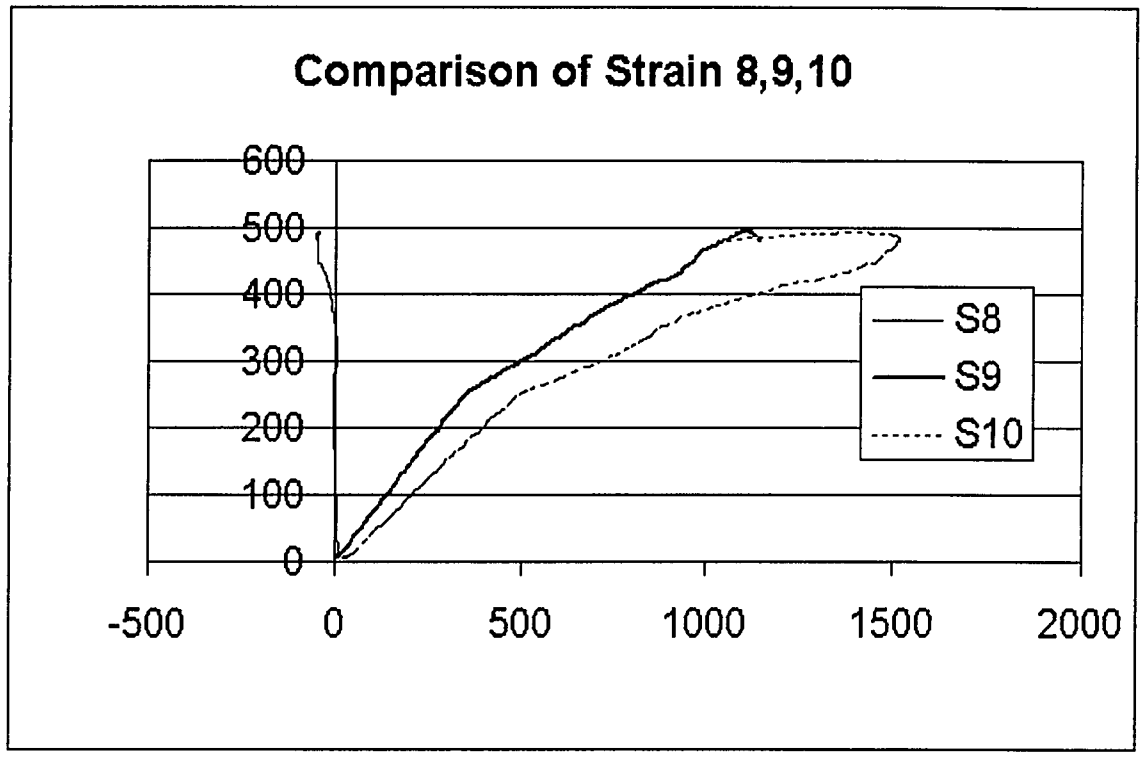

Fig. B3-4 Load vs. Strain 8,9,10 of Specimen 3

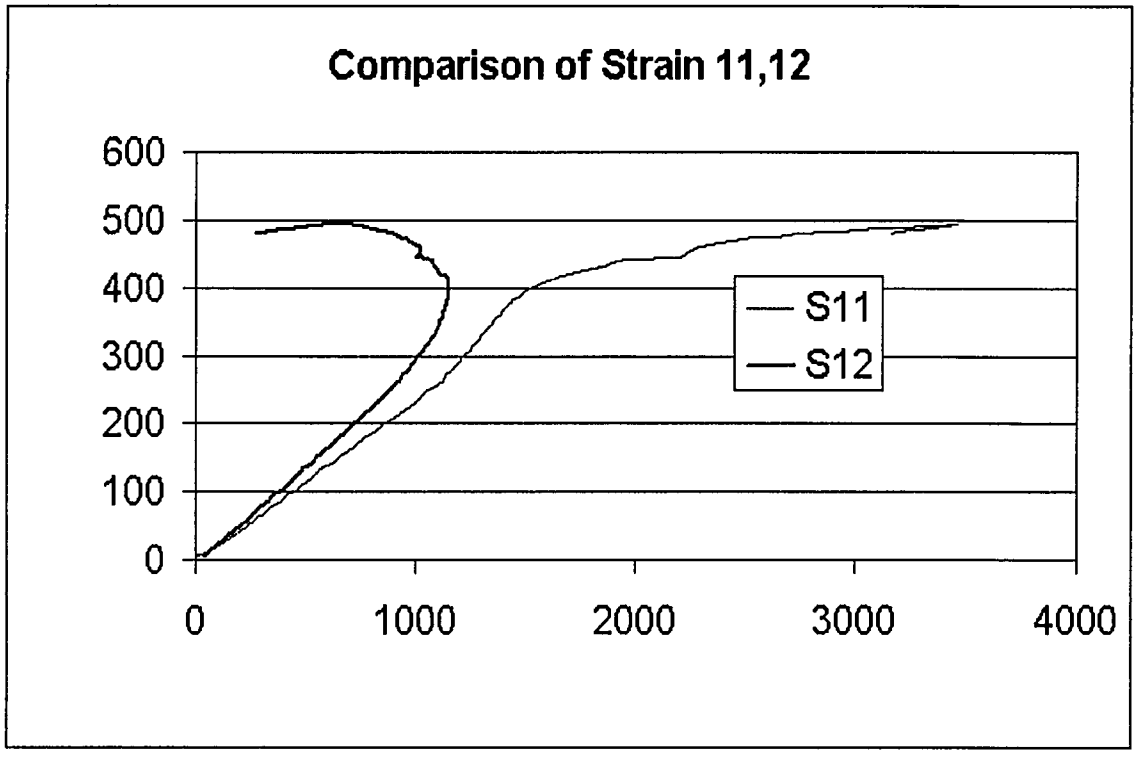

Fig. B3-5 Load vs. Strain 11,12 of Specimen 3

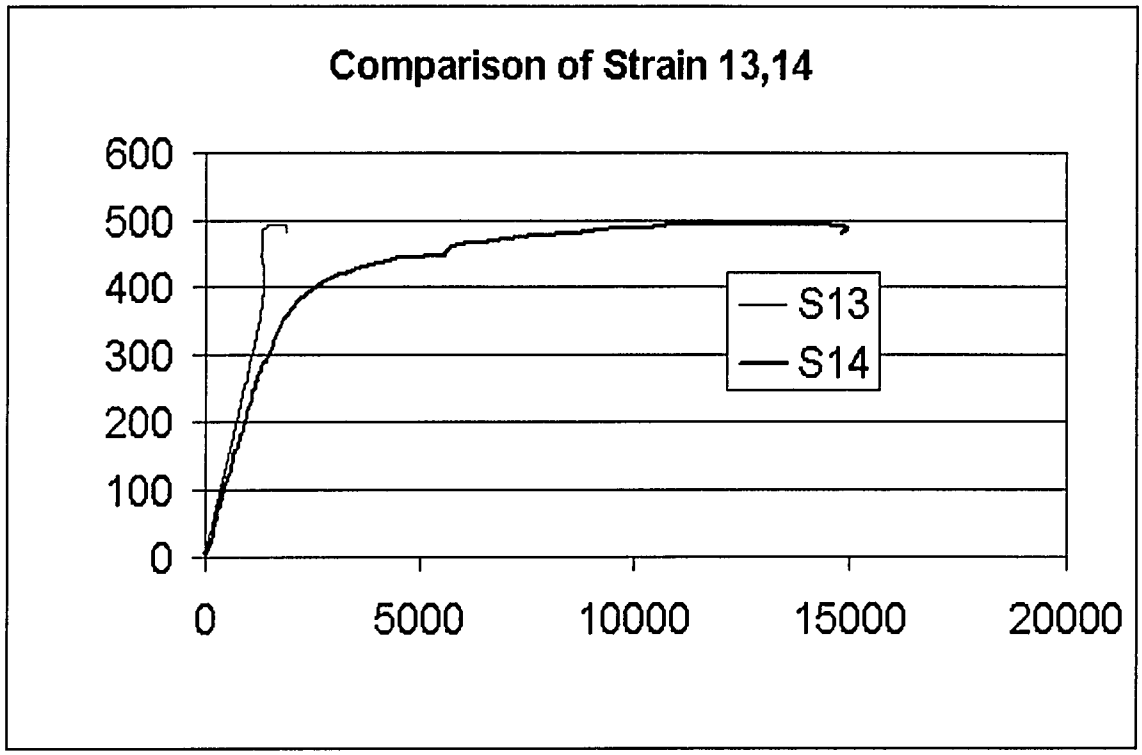

Fig. B3-6 Load vs. Strain 13,14 of Specimen 3

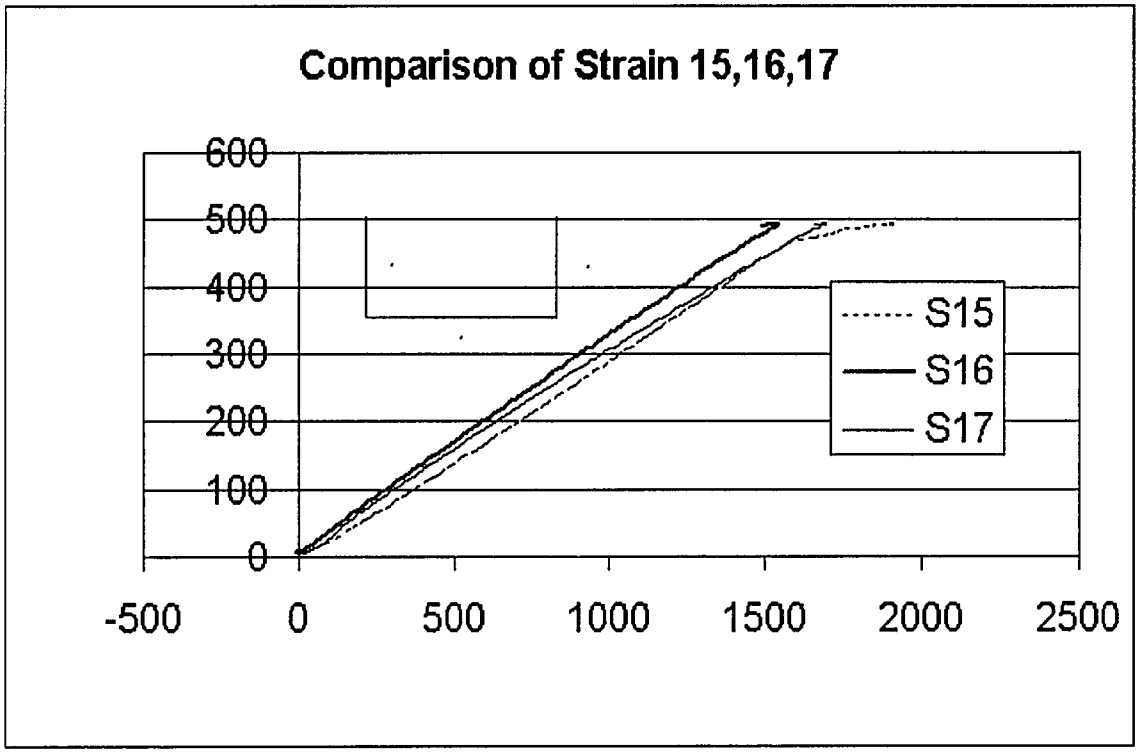

Fig. B3-7 Load vs. Strain 15,16,17 at mid-length of Specimen 3

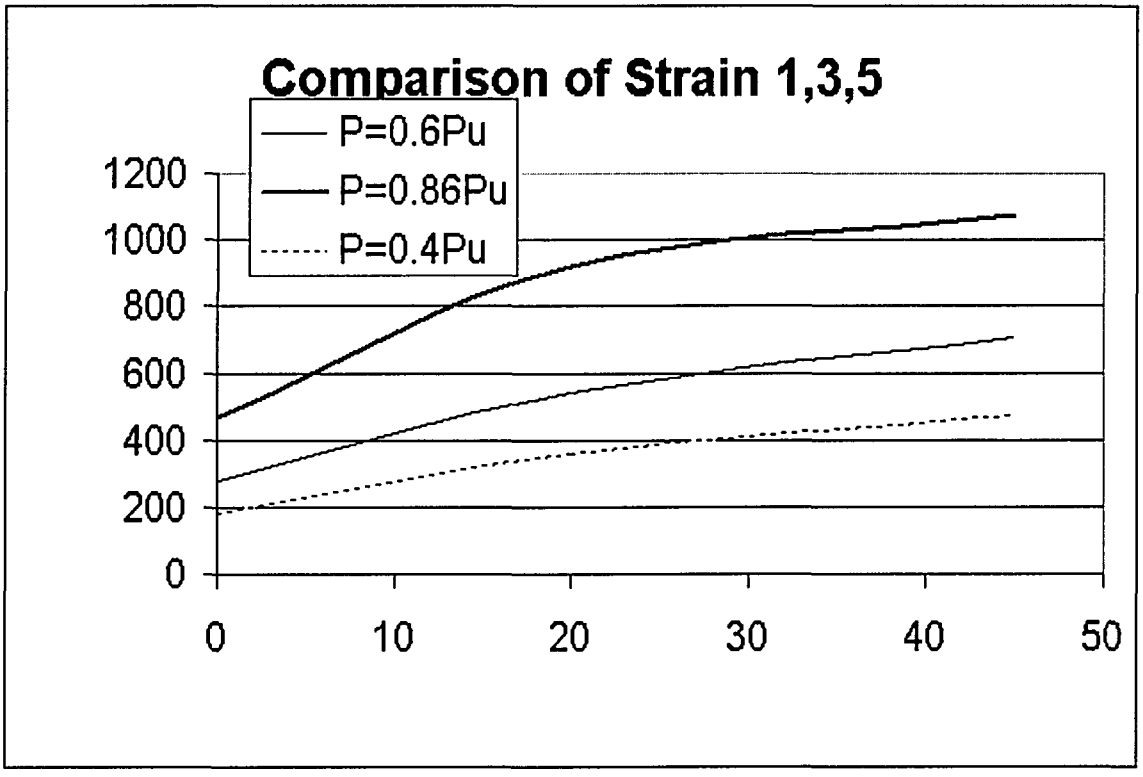

Fig. B3-8 Comparison of Strain 1,3,5 at Different Load Level of Specimen 3

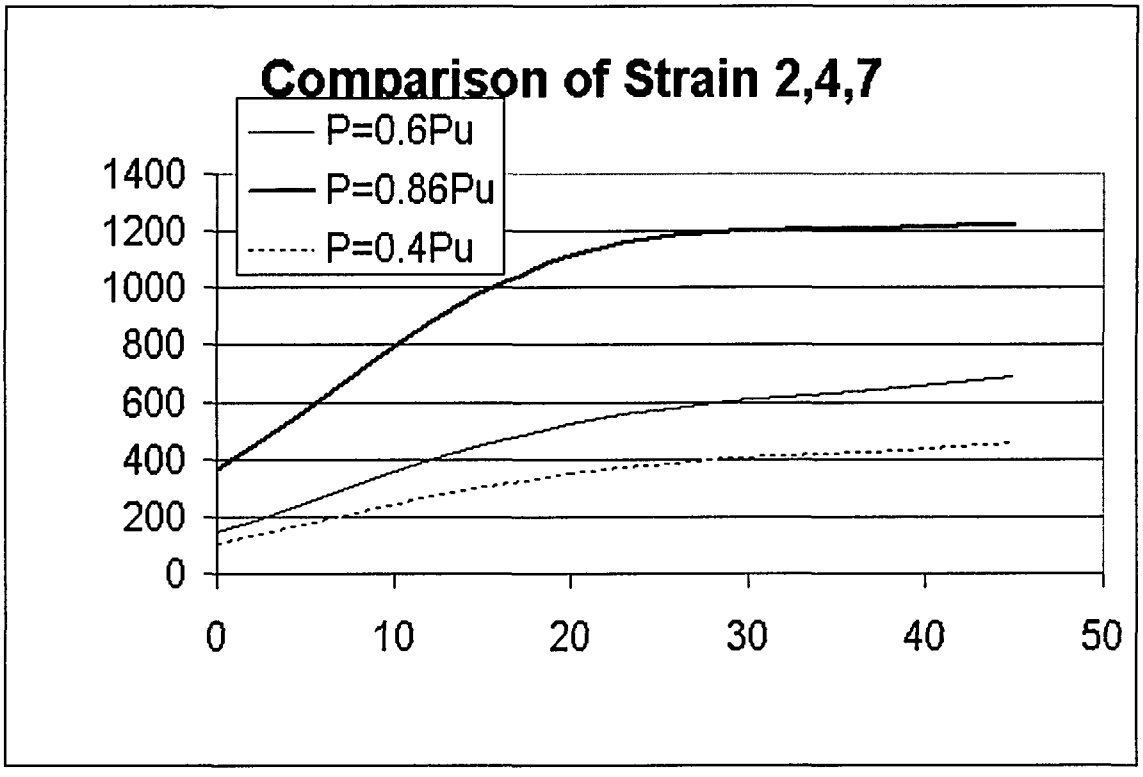

Fig. B3-9 Comparison of Strain 2,4,7 at Different Load Level of Specimen 3

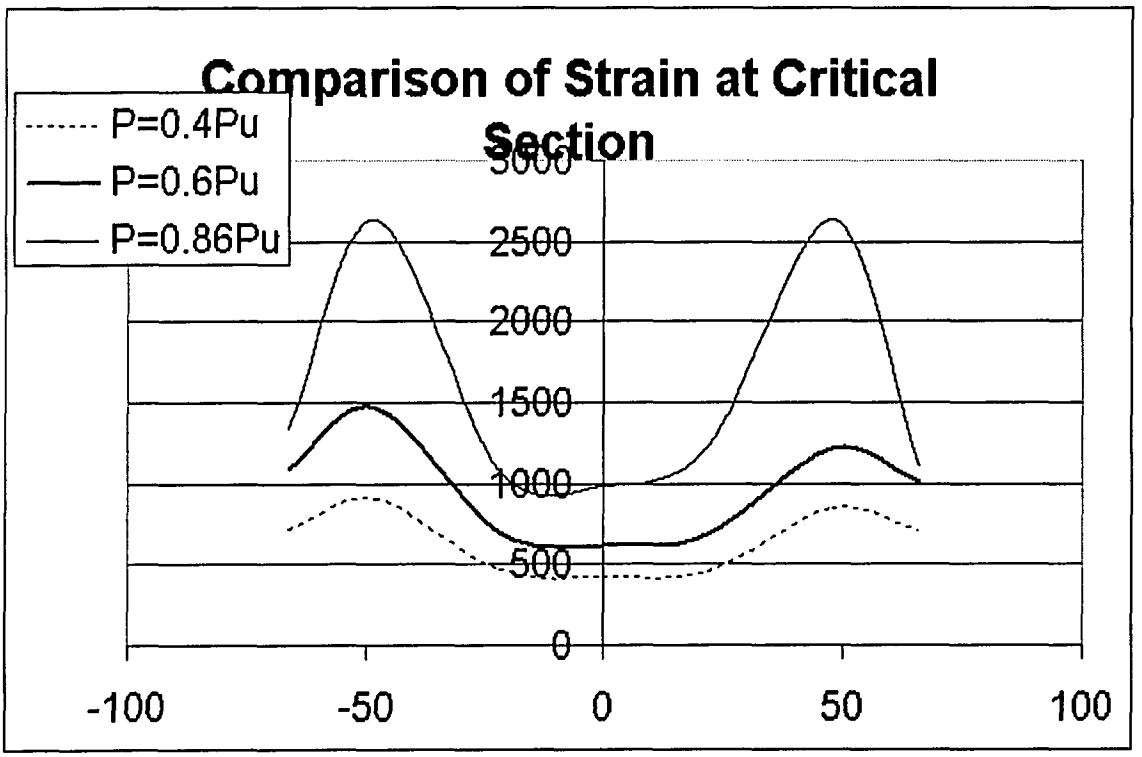

Fig. B3-10 Comparison of Strain at Critical Section at Different Load Level of Specimen 3

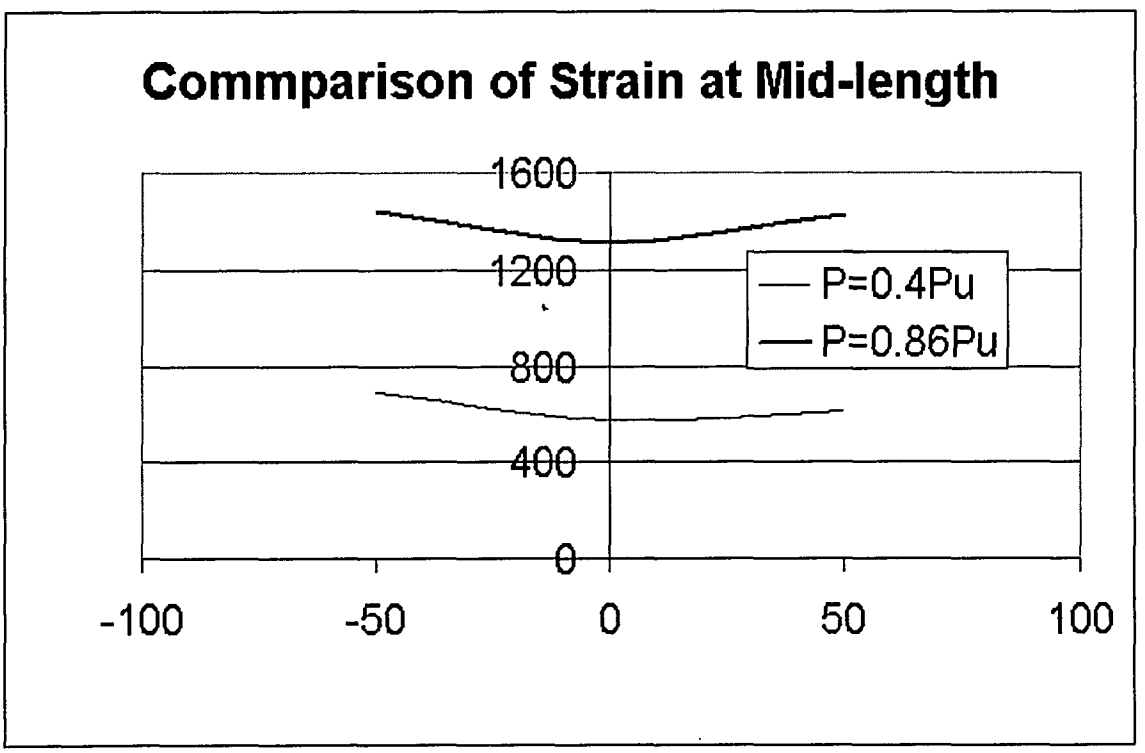

Fig. B3-11 Comparison of Strain 15,16,17 at Different Load Level of Specimen 3

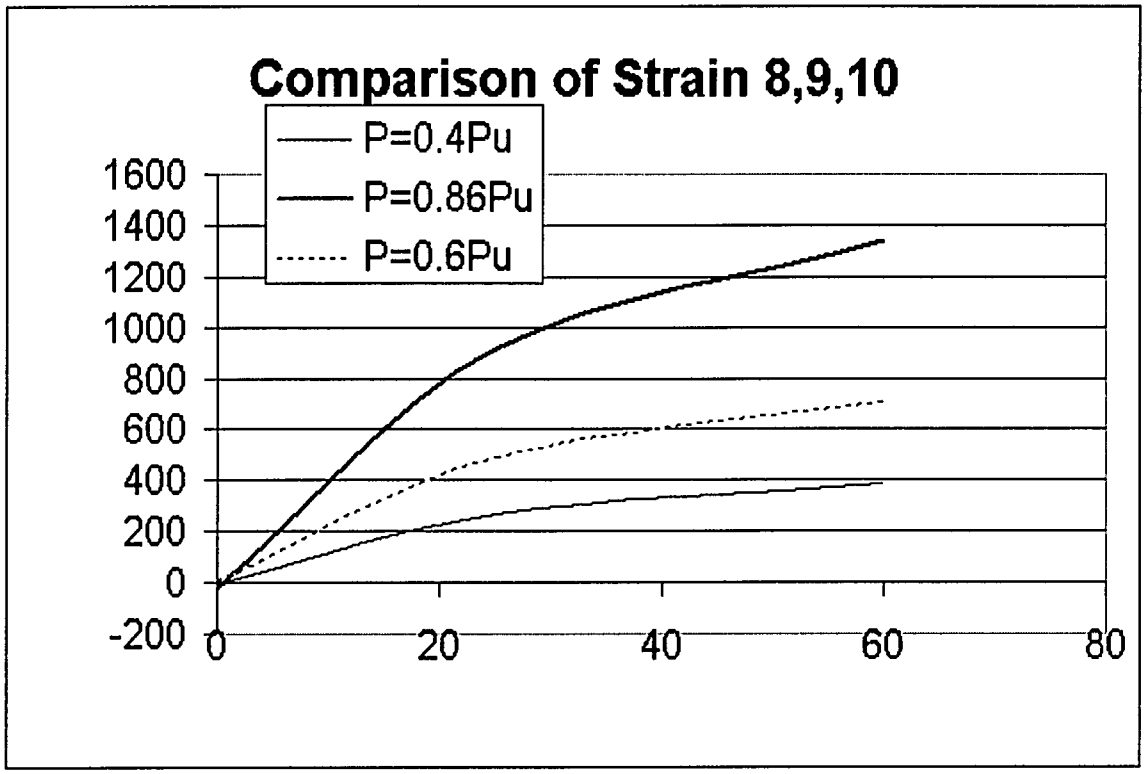

Fig. B3-12 Comparison of Strain 8,9,10 at Different Load Level of Specimen 3

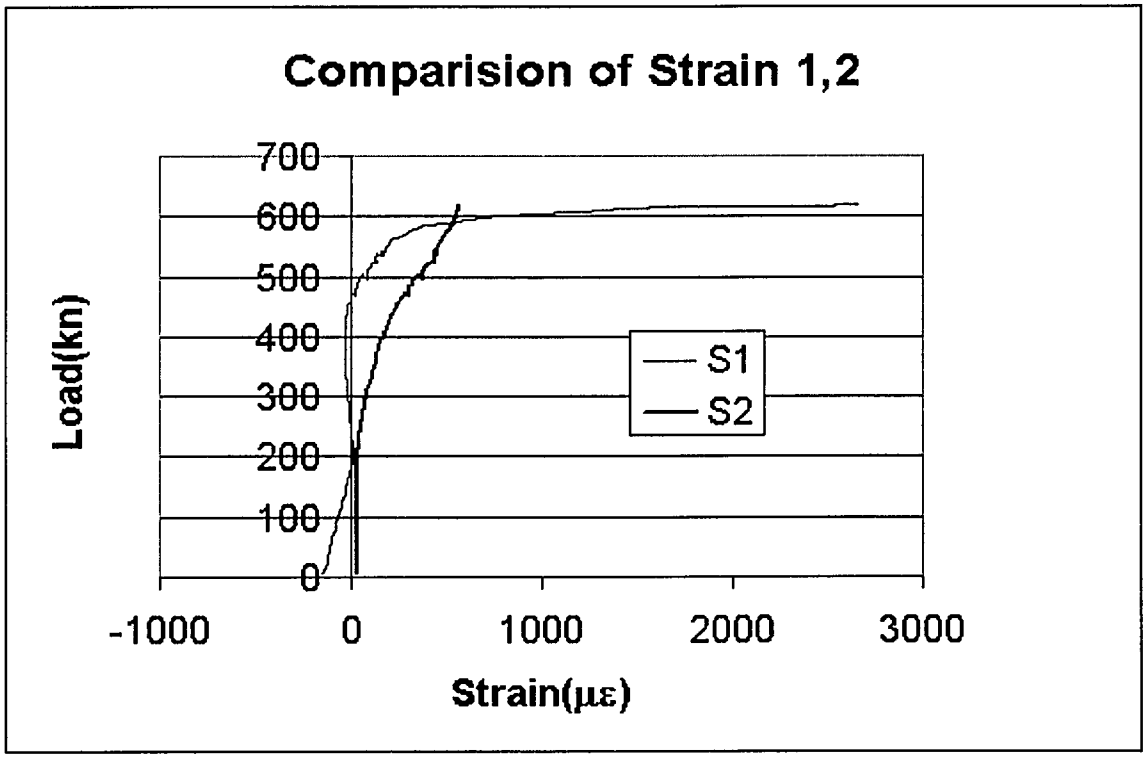

Fig. B4-1 Load vs. Strain 1,2 of Specimen 4

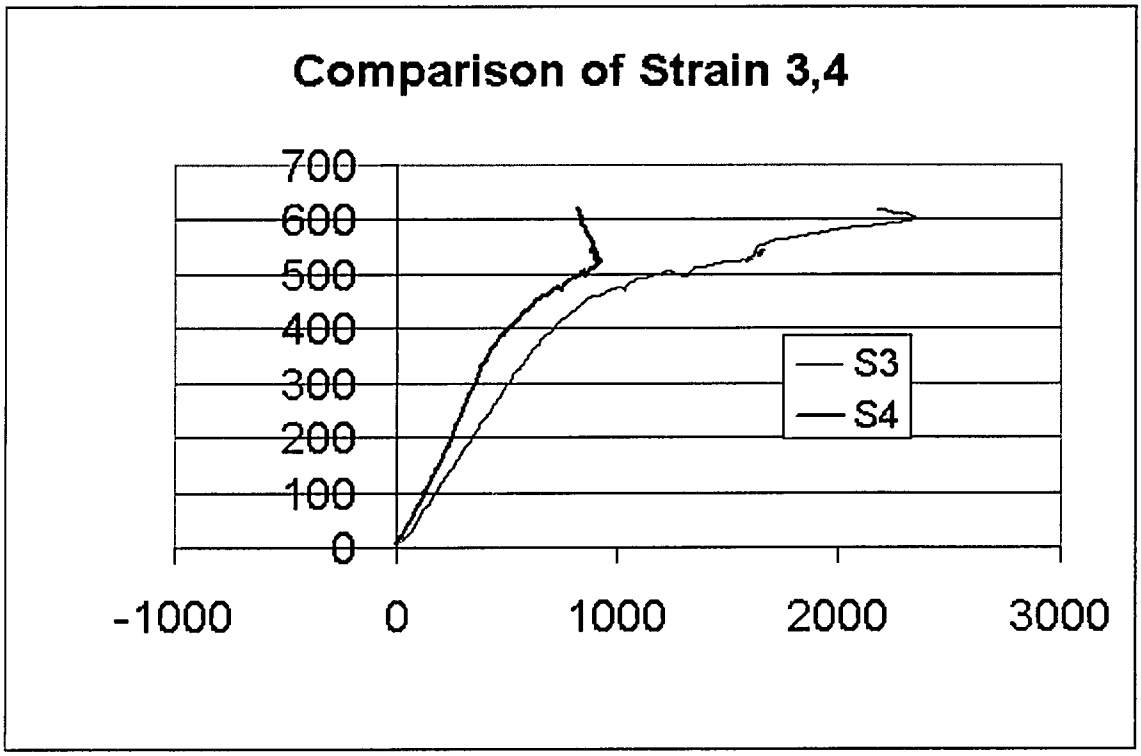

Fig. B4-2 Load vs. Strain 3, 4 of Specimen 4

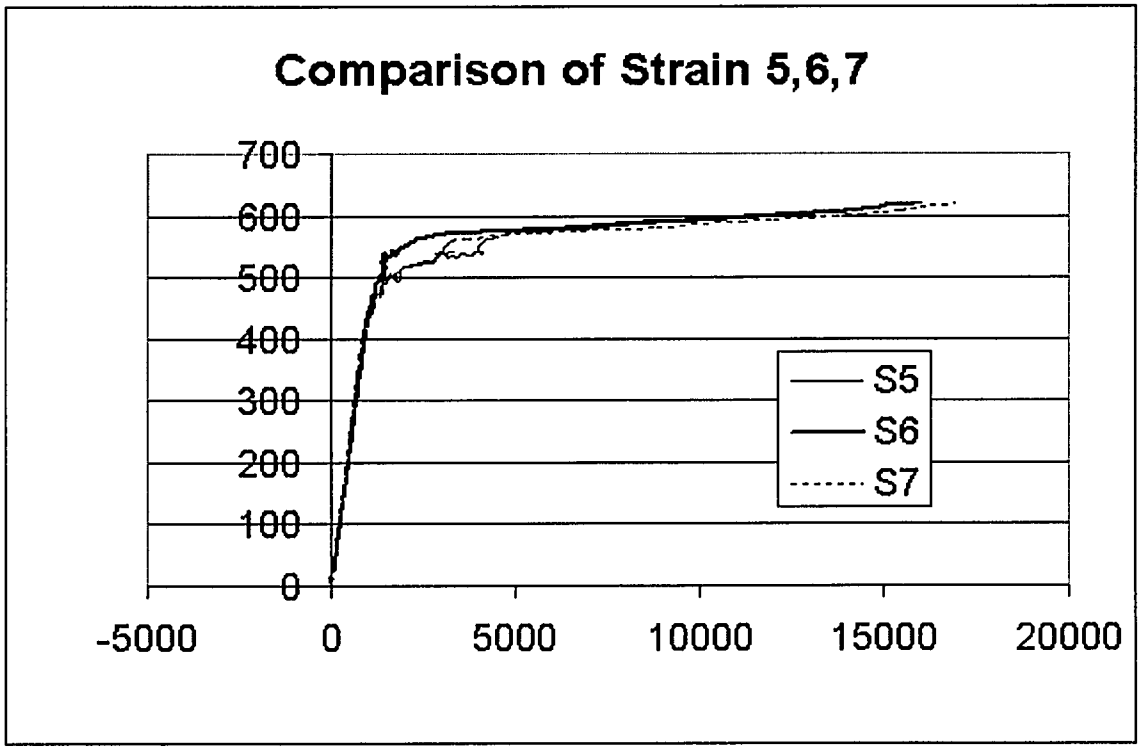

Fig. B4-3 Load vs. Strain 5, 6, 7 of Specimen 4

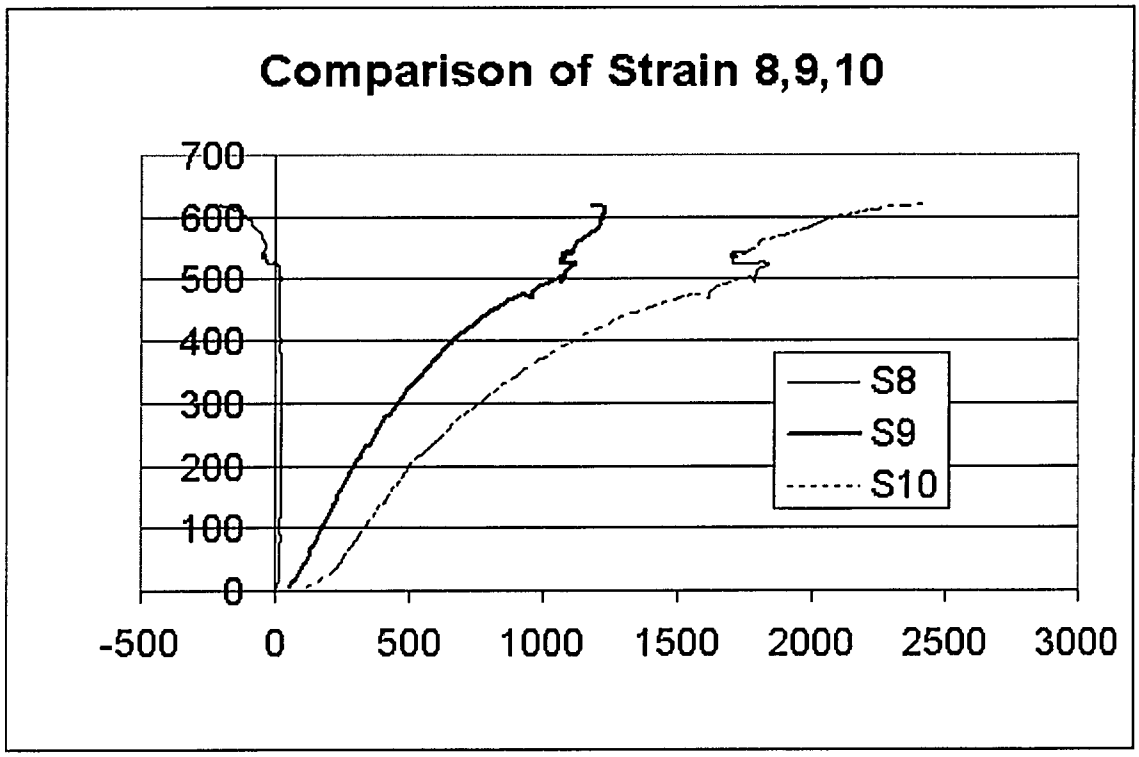

Fig. B4-4 Load vs. Strain 8, 9, 10 of Specimen 4

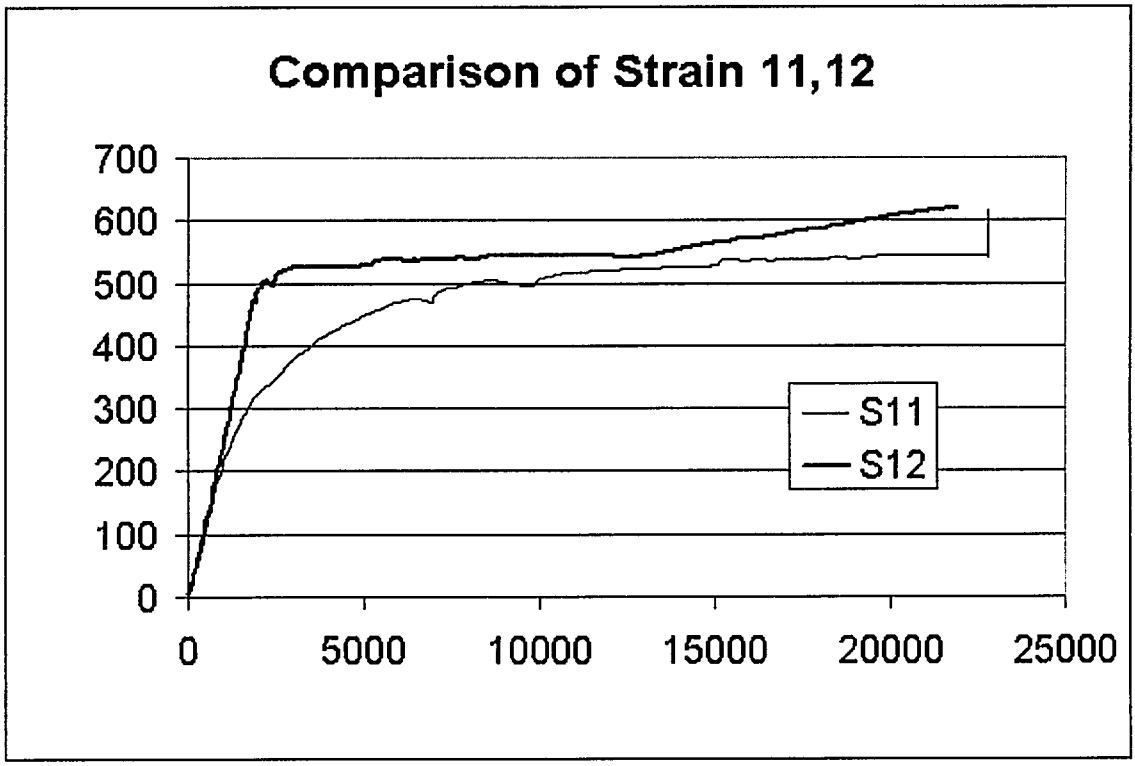

Fig. B4-5 Load vs. Strain 11,12 of Specimen 4

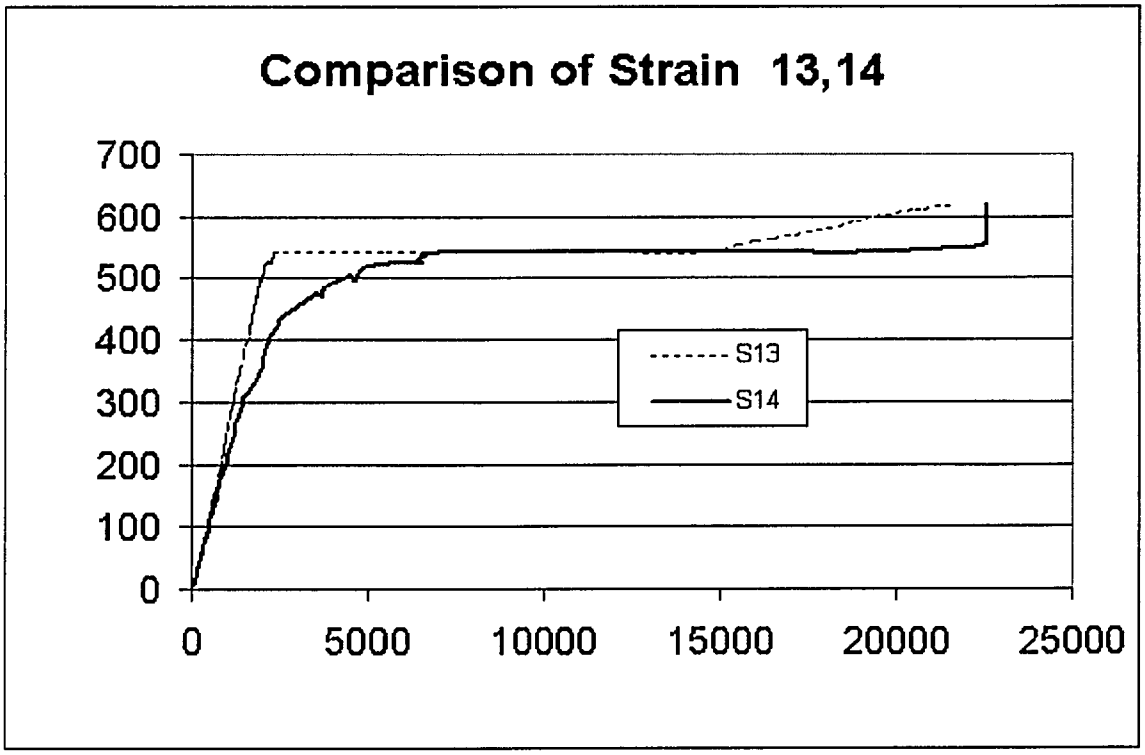

Fig. B4-6 Load vs. Strain 13,14 of Specimen 4

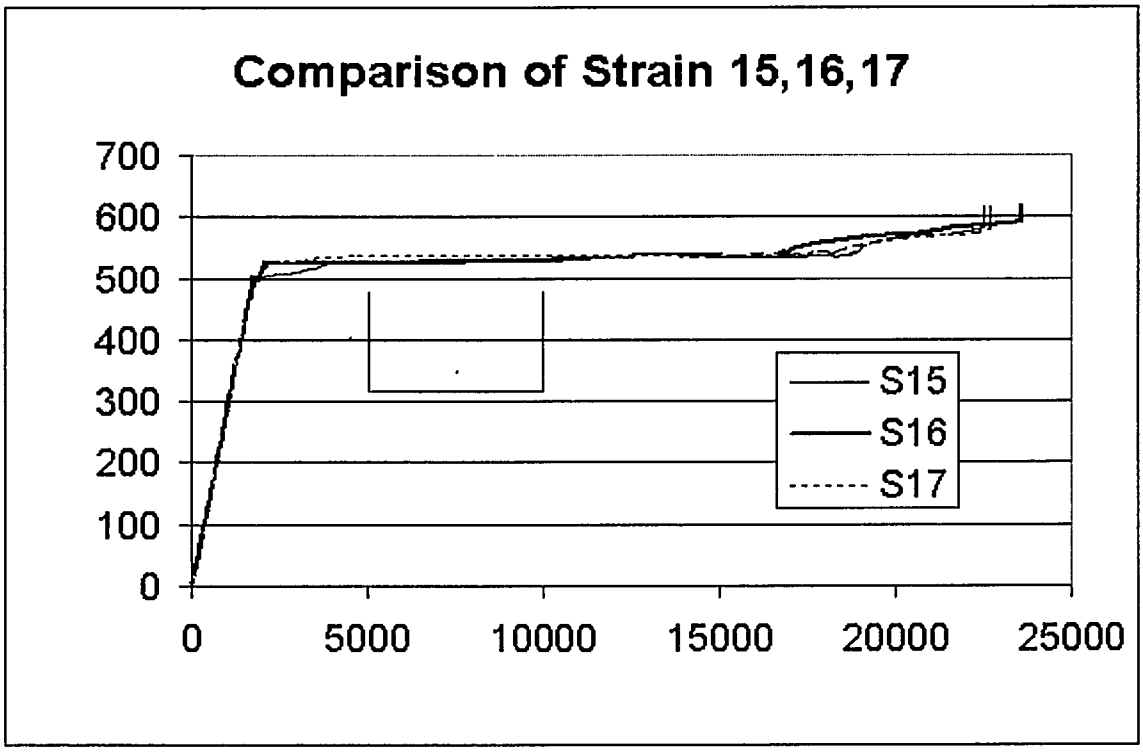

Fig. B4-7 Load vs. Strain 15,16,17 at mid-length of Specimen 4

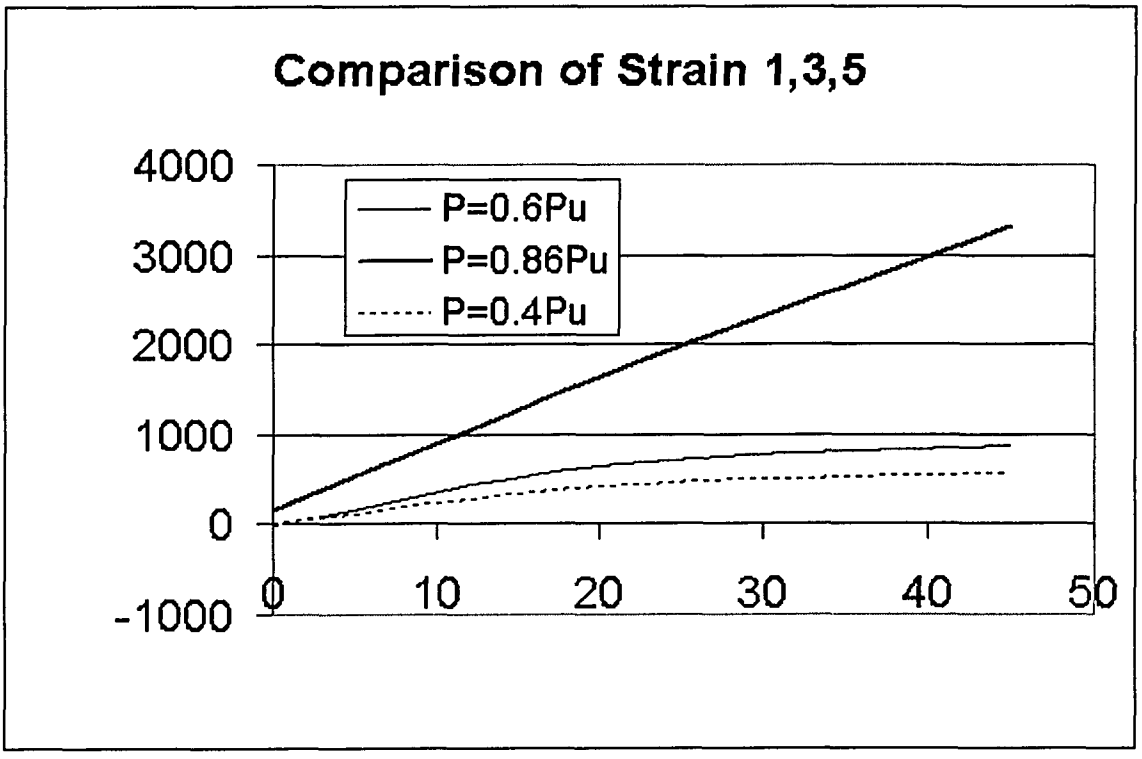

Fig. B4-8 Comparison of Strain 1,3,5 at Different Load Level of Specimen 4

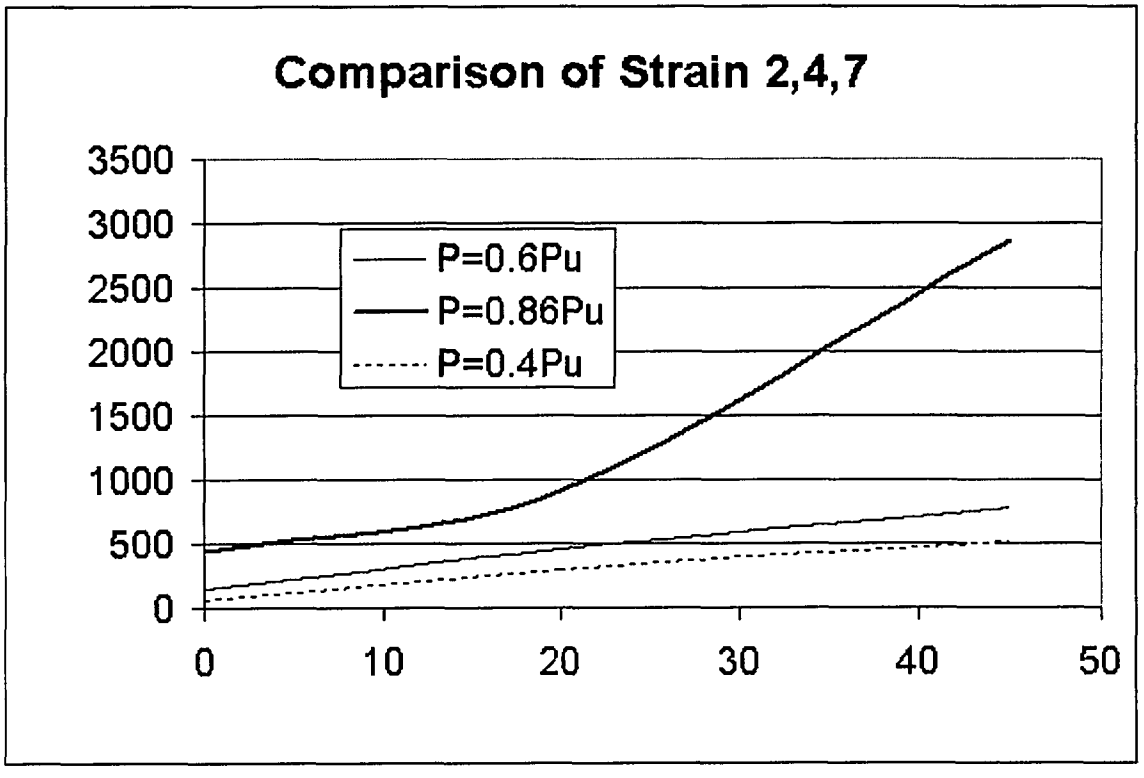

Fig. B4-9 Comparison of Strain 2,4,7 at Different Load Level of Specimen 4

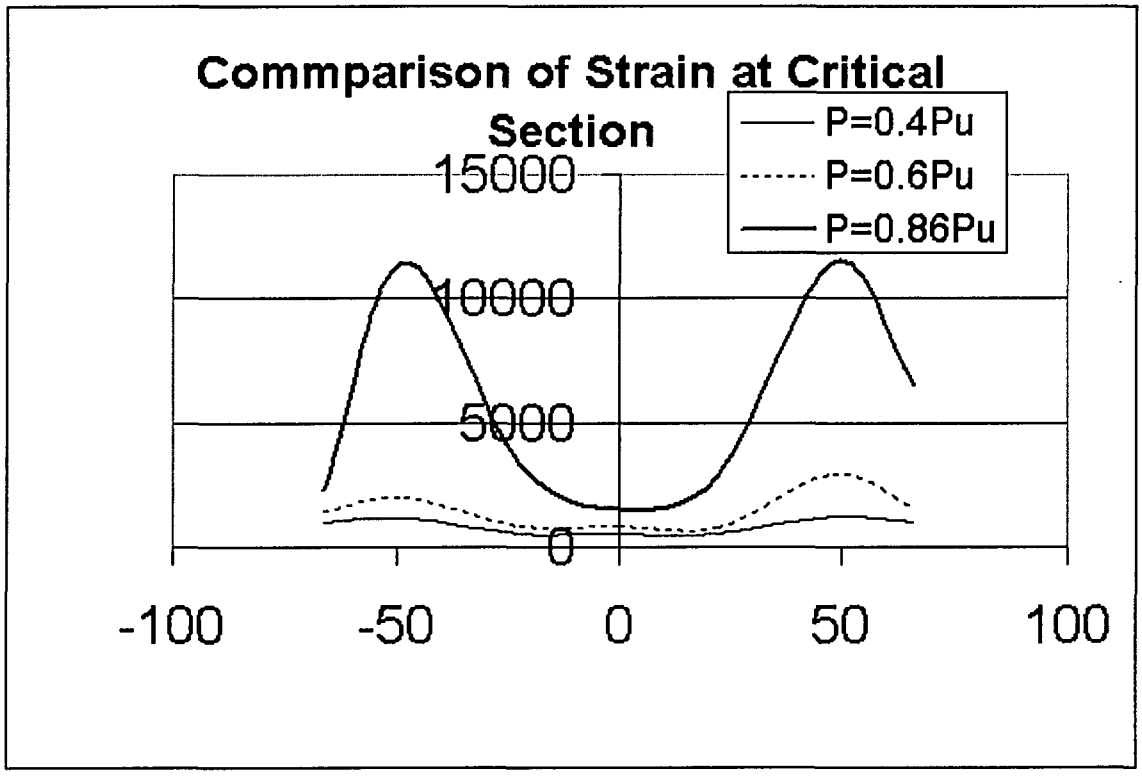

Fig. B4-10 Comparison of Strain at Critical Section at Different Load Level of Specimen 4

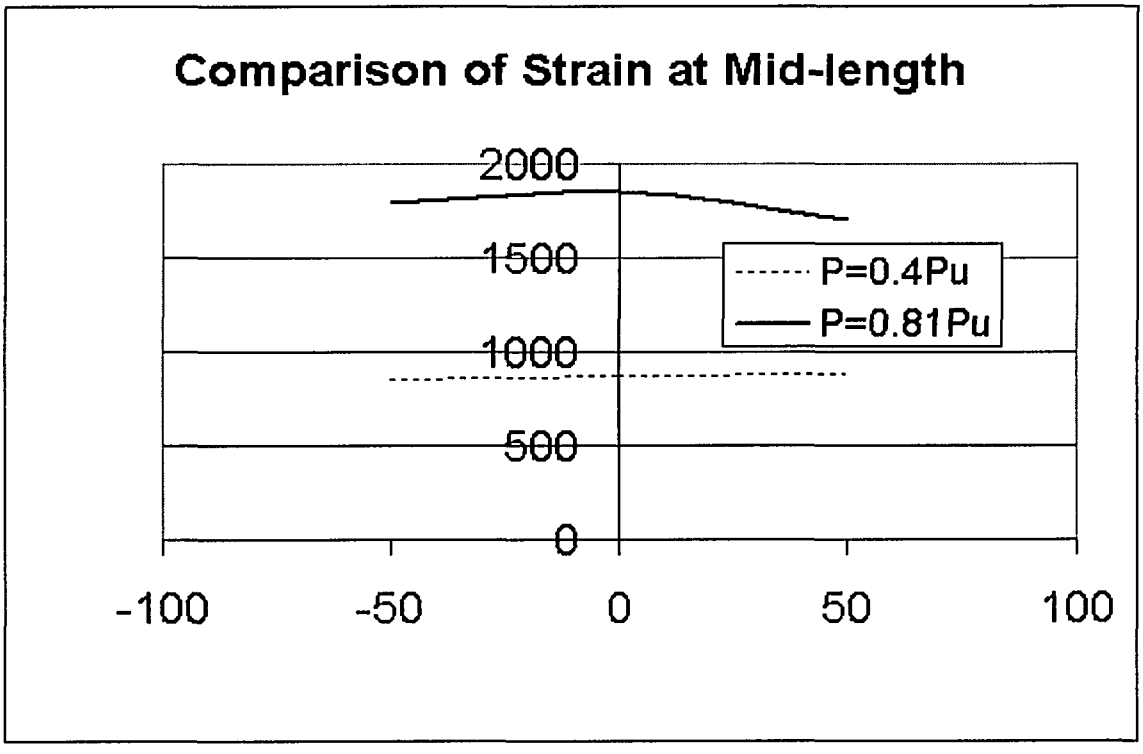

Fig. B4-11 Comparison of Strain 15,16,17 at Different Load Level of Specimen 4

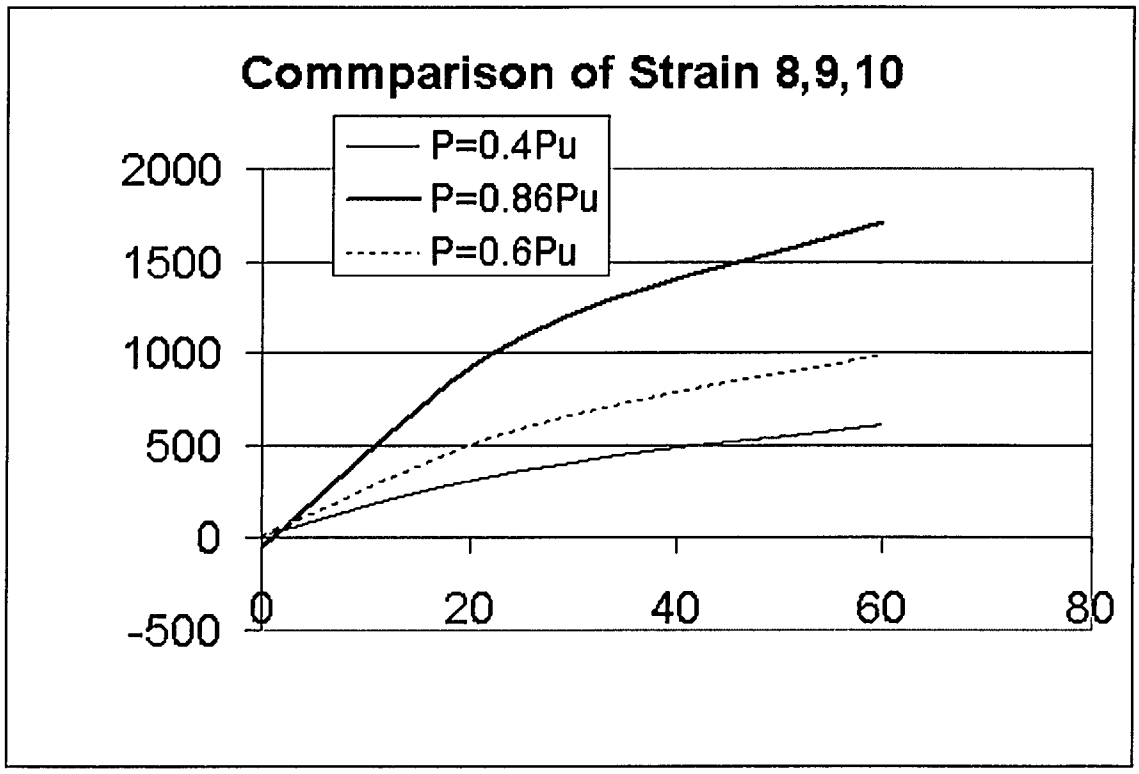

Fig. B4-12 Comparison of Strain 8,9,10 at Different Load Level of Specimen 4

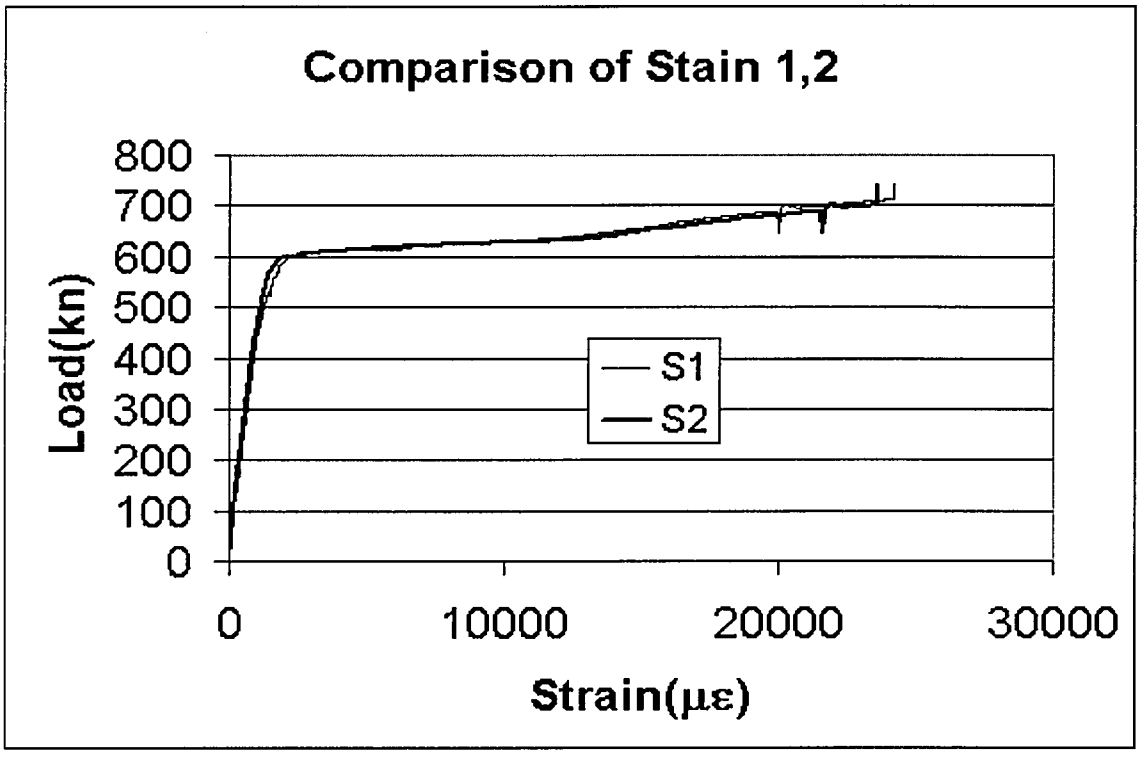

Fig. B5-1 Load vs. Strain 1,2 of Specimen 5

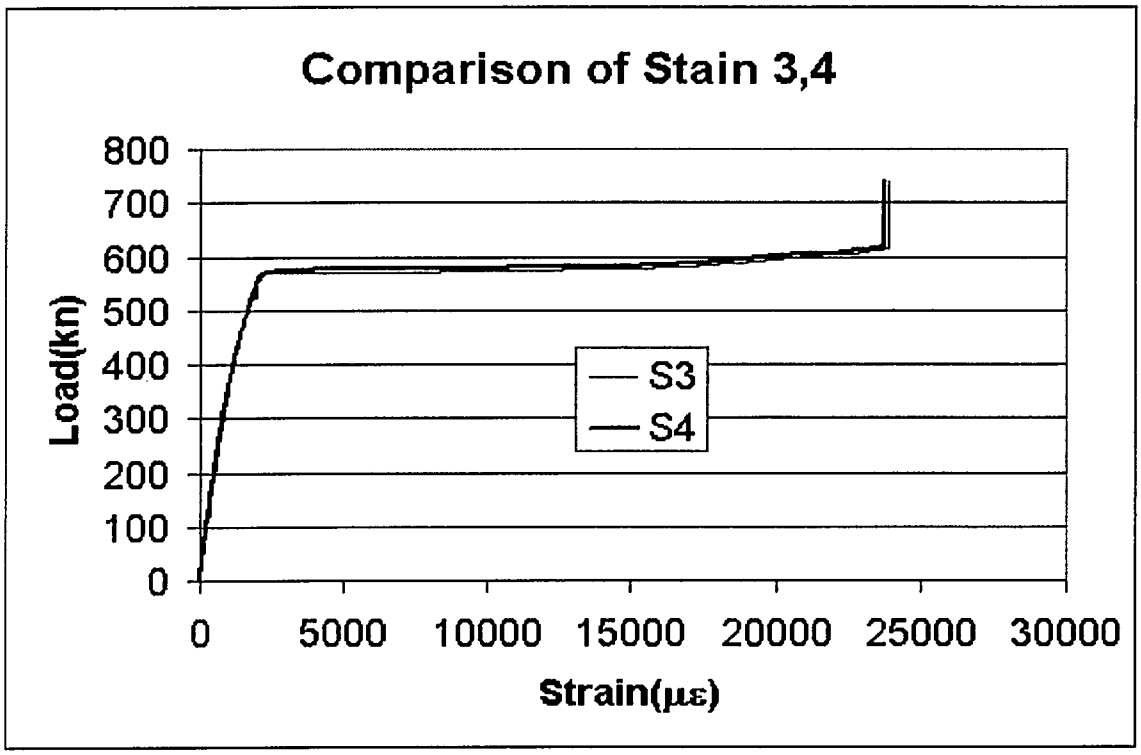

Fig. B5-2 Load vs. Strain 3,4 of Specimen 5

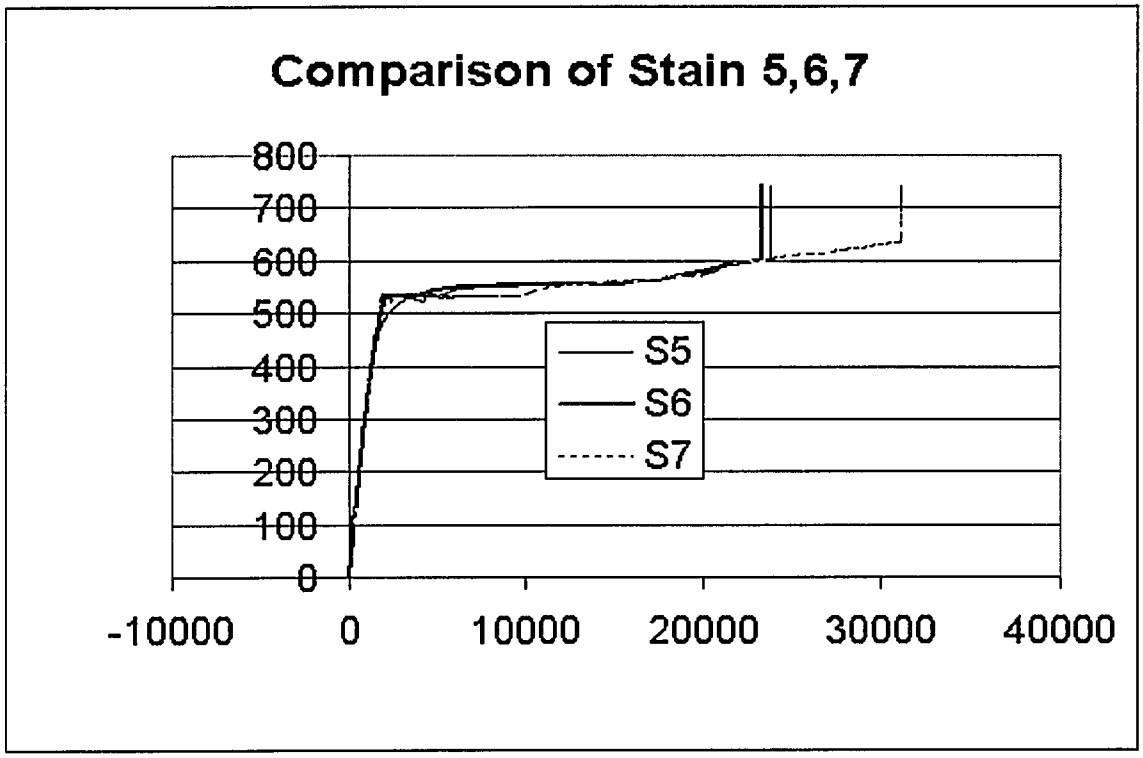

Fig. B5-3 Load vs. Strain 5,6,7 of Specimen 5

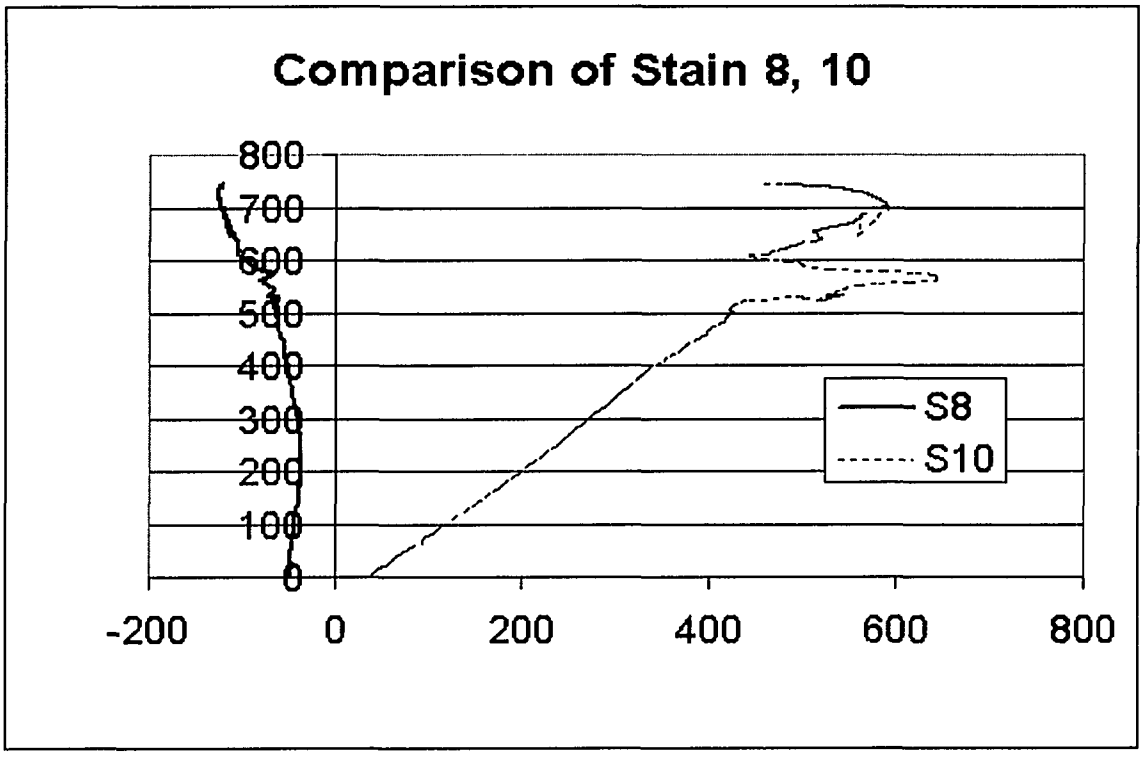

Fig. B5-4 Load vs. Strain 8,10 of Specimen 5

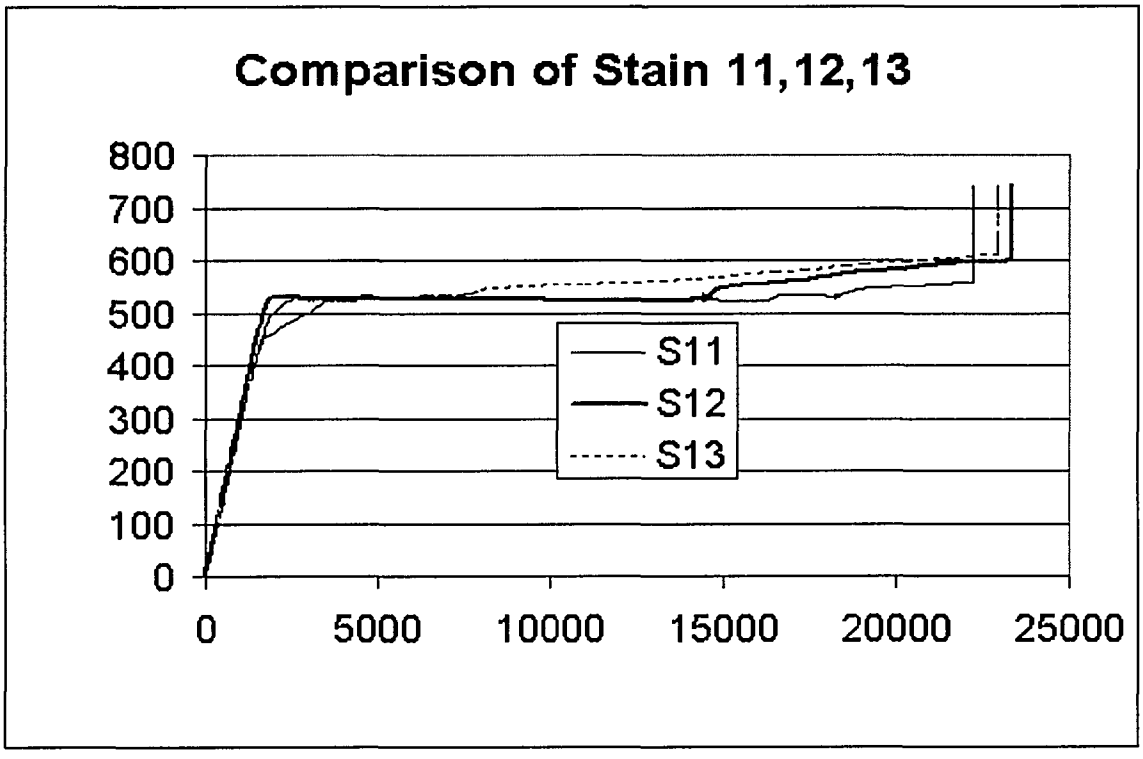

Fig. B5-5 Load vs. Strain 11, 12, 13 of Specimen 5

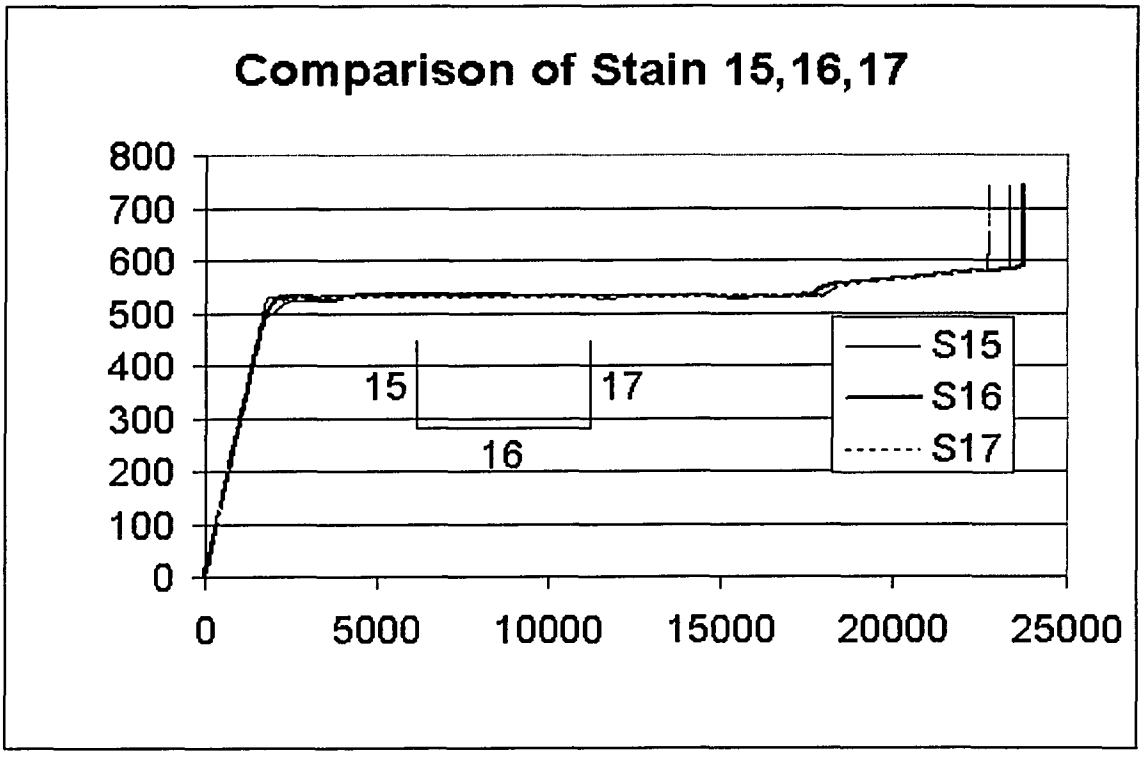

Fig. B5-6 Load vs. Strain 15,16,17 at mid-length of Specimen 5

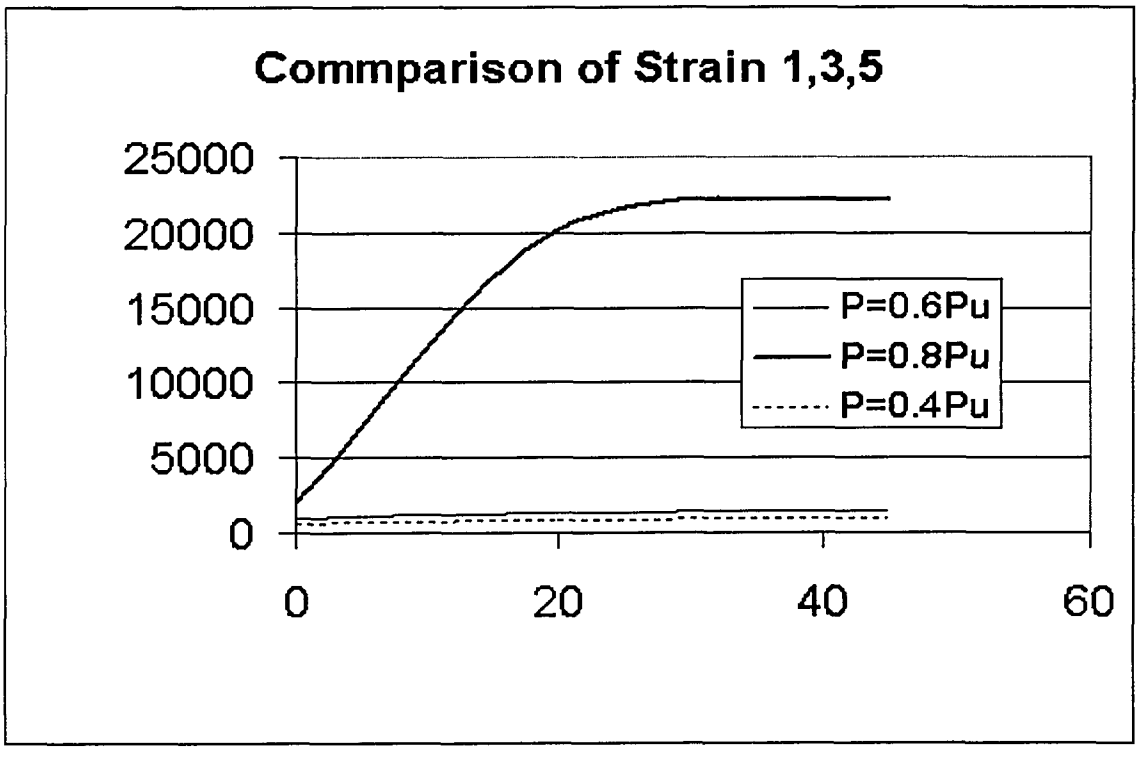

Fig. B5-7 Comparison of Strain 1,3,5 at Different Load Level of Specimen 5

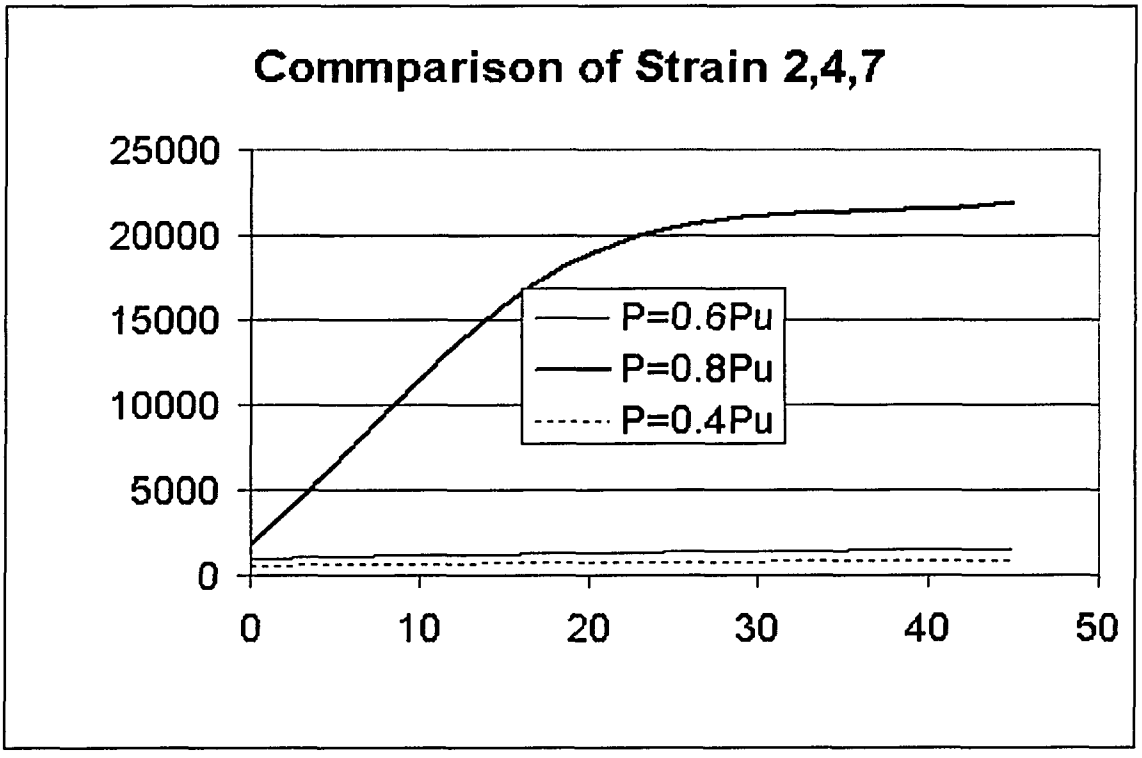

Fig. B5-8 Comparison of Strain 2,4,7 at Different Load Level of Specimen 5

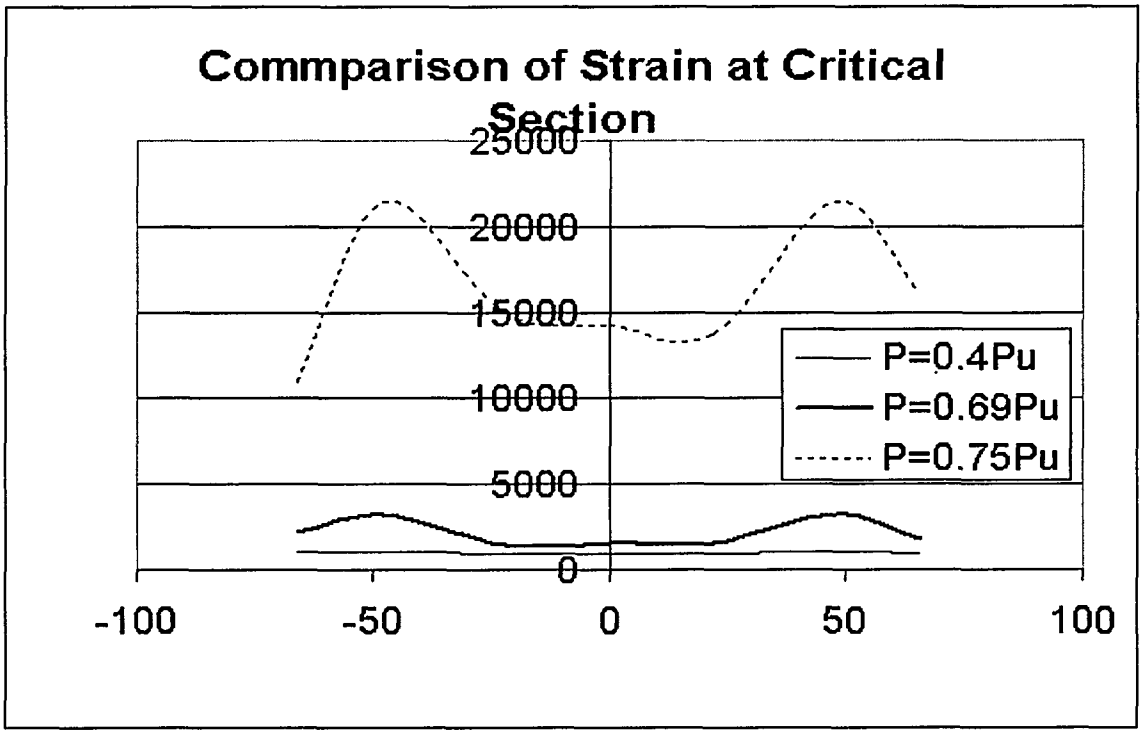

Fig. B5-9 Comparison of Strain at Critical Section at Different Load Level of Specimen 5

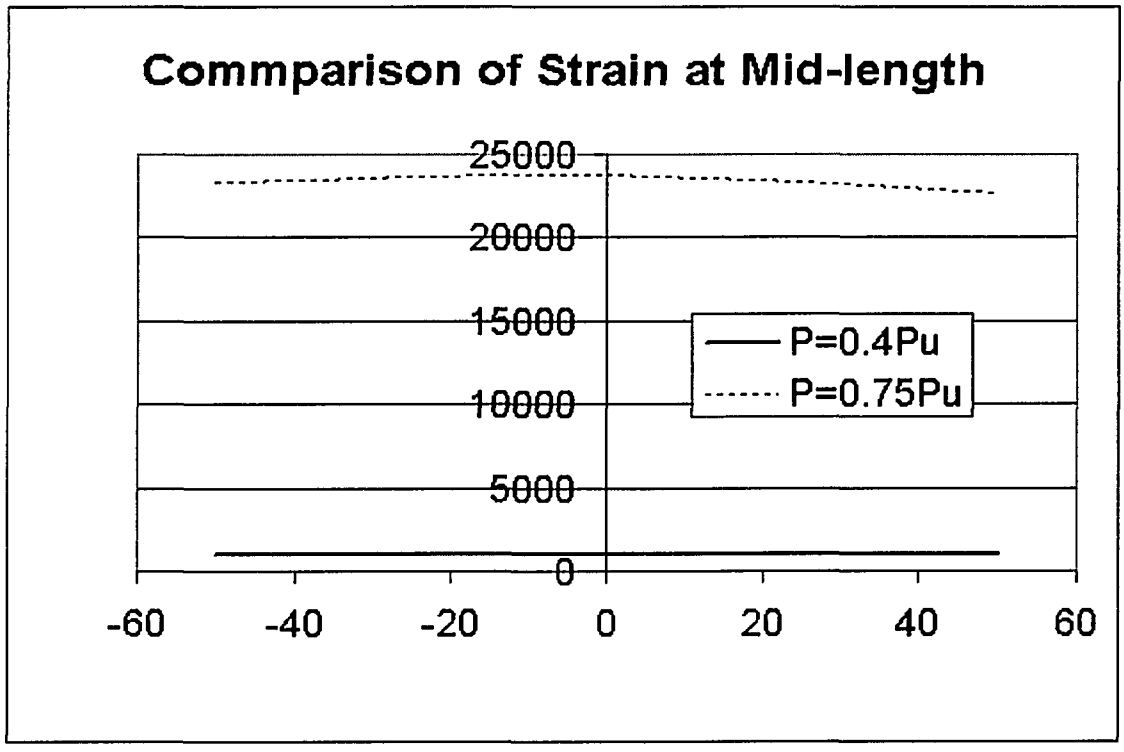

Fig. B5-10 Comparison of Strain 15,16,17 at Different Load Level of Specimen 5

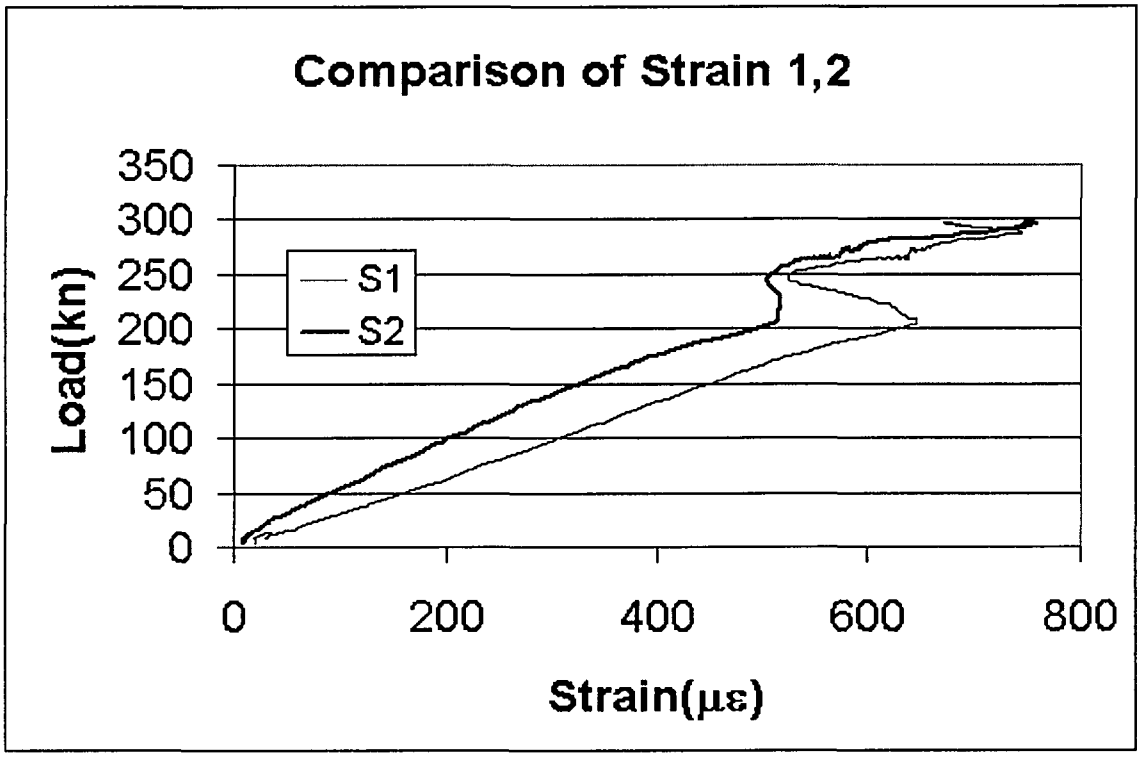

Fig. B6-1 Load vs. Strain 1,2 of Specimen 6

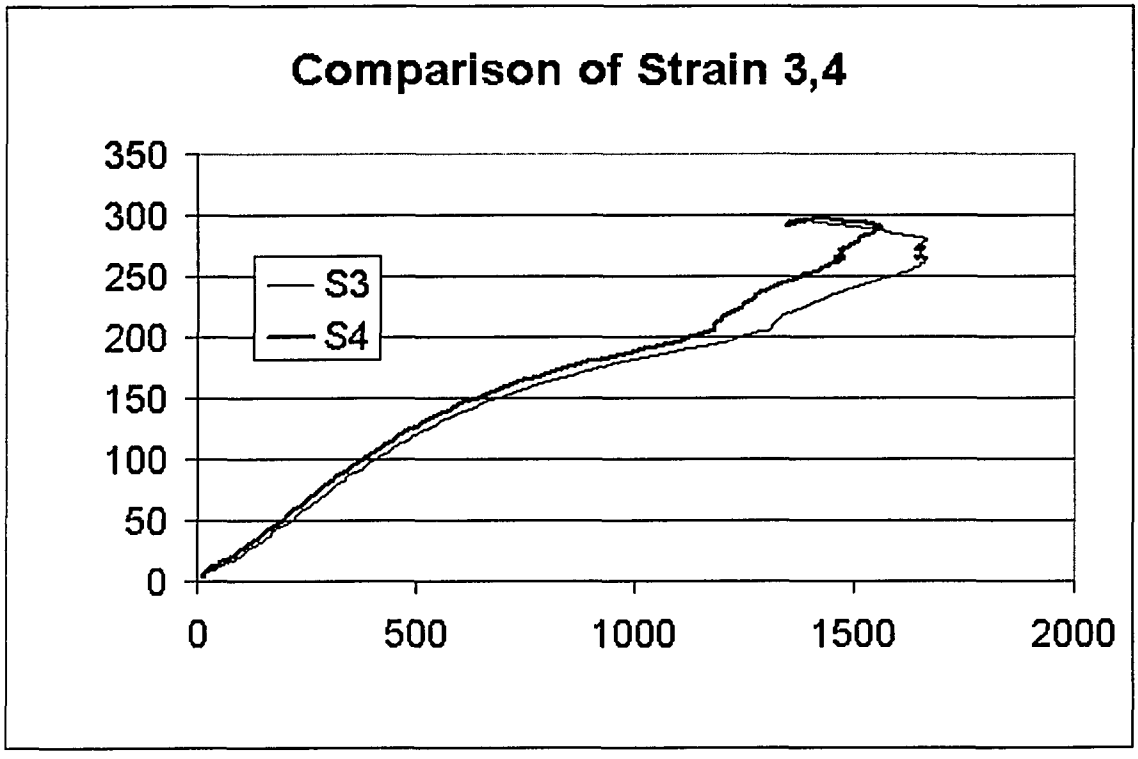

Fig. B6-2 Load vs. Strain 3,4 of Specimen 6

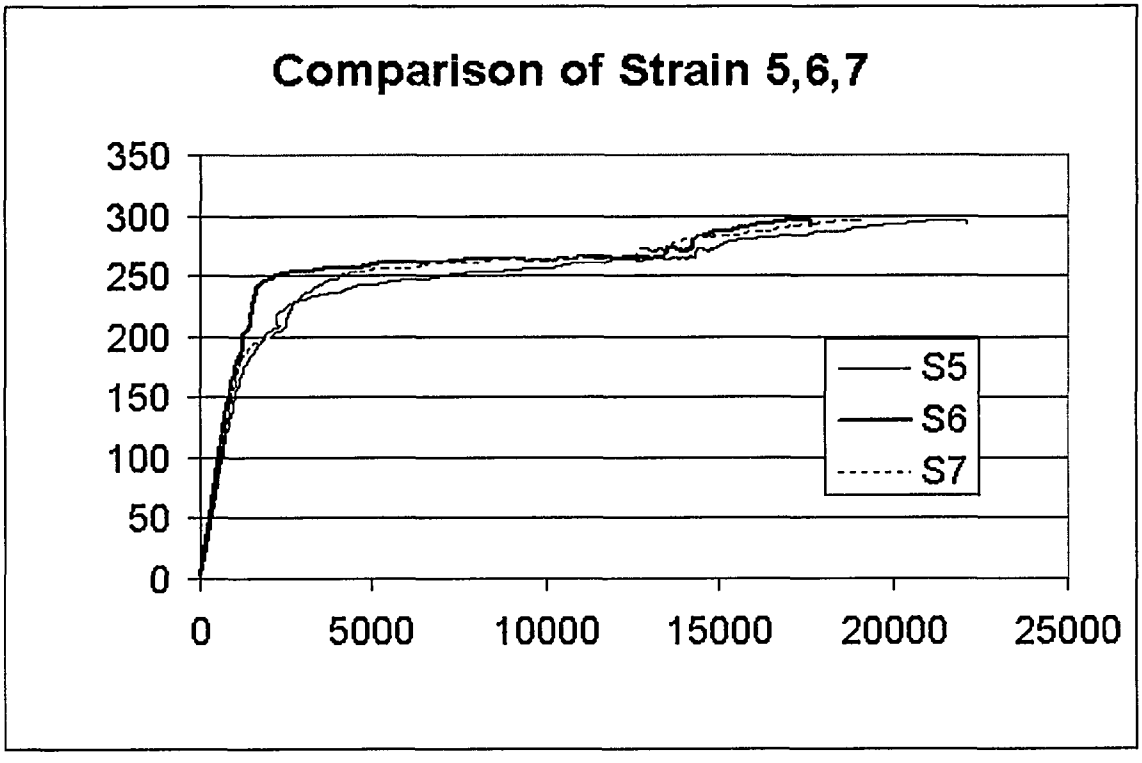

Fig. B6-3 Load vs. Strain 5,6,7 of Specimen 6

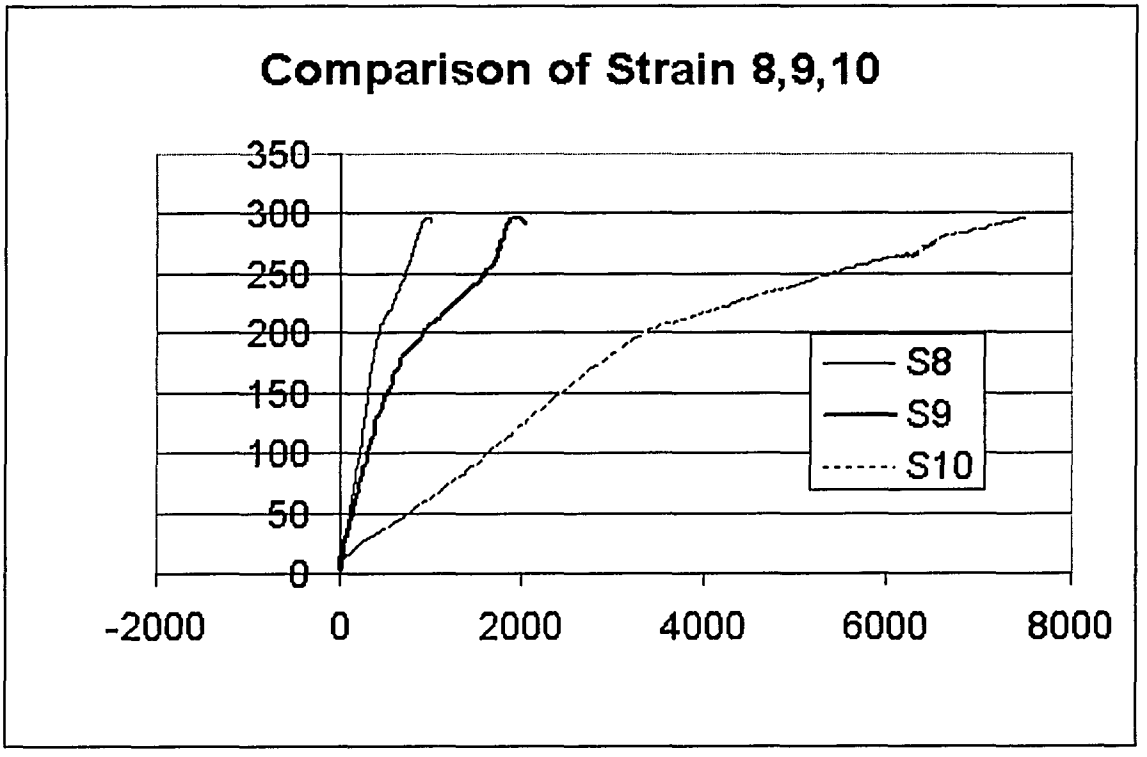

Fig. B6-4 Load vs. Strain 8,9,10 of Specimen 6

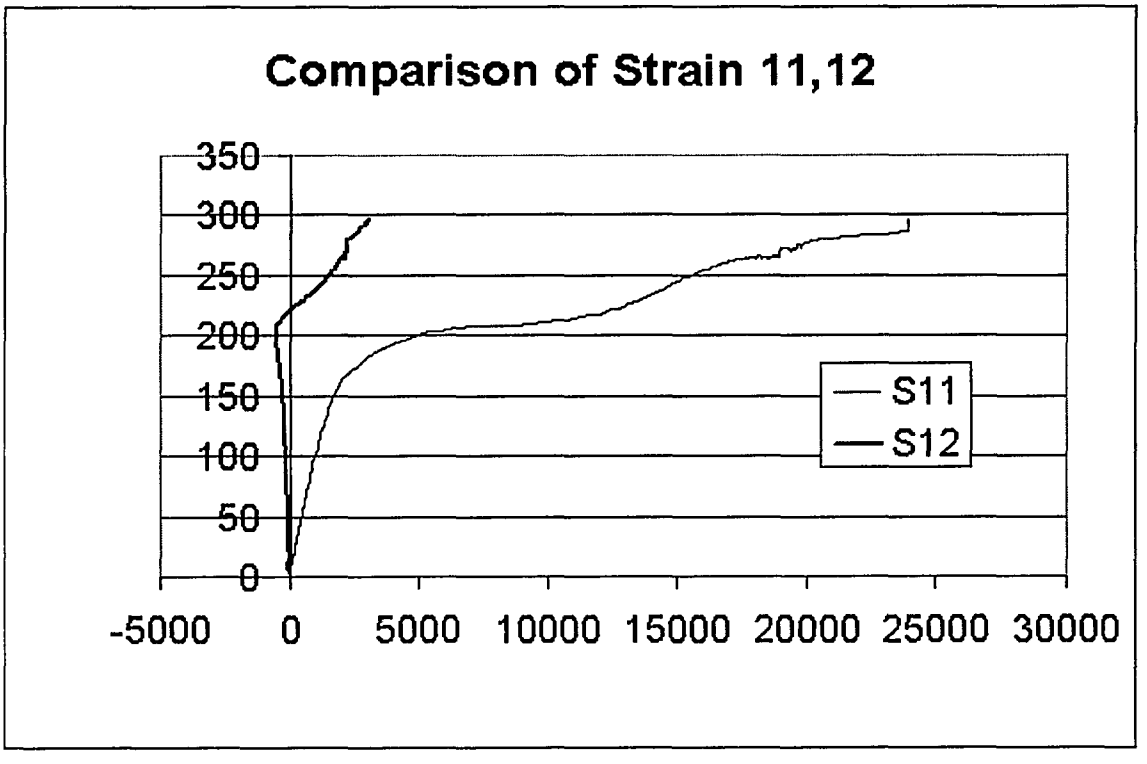

Fig. B6-5 Load vs. Strain 11,12 of Specimen 6

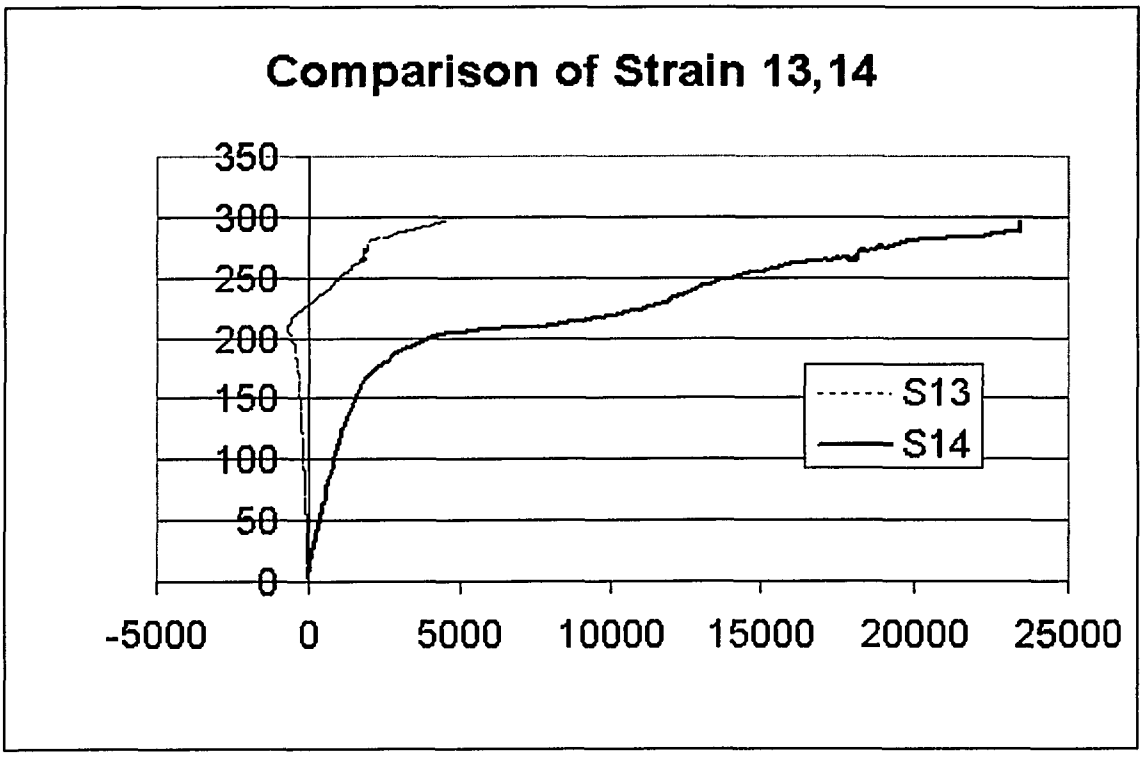

Fig. B6-6 Load vs. Strain 13,14 of Specimen 6

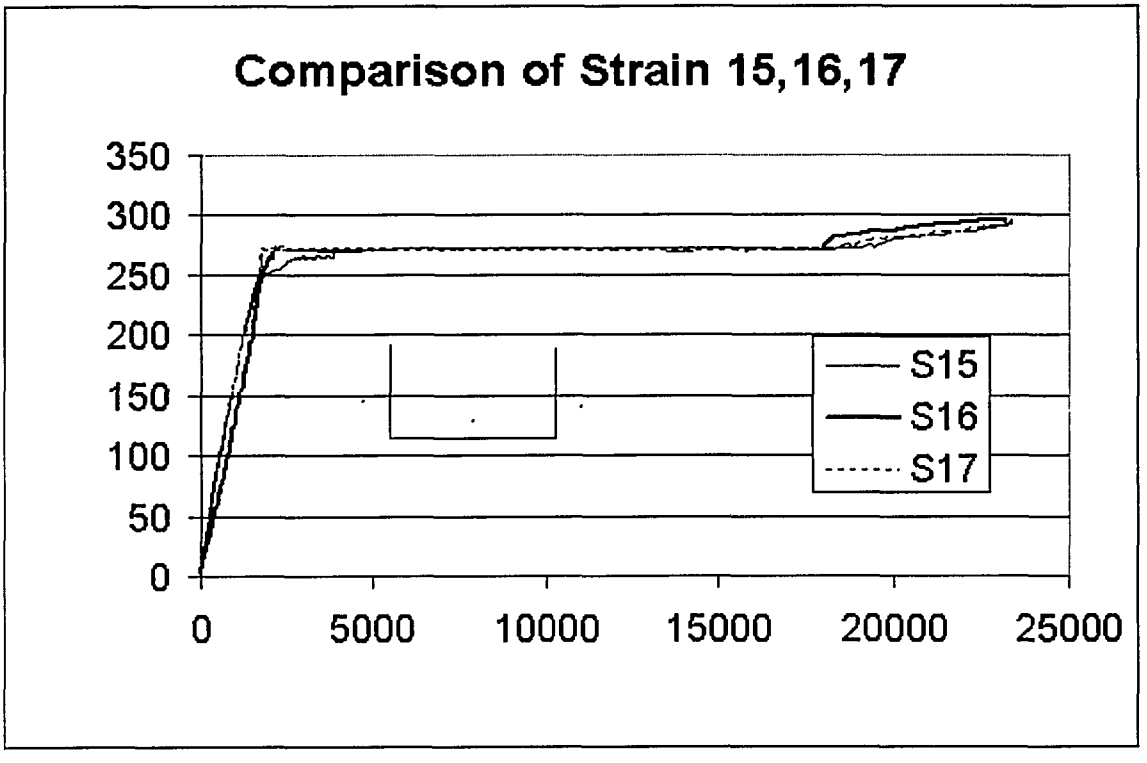

Fig. B6-7 Load vs. Strain 15,16,17 at mid-length of Specimen 6

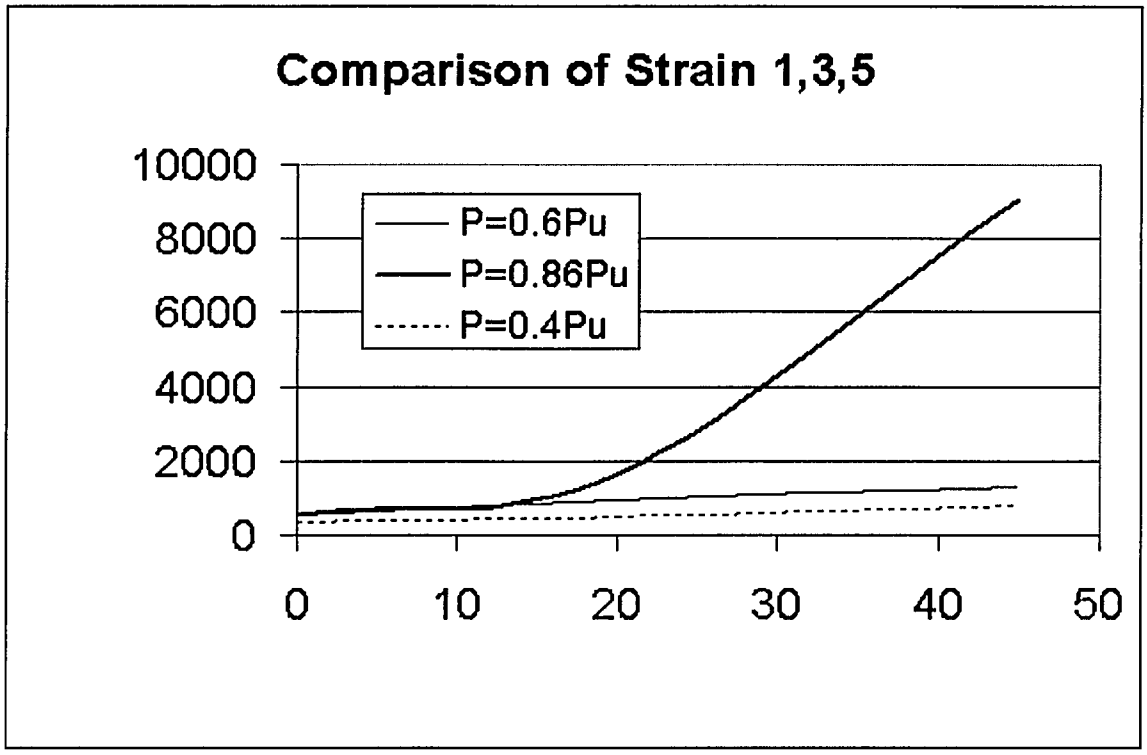

Fig. B6-8 Comparison of Strain 1,3,5 at Different Load Level of Specimen 6

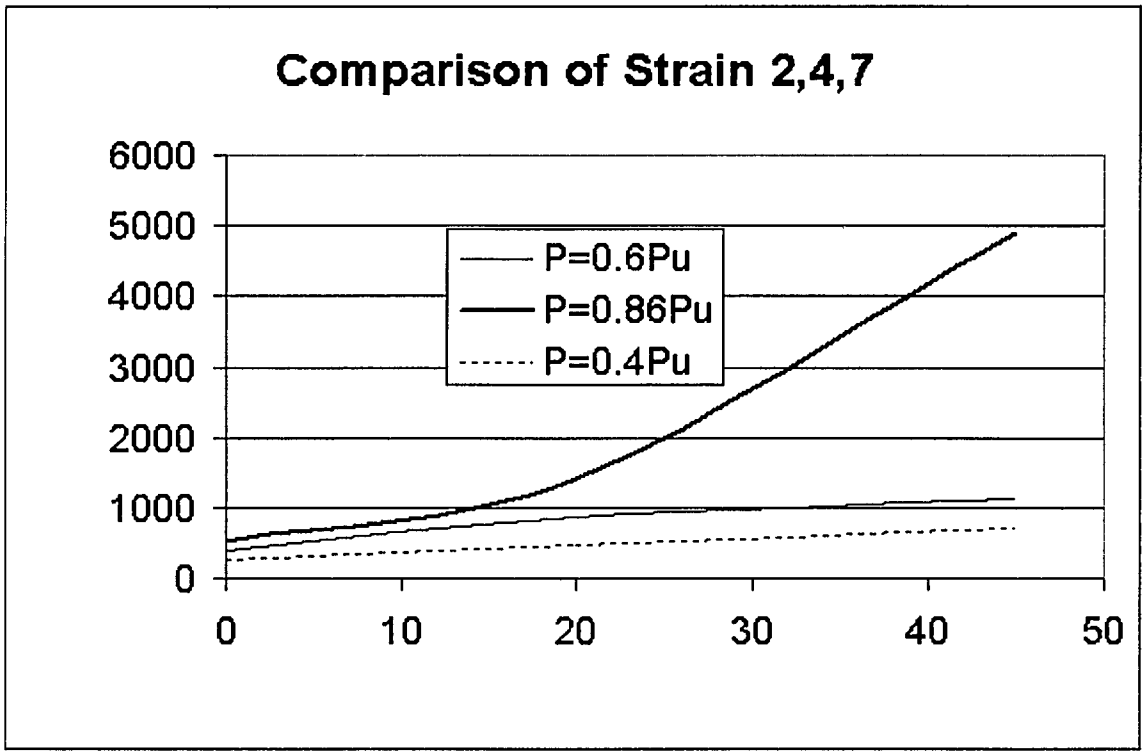

Fig. B6-9 Comparison of Strain 2,4,7 at Different Load Level of Specimen 6

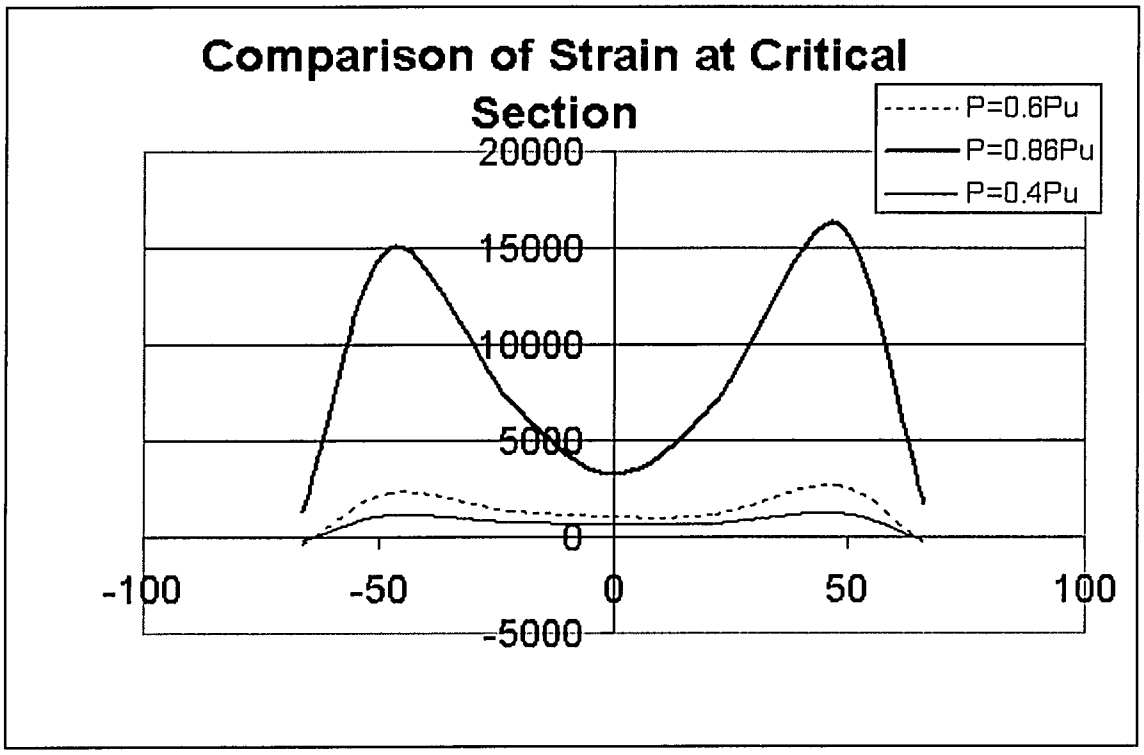

Fig. B6-10 Comparison of Strain at Critical Section at Different Load Level of Specimen 6

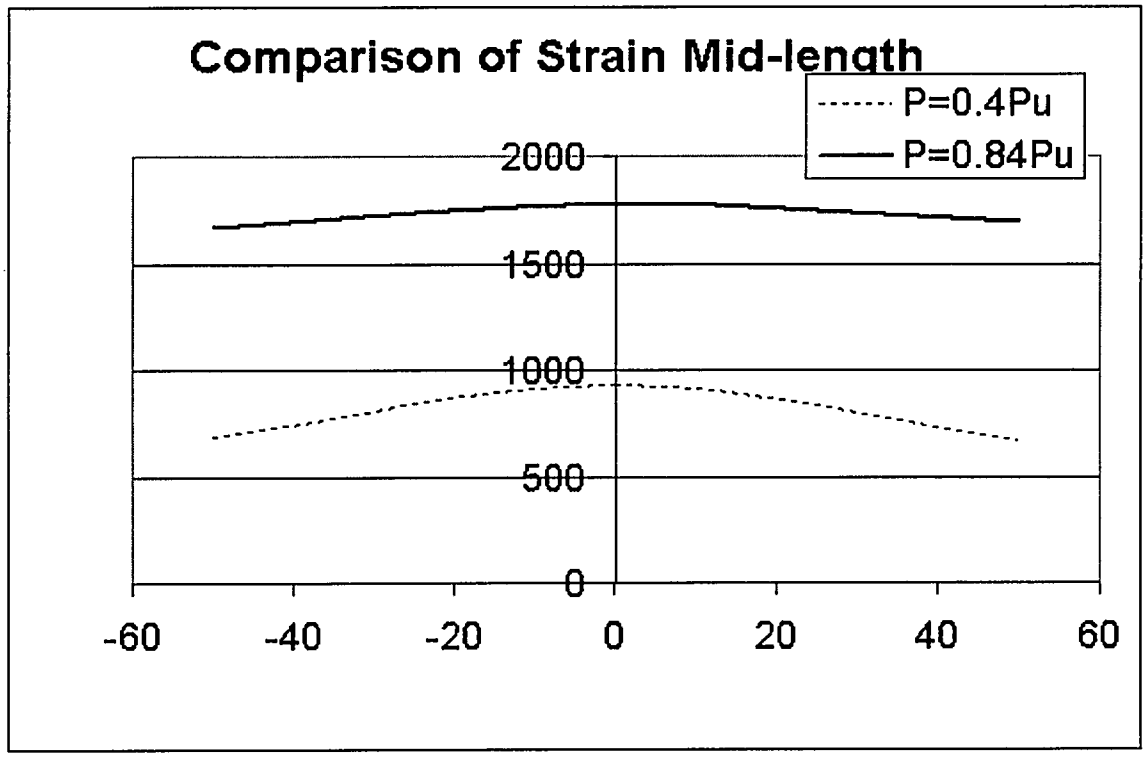

Fig. B6-11 Comparison of Strain 15,16,17 at Different Load Level of Specimen 6

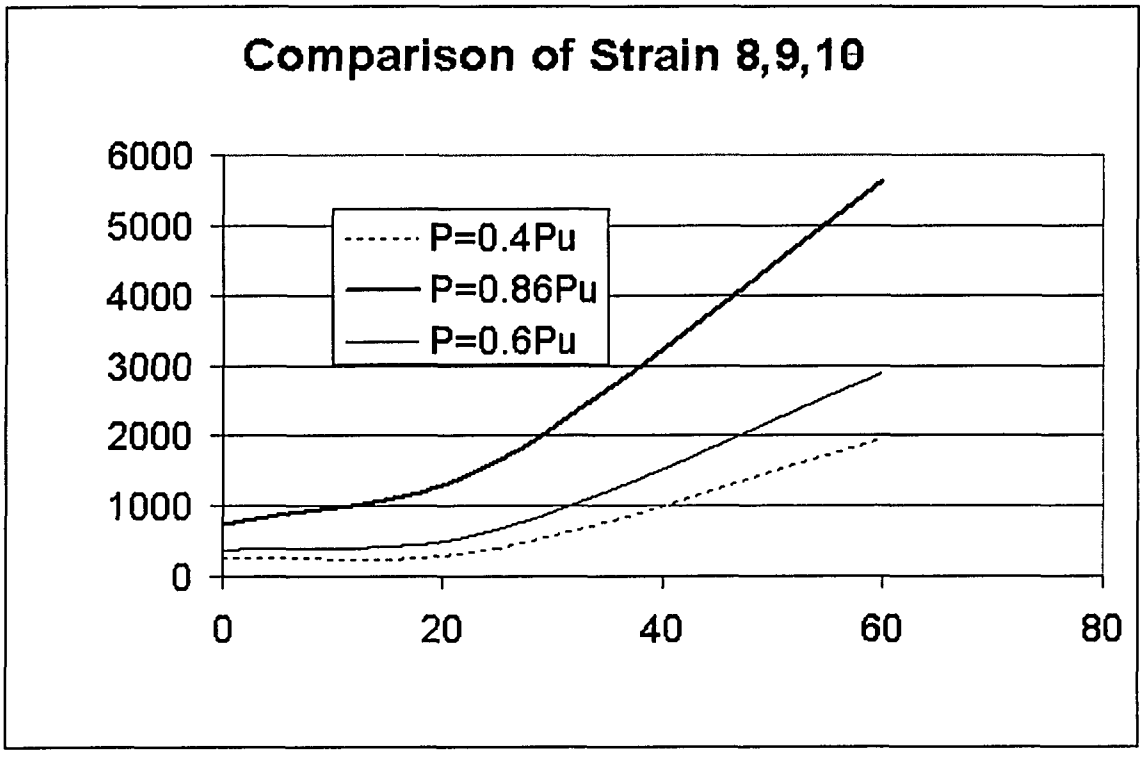

Fig. B6-12 Comparison of Strain 8,9,10 at Different Load Level of Specimen 6

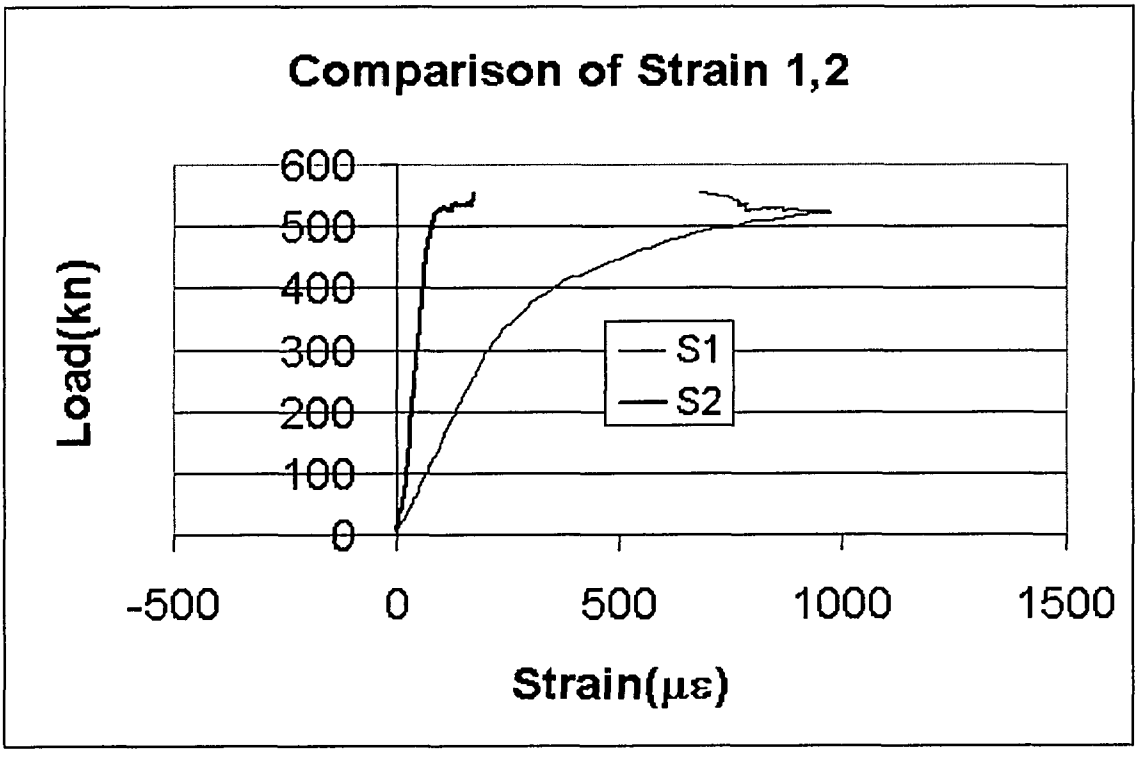

Fig. B7-1 Load vs. Strain 1,2 of Specimen 7

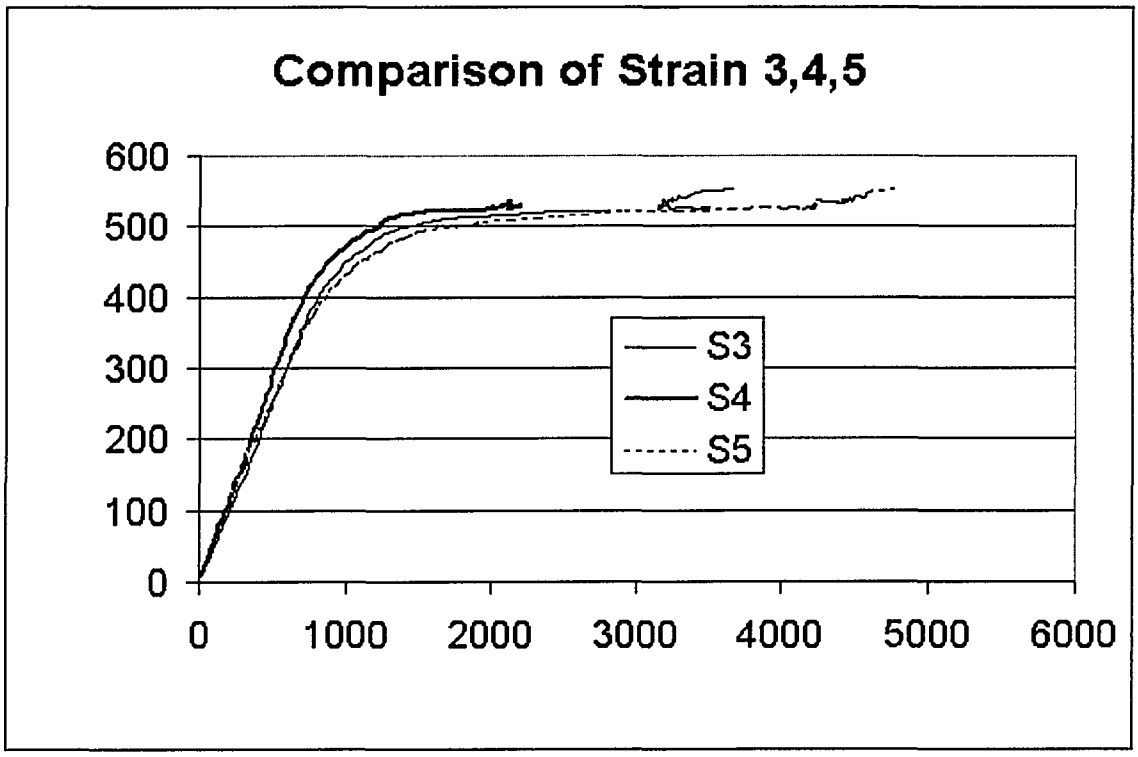

Fig. B7-2 Load vs. Strain 3,4,5 of Specimen 7

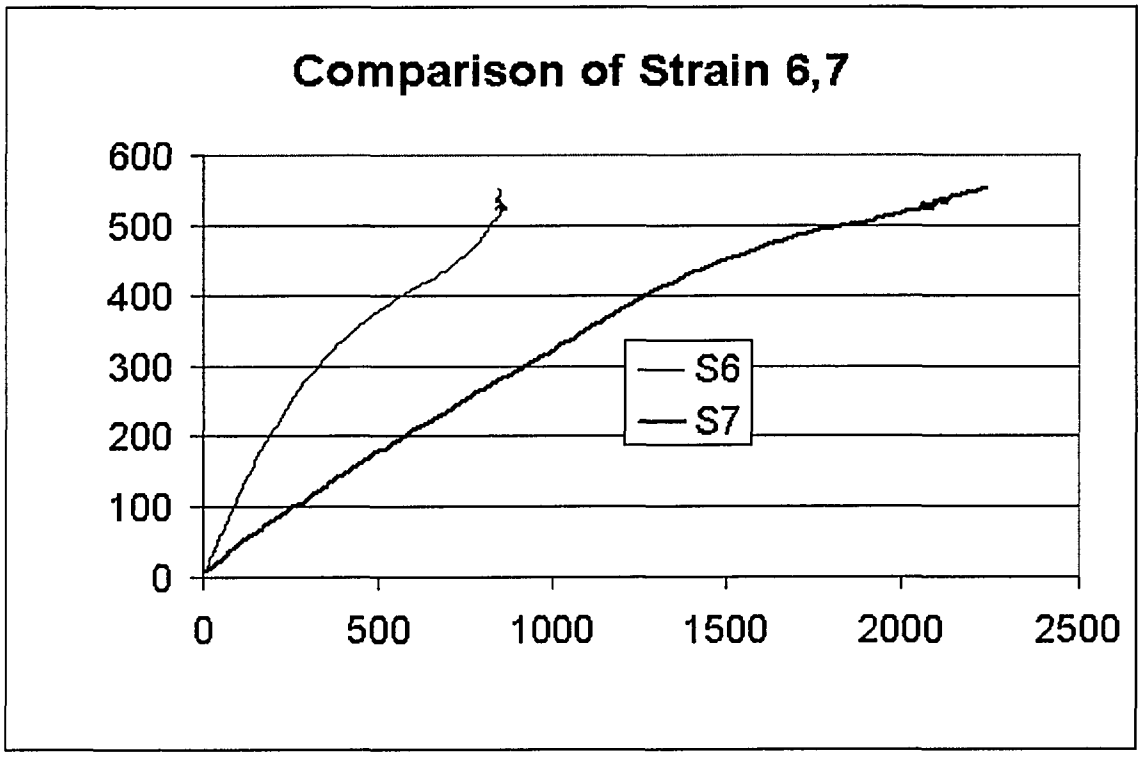

Fig. B7-3 Load vs. Strain 6,7 of Specimen 7

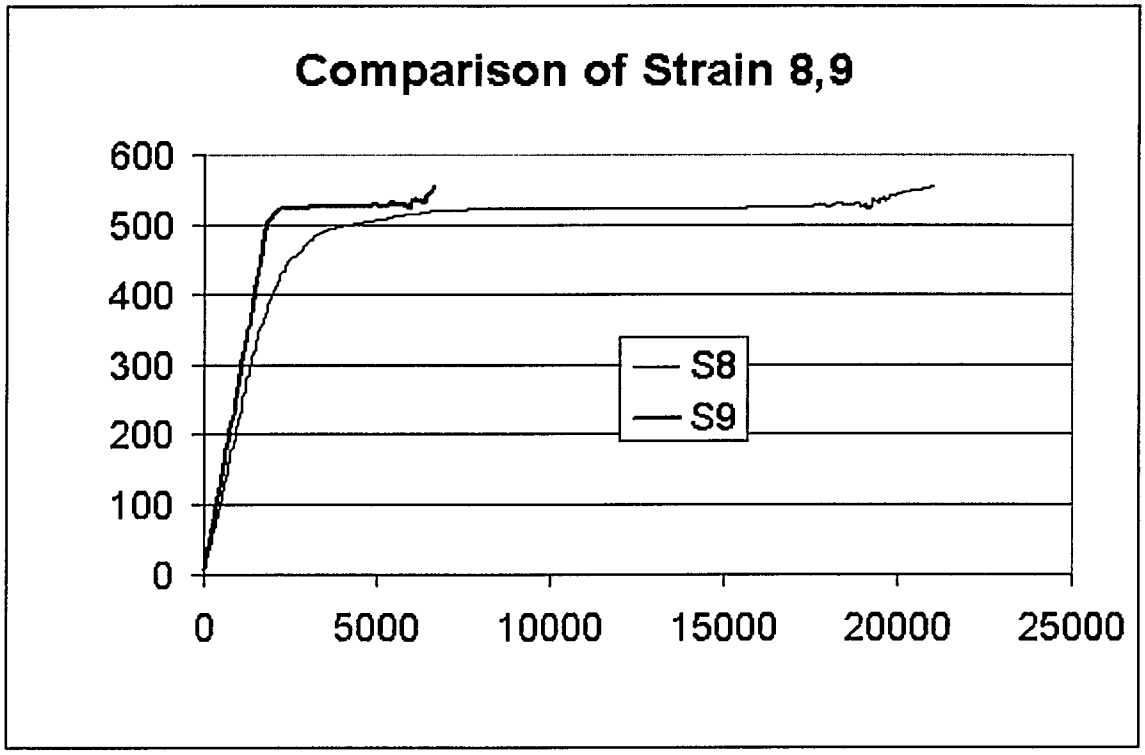

Fig. B7-4 Load vs. Strain 8,9 of Specimen 7

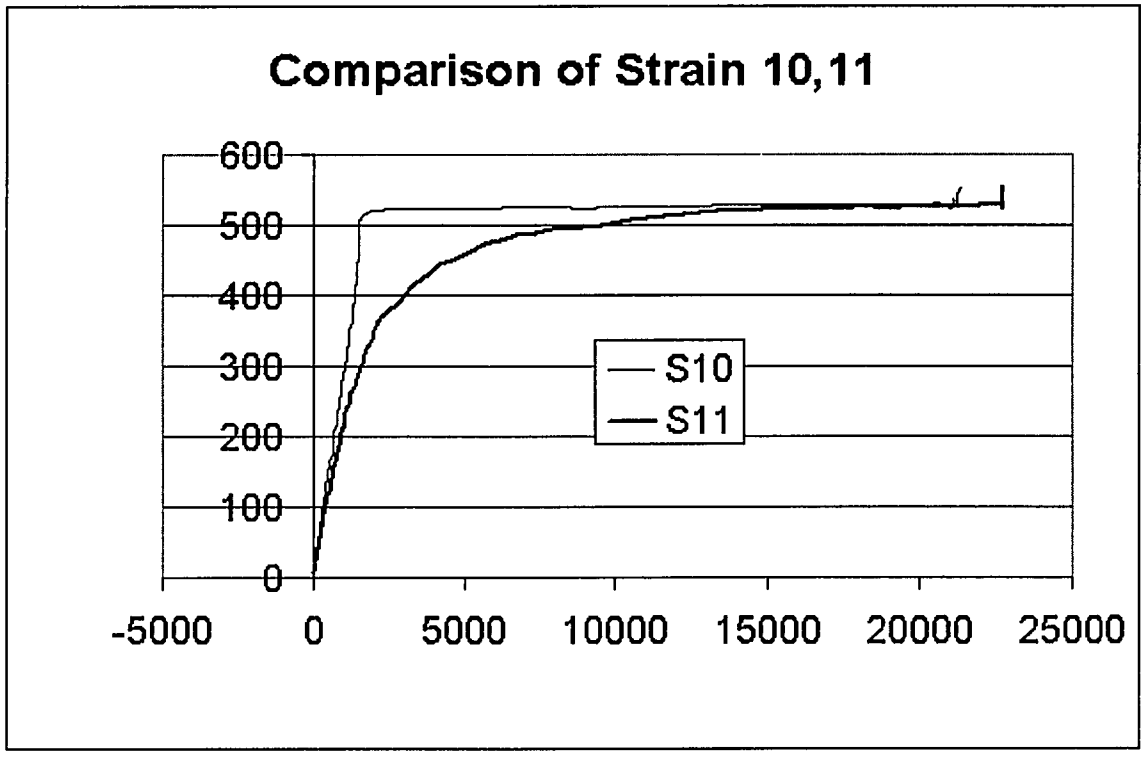

Fig. B7-5 Load vs. Strain 10,11 of Specimen 7

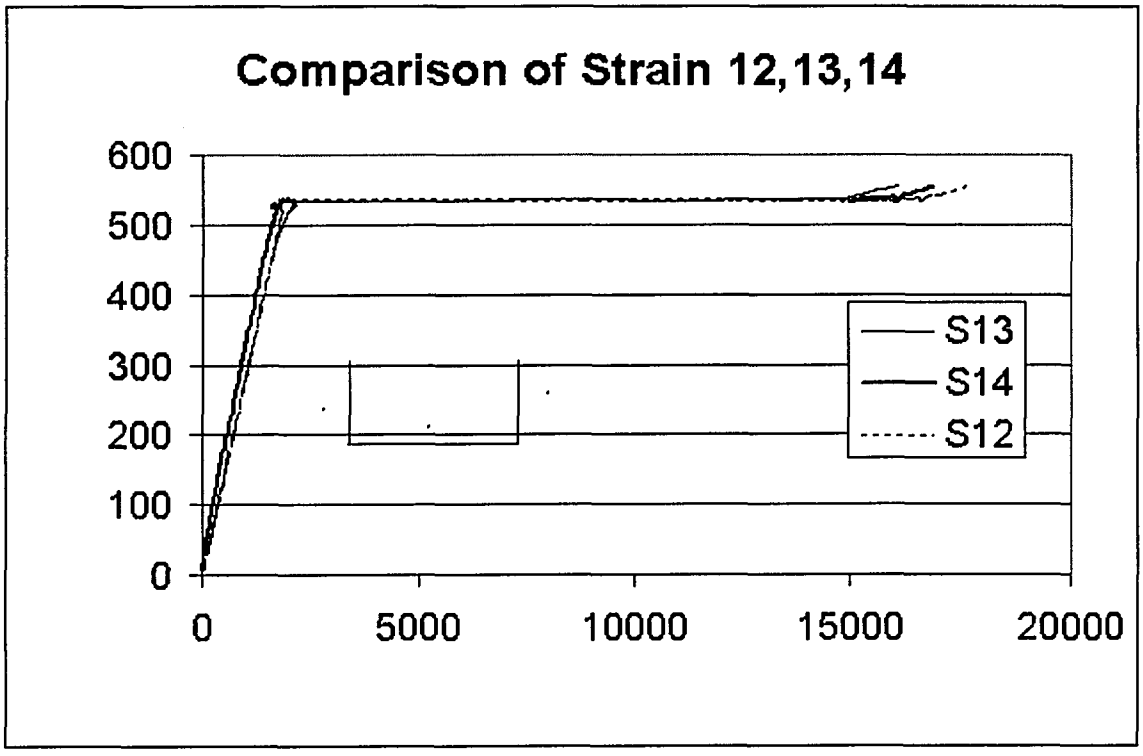

Fig. B7-6 Load vs. Strain 12,13,14 at mid-length of Specimen 7

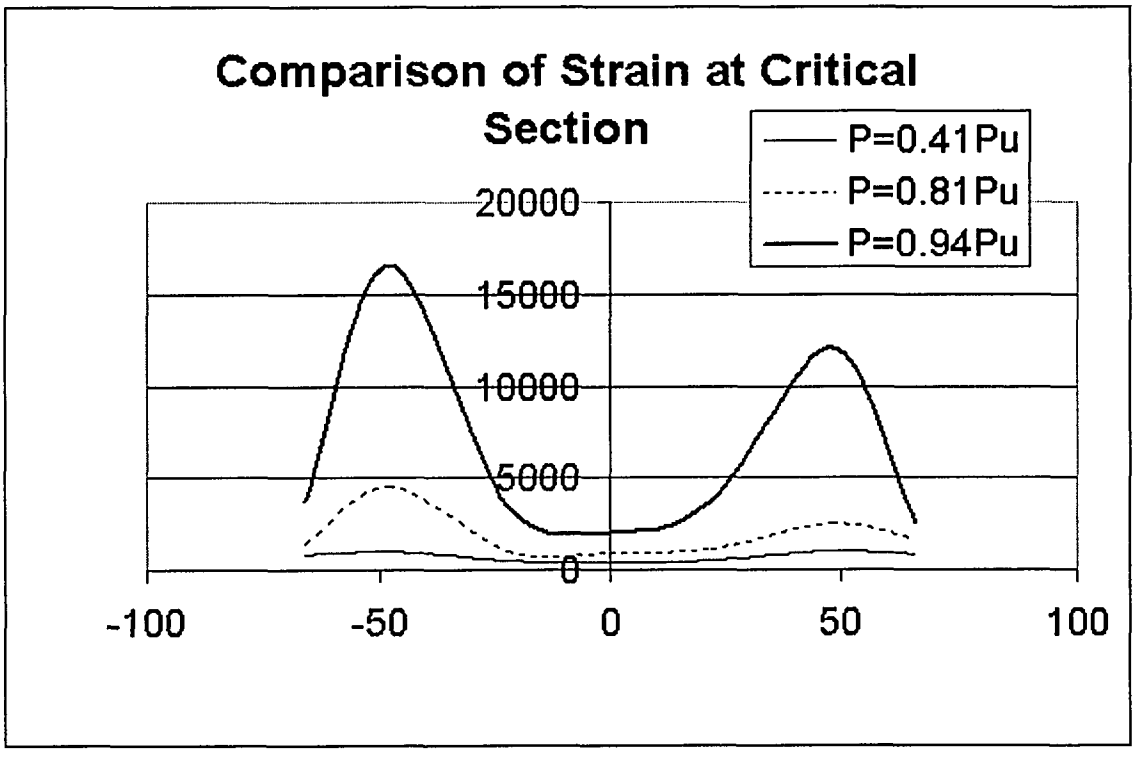

Fig. B7-7 Comparison of Strain 1,3,5 at Different Load Level of Specimen 7

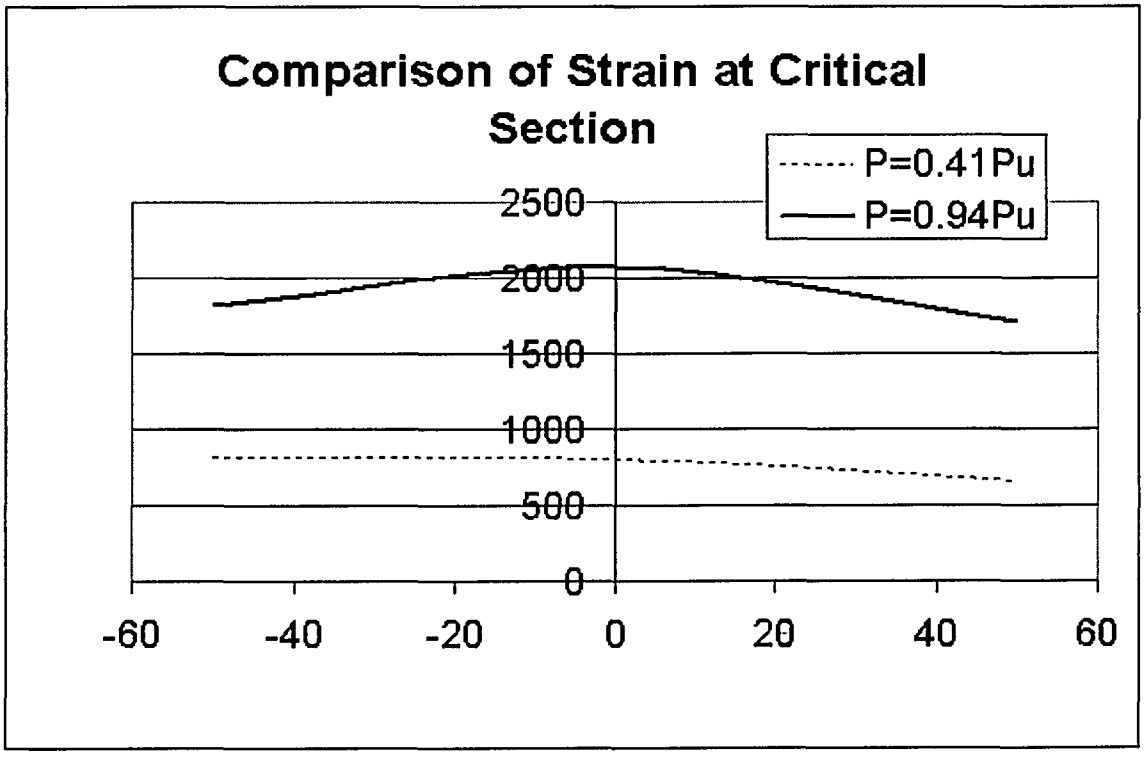

Fig. B7-8 Comparison of Strain 12,13,14 at Different Load Level of Specimen 7

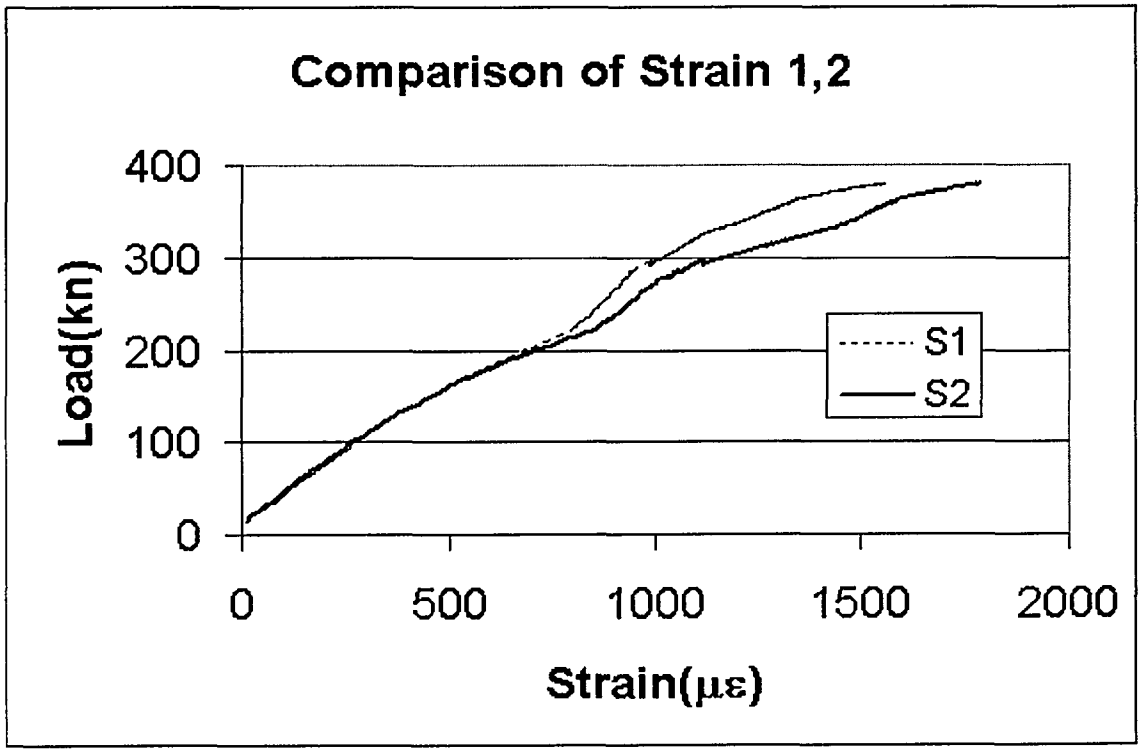

Fig. B8-1 Load vs. Strain 1,2 of Specimen 8

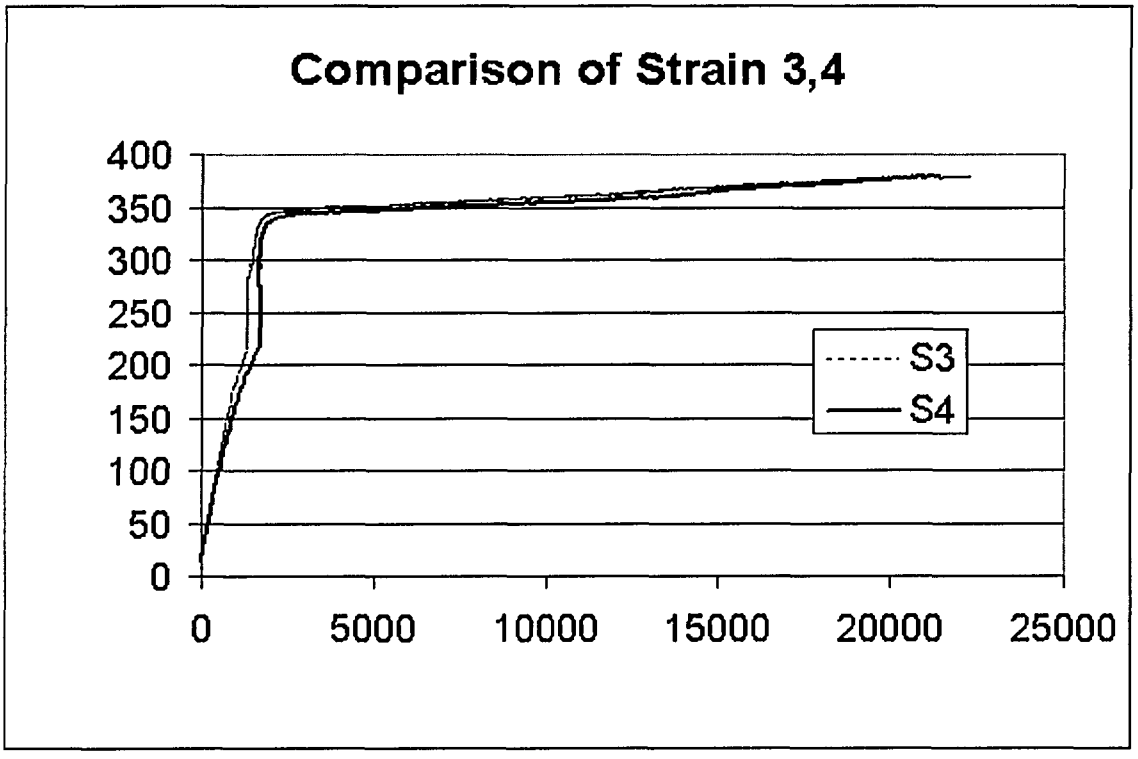

Fig. B8-2 Load vs. Strain 3,4 of Specimen 8

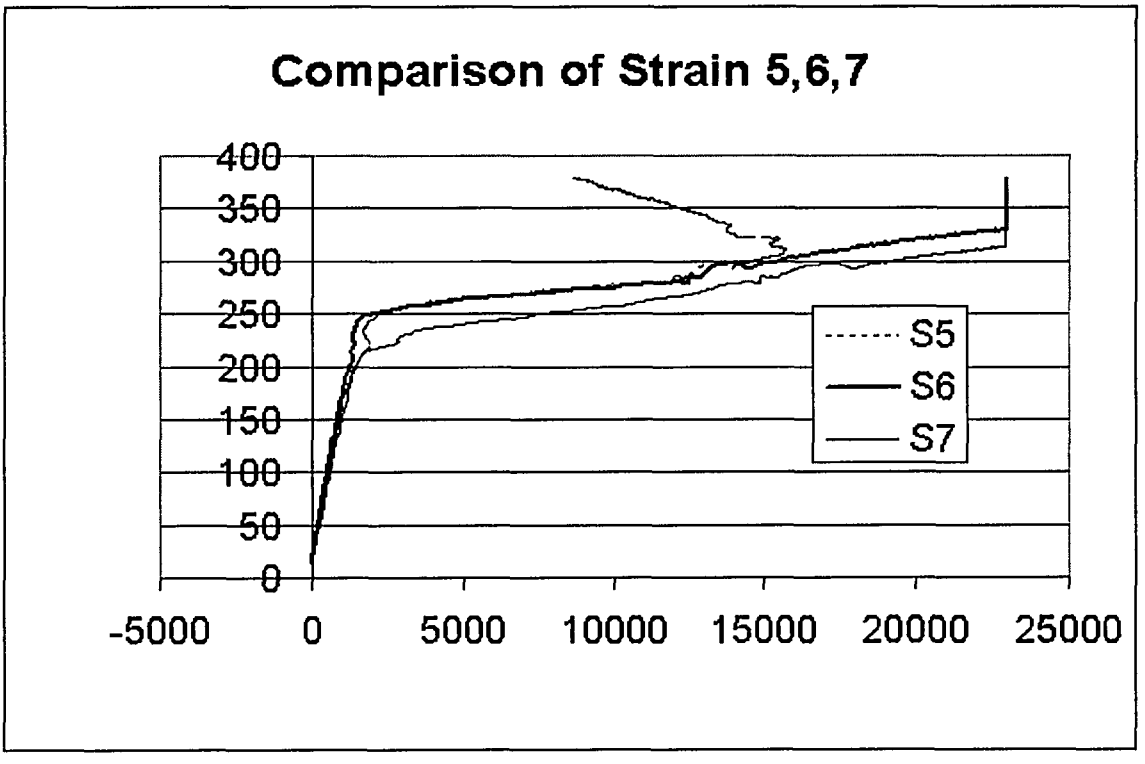

Fig. B8-3 Load vs. Strain 5,6,7 of Specimen 8

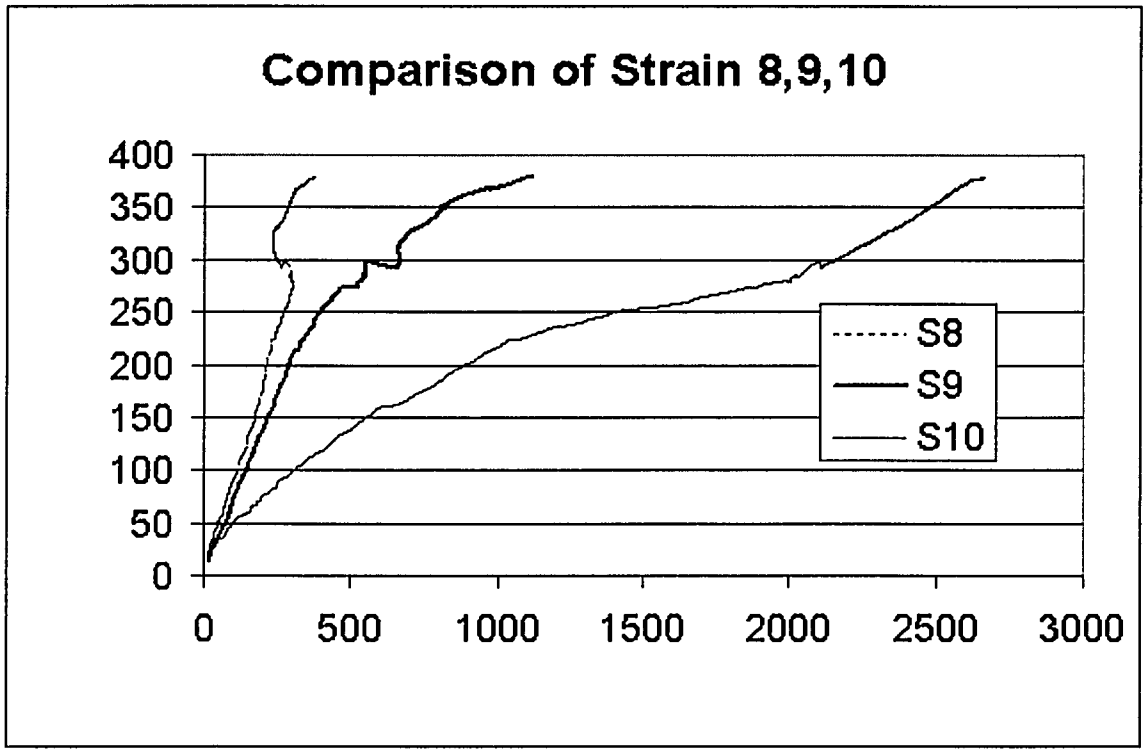

Fig. B8-4 Load vs. Strain 8,9,10 of Specimen 8

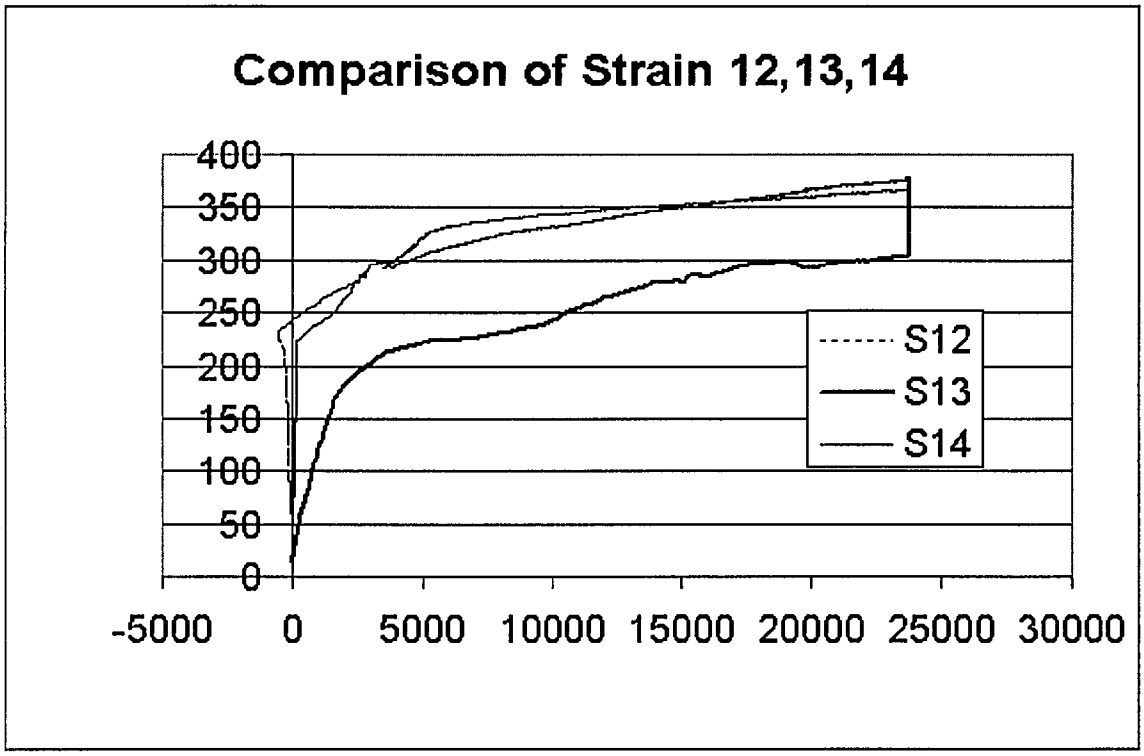

Fig. B8-5 Load vs. Strain 12,13,14 of Specimen 8

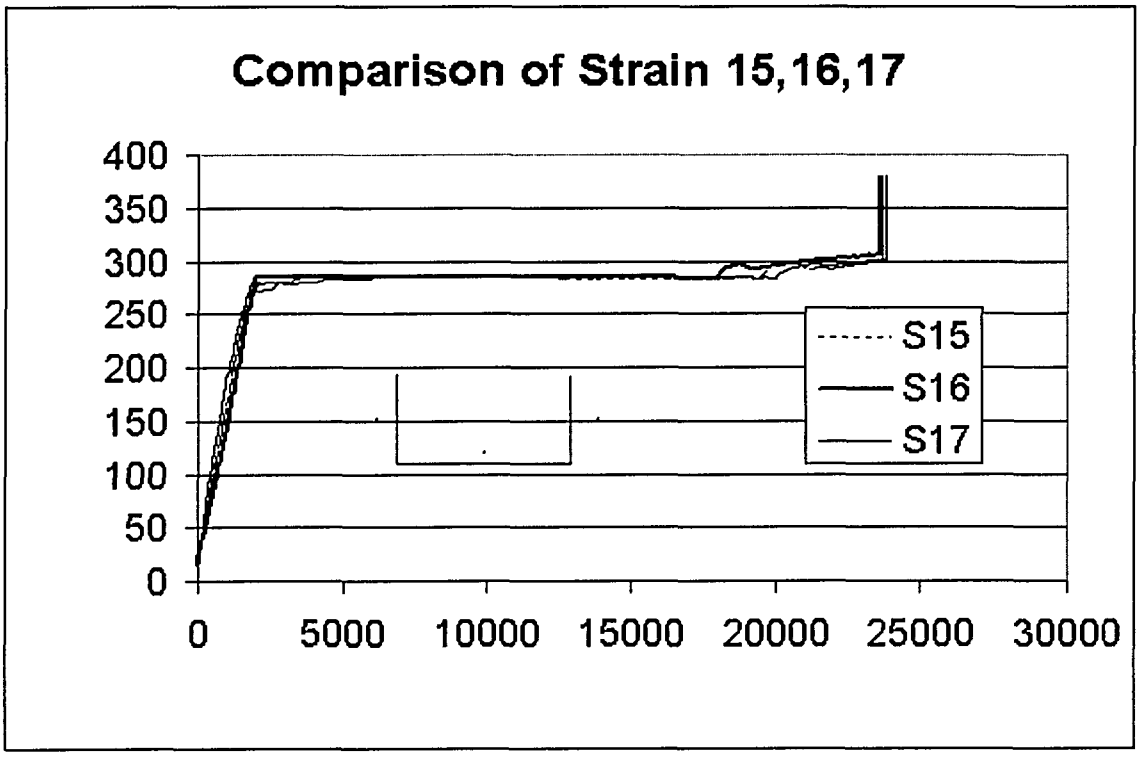

Fig. B8-6 Load vs. Strain 15,16,17 at mid-length of Specimen 8

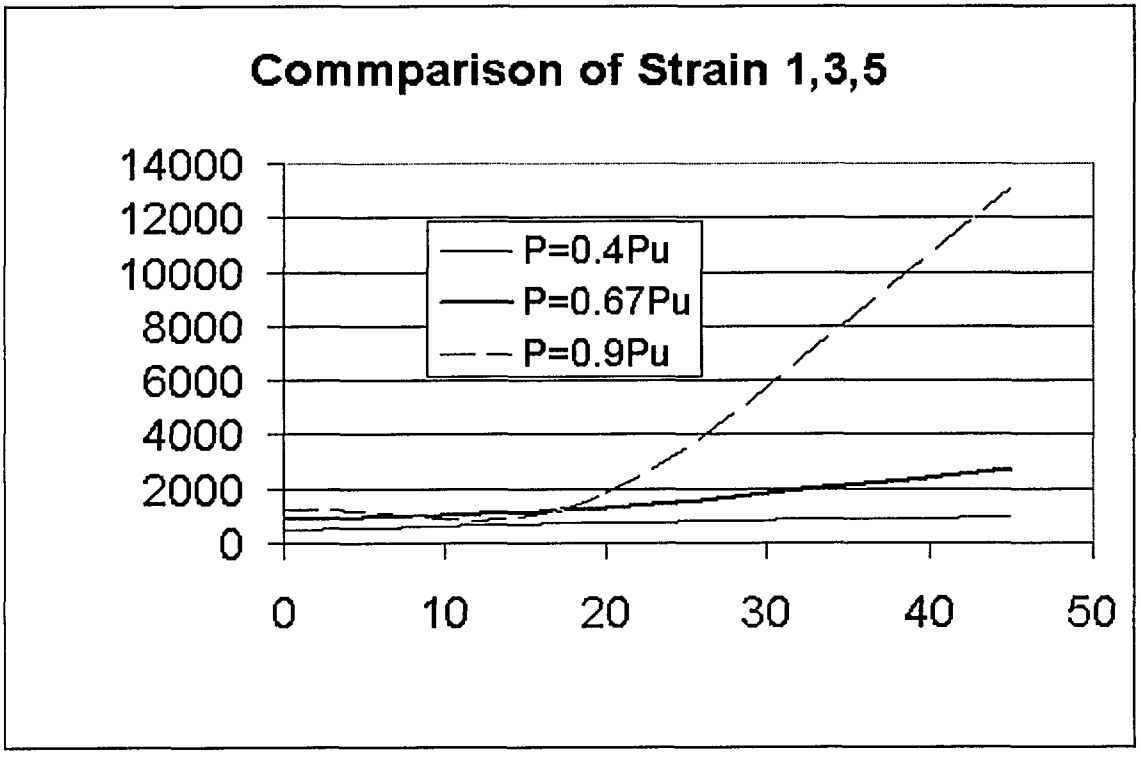

Fig. B8-7 Comparison of Strain 1,3,5 at Different Load Level of Specimen 8

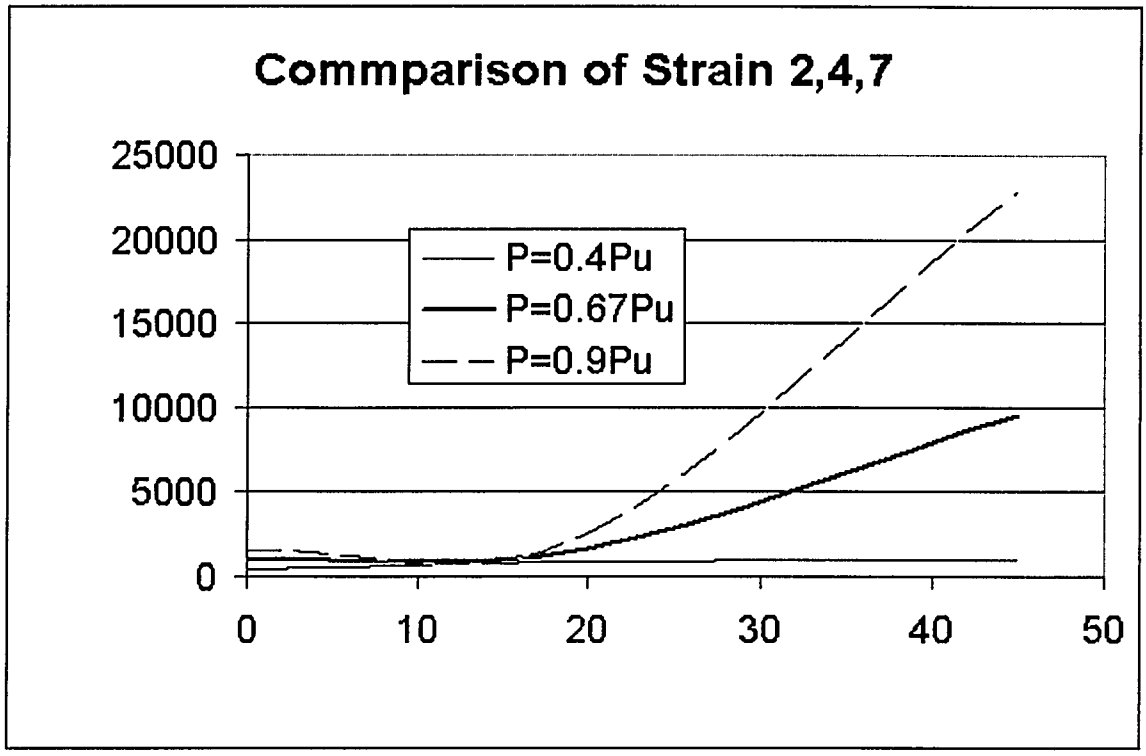

Fig. B8-8 Comparison of Strain 2,4,7 at Different Load Level of Specimen 8

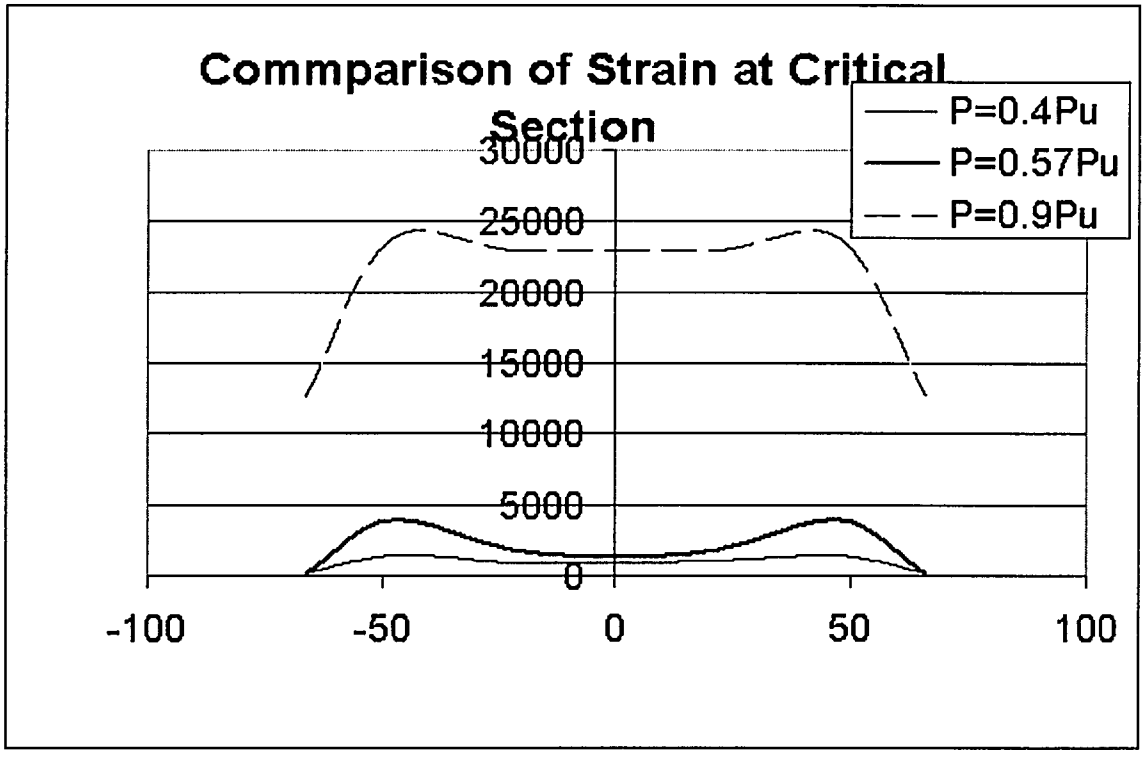

Fig. B8-9 Comparison of Strain at Critical Section at Different Load Level of Specimen 8

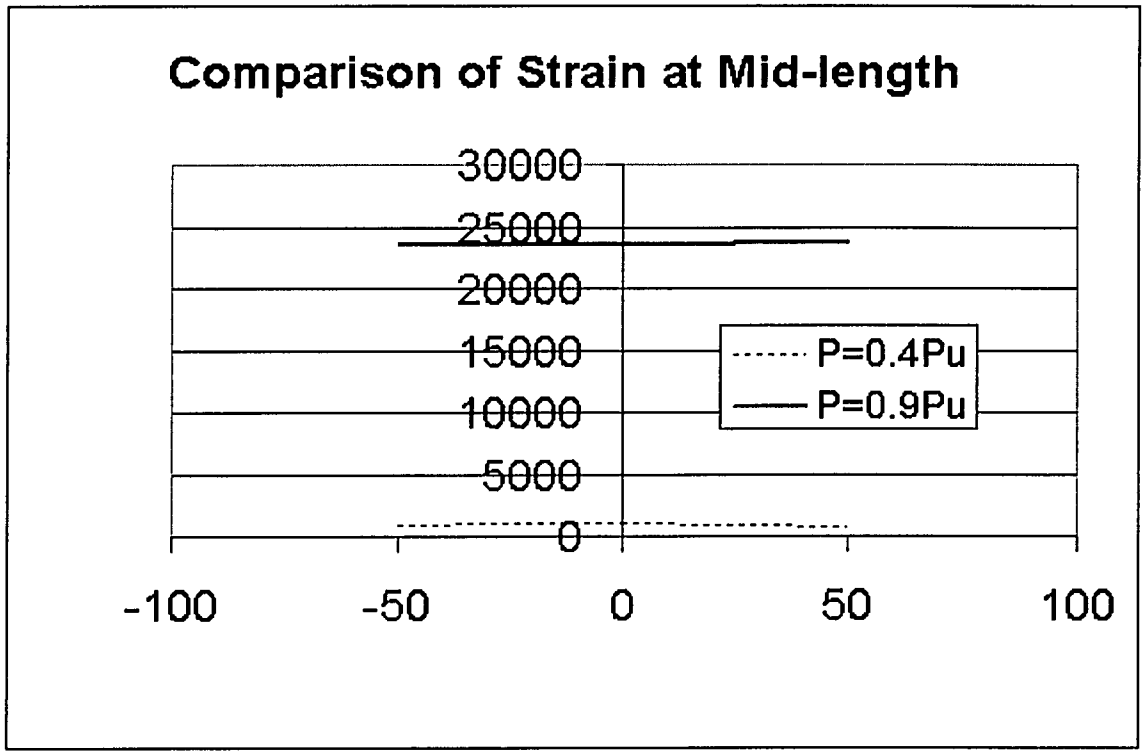

Fig. B8-10 Comparison of Strain 15,16,17 at Different Load Level of Specimen 8

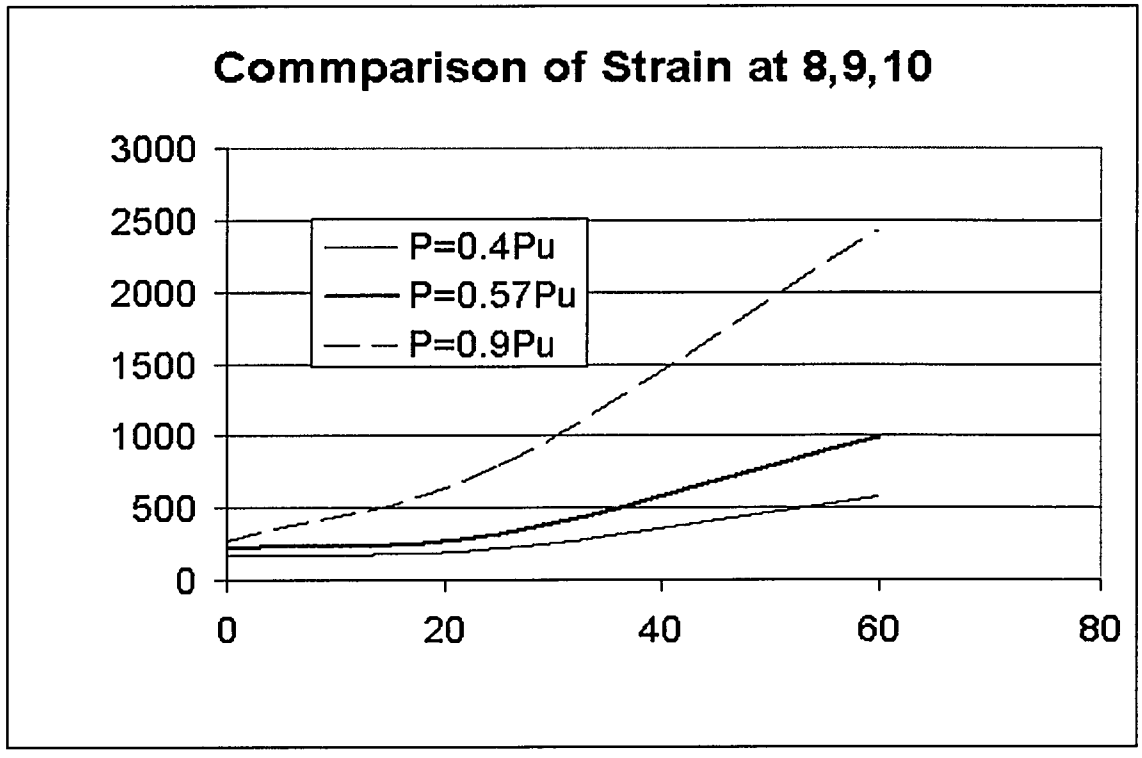

Fig. B8-11 Comparison of Strain 8,9,10 at Different Load Level of Specimen 8

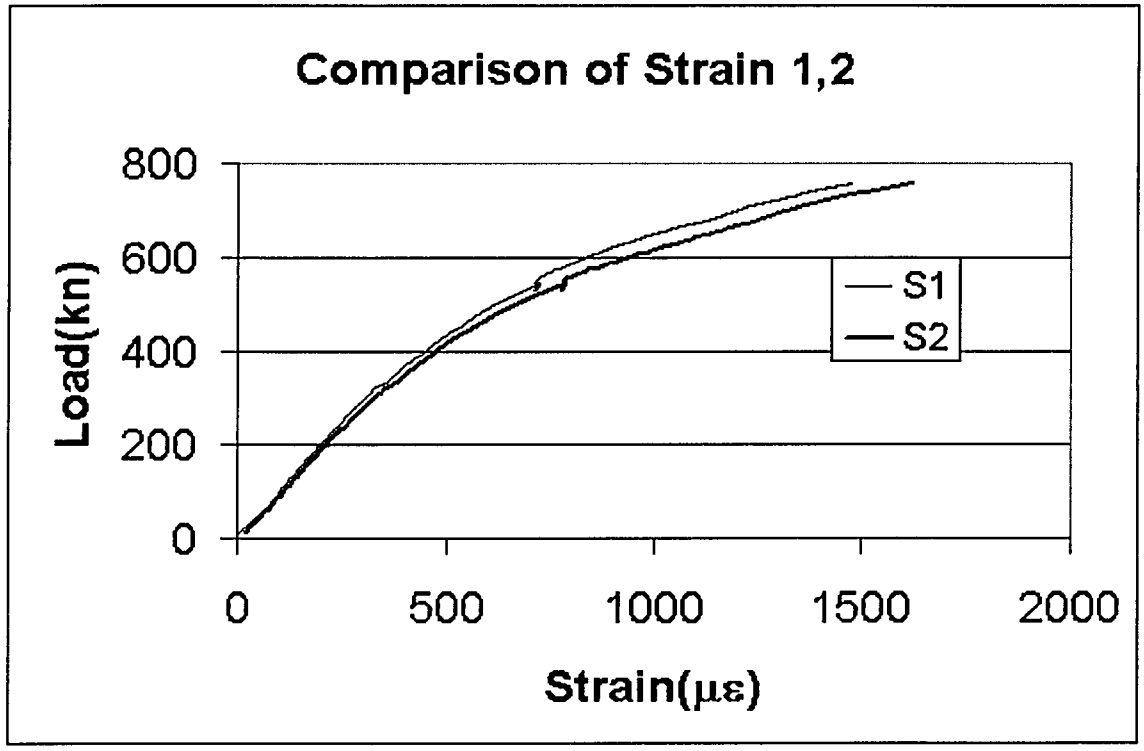

Fig. B9-1 Load vs. Strain 1,2 of Specimen 9

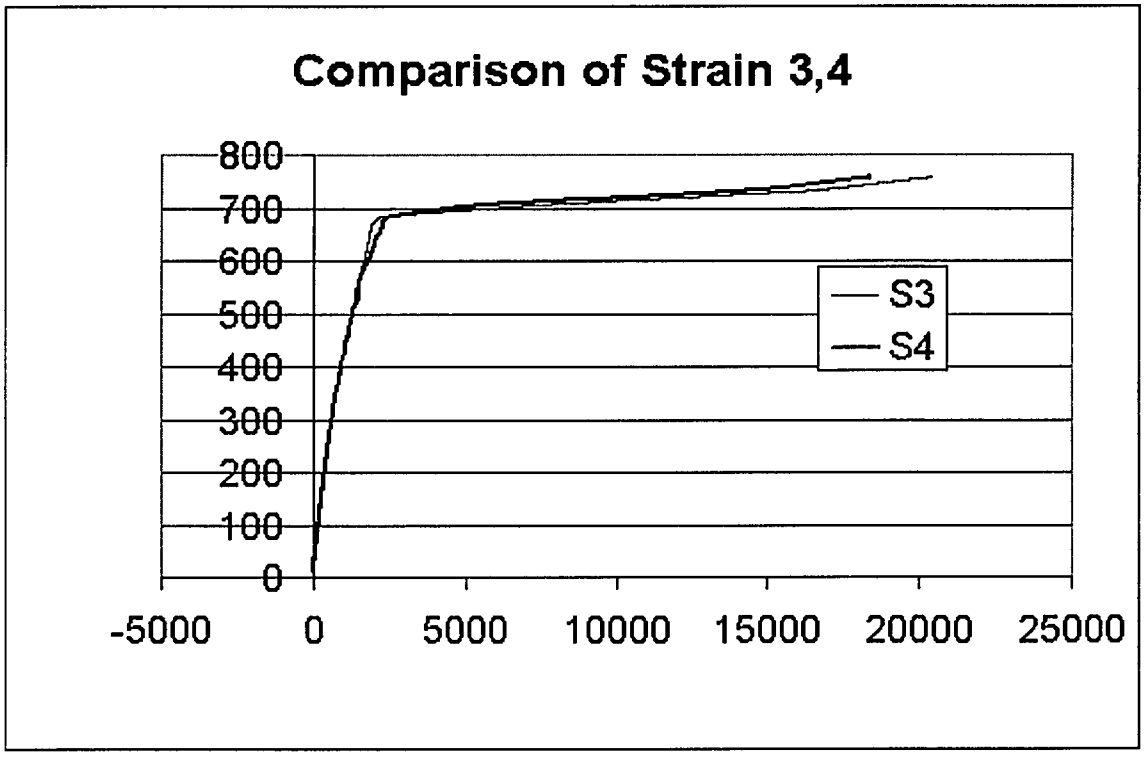

Fig. B9-2 Load vs. Strain 3,4 of Specimen 9

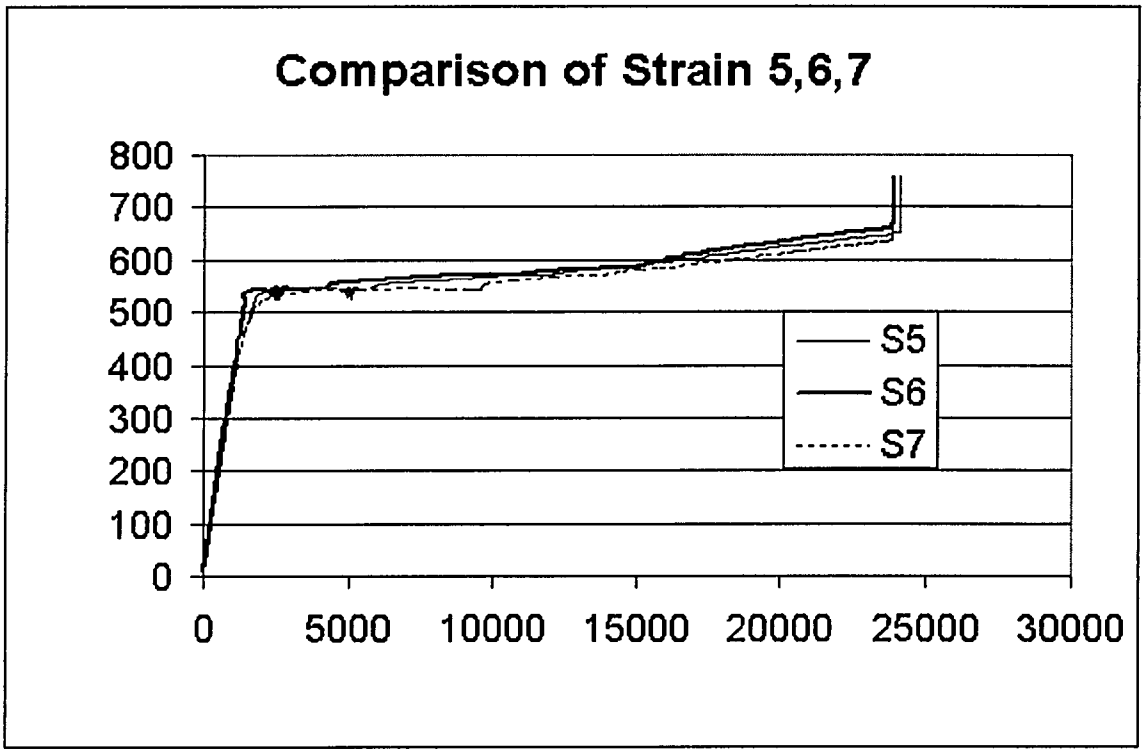

Fig. B9-3 Load vs. Strain 5,6,7 of Specimen 9

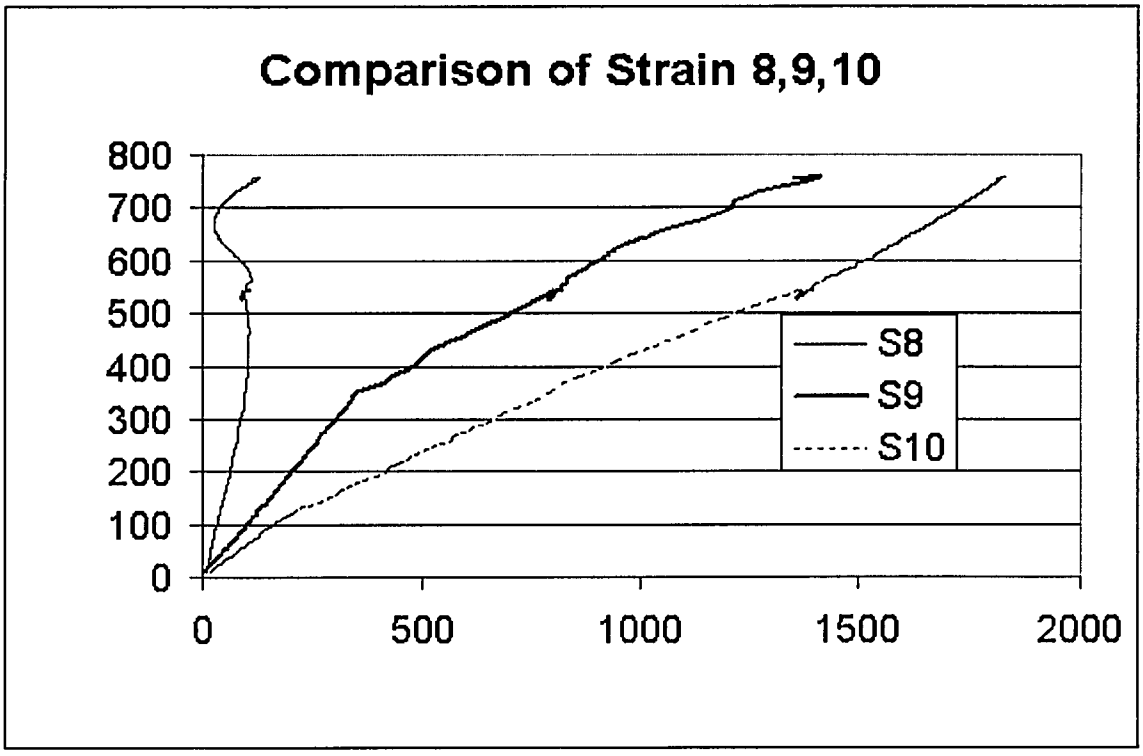

Fig. B9-4 Load vs. Strain 8,9,10 of Specimen 9

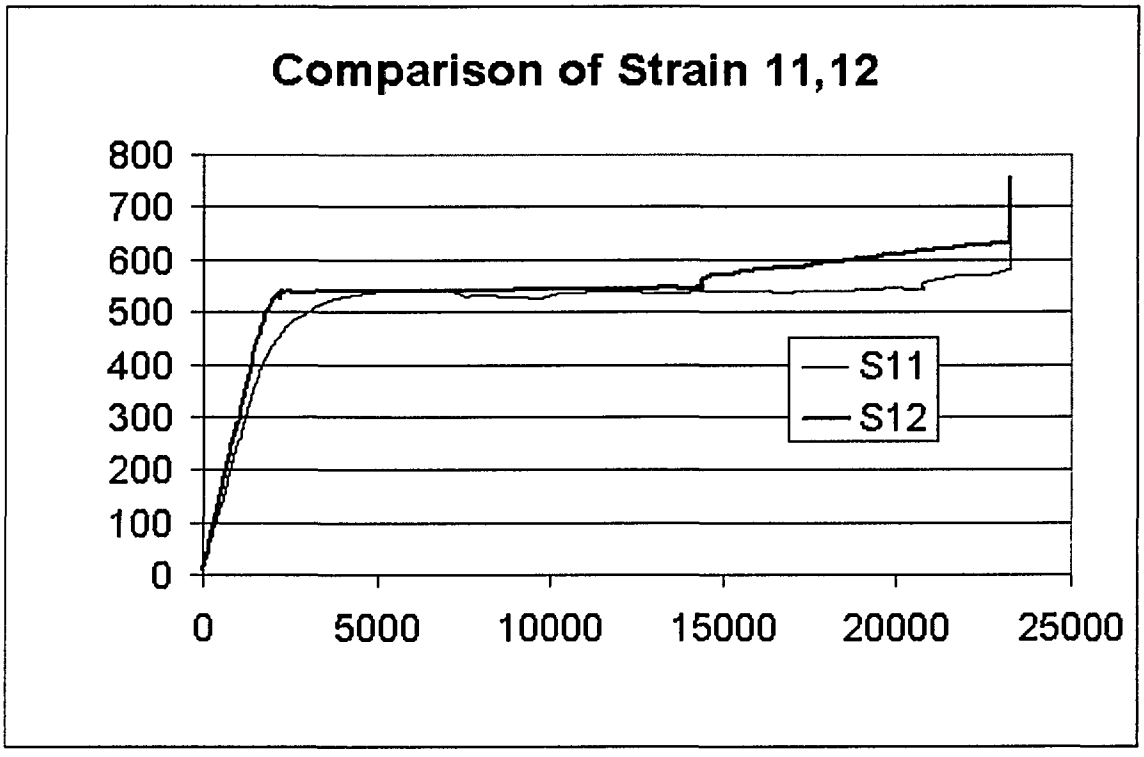

Fig. B9-5 Load vs. Strain 11,12 of Specimen 9

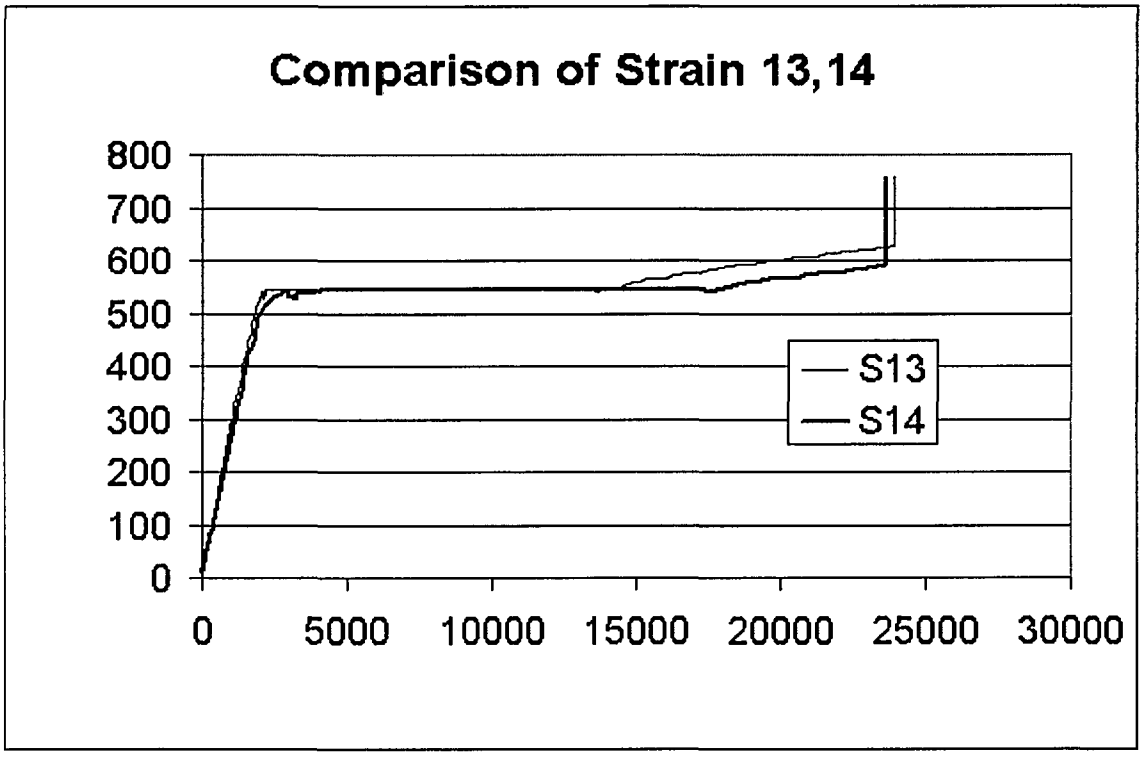

Fig. B9-6 Load vs. Strain 13,14 of Specimen 9

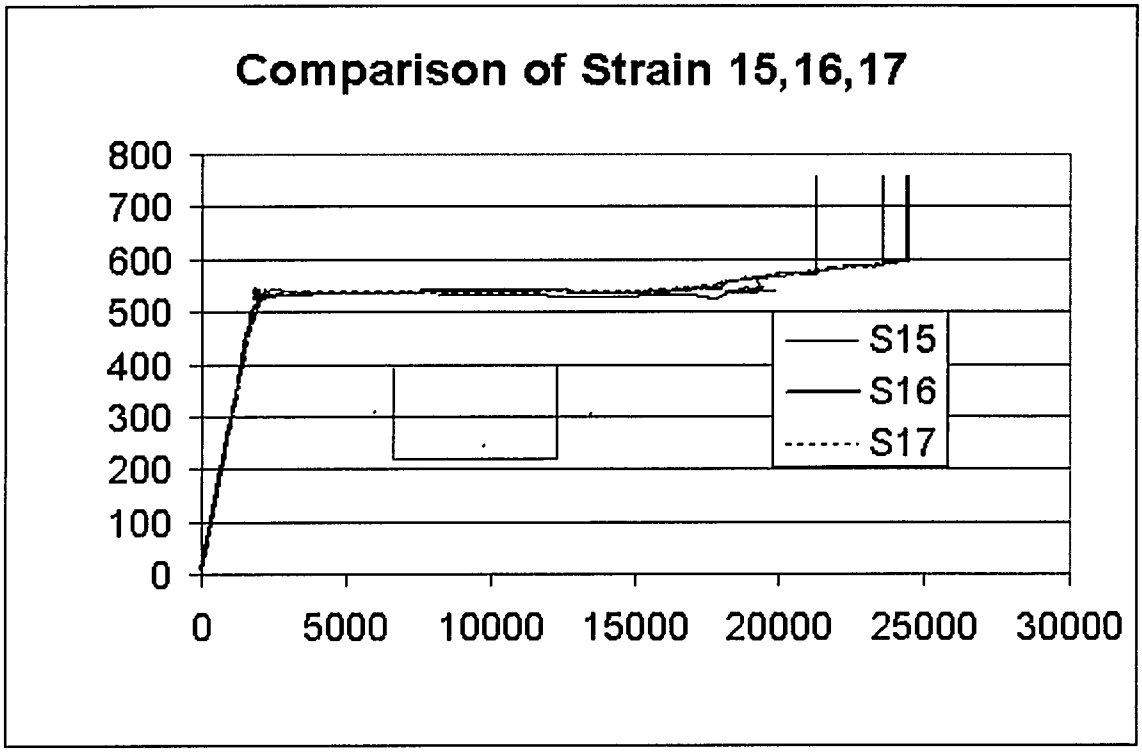

Fig. B9-7 Load vs. Strain 15,16,17 at mid-length of Specimen 9

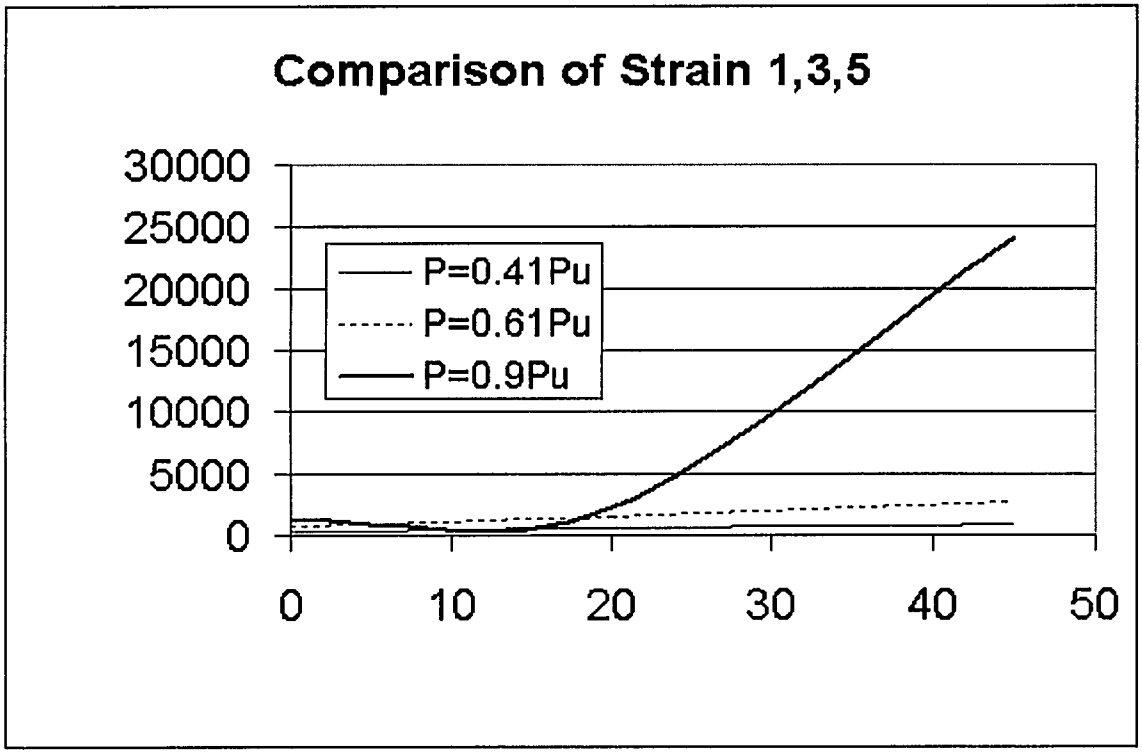

Fig. B9-8 Comparison of Strain 1,3,5 at Different Load Level of Specimen 9

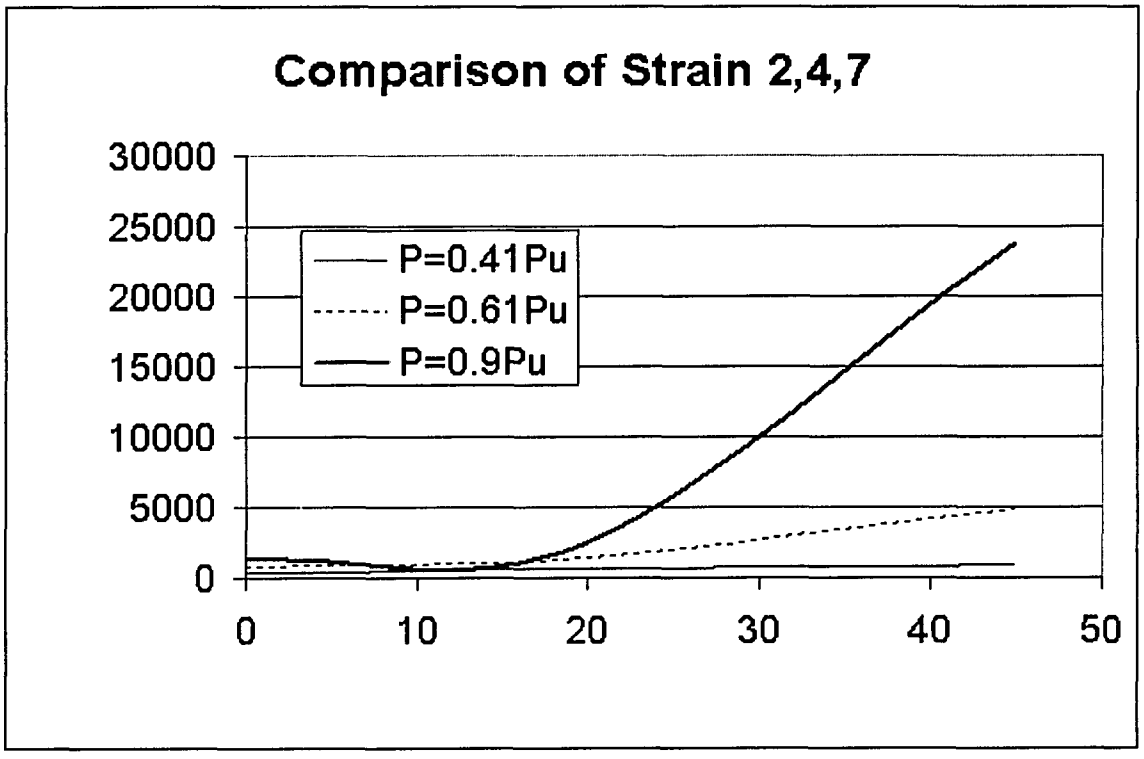

Fig. B9-9 Comparison of Strain 2,4,7 at Different Load Level of Specimen 9

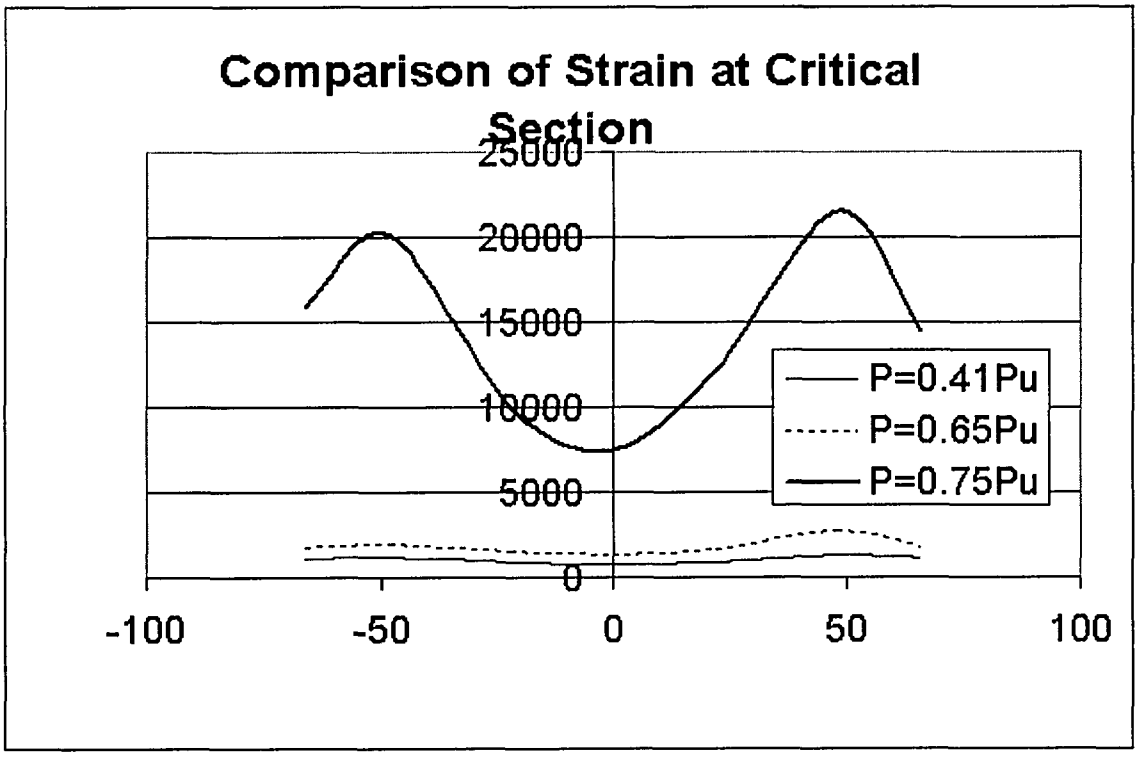

Fig. B9-10 Comparison of Strain at Critical Section at Different Load Level of Specimen 9

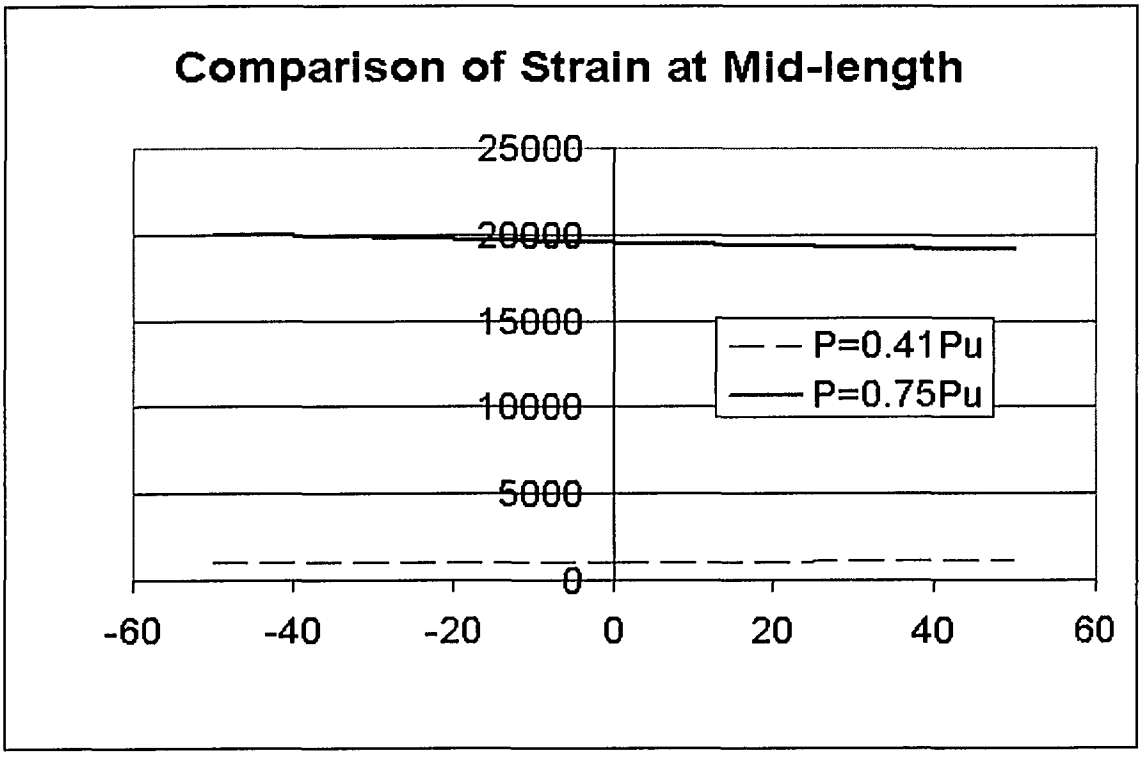

Fig. B9-11 Comparison of Strain 15,16,17 at Different Load Level of Specimen 9

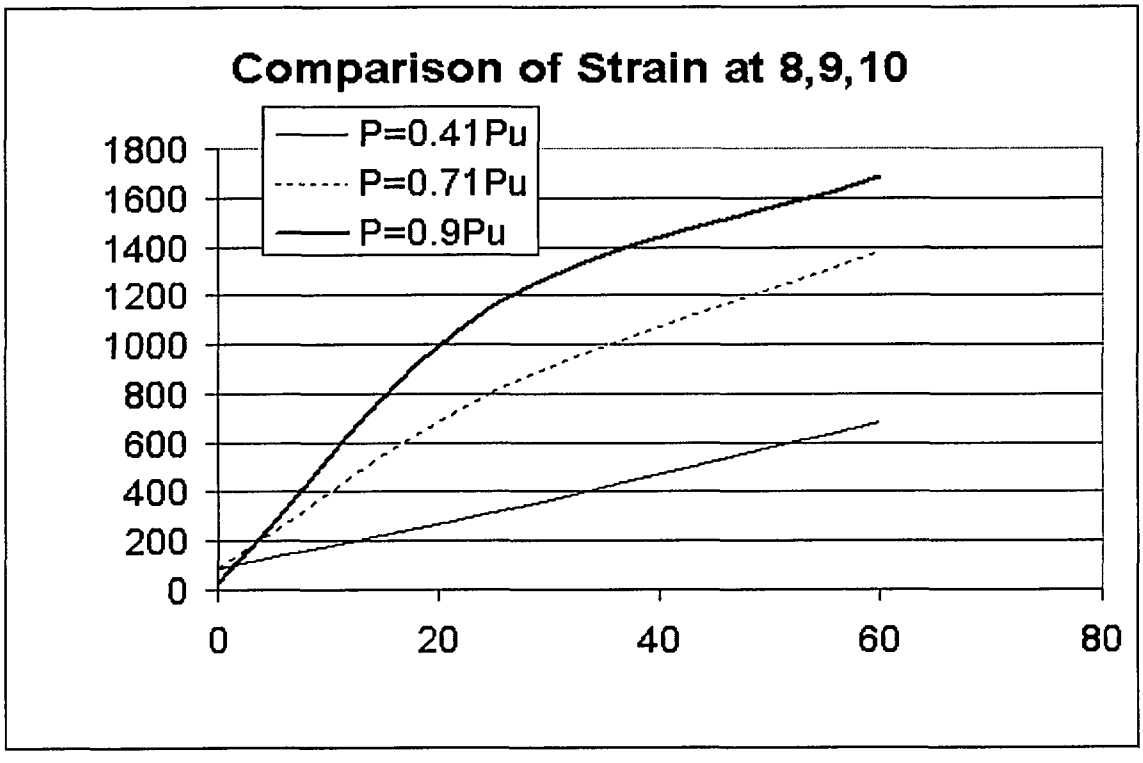

Fig. B9-12 Comparison of Strain 8,9,10 at Different Load Level of Specimen 9

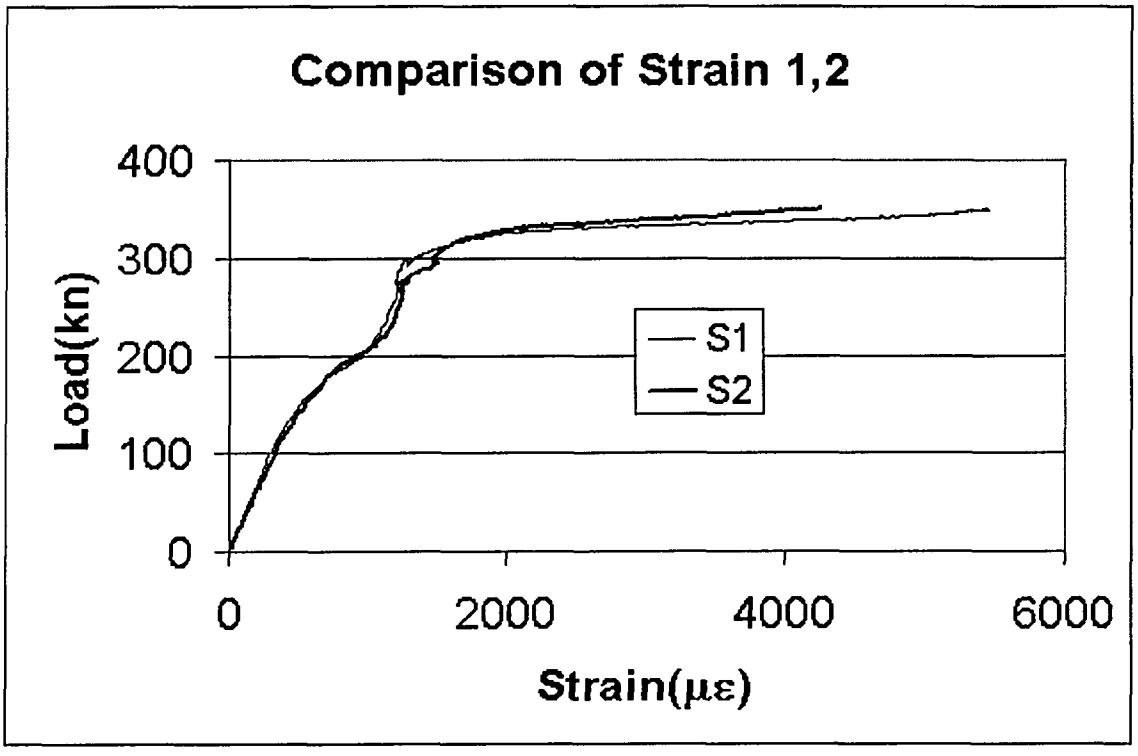

Fig. B10-1 Load vs. Strain 1,2 of Specimen 10

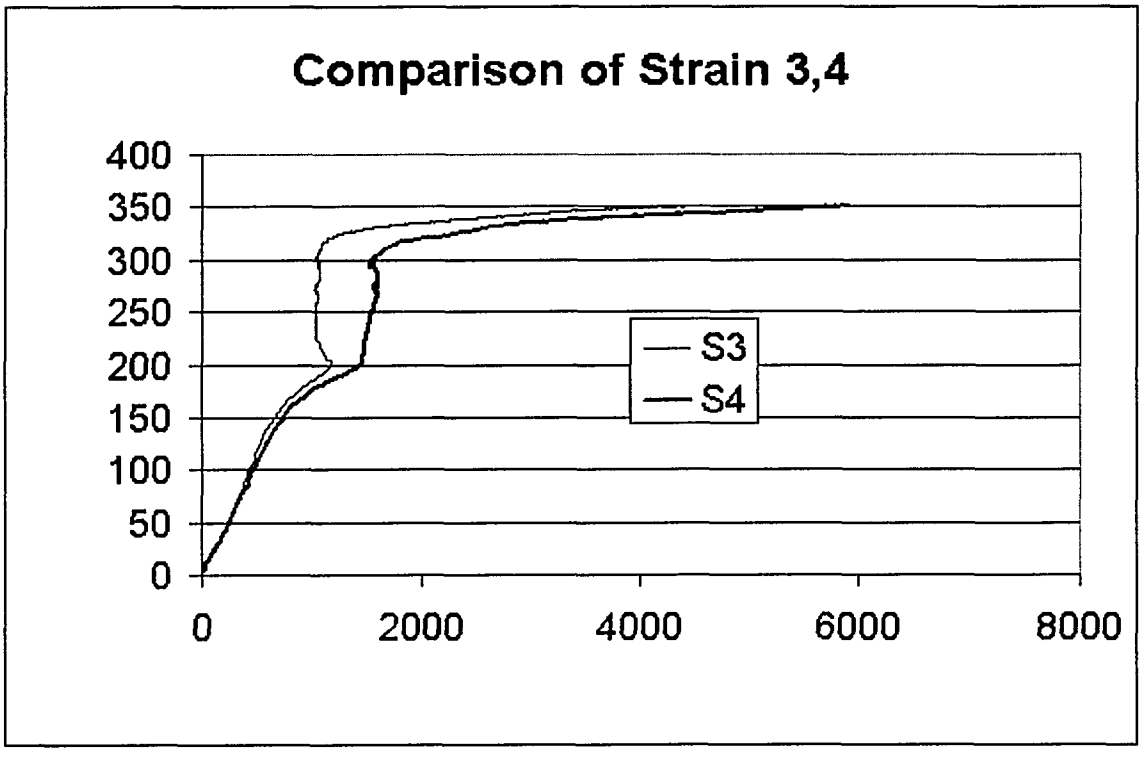

Fig. B10-2 Load vs. Strain 3,4 of Specimen 10

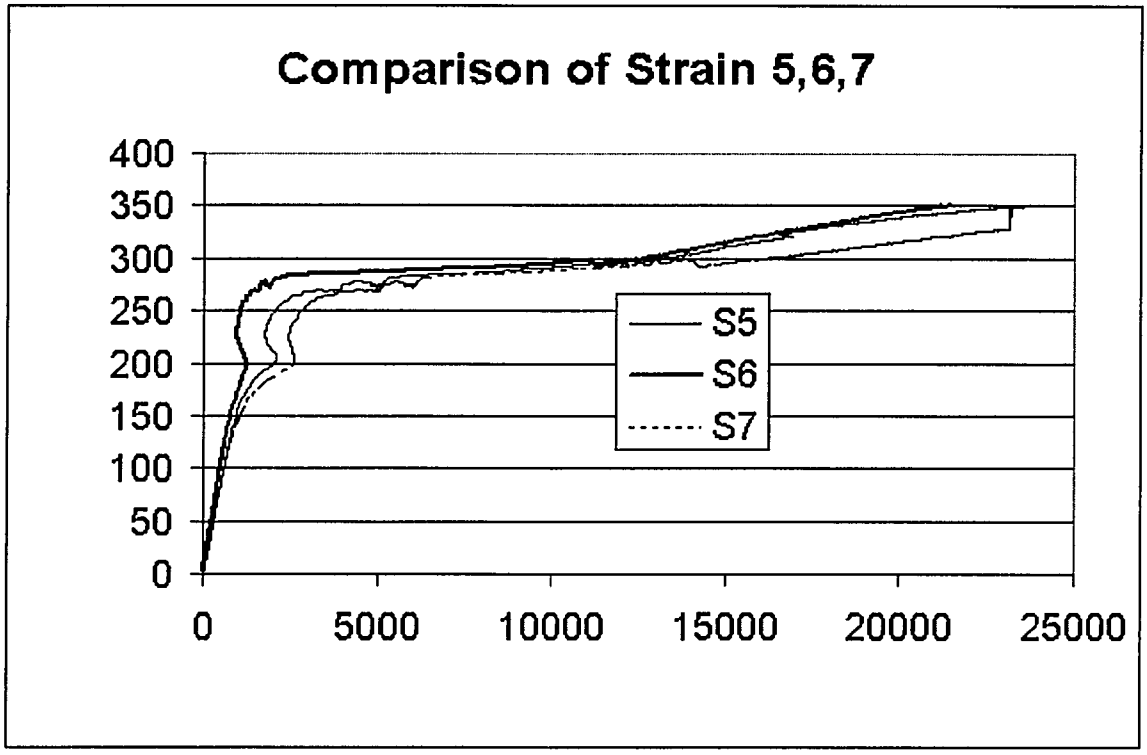

Fig. B10-3 Load vs. Strain 5,6,7 of Specimen 10

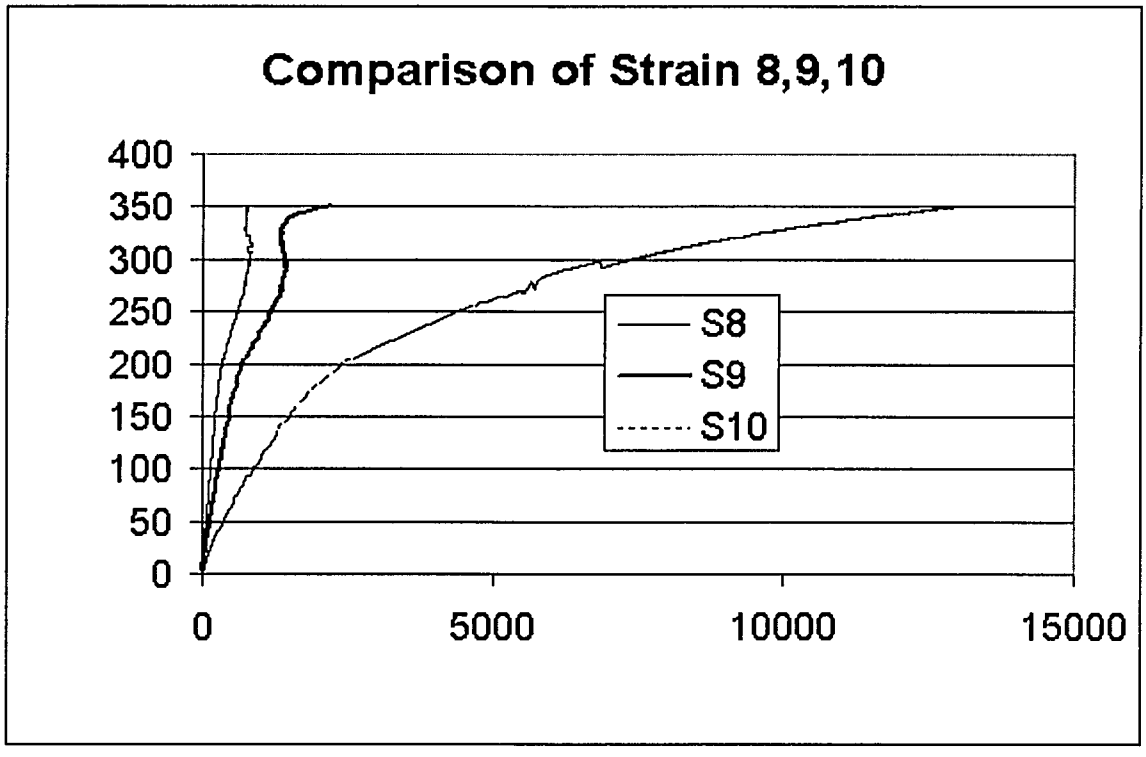

Fig. B10-4 Load vs. Strain 8,9,10 of Specimen 10

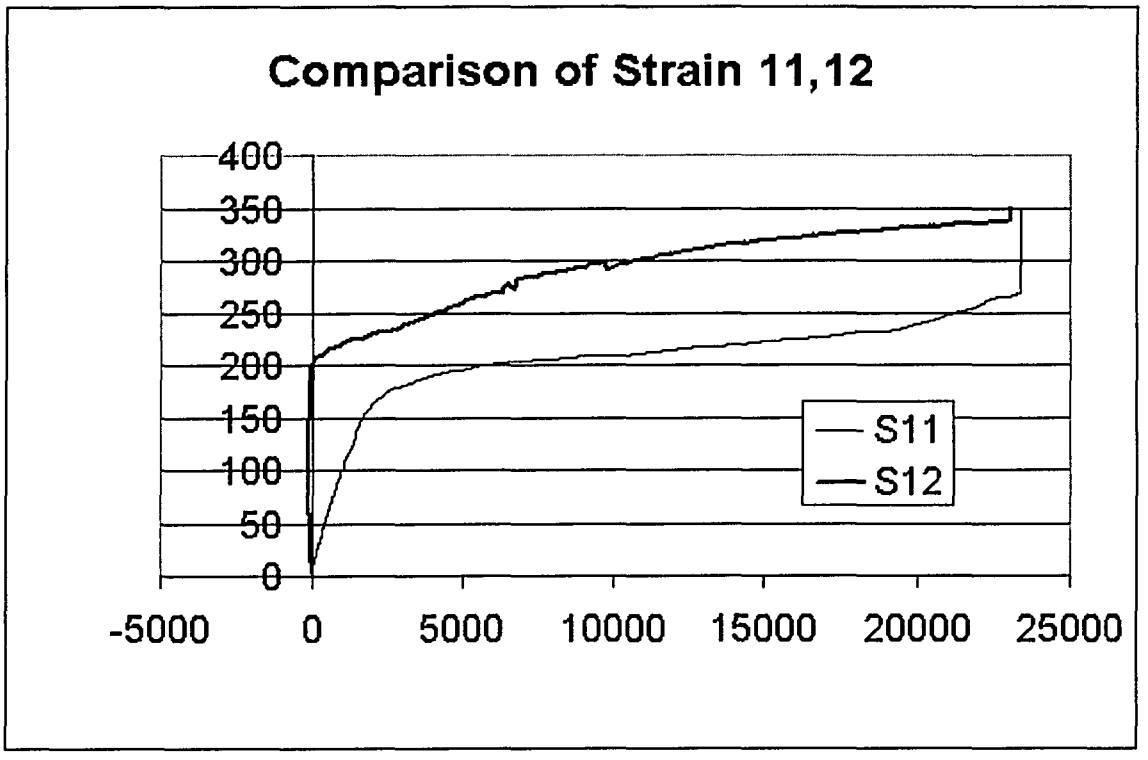

Fig. B10-5 Load vs. Strain 11,12 of Specimen 10

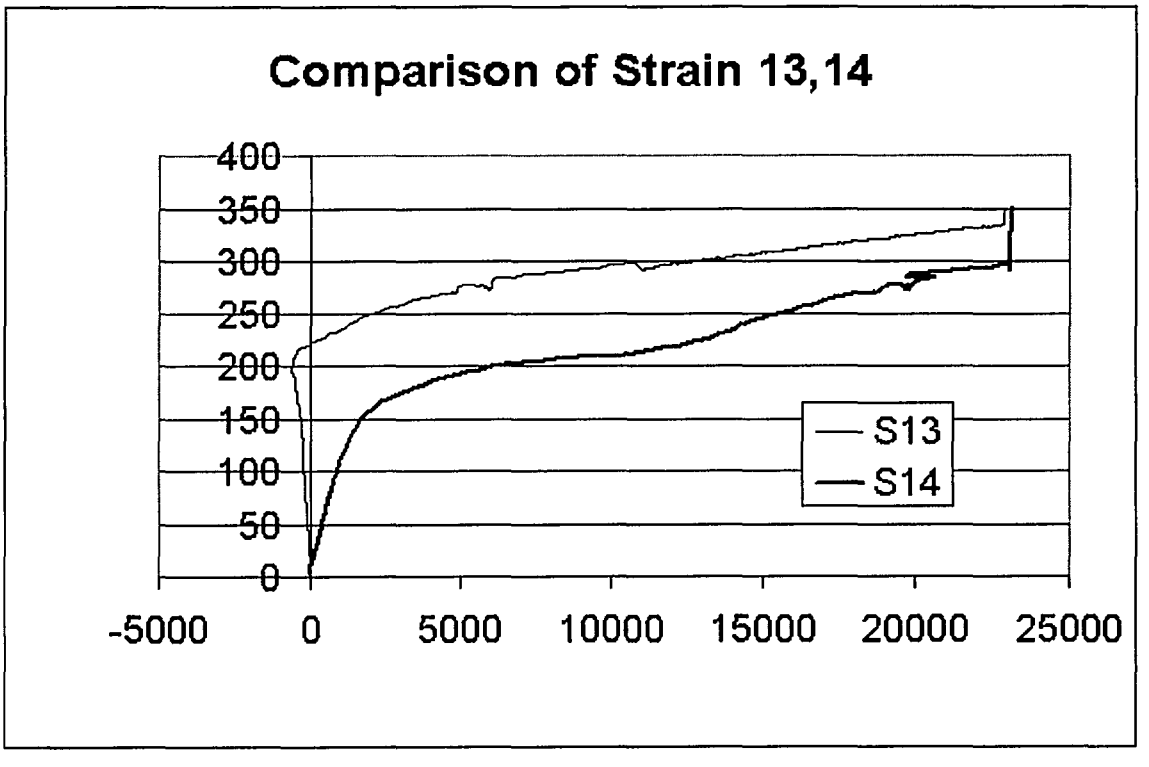

Fig. B10-6 Load vs. Strain 13,14 of Specimen 10

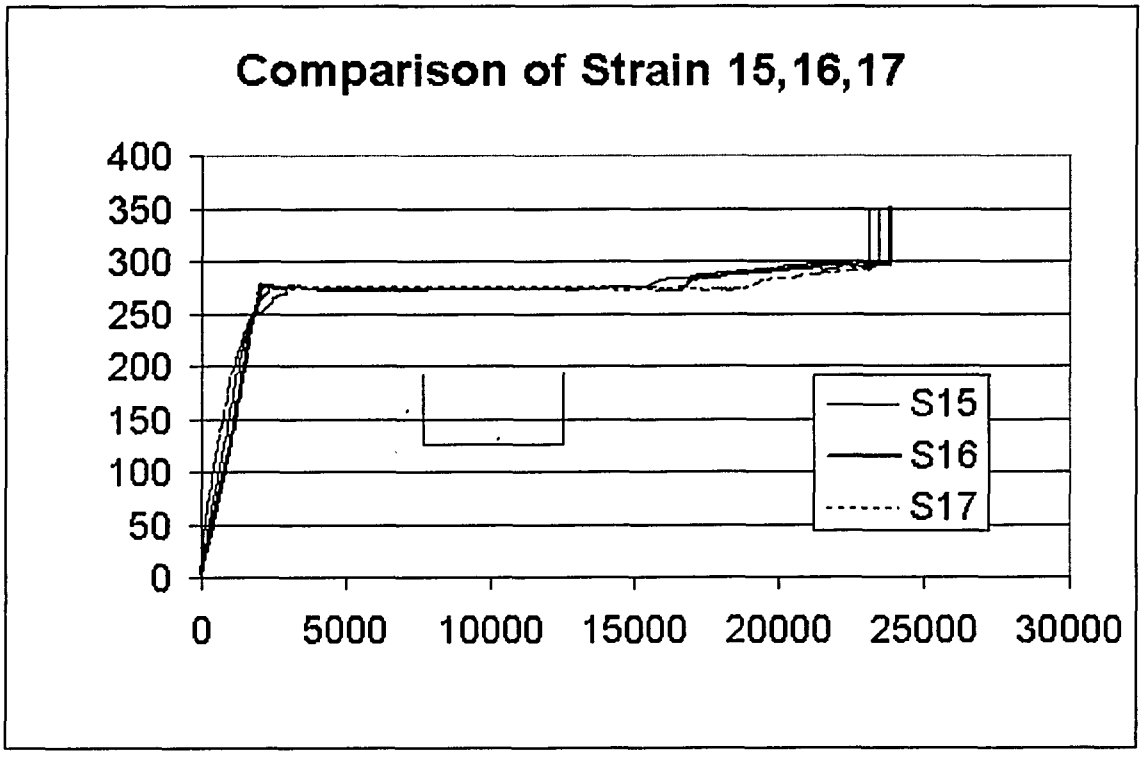

Fig. B10-7 Load vs. Strain 15,16,17 of Specimen 10

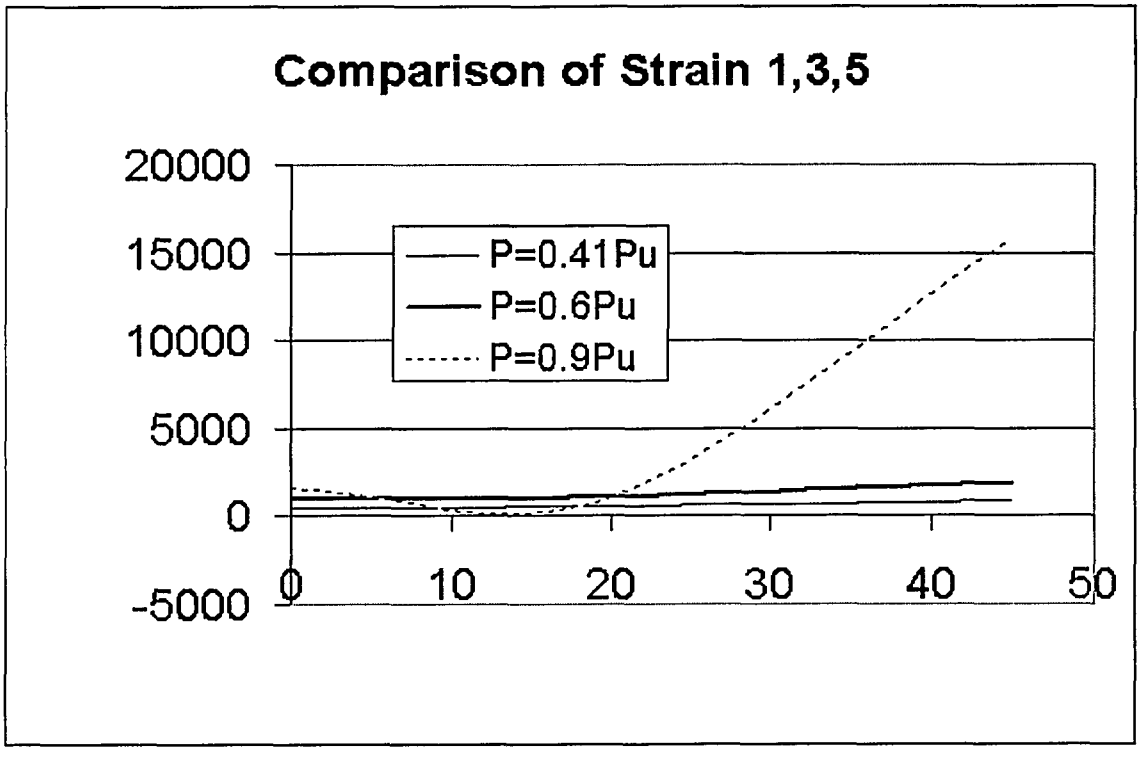

Fig. B10-8 Comparison of Strain 1,3,5 at Different Load Level of Specimen 10

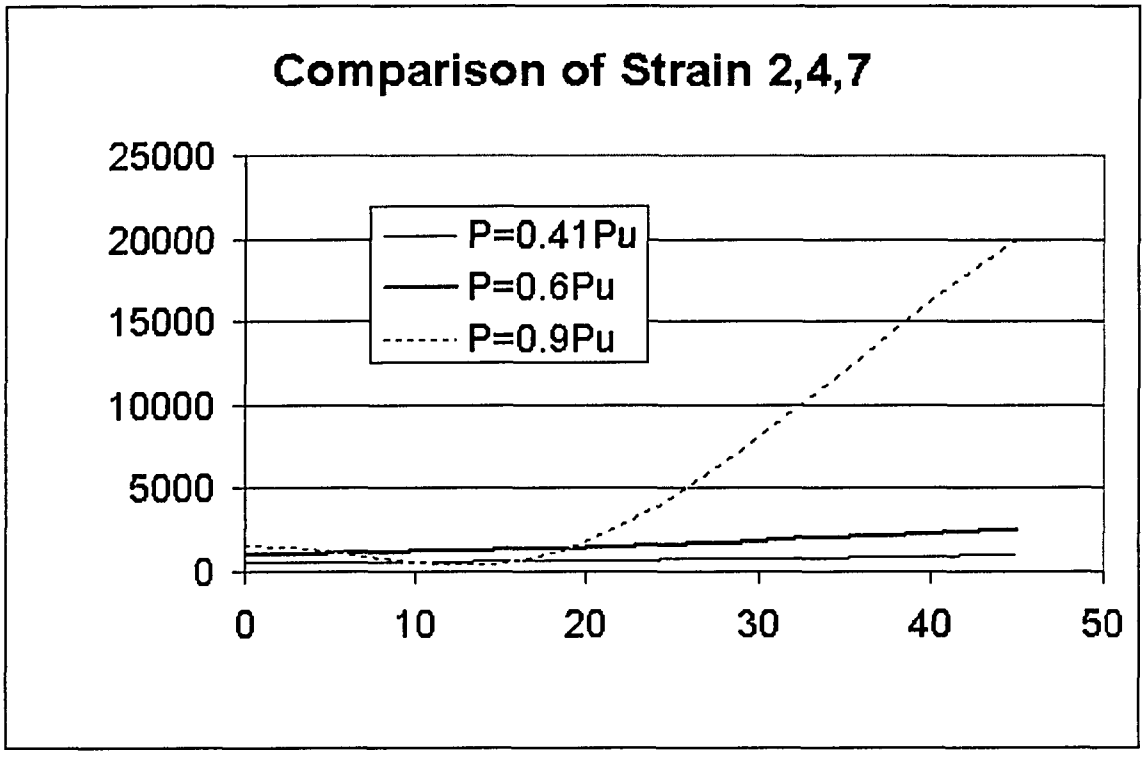

Fig. B10-9 Comparison of Strain 2,4,7 at Different Load Level of Specimen 10

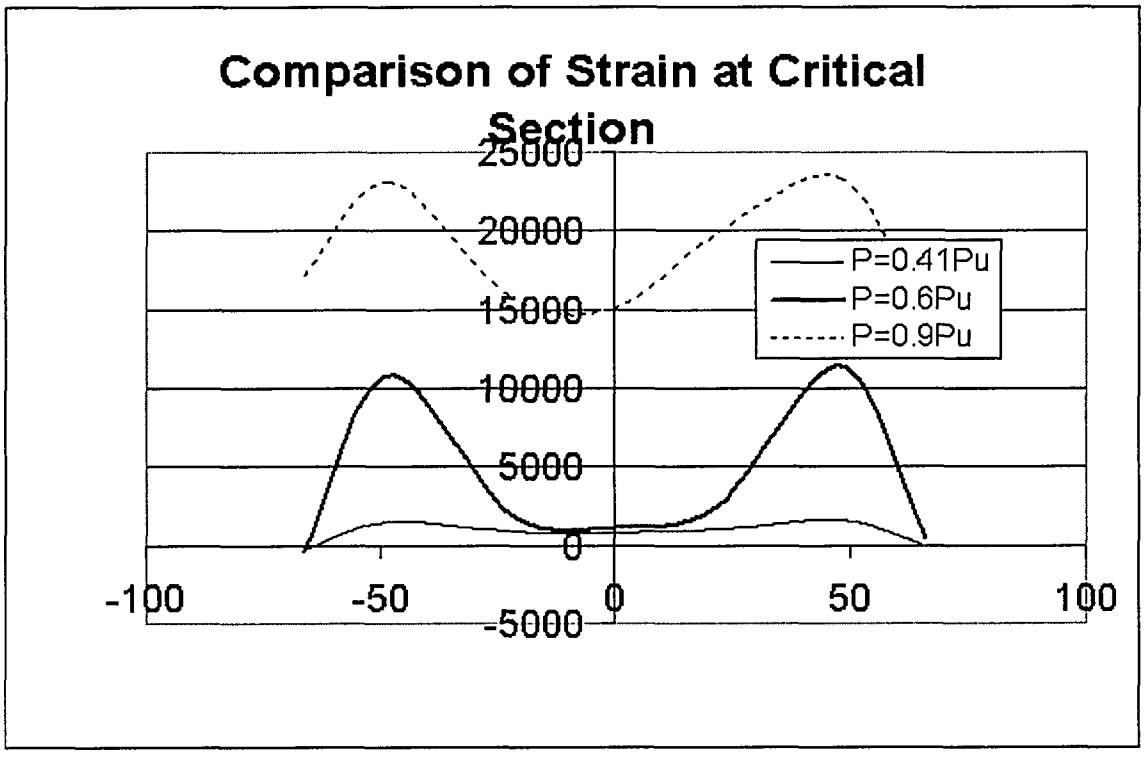

Fig. B10-10 Comparison of Strain at Critical Section at Different Load Level of Specimen 10

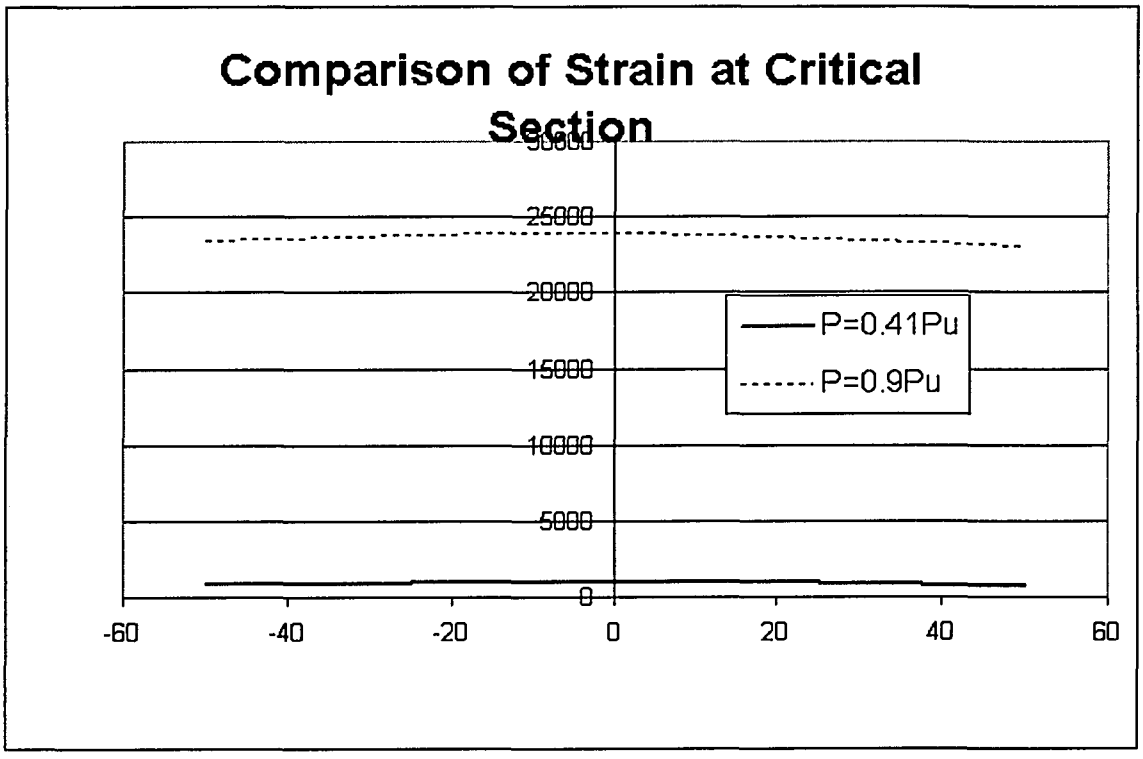

Fig. B10-11 Comparison of Strain 15,16,17 at Different Load Level of Specimen 11

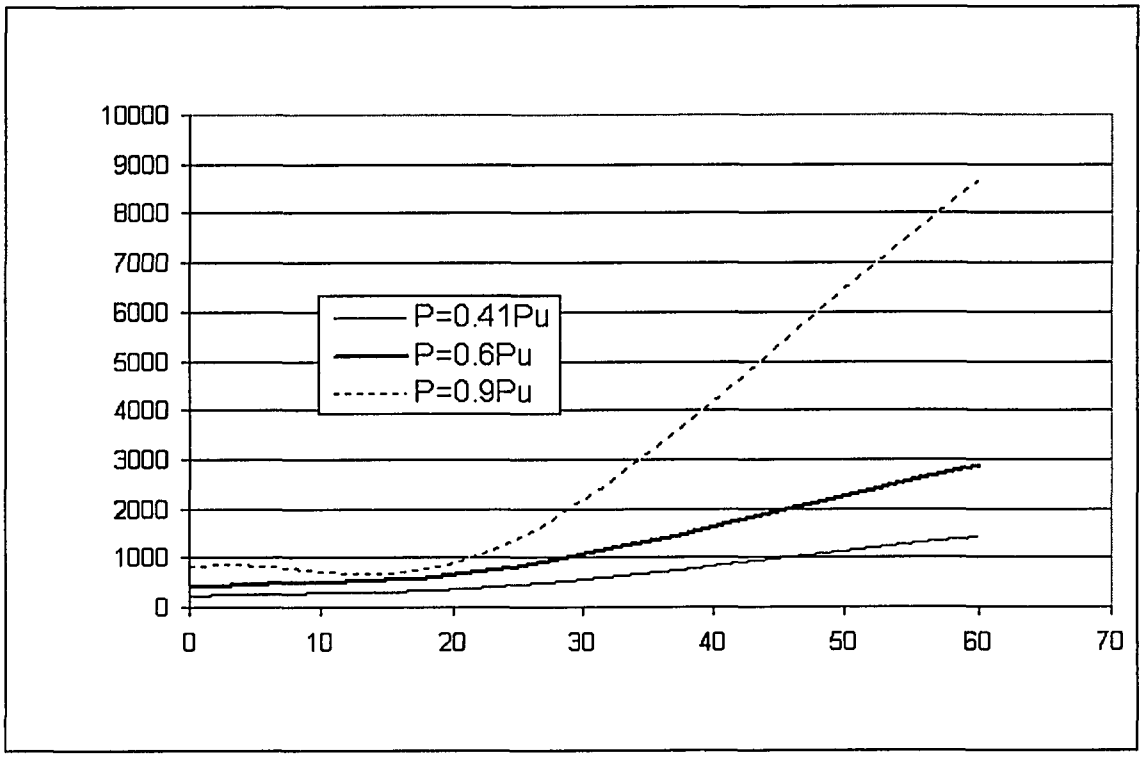

Fig. B10-12 Comparison of Strain 8,9,10 at Different Load Level of Specimen 10

APPENDIX C

Comparison of Stress and Strain at the Critical Section of Experimental Tests and Numerical Analyses

This part includes the comparison of strains of experimental test and finite element analysis at the critical section, comparison of stresses at the critical section and mid-length for specimen 4 is also presented.

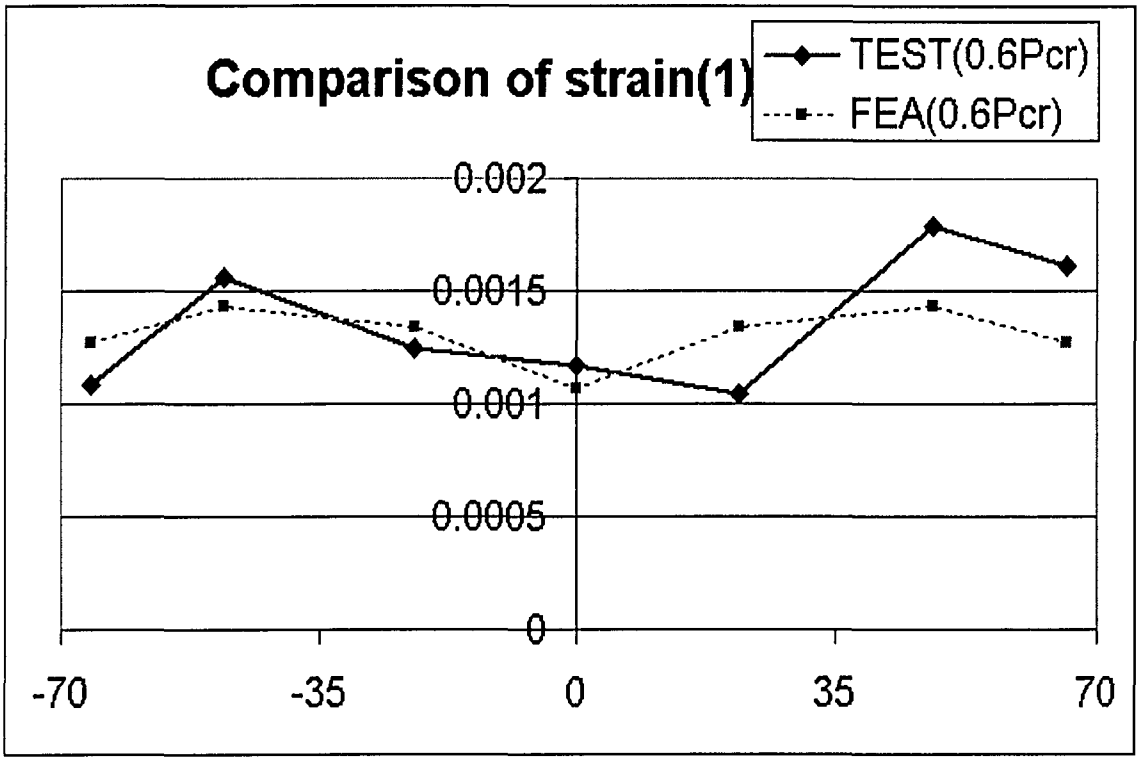

Fig. C1 Comparison of Strains at the Critical Section of Specimen 1

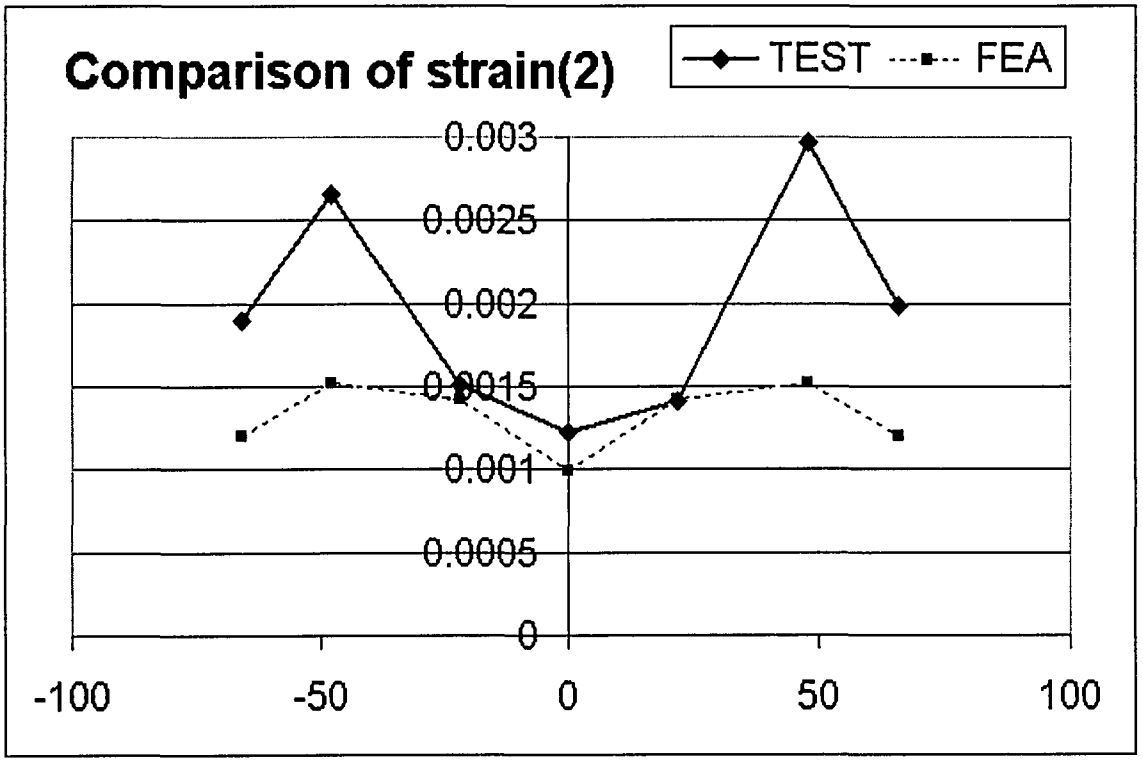

Fig. C2 Comparison of Strains at the Critical Section of Specimen 2

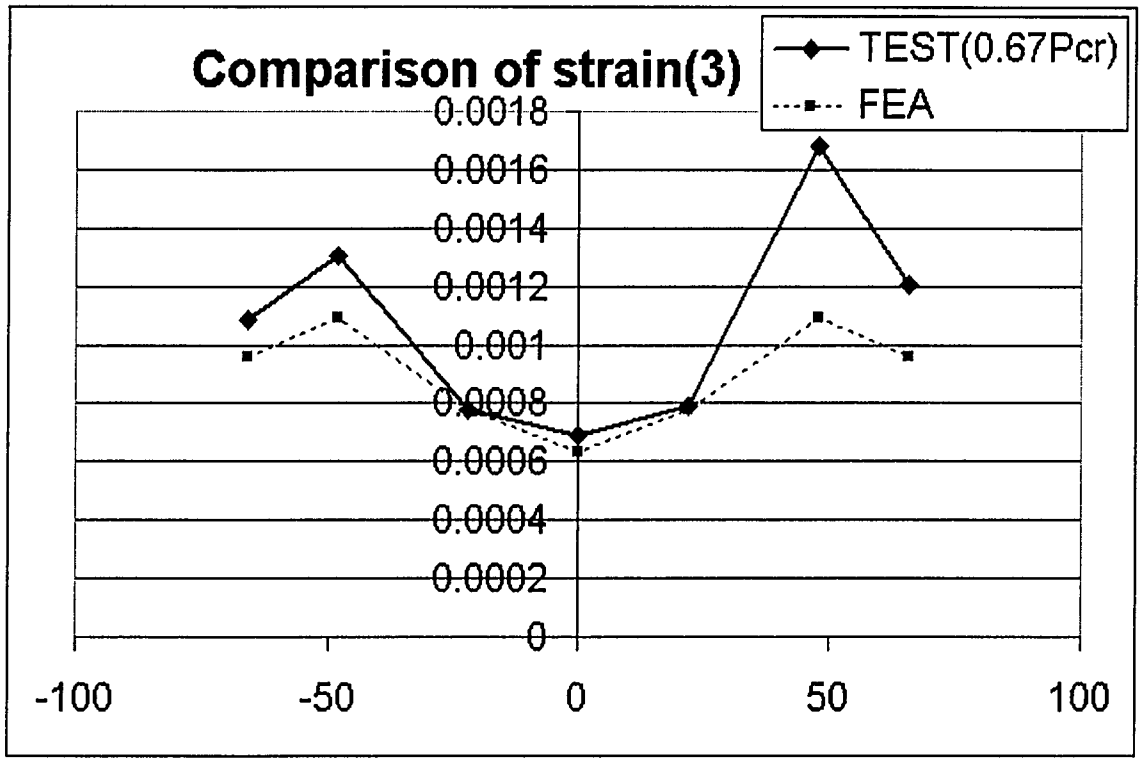

Fig. C3 Comparison of Strains at the Critical Section of Specimen 3

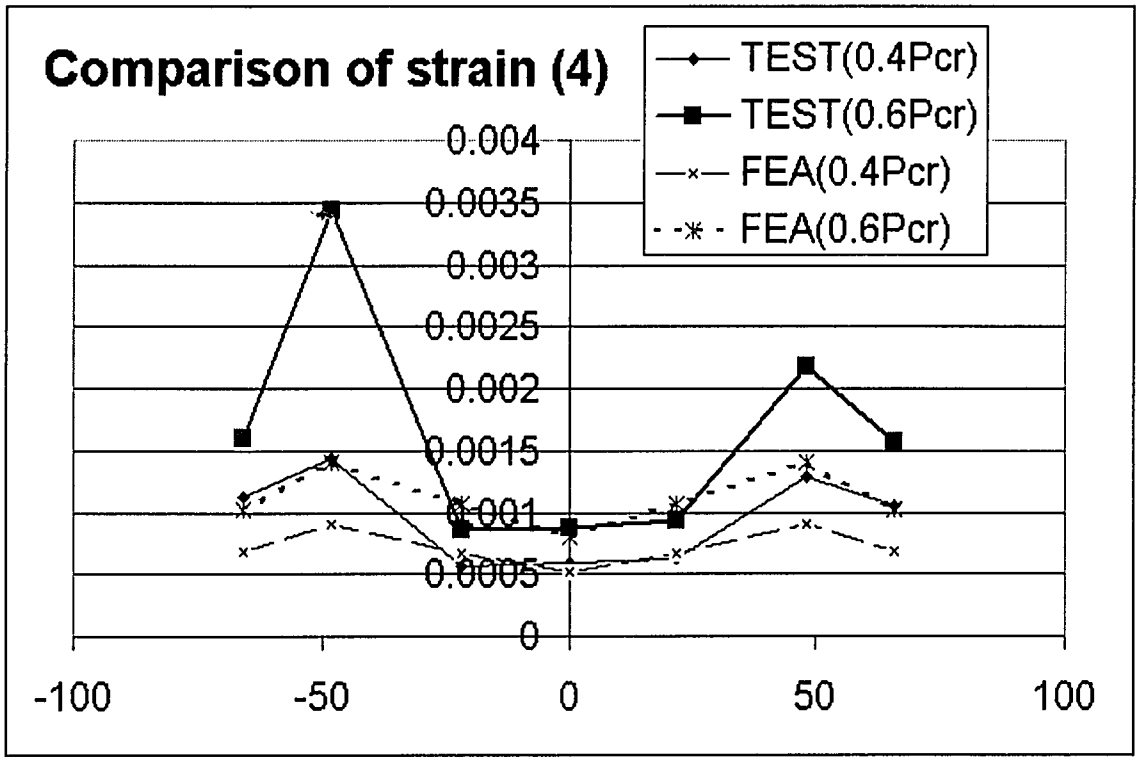

Fig. C4 Comparison of Strains at the Critical Section of Specimen 4

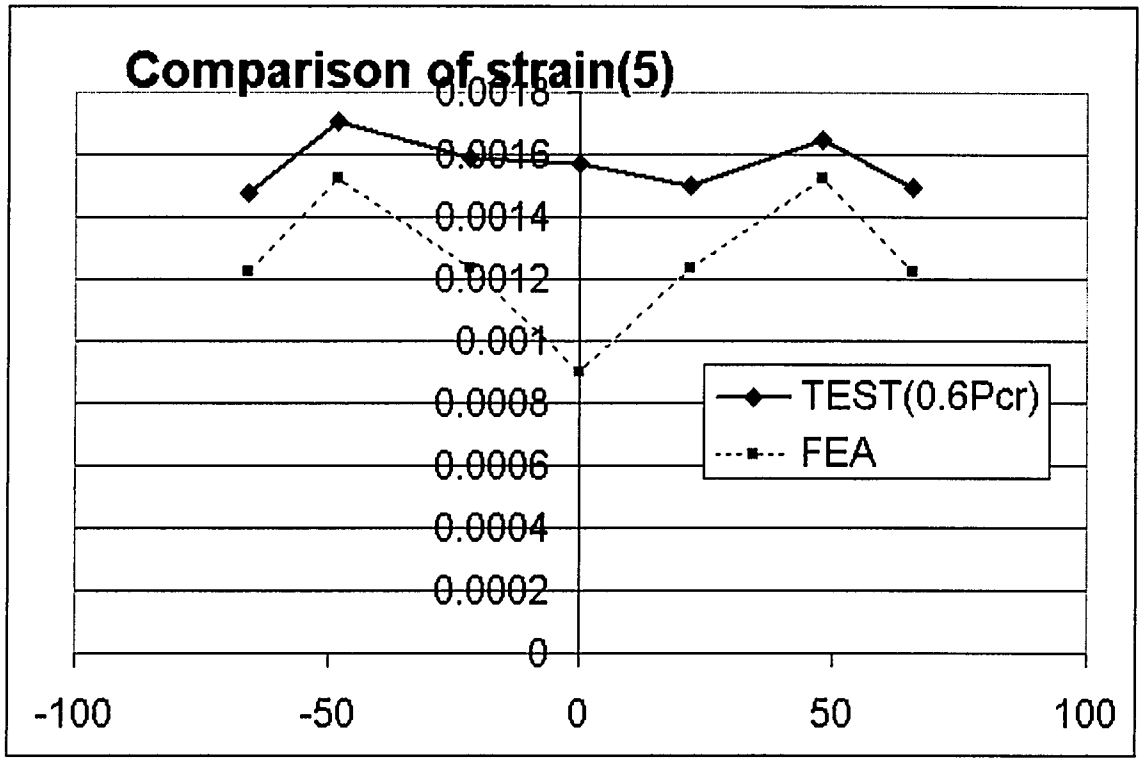

Fig. C5 Comparison of Strain at the Critical Section of Specimen 5

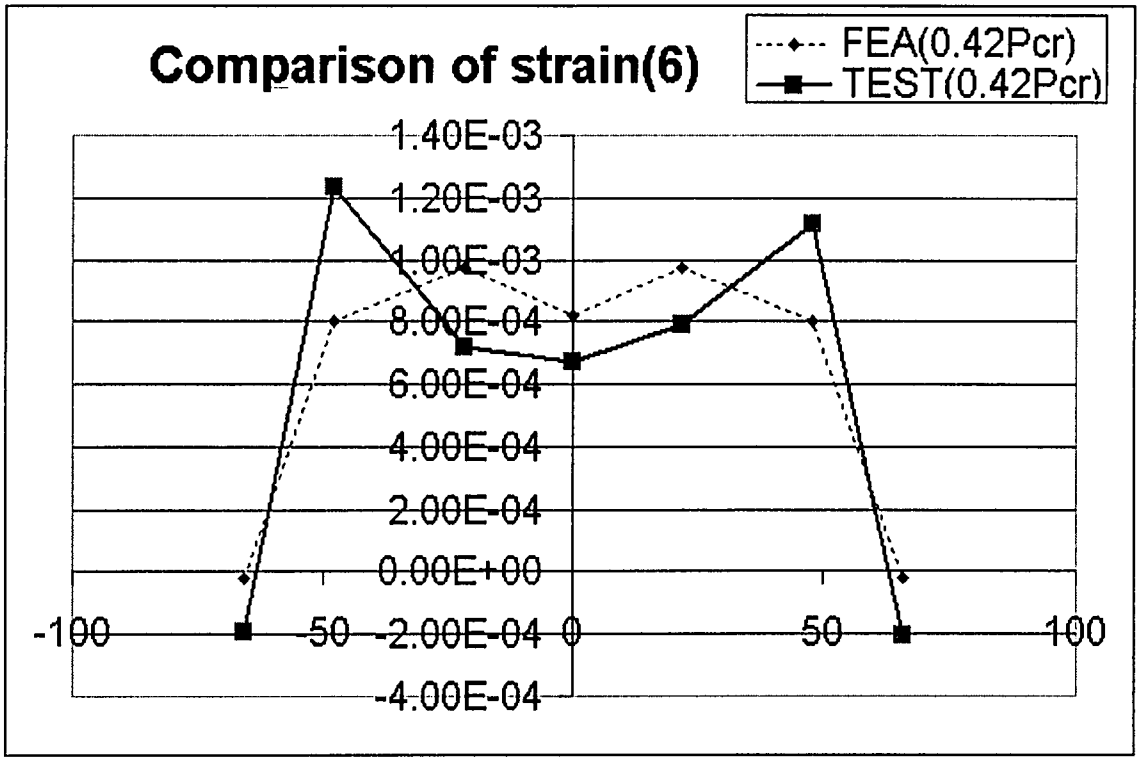

Fig. C6 Comparison of Strain at the Critical Section of Specimen 6

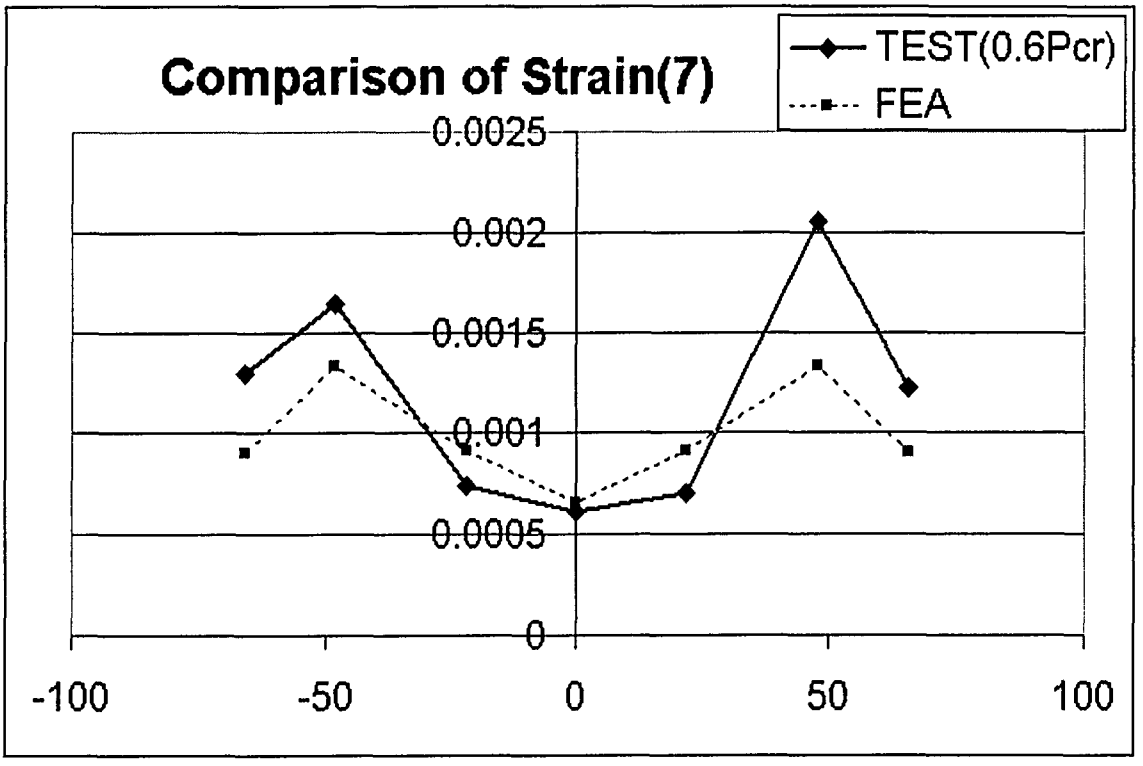

Fig. C7 Comparison of Strain at the Critical Section of Specimen 7

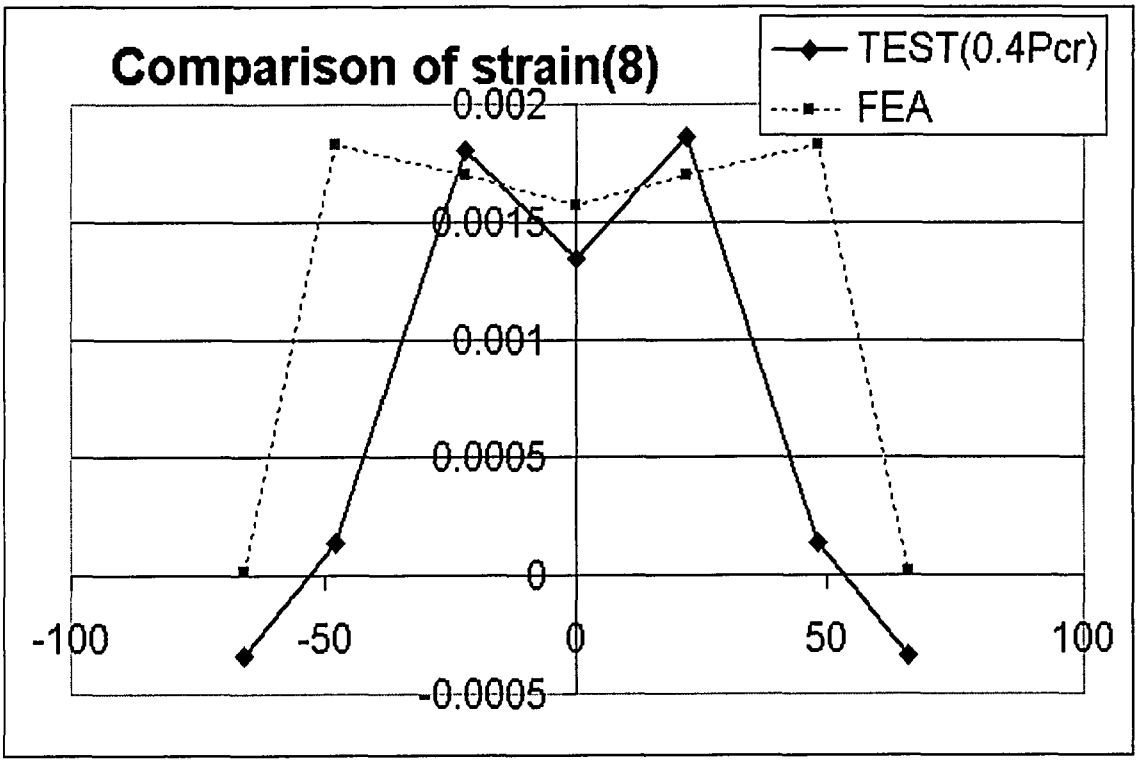

Fig. C8 Comparison of Strain at the Critical Section of Specimen 8

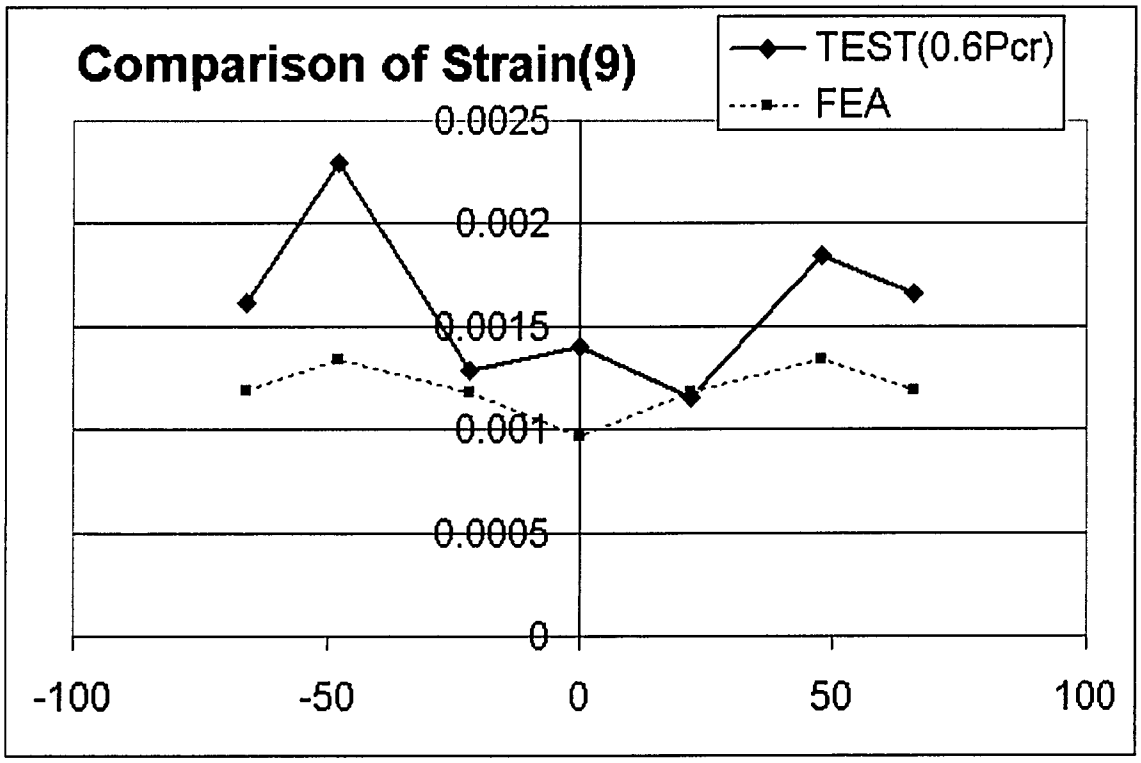

Fig. C9 Comparison of Strain at the Critical Section of Specimen 9

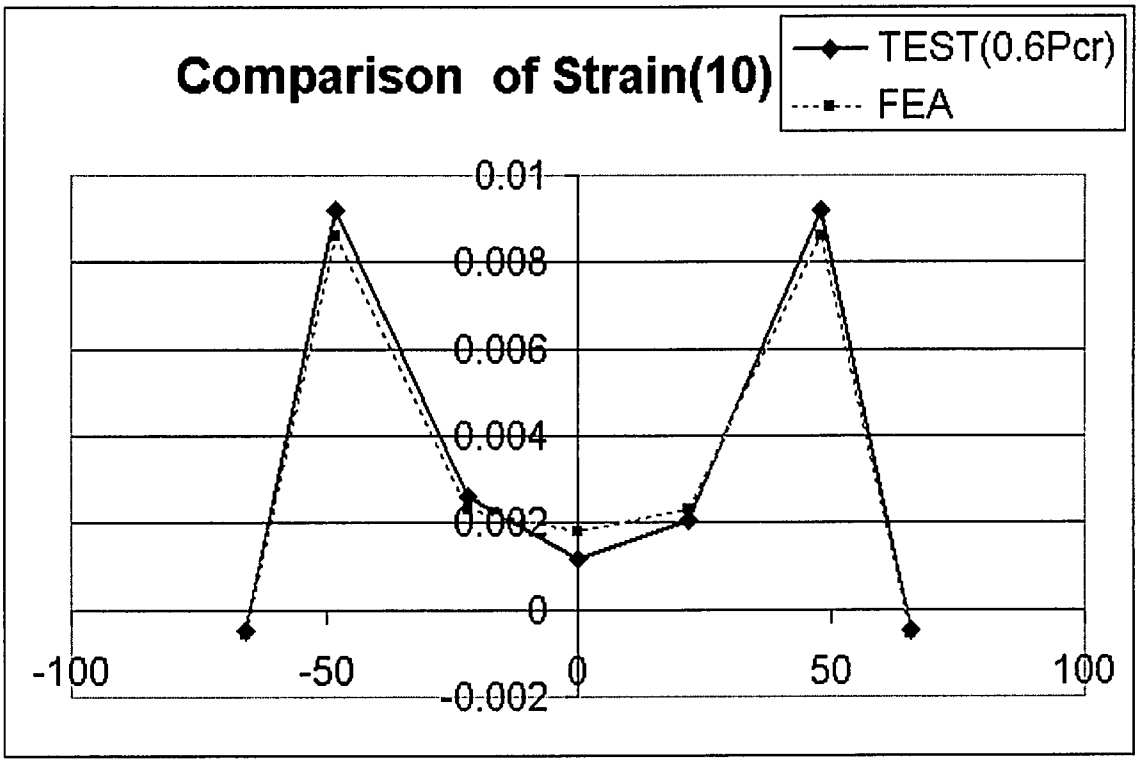

Fig. C10 Comparison of Strain at the Critical Section of Specimen 10

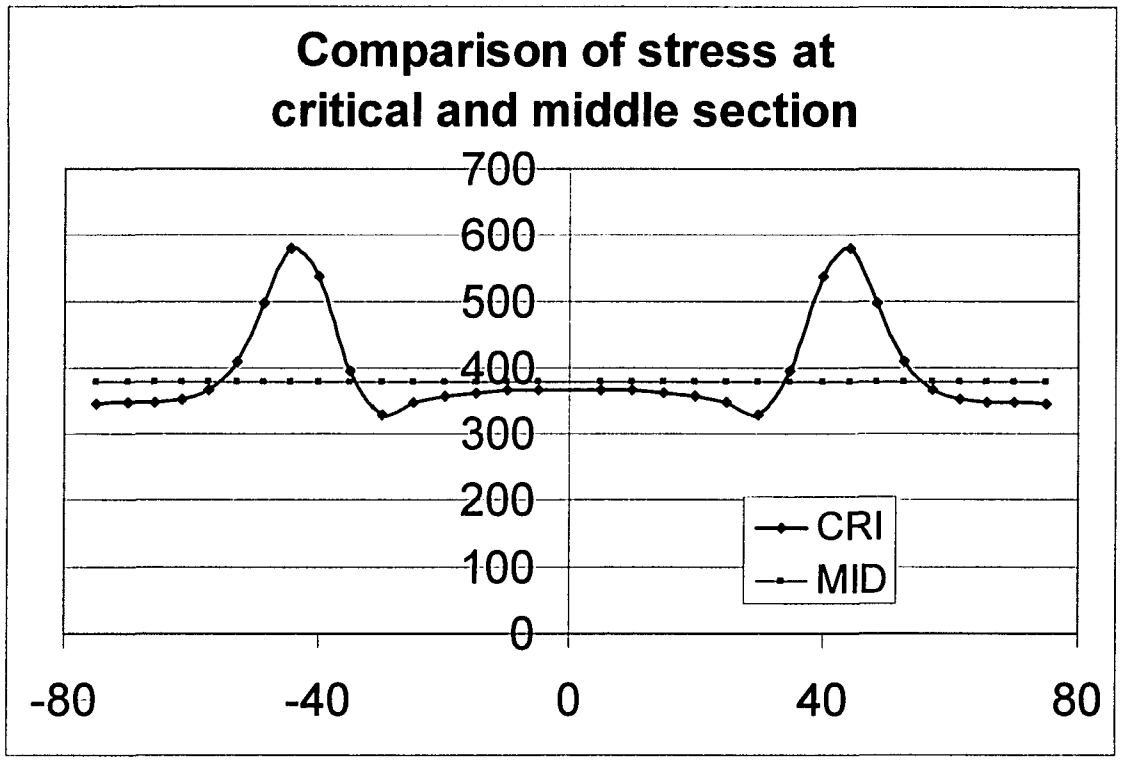

Fig. C11 Comparison of Stress at Critical Section and Mid-length of Specimen 4